



HAL
open science

Neutral Peptides in the Gas Phase: Conformation and Aggregation Issues

Eric Gloaguen, Michel Mons, Kirsten Schwing, Markus Gerhards

► **To cite this version:**

Eric Gloaguen, Michel Mons, Kirsten Schwing, Markus Gerhards. Neutral Peptides in the Gas Phase: Conformation and Aggregation Issues. *Chemical Reviews*, 2020, 120 (22), pp.12490-12562. 10.1021/acs.chemrev.0c00168 . hal-03293514

HAL Id: hal-03293514

<https://hal.science/hal-03293514>

Submitted on 21 Jul 2021

HAL is a multi-disciplinary open access archive for the deposit and dissemination of scientific research documents, whether they are published or not. The documents may come from teaching and research institutions in France or abroad, or from public or private research centers.

L'archive ouverte pluridisciplinaire **HAL**, est destinée au dépôt et à la diffusion de documents scientifiques de niveau recherche, publiés ou non, émanant des établissements d'enseignement et de recherche français ou étrangers, des laboratoires publics ou privés.

Neutral peptides in the gas phase: conformation and aggregation issues

Eric Gloaguen, Michel Mons*

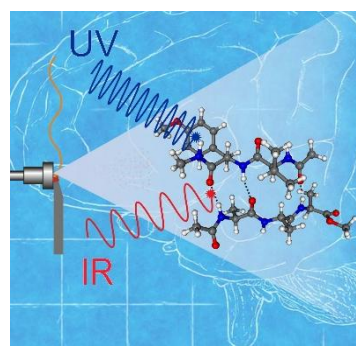
CEA, CNRS, Université Paris-Saclay, Bât 522, CEA Paris-Saclay, 91191 Gif-sur-Yvette, France

Kirsten Schwing, Markus Gerhards*

TU Kaiserslautern & Research Center Optimas, Erwin-Schrödinger-Straße 52, D-67663 Kaiserslautern, Germany

Abstract & TOC

Combined IR and UV laser spectroscopic techniques in molecular beams merged with theoretical approaches have proven to be an ideal tool to elucidate intrinsic structural properties on a molecular level. It offers the possibility to analyze structural changes by successively adding aggregation partners and thus an environment to a molecule. By this, it further makes these techniques a valuable starting point for a bottom-up approach in understanding the forces shaping larger molecular systems. This bottom-up approach was successfully applied to neutral amino acids starting around the 1990s. Ever since experimental and theoretical methods developed further and investigations could be extended to larger peptide



systems. Beyond, the review gives an introduction to secondary structures and experimental methods as well as a summary on theoretical approaches. Vibrational frequencies being characteristic probes of molecular structure and interactions are especially addressed. Archetypal biologically relevant secondary structures investigated by molecular beam spectroscopy are described and the influences of specific peptide residues on conformational preferences as well as the competition between secondary structures are discussed. Important influences like microsolvation or aggregation behaviour are presented. Beyond the linear α -peptides the main results of structural analysis on cyclic systems as well as on β - and γ -peptides are summarized. Overall, this contribution addresses current aspects of molecular beam spectroscopy on peptides and related species and provides molecular level insights into manifold issues of chemical and biochemical relevance.

Contents

1. General introduction
2. Some general aspects of amino acid and peptide structure
 - 2.1. Configuration, conformation and H-bonding pattern
 - 2.2. Frequent, naturally occurring secondary structures
 - 2.3. Further aspects of peptide structure in gas phase
3. Amino acids and peptides in the gas phase: several decades of investigations
4. Introduction to experimental methods
 - 4.1 Molecular Beams

- 4.2. Spectroscopic techniques in molecular beams
 - 4.2.1 R2PI
 - 4.2.2 UV/UV hole burning
 - 4.2.3 IR spectroscopy (IR/R2PI, UV/IR/UV)
 - 4.2.4 IR/IR/R2PI
 - 4.2.5 IR/VUV spectroscopy
 - 4.2.6 Population transfer methods
 - 4.2.7 Some aspects of spectroscopy in cold helium droplets
 - 4.2.8. Laser systems
- 4.3. Assignment strategy: principle and potential pitfalls
 - 4.3.1. UV spectroscopy
 - 4.3.2 IR spectroscopy
 - 4.3.3. Assignment
- 5. Introduction to theory
- 6. Optical probes of H-bonds and other structuring intramolecular interactions in peptides
 - 6.1. The stretching motion of the amide NH covalent bonds and other hydrides: The amide A region
 - 6.1.1. Spectroscopic probe of backbone-backbone interactions specific to uncapped peptides (COOH/NH₂): OH/NH/NH₂ hydride stretches
 - 6.1.2. Spectroscopic probe of backbone-backbone interactions: NH stretches in models of a protein chain
 - 6.1.3. Spectroscopic probe of local backbone-side chain interactions in neutral residues: backbone NH → side chain acceptors
 - 6.1.4. Spectroscopic probe of local backbone-side chain interactions in neutral residues: side chain donor → backbone CO
 - 6.2. The spectral region below 2000 cm⁻¹
 - 6.2.1. Some general aspects
 - 6.2.2. The spectral region below 2000 cm⁻¹ regarding the structural analysis of peptides
- 7. Probing biological structures
 - 7.1. β-strands
 - 7.2. β-sheet-structures
 - 7.3. γ-turns
 - 7.4. β-turn
 - 7.5. α-turn
 - 7.6. The Asx turn
 - 7.7. β-hairpins
- 8. Probing the changes induced by specific residues on the local conformation
 - 8.1. Documenting the effect of specific residues on the secondary structure through the NH stretch probe
 - 8.1.1. β-strand-like extended forms

- 8.1.2. γ -turns
 - 8.1.3. β -turns
 - 8.1.4. Uncapped peptides
 - 8.2. Documenting the effect of specific residues from the low frequency spectral region below 1800 cm^{-1}
 - 9. Competition between secondary structures; sequence-induced changes
 - 9.1. In protein chain fragment models
 - 9.1.1. At the local scale: competition between extended (5) and folded (7eq) forms in capped amino acids and dipeptides
 - 9.1.2. In capped dipeptides, competition between β -turns, 2_7 ribbons and β -strand like extended forms
 - 9.1.3. Emergence of helices: Competitions in capped trimers f-f-10-10
 - 9.1.4. Diversity in β -sheet model dimers
 - 9.1.5. Probing new secondary structures arising from specific residues in capped and uncapped dipeptides
 - 9.2. Uncapped and partially capped peptides
 - 10. Modified peptides : Homo amino acids, β - and γ -peptides
 - 10.1 Homo amino acids
 - 10.2 Capped β - and γ -amino acids
 - 10.3 Influence of cyclic structures in β - and γ -peptide chains
 - 10.4 Competition between secondary structures in larger β - and γ -peptide chains
 - 11. Microsolvation experiments: a detailed view of peptide solvation
 - 12. Specific peptides and aggregates
 - 12.1. Cyclic peptides and depsipeptides
 - 12.1.1 Depsipeptides
 - 12.1.2. Cyclopeptides
 - 12.2. Naturally relevant peptides or sequences/chain fragments
 - 12.3. Zwitterions
 - 12.4. Aggregates
 - 12.4.1. Peptide-peptide aggregates
 - 12.4.2 Non-peptide aggregates
 - 13. Conclusions and perspectives
- Author Information
- Acknowledgements
- References

1. General introduction

The main motivation to analyze the structure of biologically relevant substances on a molecular level is to gain knowledge about the structure-functionality correlation, which is a precondition to specifically influence it. In case of peptides and proteins, nature is limited to a kit with 22 proteinogenic amino acids (20 canonical ones

being directly encoded in the genetic code). Nevertheless, a different sequence of amino acids (the so-called primary structure) can already lead to different structural preferences of a relatively short peptide. Thus, the substance class of peptides exhibits a tremendous variety of structures, which is associated with the great variety of tasks they can fulfill. Structural variety also comprises the opposing aspects of structural rigidity and structural flexibility. For most peptides and proteins, their structure is a compromise between these two extrema (cf. e.g. ¹), which of them is dominant also depends on the specific functionality. In functions related to mechanical stability in supramolecular architecture (e.g. collagen in connective tissue² or transmembrane protein ion channels^{3,4}) rigidity is often required. In contrast, in processes like molecular recognition, a certain flexibility is required without losing the specificity for the corresponding binding partner (cf. e.g. ⁵⁻⁸). However, structural flexibility can also lead to structural changes disturbing the functionality of the proteins or even leading to pathogenic effects as this is the case in neurodegenerative diseases like the Parkinson's disease, the Alzheimer's disease or the Creutzfeldt-Jakob disease (cf. e.g. ^{9,10}).

Despite their high structural flexibility, proteins and peptides show repetitive structural motifs (the so-called secondary structures cf. Section 2) with characteristic hydrogen-bonding (abbr. H-bonding) patterns. Several factors influence the structural preferences: Beyond intrinsic properties, like the primary structure and the size of the system, environmental aspects like solvent effects or interactions with aggregation partners (cf. Section 12, e.g. other peptides, sugars, nucleobases, metal ions) also play a role. As a consequence, the structural analysis of proteins and peptides can quickly become a challenging task, not only with regard to experimental methods, but also to the theoretical description necessary for a further reaching interpretation (cf. Section 4.3 and 5).

From the experimental side, spectroscopic tools can be applied for structure determination. Depending on the substance and further requirements (e.g. molecular size, aggregation state, desired precision), a variety of spectroscopic methods is available: the classical techniques for structure determination of proteins like X-ray crystallography (cf. e.g. ^{11,12}) and NMR spectroscopy (cf. e.g. ¹³⁻¹⁵), via UV/VIS measurements, fluorescence spectroscopy (cf. e.g. ^{16,17}) and circular dichroism (cf. e.g. ^{18,19}), to rotational spectroscopy (cf. e.g. ²⁰⁻²⁶) and IR spectroscopy (cf. e.g. ²⁷⁻²⁹). A direct sensitivity towards inter- or intramolecular interactions can be achieved by vibrational spectroscopy, which can be applied in form of Raman spectroscopy (cf. e.g. ³⁰⁻³⁵; indirect vibrational excitation via the Raman effect) or IR spectroscopy (direct excitation of the vibrational modes). For peptide systems, the frequencies of CO, NH and OH stretching modes, are useful diagnostics to characterize H-bonding and other interactions (cf. Section 6). However, less localized modes like out of plane deformation modes or collective backbone modes in the region below 1000 cm⁻¹, including the far IR, have gained increasing importance throughout the last years (cf. Section 6). In principle, IR spectroscopy can be applied to all aggregate states, to the condensed phase (solid, liquid/solution) but also to the gas phase. Keeping in mind the rapidly increasing complexity of peptide systems with molecular size and environmental influences, a bottom-up approach makes sense. In a first step, the intrinsic structural preferences of amino acids and small peptides as building units of larger peptide and proteins are analyzed by measurements in the gas phase, where environmental effects are minimized. If spectroscopic gas phase measurements are carried out in the absorption or scattering mode as this is the case for FTIR or Raman spectroscopy in gas cells (cf. ^{36,37} and ³⁵), a sufficient sample concentration is necessary which, in turn, does not guarantee isolated conditions for the sample molecules. Isolated species, combined with the additional effect of cooling down the internal degrees of freedom, which often makes spectra less congested, can be achieved in molecular beams (cf. Section 4). Though, highly sensitive Raman (cf. e.g. ³⁰⁻³⁵) as well FTIR spectroscopic set-ups (cf. e.g. ^{30,31,38-41}) allow measurements under molecular beam conditions, neither a mass resolution nor an intrinsic isomer/conformer selectivity is given by these experiments. Similarly, rotational spectroscopy is not an isomer/conformer-selective technique either, but it can easily disentangle the contribution of each species with the help of theoretical predictions. However, due to spectral restrictions of the spectrometers, rotational spectroscopy has been limited to comparably small molecules (cf. e.g. ^{42,43}) so far: models of biomolecules (cf. e.g. ^{26,44}) to more recently analyzed sugars (cf. e.g. ⁴⁵), non-protected (cf. e.g. ⁴⁶⁻⁴⁸) and protected amino acids (cf. e.g. ⁴⁹) up to dipeptide models (cf. e.g. ⁵⁰).

In this context, laser spectroscopic techniques combining IR and UV excitations, that one can consider as belonging to the so-called 'action spectroscopies', provide an isomer-selective method of choice to tackle the

issue of structural diversity (cf. Section 4). Moreover, beyond cooled, isolated sample molecules, molecular beam experiments also offer the possibility to successively add aggregation partners to the sample molecules and thus to investigate gradual successive steps in the formation of an environment (cf. Sections 11 and 12). Though the pure experimental IR and UV data of isolated molecules can already give valuable structural hints, a further, more detailed structural description can only be achieved in comparison with theoretical tools (cf. Section 5). In that context, already successfully interpreted systems can serve as benchmark systems for higher level theory. Thus, molecular beam spectroscopy and theory are complementary and synergistic approaches, which allow to analyze intrinsic structural properties and hence to address quite specific questions on a molecular level like the interactions being responsible for the structural preferences. In that context, hydrogen bonds (abbr. H-bonds or HB) between amide backbone groups, which can give rise to well-defined (sometimes repetitive), structural patterns and secondary structure motifs (cf. Sections 2 and 7), play a decisive organizational role as well as side chain-backbone or side chain-side chain interactions (cf. e.g.⁵¹⁻⁵⁸ and with regard to gas phase cf. Sections 7 and 8). Specific aspects influencing these shaping interactions can be investigated, like the primary structure (cf. e.g. Section 8), or the L versus D configuration (cf. e.g. Section 9).

The investigation of isolated molecular systems always raises the question about the biological relevance of such an approach. Nevertheless, it could be demonstrated on a variety of examples that naturally relevant secondary structure motifs can be found under isolated molecular beam conditions without the influence of an environment (cf. Section 7-9). This further motivated gas phase spectroscopists to address biological or even medically relevant issues like the self-aggregation of peptides (cf. Section 12) and its prevention (cf. Section 12), the aggregation between peptides and sugars, e.g. being of relevance in cellular recognition (cf. Section 12), or amino acid-nucleobase complexes associated with gene expression (cf. Section 12). Furthermore, isolated gas phase conditions can be considered as being not too far away from naturally occurring hydrophobic domains in which peptide structures can be embedded (cf. Section 7). Even if the conformational landscape between solution and gas phase shows differences, the comparison helps to understand the influence of the environment. Additionally, one should keep in mind that molecular beam experiments offer the possibility to stepwise build up such an environment (aggregation: cf. Sections 11 and 12) and analyze the impact of the addition of each molecule to the system (cf. e.g. Section 11). Thus, this gain of knowledge in basic understanding of structural behaviour on a molecular level can serve as benchmark to apply these experimental and theoretical methods to larger, biologically relevant systems (cf. Section 5).

The focus of this review is to give an overview about the achievements and advances in analyzing the intrinsic structural and partly photophysical properties of neutral peptide systems by molecular beam spectroscopic methods combined with theoretical tools. The individual sections describe central topics in the analysis of isolated peptide systems as specific influences on secondary structure, microsolvation or aggregation. For readers who are not familiar with this field of research, an introduction into the basics of peptide secondary structures and molecular beam spectroscopy is given in Sections 2 and 4.

2. Some general aspects of amino acid and peptide structure

2.1. Configuration, conformation and H-bonding pattern

In the following chapters of this contribution, the predominant L-configuration of the naturally occurring amino acids will not be explicitly labelled. In contrast, the D-configured amino acids, which are only sporadically present (for example in bacterial peptides like valinomycin, cf. e.g.⁵⁹), will be denoted. The same is true for the energetically favoured, and thus dominant *trans* configuration of the amide bond and the less frequently occurring *cis* arrangement. The latter can be found if steric hindrances or tensions can be minimized, e.g. in proline containing peptides (e.g.^{60,61}) or in cyclo dipeptides (cf. e.g.⁶²⁻⁶⁵ and Section 12).

Backbone conformation

In contrast to the planar amide bond with its partly double bonding character, the rotational freedom of the single bonds of the α -C-atom leads to the structural flexibility of peptide chains. The backbone orientation around one specific α -C-atom is described by two dihedral angles as given in the extract of a peptide backbone chain in Figure 1, with $C_{\alpha,i}$ being the central α -C-atom and 'i' referring to the number of the amino acid in the sequence: $\phi(C_{amide\ i-1}-N_{amide\ i}-C_{\alpha,i}-C_{amide\ i})$ and $\psi(N_{amide\ i}-C_{\alpha,i}-C_{amide\ i}-N_{amide\ i+1})$; they are plotted against each other in the Ramachandran plot^{66,67} being subdivided into nine conformation regions. The denotation of the region and thus of the corresponding α -C-atom is given in the plot. Nevertheless, not only the backbone but also the side chain can have an influence on the peptide structure due to e.g. interactions with the backbone. Thus, its orientation is described by the dihedral angle χ_1 , frequently having three typical values gauche(+) ($\chi_1(g+) = 60^\circ$), anti ($\chi_1(a) = 180^\circ$), gauche(-) ($\chi_1(g-) = -60^\circ$). Taking all three dihedral angles into account, 27 different conformations are obtained for a single amino acid, already illustrating the structural variety of peptides. For cases in which the side chain is 'asymmetrically composed' relative to the $C_\alpha-C_\beta$ bond (e.g. in Trp or His), χ_2 as further dihedral angle rotated by 180° around $C_\beta-C_\gamma$ is introduced, basically having the two orientations '+' ($\approx +90^\circ$) and '-' ($\approx -90^\circ$). In the case of long side chains (e.g. methionine), their orientation is defined by the succession of several dihedral angles, χ_i with $i=1,2,3,\dots$, increasing again the conformational complexity of these amino acids.

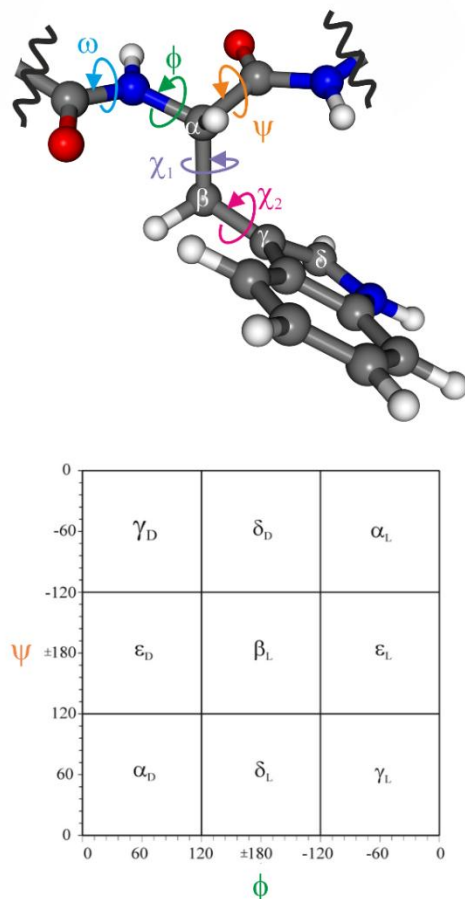


Figure 1: Definition of the dihedral angles for the structural description of the backbone and the side chain illustrated on the extract of a peptide chain. The Ramachandran plot is shown below.

Table 1: Typical average dihedral angles for secondary structure motifs⁶⁸⁻⁷¹.

structural motif	dihedral angles				nomenclature ^{a)}
	ϕ_i	ψ_i	ϕ_{i+1}	ψ_{i+1}	
pleated sheets					
antiparallel β -sheet	-140	135	the same as for ϕ_i and ψ_i		β_L
parallel β -sheet	-120	115			β_L
Helices					
right-handed α -helix	-60	-45	the same as for ϕ_i and ψ_i		α_L
3_{10} -helix	-57	-30			α_L
π -helix	-	$\phi_i + \psi_{i+1} \approx -125^\circ$ ^{b)}		-	-
turns					
classical γ -turn	75	-65	the same as for ϕ_i and ψ_i		γ_D
inverse γ -turn	-75	65			γ_L
β -turn type I	-60	-30	-90	0	$\alpha_L-\gamma_L$
β -turn type I'	60	30	90	0	$\alpha_D-\gamma_D$
β -turn type II	-60	120	80	0	-
β -turn type II'	60	-120	-80	0	-
β -turn type III	-60	-30	-60	-30	$\alpha_L-\alpha_L$
β -turn type III'	60	30	60	30	$\alpha_D-\alpha_D$

a) Nomenclature according to the Ramachandran-plot (if unambiguously defined).

b) The majority of π -helices does not adopt very regular dihedral angles but the ψ_i and ϕ_i angles usually sum up to roughly -125° (except of the first and the last residue).

The sequence of amino acids within a peptide chain is called primary structure, whereas the term secondary structure denotes the spatial arrangement of amino acid residues close to each other in the linear sequence. These steric relations can be regular and repetitive and can thus lead to periodical structures, among them helices and pleated sheets (cf. Section 2.2). Structural periodicity originates from identical or similar dihedral angles of adjacent α -C-atoms (cf. Table 1). The turns (cf. Section 2.2), as the third famous secondary structure motif, are frequently not repetitive, but have well-defined structures. Combined with helices and pleated sheets, they decisively shape the structure of peptides and proteins. Nowadays, it is generally accepted that the structure of peptides and proteins is determined at the level of the primary structure and thus by the amino acid sequence, since it influences the backbone (abbr. bb) in different ways: On the one hand, the steric requirements of the side chains (abbr. SCs) can indirectly narrow the number of possible amidic H-bonds, or, on the other hand, SCs can directly influence the backbone conformation by SC–bb interactions (NH \cdots π , NH \cdots SCH₃, NH \cdots SH, SH \cdots CO) or SC–SC interactions (e.g. $\pi \cdots \pi$, SH $\cdots \pi$).^{51-54,57,58} To investigate peptide folding, resulting from numerous interactions of different natures, gas phase spectroscopy experiments are ideal to disentangle all these contributions and to analyze detailed aspects of structure formation in peptide systems (cf. esp. Sections 7, 8, 9 and 12) for naturally occurring secondary structure motifs and partly biologically relevant structures (examples cf. Sections 7 and 12).

H-bonding content

The preceding section addressed the denotation of a peptide sequence by labelling the conformation of each α -C-atom within the peptide sequence according to the characteristic dihedral angles. Another classical nomenclature addresses the pattern of intrabackbone H-bonds: the term C_n (or C_n) interaction (or structure) is used when the H-bond leads to the formation of a n-membered ring, including the donating NH and the accepting CO group (see examples of such bb–bb interactions in Table 2 left).

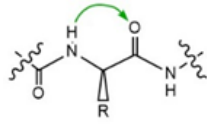
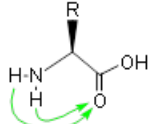
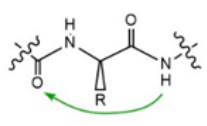
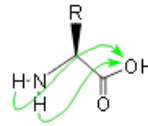
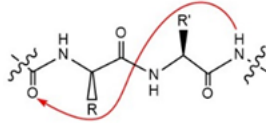
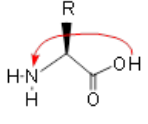
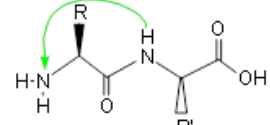
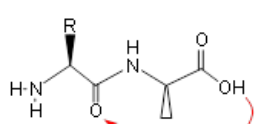
without inclusion of N- or C-terminus		including N- or C-terminus	
structural motif	notation	structural motif	notation
	5 $i \rightarrow i$		N_5^C
	7 $i \leftarrow i+2$		$N_5'^C$
	10 $i \leftarrow i+3$		C_5^N
Frequent alternative denotation: 5: C5 or C_5 7: C7 or C_7 (secondary structure motif of a γ -turn, cf. section 'turns' here and Section 6) 10: C10 or C_{10} (secondary structure motif of a β -turn, cf. section 'turns' here and Section 6)			5^N
			C_7

Table 2: Examples for bb – bb interactions and corresponding notation according to the H-bonding pattern with 'i' being the number of the amino acid in the sequence (cf. Section 6).

Owing to the prominent role of the donating NH groups along the backbone and their specific vibrational signatures (cf. Section 6.1), the sequential listing of individual H-bonding status of the NH bonds along the backbone provides an efficient way to characterize the H-bonding pattern and the overall structure of the peptide, especially beyond two-residue peptides. Several more or less elaborated notations have been developed by several groups,⁷²⁻⁷⁶ leading to a concise H-bond nomenclature: Cn bonds (cf. above) are indicated by 'Cn' or simply 'n'; a free NH group is labelled with 'f'; an interaction with a π -system with ' π '. A more complex nomenclature is needed when SCs are involved in H-bonding⁷⁷⁻⁸³: the size of the ring formed is again denoted with 'n', but the way the bb/SC nature of the bonding is indicated differs. Some authors simply mention them separately from the previous backbone bonds;⁷⁷⁻⁷⁹ others adopt a more sophisticated nomenclature,^{81,82} which enables distinction between a donor or an acceptor SC, the position of the side chain group relative to its α -C-atom being given by Greek letters (e.g. γ , δ , ϵ) as superscript (left hand side if it is in a donating function, right hand side for an acceptor function), cf. Table 3.

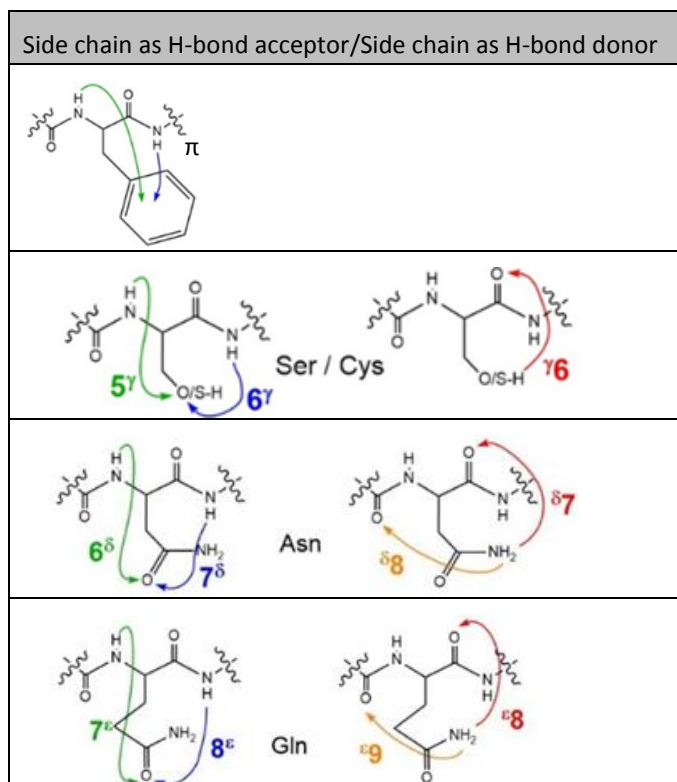


Table 3: Examples for bb – SC interactions and corresponding notation according to the H-bonding pattern (cf. Section 6).

A similar terminology can be proposed if the N and/or C terminus participate in an H-bond (cf. Table 2. right hand side): Again, the number of atoms included in the ring formed by the H-bond is indicated with ‘n’. The N- or C-terminus participating in the H-bond is marked with ‘N’ or ‘C’ as superscript to the number ‘n’ of the ring size. If the terminus acts as an H-bond donor, the superscript is placed on the left hand side of ‘n’, in case of a role as H-bond acceptor, it is on the right hand side.

2.2. Frequent, naturally occurring secondary structures

Helices

Helices belong to the most common secondary structure motifs and can be distinguished by their different hydrogen bonding patterns.

Pauling and Corey were the first to propose a structure for the α -helix⁸⁴; it is characterized by $i \leftarrow i+4$ H-bonds between the CO group of the amino acid i and the NH group of the amino acid $i+4$, which is four residues apart in the sequence (cf. Figure 2). This interaction could also be denoted as C13. Due to this H-bonding pattern, 3.6 amino acids per turn are found, resulting in a spatial proximity of amino acids being quite far apart in the linear sequence. In nature, the clockwise arrangement is preferred based on the lower steric hindrance compared to the counter clockwise arrangement.

In the 3_{10} helix,⁷¹ H-bonds are formed between the amino acid residues i and $i+3$, leading to three residues per turn and thus a more stretched appearance in comparison to the α -helix (cf. Figure 2). The H-bonding pattern results into a ten-membered H-bonded turn, so that the helix can be considered to be constituted of successive β -turns (cf. Table 1.) In comparison to α -helices, 3_{10} helices are usually shorter, i.e. they span over a smaller number of residues than α -helices.

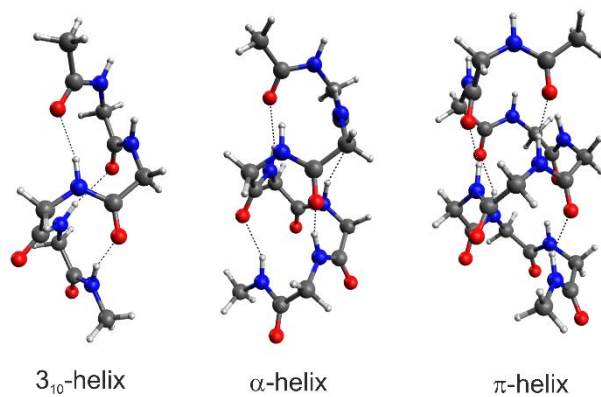


Figure 2: Schematic illustration for the three most abundant types of helices.

The π -type helix⁸⁵ exhibits the most compressed appearance with a $i+5 \leftarrow i$ hydrogen bonding pattern and 4.4 residues per turn (cf. Figure 2). It is naturally less abundant than the other two types of helices, and often comprises not more than 7 residues with much less regularly repeating dihedral angles than the other two types of helices.

The β -sheet structure

After the α -helix, the β -sheet was the second secondary structure that was described by Pauling and Corey⁸⁶, in which the planes of the backbone amide bonds are oriented like a pleated sheet. In these structures, at least two stretched polypeptide chains, called β -strands, are opposite each other and are linked by a series of sequential interstrand H-bonds forming a β -sheet.

In a β -strand, the conformation of the amino acids is mainly β_L , and the extended shape of a non-aggregated β -strand is stabilized by weak intraresidue C5 H-bonds between the carbonyl and amino group of the same amino acid.

In a parallel β -sheet the two β -strands have the same orientation with regard to the N- and C-terminus, whereas in an antiparallel β -sheet they have the opposite direction (cf. Figure 3). In the latter, the H-bonding pattern adopts an alternating sequence of ten- and fourteen-membered rings, so that a β -sheet unit cell is composed of these two components. In comparison, the unit cell consists of an H-bonded twelve-membered ring in a parallel β -sheet. Frequently, β -sheet structures with up to 4-5 strands are found, which can be of purely parallel, antiparallel or of mixed character. Biologically relevant examples with β -sheet structures are the protein chains of natural silk (cf. e.g.⁸⁷) or immunoglobulins (cf. e.g.⁸⁸), but they are also found in context with neurodegenerative diseases (cf. e.g.⁸⁹⁻⁹⁵ and Section 12). A further structure associated with these diseases (cf. e.g.⁹⁶) is the β -helix, which presents a protein structure of several parallel β -strands in a helical arrangement with a frequently repetitive amino acid sequence. The structure is stabilized by H-bonds, sometimes ionic interactions or so called protein-protein interactions, which e.g. include electrostatic and hydrophobic effects.

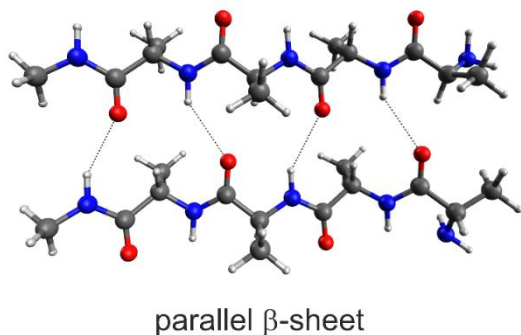
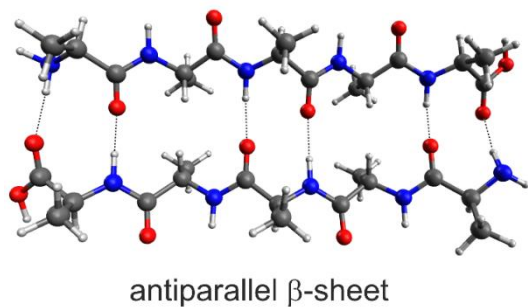


Figure 3: Schematic illustration of antiparallel and parallel β -sheet arrangements.

Turns

A direction change within a peptide chain, which is necessary for the compact structures of proteins, can be achieved by turns, which connect regions of defined secondary structure. Within such turns, the participating amino acids form sixteen- (π -turn⁹⁷), thirteen- (α -turn⁹⁸), ten- (β -turn^{99,100}) or seven-membered (γ -turn¹⁰¹) H-bonded rings. Turns often exhibit characteristic dihedral backbone angles and changing their sign often converts them into their inverse form (cf. Table 1).

γ -turns (C7 interaction) and β -turns (C10 interaction) belong to the frequently occurring structures (cf. Figure 4 and Section 7). The latter ones are of special importance since they can be involved in loops. Those can effect a direction change within a β -strand, which can lead to a folding and finally to the formation of an antiparallel β -sheet structure.

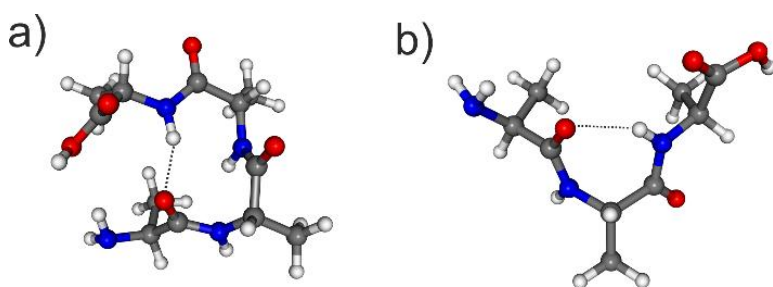


Figure 4: Schematic illustration of a) a β -turn type I and b) an inverse γ -turn.

2.3. Further aspects of peptide structure in gas phase

The role of protection groups

With the unmodified N- and C-terminus amino acids and peptides can exhibit strong preferences for intramolecular H-bonds involving the N- and C-terminus, and can also form intermolecular H-bonds leading to polymer chains. Nevertheless, in a context where the description of the properties of a protein or a long peptide (with respect to its backbone) by smaller peptides is targeted, the introduction of protecting groups at the N- and C-terminus is a useful approach. The protection groups help to get rid of edge effects due to the N- and C-terminus, especially with regard to the bottom-up approach of gas phase spectroscopy. Thus, the resulting protected or capped peptides can be considered as suitable model systems for extracts of larger polypeptide chains and their structural preferences. In many gas phase spectroscopic investigations, the acetyl group (Ac) is the preferred protection for the N-terminus, while the C-terminus is frequently esterified or amidated (also cf. Section 3). The hydroxyl group of the tyrosine residue can also be protected with a methyl group. These caps at the termini do not only reduce the 'undesired' formation of inter- and intramolecular H-bonds, but they also introduce additional amide bonds elongating the peptide backbone (e.g. Ac-Val-Tyr(Me)-NHMe is a dipeptide but can also denoted as tripeptide model¹⁰²). Beyond, certain protection groups like the Z-group (also abbrev. by Cbz, denoted as benzyloxycarbonyl or carbobenzyloxy) introduce a UV chromophore required for R2PI (resonant 2 photon ionization) or laser induced fluorescence (LIF)-based spectroscopic methods (cf. Section 4) when no aromatic side chain is available in the peptide sequence (cf. e.g.^{61,74,103}).

Isomers and conformers

The flexibility of the peptide backbone chain leads to a variety of possible conformers, which can formally interconvert by rotations around single bonds (here of the α -C-atom). In the context of monomeric amino acids and peptides investigated in molecular beam experiments, the discrimination between these conformers is a decisive issue. Nevertheless, in a peptide aggregate, not only the different possible conformers of the peptide backbone but also the different binding sites for an aggregation partner (e.g. another peptide, cf. Section 12, or a solvent molecule, cf. Section 11) must be taken into account, increasing the numbers of possible structures. Structures of a specific peptide aggregate differing in the binding sites for the aggregation partner should be denoted with the more general term 'isomer'. The spectroscopic methods addressed in Section 4 can be isomer- and conformer-selective.

3. Amino acids and peptides in the gas phase: several decades of investigations

Gas phase spectroscopy provides such a detailed level of information that much can be learnt from what could be seen as simplistic systems. This is why, at the beginning of the road towards polypeptide investigations, the peptide bond itself received much attention. Indeed, formamide,^{38,104} N-alkyl-formamides,^{38,105-114} alkylacetamides,¹¹⁵ N-alkylacetamides^{38,116} and other derivatives¹¹⁷⁻¹¹⁹ served as model molecules to address several basic issues: the cis-trans isomerization of the peptide bond,^{105,110,116,120} its hydration sites,^{104,106-109,111,113-115,117-119} the aggregation of peptide motifs^{38,109,115} or simply the knowledge of spectroscopic benchmarks such as vibrational modes^{38,109} or rotational constants.^{110,112,116,120} These model systems are still used to improve benchmarks,³¹ increase knowledge on peptide bond hydration¹²¹ or aggregation,¹²² explore new spectral domains¹²³ or develop new techniques.¹²⁴

Uncapped amino acids were among the first targets of gas phase investigations by spectroscopic techniques. However, while a terminal carboxylic acid and an amino group characterize their ground electronic state in the gas phase, these ends are charged in aqueous solution, forming a zwitterionic state made of a carboxylate and an ammonium group. Despite this difference between gas and solution phases, isolated amino acids present a rich conformational landscape of general interest. The most simple amino acids, starting by glycine,^{125,126} were first investigated by microwave spectroscopy. As this technique is particularly well suited for systems of this size, numerous studies followed.⁴³ Beyond the benchmarking aspect of this work on amino acids, several side-chain issues, such as the alkyl chain conformations of valine,¹²⁷ isoleucine¹²⁸ and leucine,⁴⁶ or histidine tautomerism¹²⁹ were conveniently addressed. In contrast, optical spectroscopy, i.e. UV and IR spectroscopy,

was perfectly adapted (cf. Section 6), but also often limited (cf. Section 4.2), to study amino acids containing UV chromophores such as tryptophan,¹³⁰ phenylalanine,¹³¹ or tyrosine.¹³² However, their conformational distribution being governed by the -COOH and -NH₂ ends, which are of limited biological relevance, amino acids were not the best models to address biological issues, and alternative systems were considered.

In this context, amino acid derivatives were designed with the aim i) to avoid the non-zwitterionic ends specific to gas phase studies, ii) to avoid non-covalent interactions involving these end groups, iii) to create peptide bonds at either side of the amino acid and make the backbone chain longer in order to mimic the environment found in longer peptide chains or proteins, and thus have a better model to address residue-related issues. Acetyl (Ac) or carbobenzyloxy (Cbz or Z) caps on the N-terminus side, and primary (-CO-NH-Me) or secondary (-CO-NH₂) amides, methyl or benzyl esters (-CO-O-Me or -CO-O-Bn) on the C-terminus side were commonly used. The resulting capped amino acids allowed the characterization, for the first time, of isolated γ -turns and β -strands in tryptophan,¹³³ and β -sheets between phenylalanine derivatives.^{134,135} Analyzing archetypical biological structures with the accuracy of gas phase techniques became thus possible. These successes triggered numerous optical spectroscopy experiments (cf. Section 7), where shaping interactions at the residue scale were characterized, shedding light on the relationship between primary and secondary structures with an unprecedented level of detail.¹³⁶ Another benefit of capped amino acids is the possibility to have a UV chromophore already incorporated in the caps instead of the residues,¹³⁷ making any peptide sequence accessible to optical spectroscopic techniques (cf. Section 4.2), although undesired/biologically irrelevant folding might occur.¹⁰³ In turn, microwave investigations were historically limited by the rotation of the methyl groups typically used in the caps, but recent successes were reported on capped alanine, proline, serine and valine.^{49,50,138,139}

For sizes larger than amino acids, optical spectroscopy techniques (cf. Section 4) have proven to be the most efficient to characterize isomer/conformer landscapes. These larger systems offered the possibility to observe the first β -turns,¹⁴⁰ 3_{10} helices,¹⁴¹ β -hairpins,⁷² and several combinations of different types of secondary structures.^{142,143} Peptide folding in the gas phase often revealed rich conformational distributions which are ideal for rationalizing the dependence of the structure with the peptide sequence (cf. Sections 8 and 9). Peptide lengths up to tetrapeptides are commonly found in the literature. The characterization of an intramolecular salt bridge in a pentapeptide sequence containing ionic residues of opposite charges is also a noteworthy achievement illustrating the potential of this type of approach (cf. ¹⁴⁴ and Section 12). Larger molecules, like *e.g.* a capped hexapeptide sequence of the tau peptide involved in the Alzheimer's disease,¹⁴⁵ are occasionally reported, gramicidins being the largest (cyclopentadecapeptides) for which the IR and UV signatures were obtained¹⁴⁶ (cf. Section 12). However, two limitations rapidly appeared and are still relevant today: vaporization of large neutral systems is so challenging that neutral α -helices are still to be characterized, whereas their ionic counterparts produced by electrospray ionization were readily reported;¹⁴⁷ a complete structural characterization results from an interpretation of IR and UV spectra which relies on relatively advanced, and thus size-limited, theoretical methods (cf. Section 5). Furthermore, one must mention the recent progress of microwave spectroscopy techniques which can now target neutral dipeptides such as Gly-Gly.¹⁴⁸ An overview of this field can be found in reviews dedicated to microwave spectroscopy.⁴³ Optical spectroscopies are thus the focus of the rest of this review.

Non-standard peptides are perfectly suitable for gas phase investigations. One can cite the first studies on cyclopeptides⁶² and depsipeptides¹⁴⁹ (cf. Section 12), on β -^{150,151} or γ -¹⁵² peptides belonging to the class of foldamers (cf. Section 10), as well as on other rare or non-natural residues such as a methyl capped tyrosine Tyr(Me)¹⁰² (cf. Section 7), Aib¹⁵³ (cf. Section 9), homophenylalanine (hPhe)¹⁵⁴ and homotryptophan (hTrp)¹⁵⁵ (cf. Section 10), and selenocysteine¹⁵⁶ (cf. Section 8).

Non-covalent complexes offer also the possibility to investigate specific intermolecular interactions of a peptide or protein. Homogeneous peptide clusters are indeed ideal to characterize isolated β -sheets or focus on self-aggregation issues (cf. ¹⁵⁷, overview in ¹⁴³ and Section 12). Gas phase heterogeneous clusters provide also a unique way to investigate the interaction between a peptide and a particular molecule of the biological medium (cf. Sections 11 and 12). Interactions between peptides and solvent molecules were early investigated by vibrational spectroscopy in microsolvation experiments¹⁵⁸ where several solvent molecules can be added to a peptide one by one. Remarkably, once surrounded by several water molecules, an amino acid can eventually

be observed in its zwitterionic state typical of aqueous solutions.¹⁵⁹ The conformational changes induced by the successive addition of water molecules to a protected amino acid were analyzed¹⁶⁰ and for a dipeptide microsolvated by methanol molecules it was demonstrated that it may ultimately fold the same way as in solution.¹⁶¹ Gas phase non-covalent complexes are thus interesting models capable to reproduce a minimalist, but biologically-relevant environment around the peptide in order to address issues typical of the condensed phase (cf. Sections 11 and 12). In particular, aspects of molecular recognition, like binding sites or induced fit, can be uniquely documented by studying peptide-containing non-covalent complexes: interactions with ligands like sugars,¹⁶² aminopyrazoles,¹⁶³ or toluene¹⁶⁴ illustrate the potential of this approach. Complexes between neutral peptides and ions were also early targeted,¹⁶⁵ but being formed by electrospray, the related issues can be found in other reviews dedicated to biomolecular ions.¹⁶⁶

Finally, beyond the motivation of pure structural elucidation, the isomer/conformer-selectivity of the experimental optical techniques (cf. Section 4), gives the opportunity to investigate intrinsic molecular properties not only at the molecule level, but at the isomer/conformation level by disentangling their respective contribution to a given property. Several photophysical properties of aromatic residues have been rationalized this way. Early works analyzed the electronic absorption spectrum¹⁶⁷ or the dispersed fluorescence,¹⁶⁸ before other observables were used to document the first electronic excited states, such as their vibrational spectra¹⁶⁹ or their lifetimes.¹⁷⁰ Further experimental and theoretical works on neutral peptides followed,^{133,171-185} and are mentioned throughout this review, but more details can be found in another review dedicated to photophysical aspects.¹⁸⁶

4. Introduction to experimental methods

General methods for structure determination were already briefly addressed in the introductory section. The focus of our contribution and in particular of this section is on electronic and vibrational spectroscopy under the cooled isolated conditions of molecular beams; some aspects of spectroscopy in helium droplets will also be briefly addressed at the end of Section 4.2. In the following we will use the term 'conformer' where appropriate but also the more general term 'isomer', automatically including conformational isomerism (cf. Section 2.3).

Though electronic spectroscopy cannot directly probe molecular structure in general, the electronic excitation energy of a chromophore is nevertheless influenced by inter- and intramolecular interactions and is therefore expected to be sensitive to the structure (more details in Section 4.3). Beyond this, certain electronic molecular beam spectroscopic methods also allow to draw conclusions about the number of isomers present in the experiment (cf. Section 4.2). A much more direct structural probe is vibrational spectroscopy since the vibrational frequency of substance specific (functional) groups (for peptides e.g. NH and CO) is sensitively influenced by binding relations like H-bonds or interactions with π -systems (more details in Section 4.3 and 6). Molecular vibrations can be directly excited, which is the task of IR spectroscopic techniques, or indirectly by Raman or SEP (stimulated emission pumping) processes (cf. Section 4.2).

As mentioned in the introduction, FTIR (cf. e.g.^{30,31,36-41}) and Raman (cf. e.g.³⁰⁻³⁵) spectroscopic techniques have been used to characterize amino acids and peptides in gas cells (cf. e.g.³⁵⁻³⁷) and jet expansions (cf. e.g.^{30-35,38-41}). Apart from that, combined IR/UV laser spectroscopic investigations in molecular beams are nowadays established experimental methods to analyze intrinsic structural behaviour and reactivity of isolated molecules, molecular aggregates or ions in the gas phase. The sample concentration in molecular beams is low so that the absorbance of light is difficult to detect; instead, the effects of light-molecule interaction like fluorescence or ionization (cf. Section 4.2) are detected, so that these spectroscopic methods are also denoted as action spectroscopy. Except for a few applications (cf. e.g.^{187,188}) most of the spectroscopy is performed with ns-laser systems having a pulse width around 10 ns, which defines the temporal resolution. In the context of this review, we can only give a short overview on a selected number of combined IR/UV methods covering the investigations on neutral peptide molecules or peptide containing aggregates in molecular beam experiments. For more references and details on action spectroscopy, the reader can also refer to the reviews^{142,143,189,190}.

Though spectroscopic measurements can give a first idea about basic structural motifs in amino acids, peptides and their aggregates, a detailed structural analysis can only be performed in comparison to theoretical calculations (cf. Section 5), in which the spectroscopic data (UV excitation energies, IR and/or Raman vibrations) for different isomers or conformers of a defined system are calculated (details cf. Section 4.3).

4.1 Molecular Beams

Generally, molecular beams¹⁹¹ are generated by expanding a sample-containing carrier gas (frequently monoatomic, inert gases like helium, neon or argon) from a high-pressure vessel via a nozzle (a pulsed valve) into vacuum. (In the following we refer to the high pressure region as being located 'before' the nozzle whereas the low pressure region is located 'after' or 'behind' the nozzle). The spectroscopic investigations we refer to in this article are mainly performed in supersonic beams, which are formed if the diameter d of the nozzle orifice is larger than the mean free path λ in the high-pressure region, where the (inelastic) collision frequency directly behind the nozzle is high, leading to an effective energy transfer from the sample molecules to the carrier gas. As a consequence, internal energy of the sample molecule is abstracted from the internal degrees of freedom leading to an energy distribution that can be described by the following temperatures: T_{trans} (which can drop below 1 K^{192,193}) $< T_{\text{rot}}$ (which can be reduced down to a few Kelvin¹⁹³⁻¹⁹⁵) $\ll T_{\text{vib}}$ (which is, in larger molecules, of the order of a few tens of Kelvin^{190,192,196}). Beyond this cooling effect, the disordered molecular movement is transferred into a directed mass flux. Both effects lead to a narrowing of the velocity distribution. Behind the nozzle, the particles of the beam already fly in a collision-free regime ('isolated') at distances as large as a few nozzle diameters (e.g. 500 μm orifice).

Without going into details for individual systems, most molecular beam apparatuses consist of a differentially pumped system, in which the first chamber is the source chamber. In the second chamber (separated from the first one by a skimmer to cut off the turbulent flanks of the beam) the IR and UV lasers interact with the isolated sample molecules in the collision free region. In photoionization-based methods the (UV laser generated) ions are accelerated by high voltages (e.g. of a Wiley-McLaren arrangement¹⁹⁷) into a time-of-flight mass spectrometer (TOF, occasionally denoted as third chamber). It can either be a linear (schematic illustration cf.¹⁴³) or a reflectron arrangement (schematic illustration cf.¹⁴³, for more details on Re-TOFs cf. e.g.¹⁹⁸⁻²⁰¹). The mass-selected ions are detected on e.g. a microchannel plate detector, amplified and analyzed by an oscilloscope and specialized software. In LIF-based spectroscopies, apparatuses are slightly less demanding: normally one vacuum chamber containing the sample supply and the pulsed valve are used. The formed molecular beam is crossed perpendicularly by the excitation laser and the fluorescence is collimated and measured perpendicular to the excitation light by either a photomultiplier or a CCD camera (cf. e.g.²⁰²). Most molecular beam experiments are normally operated in a pulsed mode (e.g. 10 Hz) with e.g. the pulsed valve serving as master trigger.

In the source chamber, the sample molecules are brought into the carrier gas by thermal evaporation or by laser desorption. For thermal evaporation the carrier gas can be guided over the heated sample (cf. e.g.^{134,158,203,204}) and temperatures up to about 200 °C can be used depending on the pulsed valve. Occasionally, arrangements are used in which the sample is not located in the high pressure region but in front of (= behind) the valve and is thus connected to the vacuum of the source chamber (cf. e.g.²⁰⁵). In a similar arrangement, a heatable brass block with a cylinder channel in which the carrier gas expands is fixed in front of the valve; the sample solution is sprayed by a capillary into the expansion channel, so that, after evaporation of the solvent, the sample is deposited on the channel walls and can be picked up by the carrier gas, making the vaporization of thermally fragile molecules possible¹³⁰. In a further elaborate set-up for thermally fragile substances, the sample molecules form nanoparticles in an aerosol; the aerosol beam is guided into the vacuum of a TOF mass spectrometer where the biomolecules are thermally vaporized by passing a thermodesorber (e.g. a heatable tip) inserted between the optics of the TOF (cf. e.g.^{206,207}) where they are photoionized. An advantage of thermal sources is the generation of a quite constant sample concentration supporting the measurement of spectra with a good signal to noise ratio (cf. spectroscopic methods Section 4.2). Alternatively, laser desorption sources are available to bring larger or unprotected peptides into the gas phase, which have a tendency to decompose via CO₂ elimination. In this technique, the sample is mixed with a matrix substance (e.g.^{83,194,208-219}), which can for example be graphite-based (e.g.^{194,214-216,218,219}), based on carbon black powder,⁸³ or, in former

times, a dye as matrix (e.g. ^{211,212}). This matrix absorbs the laser energy (e.g. in case of graphite, the fundamental or second harmonic of a Nd:YAG laser, with frequently nanosecond or sometimes picosecond pulse width²²⁰), leading to a fast evaporation of the sample molecules before they are cooled down in the beam. The sample-matrix mixture is often coated on a rotating rod, disc or translating bar (e.g. ^{83,194,214-216,218}) directly placed behind the nozzle, so that the sample volume can be exchanged during the measurement.

If the aggregation behaviour should be investigated, the aggregation partners are coexpanded so that the cluster formation occurs during molecular beam expansion. In case of a thermal evaporation source, individually heatable sample chambers each containing one aggregation partner can be advantageous (cf. e.g. ^{143,163}). Otherwise, if one of the aggregation partners is liquid at room temperature (e.g. water), the carrier gas can be enriched with this component by guiding it over an (optionally cooled) reservoir. This carrier gas enriched with the first aggregation partner can afterwards enter a heated sample chamber (cf. e.g. ^{160,204,221}), taking up the second aggregation partner before being expanded into the vacuum. For laser desorption sources, both solid components can be mixed with the matrix and codesorbed²¹⁸. If one partner is volatile, the carrier gas can be enriched as described previously, and expanded via a pulsed valve directly crossing the region of laser desorption, in which the second component is evaporated (cf. e.g. ^{159,222}). Alternatively, also liquid components can occasionally be laser-desorbed by mixing them with matrix substance and a further solid component (cf. e.g. ²¹⁹). The formation of aggregates is a delicate process depending for example on the stagnation pressure and the kind of carrier gas both correlating with its ability to abstract internal energy by inelastic collisions from the monomeric aggregation partners before clustering (occurring in the warm part of the molecular beam) but also afterwards. A further aspect is the molar ratio between aggregation partners in the carrier gas (also indirectly effected by the stagnation pressure and the vapour pressure of the involved substances). How such factors influence aggregation depends specifically on each individual system.

After this brief overview, the question about advantages of spectroscopy in supersonic beams arises: on the one hand, isolated molecular systems and thus their intrinsic properties can be investigated without the influence of a bulk environment. On the other hand, it offers the possibility to successively add further aggregation partners like solvent molecules so that structural changes during a stepwise formation of an environment can be traced. The cooling of the internal degrees of freedom, the associated narrowing of the velocity distribution in the jet as well as the performance of the spectroscopy perpendicular to the beam effects a better interpretability of the data due to less congested spectra (few or no hot bands, reduction of Doppler broadening, inhibition of cluster dissociation on lower mass traces).

Beyond the issue of the internal energy distribution among the several degrees of freedom of the molecules, however, the flexibility of amino acids and peptides (cf. Section 2) endows these species with a more or less complex potential energy surface (conformational landscape), characterized by a vast number of minima (conformations). These minima are often organized in basins or families of conformations, inside which interconversions are facilitated by relatively low barriers as compared to more energy demanding isomerizations between different basins (Figure 5).^{133,223} An important task is therefore to identify those conformations that can be observed in the supersonic expansion.

The initial population of the conformational minima can be estimated from the temperature at which the sample is initially brought into gas phase in the experiment. In a thermal evaporative process where the reference temperature is well defined (typically in the 400-500 K range), one can assume a Boltzmann equilibrium distribution (taking Gibbs energies and thus entropy effects into account). In case of laser desorption, the description using a Boltzmann distribution is much more questionable given the pulsed character of the heating (tens of ns), but rather high initial internal temperatures (~350-500 K) are reported,²¹³ suggesting that in both cases the conformational memory of the solid peptide sample is lost. This is confirmed by recent studies on laser desorbed synthetic peptides, where both solid structure and gas phase structures subsequent to laser desorption were determined and found to be very different.²²⁴

Then, the question remains in how far this high temperature conformational distribution is conserved during the supersonic cooling process. Generally speaking, the number of conformers that one eventually observes results from a competition between i) the cooling rate in the supersonic expansion, which depends upon the carrier gas and of its ability to take away molecular internal energy during the collisions and ii) the

isomerization rate between the conformers initially populated, which will mainly depend upon the height of the barriers, which separate them, and the initial internal energy of the molecules.

Owing to the range of initial temperatures achieved (350-500 K), fast interconversions are expected to take place in the early expansion (Figure 5). In the hypothesis of an ideal, infinitely slow, adiabatic cooling, the conformational distribution would always be described by a Boltzmann distribution at any temperature achieved by the cooling process. Additionally, if the slow cooling process would be long enough to achieve low final temperatures, it would lead to a complete conformational relaxation characterized by the exclusive observation of the most stable conformer. The co-existence of multiple conformers at the end of the expansion comes from the relatively fast cooling rate (typically several 10 K/ μ s in an expansion), which causes a drastic drop in the isomerization rate, leading to the kinetic trapping of conformers that belong to isolated basins. A slower cooling rate would have enabled a relaxation to the conformer of lowest energy.^{133,190,225,226}

Of course, within the isolated basins, the same picture still holds. The barriers within such a conformational family being much lower than the inter-basin barriers, interconversion can take place for a longer time along the expansion, so that an efficient conformational relaxation can occur (Figure 5), eventually funneling the population of the basin down to its lowest energy form (at a low temperature). Experimental data suggest that barriers as low as ca. 4 kJ mol⁻¹ can easily be crossed over in the expansion, whatever the carrier gas is.²²⁷ Conversely, much higher barriers will be crossed only very early in the expansion.

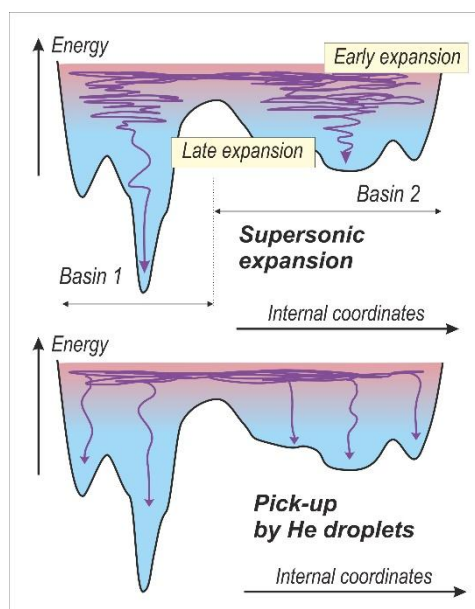


Figure 5: Scheme of the conformational dynamics during the cooling process. Top panel: case of comparable cooling and isomerization rates (e.g. supersonic expansion). Isomerizations take place in the early expansion, with conformer population described by a high temperature. As the expansion develops, the cooling rate becomes slow and the isomerization rate between basins of different conformational families decreases (kinetic trapping) but conformational relaxation keeps going on into the local basins of a conformer family (in case of an efficient argon expansion). Bottom panel: Case of a much faster cooling rate than isomerization rate (case of an ideally fast collisional trapping in He droplets). The cooling rate is so fast that the initial conformational distribution is preserved.

From this picture, the relative populations of the conformational basins taken two by two are expected to be roughly described by an apparent conformational temperature T_{conf} which can be viewed at the last range of temperatures along the expansion for which the interconversion time between the basins considered was still comparable to the characteristic time scale of the supersonic expansion, i.e. typically the μ s range. In this case, assuming that each basin is dominated by a single form, the population ratio observed is expected to match that predicted from the relative free enthalpy of these two forms at T_{conf} . In practice, T_{conf} is intermediate between the initial temperatures discussed above and the early expansion temperature ($\frac{1}{4} T_0$ at nozzle, where T_0 is the reservoir temperature, yielding ~ 350 K for thermal evaporation and 225 K for a room temperature reservoir). 300 K is thus a fair estimate of T_{conf} , and Gibbs energies (free enthalpies at 300 K) are considered to characterize population ratios.^{72,73,103,133,142,228} Owing to this, conformers higher than the global minimum by up to 10 kJ·mol⁻¹ at a high temperature (~ 300 K) are expected to be observed in molecular beam experiments,¹⁴² provided that the interconversion barrier with the minimum is large enough, typically higher than 10 kJ·mol⁻¹.^{190,225,226}

This property is especially interesting for two reasons. First, the conformational population observed in the expansions, which turns out to correspond to a finite temperature (in the 300 K range), is much more relevant

to biological conditions than one could suspect from the extreme cooling eventually achieved in a supersonic expansion. Second, it makes possible the observation of intrinsically unstable (high energy at 0 K) forms provided that they are entropically favoured, for example due to the presence of a loose backbone, such as the extended β -strand forms of peptides.⁷⁵

While the barrier heights between different conformers modulate the isomerization rate, the efficiency of the energy transfer during the collision of the molecule with the carrier gas (and thus the nature of the carrier gas, cf. e.g.^{142,190,219,229}) also plays a decisive role on the cooling rate. The conformational relaxation efficiency increases with the mass of carrier gas collision partner, with helium having the lowest cooling efficiency.²²⁷ The nature of the carrier gas is thus a critical parameter able to tune the degree of complexity of the isomerizational distribution of the systems investigated: whereas argon expansions usually give rise to a limited number of conformers, additional less stable forms can be revealed in He or Ne expansions (cf. e.g.^{142,190}). The choice of the carrier gas is thus intimately linked to the aim of the experiment (investigation of a specific conformer vs. documentation of the potential energy landscape)

Against this background of questioning isomer distributions and isomerization experiments in molecular beams, Zwier and coworkers introduced the population transfer methods, which will be described in Section 4.2.

Beyond molecular beam expansions, cold isolated conditions for spectroscopy can also be generated in helium droplets (e.g.²³⁰⁻²⁴²); some specific aspects are briefly addressed at the end of Section 4.2. In this case, however, the molecules of interest are captured by helium droplets in a collisional trapping process (pick-up). The sudden contact of the hot molecules with the superfluid medium enables a very strong cooling rate, which is thought to greatly inhibit isomerization during the process. In these experiments, the conformational temperature in the droplets is assumed to be determined by the temperature of the pick-up cell, since the following cooling process is thought to be so fast that it freezes the conformer distribution (bottom picture in Figure 5). The measurement of the relative abundances of two conformers in a small peptide,²⁴¹ which was shown to depend on the gas cell temperature on a wide temperature range (400-600 K), corroborates such a picture. A slow cooling process internal to the droplets would still allow isomerization barrier crossing so that the conformational distribution would be independent from the (cell) gas temperature. Such a behavior was not observed. Nevertheless, it should be noted that in some instances, conformer distributions of the Trp and Tyr aromatic amino acids in He droplets and expansions could be compared²³¹: the He droplet distribution was found to be narrower, with a limited number of conformations observed, suggesting that the simple freezing picture could be questioned in such large polyatomic systems.

4.2. Spectroscopic techniques in molecular beams

4.2.1 R2PI

The R2PI (resonant 2 photon ionization) spectroscopy (cf. e.g.¹⁶⁷), also occasionally denoted with the simplified term UV spectroscopy in the following sections, represents a method to obtain information on neutral systems in their electronically excited state: In a first step, the neutral species is excited by an UV photon into the electronically excited state (frequently the S_1), from which it is afterwards ionized by a second UV photon (cf. Figure 6). Since this process is only efficient if vibrational levels of the S_n states are resonantly excited, the R2PI method is often also denoted as resonance-enhanced multiphoton ionization (REMPI). Afterwards, the singly-charged ions are detected in a time-of-flight mass spectrometer (TOF), leading to the mass selectivity of this method. Depending on the energetic gaps between S_0 and S_n and S_n and D_0 , the UV photon can either be of the same (one colour (1 + 1) process) or of different energies (two colour (1 + 1') process). The latter one has the advantage that the excess energy and thus fragmentation can be minimized, especially in the case of clusters. For this purpose the ionization energy can in principle be estimated by theory or experiments (ion current curves, e.g. cf.²⁴³, PFI-ZEKE (Pulsed Field Ionization–Zero Kinetic Energy, cf. e.g.²⁴⁴⁻²⁴⁶) or MATI (Mass Analyzed Threshold Ionization) cf. e.g.^{247,248}) spectroscopy). Nevertheless, due to their efficient one-color R2PI process, these experimental techniques do not turn out to be necessary for peptides.

To obtain electronic excitation energies, an R2PI spectrum is measured by recording the ion yield when scanning the UV photon energy. In case of a single isomer, the intensity of the vibronic transitions in the R2PI spectrum depends (for an electronically allowed transition) on the Franck-Condon (abbr. FC) factors. This factor decreases for higher energetic modes, in particular the structure-sensitive (stretching modes) modes like CO-, NH- and OH-modes, which can seldom be directly analyzed from the R2PI spectrum. For this purpose, other methods, such as UV/IR/UV (cf. subsection about IR spectroscopy) are available. Another possibility for the observation of several R2PI transitions in the mass-selected R2PI spectra is the presence of several isomers, which are all successively excited and ionized during a wavelength scan. In case their contributions to the electronic spectrum overlap, several isomers can be excited and ionized for a given wavelength, so that the R2PI process is not isomer-selective, requiring alternative methods (see below). Nevertheless, isomer selection can be achieved if there is no or limited overlap between the electronic signature of each isomer: an excitation laser frequency fixed to an isomer specific transition will generate a R2PI ion signal from the vibrationless level of a single isomer. This is the basis for the isomer-selective IR spectroscopic techniques presented below.

An alternative to R2PI for visualizing the excitation into vibronic levels is the detection of the integral fluorescence (LIF: laser induced fluorescence, e.g. ¹³², cf. Figure 6). Despite the less sophisticated experimental set-up (cf. Section 4.1), which only requires a single UV laser, the main disadvantage of LIF is the lack of mass selectivity. This is especially true if combined with laser desorption sources often producing undesired species. (LIF should not be mixed up with dispersed fluorescence (DF) in which the emitted light is spectrally split into its wavelength contributions and from which information on ground state vibrational levels can be obtained; for early DF investigations on amino acids cf. e.g. ¹⁶⁸).

Both methods (R2PI and LIF) require an efficient chromophore, e.g. an aromatic system as found in the side chains of the amino acids Phe, Tyr and Trp. If none of those amino acid is in the sequence, UV chromophores can be introduced in the protection groups at the N- or C-terminus (cf. Section 2.3) like the Z-group (benzyloxy) at the N-terminus (cf. e.g. ^{61,74,78,137,153,249}) or at the C-terminus O-benzyl (cf. e.g. ¹⁰³) or NH-benzyl (cf. e.g. ^{77,79,162,250}). A further possibility are non-covalently bound UV chromophores acting as aggregation partners (cf. e.g. ¹⁶⁴). In case of peptide aggregates, only one of the non-covalently binding partners needs to carry such a chromophore (cf. mixed peptide dimers¹⁴³ in Section 12). For amino acid and peptides deprived from an aromatic UV chromophore, VUV photoionization with ion^{124,206,251-258} or photoelectron detection²⁵⁹⁻²⁶¹ have been applied (non-resonant multiphoton ionization, e.g. with a 800 nm pulse^{188,262,263}, is another solution although not used for peptides or amino acids yet).

Beyond the excitation energy, also the lifetime of the excited state is of relevance since the R2PI based methods are mainly performed with lasers having pulse half widths of several ns, requiring lifetimes in that regime or slightly below. Since the lifetime can be isomer-dependent the pitfall can occur that certain isomers are not detected in the measurements, as this was already the case for DNA bases^{264,265}. In case of amino acids and peptides, with the side chains of Phe, Tyr and Trp as the most important UV chromophores, experiments imply that isomer-dependent lifetimes of the relevant first $\pi\pi^*$ state are in a range making ns-excitation and ionization possible (cf. e.g. for Phe ^{173,174}). The suspicion that theoretically predicted conformers were not found in the experiment due to a sub ns excited state lifetime remain rare: they have been evoked only for some Trp and Phe containing uncapped peptides (cf. e.g. ^{177,266,267}).

With regard to LIF or REMPI spectroscopy combined with a laser desorption source, pioneering work was performed by Levy and coworkers^{130,211,212} in which amino acids up to tripeptide species were analyzed ²¹¹. Despite this pioneering spectroscopic work, main drawbacks were: (1) LIF and R2PI only offered excess to low (structurally often less relevant) vibrational levels in the S_1 state and no vibrational information of the electronic ground state could be obtained. (2) A discrimination between isomers was not easily possible (except for power dependent measurements cf. e.g. ^{132,167} and Section 4.3). (3) A comparison with reliable calculations was missing since sufficient computer power was not available in the 1980s. The development of double resonance spectroscopic methods as well as the increasing computational power allowed the first structural assignments for amino acid model systems, amino acids and peptides in the late 1990s (cf. Sections 6 and 7).

4.2.2 UV/UV hole burning

Since the R2PI spectrum via one mass trace is not necessarily isomer-selective, additional so-called hole burning or double resonance methods based on a pump-probe principle were developed (e.g. UV/UV and IR/R2PI, for latter see section below) to correlate the observed electronic transitions with the corresponding isomer species. In the UV/UV method, the UV probe laser is tuned to an electronic transition of the originally measured R2PI spectrum to generate a constant ion signal (for amino acids and peptides in most of the cases via a (1+1) R2PI process). Prior to this, the wavelength-scanned UV pump laser excites the sample and each time a resonance is excited belonging to the probed isomer, the constant ion signal is depleted since, figuratively spoken, the wavelength-tuned pump laser has burnt a hole into the population of the corresponding isomer. The term double resonance spectroscopy arises from the fact that both lasers must be in resonance. By this, the UV/UV spectrum allows to identify the contribution of the probed isomer to the UV (=R2PI) spectrum. The repetition of UV/UV measurements via different UV transitions and the comparison between both spectra finally enables to reveal the different isomer contributions to the UV spectrum, however, without any hint about structural assignment.

It is worth noting that both spatially overlapped pump and probe lasers are fired within 100 – 300 ns and generate an ion signal of the same mass but with different temporal origin, requiring a TOF mass spectrometer with a sufficient temporal resolution. For the UV/UV measurements the depletion effect is detected on the ion signal generated by the frequency fixed UV probe laser. The issue is still more critical when using a 1 + 1' R2PI probe process. As an alternative, the ions produced by the wavelength-tuned pump laser can be temporally discriminated using a transient high voltage pulse. (For application of UV/UV hole burning measurements to neutrals cf. e.g. ^{62,154,215,268-270}).

4.2.3 IR spectroscopy (IR/R2PI, UV/IR/UV)

To gain structural information, structure sensitive IR spectroscopy presents a powerful tool. For the electronic ground state (of a mass selected species) the IR/R2PI method (also denoted as IR/UV or even shorter as IR) is applied (cf. Figure 6), in which the UV excitation probe laser is set to a transition of the R2PI spectrum, generating a constant ion signal by the R2PI process. If a wavelength-tunable IR pump laser arrives prior to the R2PI process and resonantly excites a vibrational mode, the vibrational level of the ground state isomer probed is depopulated. Under isolated molecular beam conditions, the vibrational energy cannot be released into the environment but is redistributed by internal vibrational redistribution (IVR), preferentially among low vibrational modes. During this relaxation process, the molecule does not return into its original vibrational ground state and remains vibrationally hot, generally making the original R2PI process less efficient, since the UV spectrum of hot species is usually shifted relative to that of cold molecules. This leads to a depletion of the probe ion signal, justifying the alternative notation as IR/ion dip spectroscopy (cf. e.g. ^{271,272}).

In cases in which the R2PI process is isomer-selective, the IR/R2PI spectroscopy measures not only mass- but also isomer-selective IR spectra (for non-isomer selective R2PI process cf. subsection about IR/IR/R2PI). If the different isomer contributions to the UV spectrum are exactly known from UV/UV spectra, only a few IR/UV spectra need to be recorded; alternatively, the same information can be obtained by comparing the IR/UV spectrum obtain via the different UV transitions of the R2PI spectrum. When using the LIF process instead of R2PI the fluorescence is depleted if the molecule is vibrationally excited (IR/LIF or IR/FD with FD as abbr. for fluorescence dip).

For electronically excited states, an IR spectrum can also be measured by a variant of the IR/R2PI method. Here an IR laser is inserted between the two photons of a (1 + 1') R2PI probe process (UV/IR/UV, cf. Figure 6), which can lead to excitation of vibrational levels in the electronically excited state (cf. e.g. ^{75,273-277}, first application for a peptide ⁷⁵, FD dip based cf. e.g. ^{169,271,278,279}). The most frequent effect is again an ion yield decrease, though the depletion effect might be less in comparison to ground state effects in IR/R2PI due to a reduced photoionization efficiency. In rare cases however, the photoionization efficiency can increase after a vibrational excitation in the electronically excited state, leading to an enhancement of the ion signal. Requirements for such experiments are a sufficient lifetime to insert the wavelength-tuned IR laser and an optimization of the

two-colour R2PI process, which is necessary in case of amino acids and peptide systems, since for the Phe, Tyr and Trp chromophores the one-colour process dominates.

In case of amino acid and peptide systems, the mass-, isomer- and state-selective IR/R2PI spectroscopy represents an ideal tool to investigate the regions of structurally relevant vibrations. In general, the first applications of IR/R2PI were performed in the Lee group for CH-stretching modes²⁸⁰, followed by C-O-stretching vibrations by Brutschy and coworkers²⁸¹ and extended to OH-stretching vibrations by the groups of Mikami²⁸² and Zwier²⁸³. Later on, first measurements on amino acids and amino acid models followed in the groups of Simons²⁰⁵ and Mons¹¹¹, which were further extended to the C=O-stretching and NH-bending region by the Gerhards^{284,285} group and were finally extended in the region down to the far IR region in by Bakker et al.²⁸⁶. (Further literature regarding the different spectral regions can be found in Section 6).

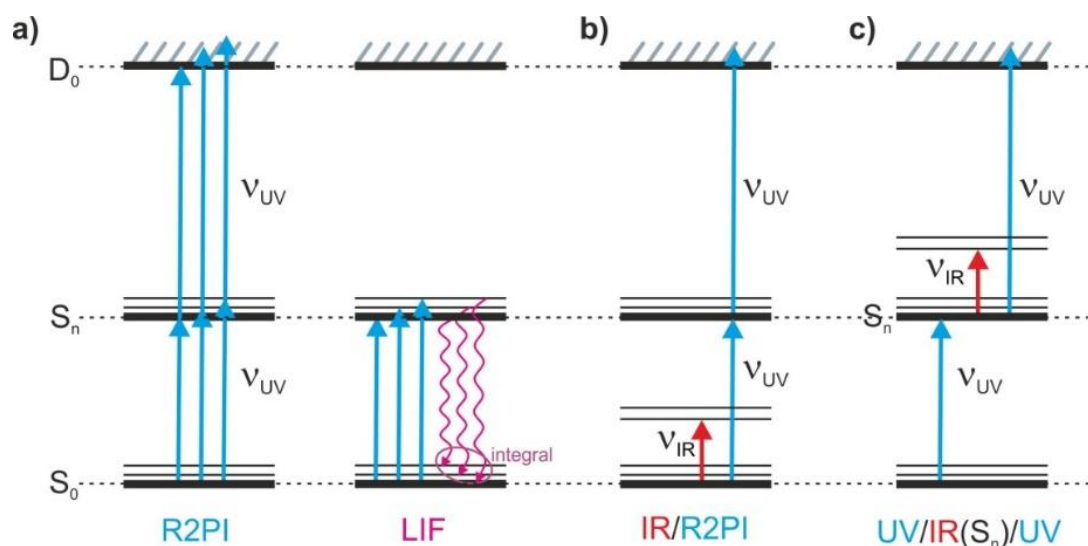


Figure 6: Schematic illustration of spectroscopic methods: a) R2PI and LIF (fluorescence magenta arrows), b) IR/R2PI for the S_0 state, c) UV/IR/UV for the S_n state. Bold lines present the zero-point vibrational levels of the corresponding electronic state, thin lines represent vibrational levels for the different modes of the molecule. In all figures, red arrows represent the IR photons, blue ones the UV photons and the arrangement of the arrows from the left to the right corresponds to the chronological sequence of lasers.

As also mentioned before, the effectiveness of ionization of the R2PI process strongly depends on the resonance of especially the exciting photon. This frequently missing resonance in the excited state of a (vibrationally) hot species is the main reason why an UV excitation from a vibrationally excited S_0 level in the IR/R2PI scheme is less effective, leading to the hole burning effect and the ion dip observed. Nevertheless, depending on the molecular systems, such a resonance can occur leading to an IR+UV effect and thus to an enhancement of the R2PI signal. Such an IR+UV process can also be forced by setting the sum energy of the exciting and ionizing UV photon(s) below the ionization threshold, so that no ion signal is generated. Then, only an excitation from a vibrationally excited level (sum IR+UV photon) exceeds the threshold, leading to ionization. Thus, this IR+UV method measures against a zero baseline, and the vibrational excitation as an increase/occurrence of an ion signal, which often makes this spectroscopy more sensitive than the IR/R2PI spectroscopy (cf. e.g. ²⁸⁷⁻²⁸⁹). A main reason for the lower sensitivity of the IR/R2PI compared to an IR+UV approach is the fluctuation in the R2PI signal. One reason is a fluctuating sample concentrations in the beam caused by the pulsed sources, with the desorption sources often generating less constant ion signals than the thermal sources. As additional reason long-term changes in the UV laser power must be taken into account. Compensation of the ion signal fluctuations can partly be achieved by increasing the averaging time. A possibility to further improve the stability of the base line is the application of difference measurements: This can be implemented in the experimental set-up by firing the IR laser at half the frequency of the UV laser(s) and a real time subtraction between the signal with and without the IR laser (cf. e.g. ^{61,83,290,291}). As alternative, a reference ion signal can be generated for subtraction by sending back the UV laser into the molecular beam downstream to the point in which IR and UV laser overlap (cf. e.g. ²⁹²).

4.2.4 IR/IR/R2PI

The isomer selectivity of the excitation in the R2PI process is a necessary requirement for the isomer-selectivity of the IR/R2PI method. Nevertheless, in larger systems, e.g. biomolecules in which the UV chromophores are far away from the regions of isomerizational or conformational diversity, or in photoreactive systems, overlapping UV transitions can occur. In such a case the R2PI process can excite and ionize more than one isomer. As a consequence, the IR/R2PI method loses its isomer selectivity and the IR spectra represent an overlay of the vibrations of different isomers. As a solution to this issue, IR/IR methods (cf. Figure 7) were established for the electronic ground state by Zwier and coworkers^{293,294}, and further applied in the Gerhards group^{277,295}. The latter introduced this method for the electronically excited state (cf. ^{277,295}) which was varied by the Fernández^{188,262} group.

The principle of the IR/IR methods for the S_0 state can be briefly described the following way: an IR/IR/R2PI spectrum is measured with a first IR laser frequency-fixed to a vibration of the originally measured IR/R2PI spectrum (for which an overlay of two isomers e.g. A and B is assumed). The frequency fixed IR laser excites the sample prior to the wavelength-tuned IR laser (IR_{fix}/IR_{scan}/R2PI scheme). If the IR burn laser (= IR_{fix}) is set to an isomer specific vibration, it only depopulates the vibrational ground state of the corresponding isomer (e.g. A). As a consequence, all the other vibrations of this isomer should also be influenced in the IR_{fix}/IR_{scan}/R2PI spectrum. In contrast, no effect on the vibrations of the remaining isomers (e.g. B) should be observable, i.e. the relative intensities of their IR bands in the IR/R2PI and IR/IR/R2PI spectrum should be the same. In short, the IR/IR methods present triple- and quadruple resonance methods (with one or two colour R2PI), which enable to recover the isomer-selectivity which is lost in an insufficiently selective R2PI probe process.

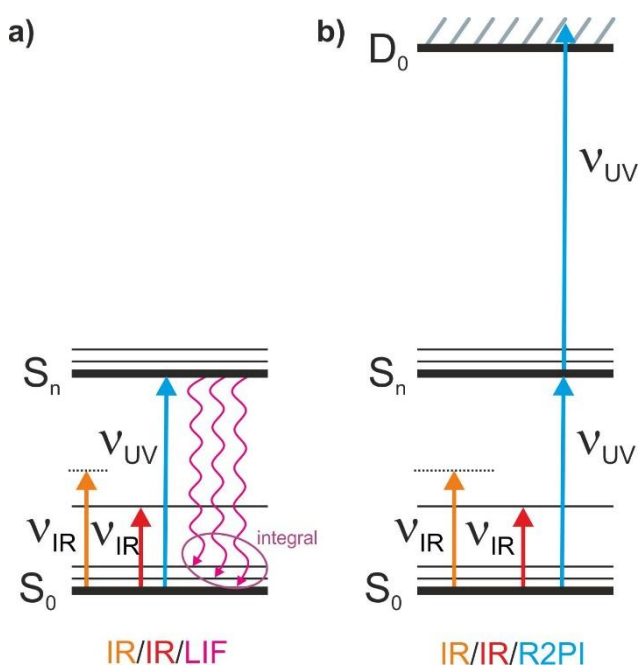


Figure 7: Schematic illustrations of IR/IR spectroscopic methods for the electronic ground state (details cf. ¹⁸⁹). The detection is either based on a) fluorescence or b) ionization. The orange arrows represent the frequency-fixed IR burn laser exciting one isomer, the red one the scanned IR-laser.

4.2.5 IR/VUV spectroscopy

The R2PI- and fluorescence-based measurements both require an efficient UV chromophore, like in the side chains of the amino acids Phe, Tyr or Trp. If this is not the case, alternative ionization methods can be applied (cf. Figure 8) either based on VUV^{124,206,251-261} or multiphoton fs-IR ionization^{188,262,263} (with the latter not further described here as not applied to amino acids or peptides yet).

For the single photon-based VUV method, the 118 nm radiation is frequently used, which is based on the tripling of the third harmonic of a Nd:YAG-laser (355 nm) in a noble gas as a nonlinear optical medium²⁵⁶. A variety of non-aromatic systems have ionization potentials around the corresponding energy of 10.5 eV and are thus accessible by IR/VUV methods. Those can be applied as hole burning or IR+VUV methods (cf. Figure 8). For the latter, the VUV photon is set below the ionization threshold so that only the sum energy of the vibrational excitation and the UV photon is enough to ionize the system and generate an ion signal. If further dissociation after ionization occurs, the increase of ion signal might have to be measured in the fragmentation channels instead of the parent mass channel. In comparison, the IR/VUV method can be analogous to the IR/R2PI method, measuring an ion dip spectrum via a parent mass, if the VUV photon energy exceeds the ionization energy of the parent molecule. If the VUV induces a fragmentation after ionization, a preceding IR excitation in the electronic ground state can either affect a depletion on these fragmentation channels or conversely enhance the fragment masses. The latter (depletion of the parent mass and enhancement of fragmentation channels) can especially be observed if a strong laser pulse induces IRMPD of the neutral species, so that the VUV processes ionizes (the remaining parent molecules) as well as the IRMPD-generated fragments^{124,257}.

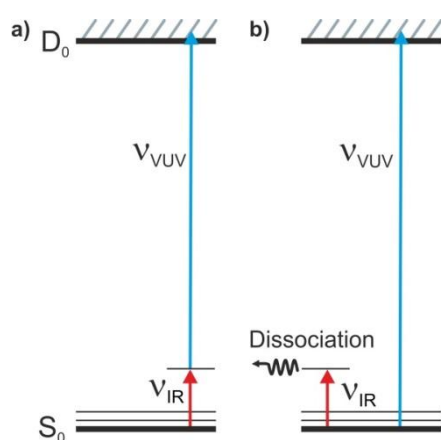


Figure 8: Spectroscopic methods not requiring a UV/VIS chromophore: a) IR+VUV techniques, b) IR/VUV.

4.2.6 Population transfer methods

Due to their high structural flexibility, peptides can adopt a variety of conformations and experimentally accessible isomers are frequently calculated with energy differences within a few kJ/mol. Thus, the experimentalist is often faced with the problem that, even in investigations on isolated cooled systems, more than one conformer is observed. Hence, the question about the conformer relative energies and distributions as well as the energy barriers for isomerisation between them arises.

Against this background, Zwier and coworkers established the hole filling (HFS) and population transfer spectroscopy (PTS) (cf. Figure 9). A detailed description is beyond the scope of this review, but reference should be given to^{113,203,296-300}. Both methods follow the same principle: in the 'warm' part of the molecular beam (i.e. at nozzle distances within a few nozzle diameters, where the collision rate is still significant), a well-defined vibration of a conformer known from IR/LIF measurements (e.g. an NH-stretching mode of a small peptide) is excited. If the vibrational excitation introduces enough additional internal energy, it is possible to exceed barriers for conformational isomerization. The population change induced by the vibrational excitation is then probed by a LIF process (difference measurements) in the cold part of the molecular beam.

The main difference between HFS and PTS is the wavelength tuning of the participating photons. In HFS, the vibrational excitation of one isomer in the warm part of the beam is frequency-fixed whereas the LIF laser is scanned in the collision-free region, giving a first idea of the population redistribution after a defined vibrational excitation. In the population transfer method, the vibrational excitation is wavelength-tuned whereas the UV laser is frequency-fixed to a conformer-specific electronic excitation, giving an idea about the effect of vibrational excitation onto the population of a specific conformer.

Different approaches exist depending on how this vibrational excitation is achieved. In the IR-HFS and IR-PTS,^{203,296,297,300} the IR laser is applied in the 'warm' part of the supersonic beam, whereas in case of the SEP

(stimulated emission pumping) methods^{113,298-300} a defined conformer is electronically excited and afterwards specifically stimulated back into defined vibrational levels of the ground state. In both cases, the PT methods offer the possibility for more quantitative analysis, with IR-PTS yielding fractional isomer populations or quantum yields,^{203,296,297,300} and SEP-PTS allowing conclusions about isomerization barriers^{298,300}. The latter is more suitable for estimations regarding isomerization barriers since, in comparison to a pure IR excitation, the SEP process can generate a larger variety of different vibrational states (in the S_0 state), offering access to a broader range of internal energies.

Another approach is the IR excitation of a selected species further probed by IR/R2PI (cf. Figure 7). The Gerhards group made use of this method in measurements on the 3-hydroxychromone water cluster²⁷⁷ and detected (in comparison with the original IR/R2PI spectrum) a new isomer originating from a rearrangement reaction of the 3-hydroxychromone water cluster, vibrationally excited by the first frequency-fixed IR laser. In the context of such IR_{fixed}/IR_{scan} measurements on a depsipeptide having three conformers,³⁰¹ the Gerhards group provided evidence for an IR induced-rearrangement between these conformations (cf. Section 12). As a last remark, it should be pointed out that comparable (IR-induced) population transfer methods for charged species were established by Rizzo and coworkers (cf. e.g.³⁰²).

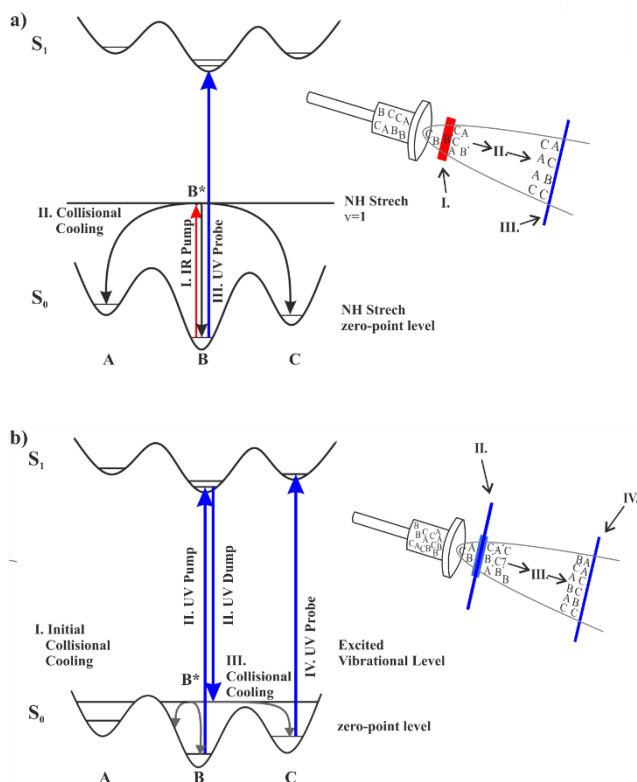


Figure 9: Generalized energy level diagrams for a) the IR-HFS and IR-PTS techniques as well as b) the SEP-HFS and SEP-PTS method. On the right side of each energy diagram, the principle spatial (and indirectly temporal) arrangement of the lasers is illustrated (redrawn from Ref.^{203,299}).

4.2.7 Some aspects of spectroscopy in cold helium droplets

Beyond molecular beam expansion, cold or even ultracold conditions can be achieved in superfluid helium droplets ($T = 0.37$ K in ^4He droplets, or 0.15 K in ^3He droplets),²³⁶ which, in comparison to other matrices, are known to have the weakest interactions with the embedded sample molecules.^{242,303} To perform spectroscopy, basically three kinds of detection methods exist: LIF^{230,231,235}, electron impact ionization combined with mass detection of the generated ions^{230-232,234,238} and detection of the helium beam intensity using a helium cooled bolometer^{230,236,237,241}. The detection of laser-induced fluorescence of course only works for electronic excitation. In contrast, the latter two detection methods are both based on the evaporation of helium as a

consequence of the photon energy absorption by the embedded molecule and the subsequent energy redistribution into the helium droplet environment. In the bolometer detection, a decrease of the helium beam intensity is detected, whereas for the EI method the droplet ionization cross section is reduced and thus the corresponding ion signal. A slight disadvantage of these (detection) methods is that they are not necessarily isomer- or conformer-selective so that e.g. in bolometer-based methods additional efforts are often required. For example, in bolometer-based methods, vibrational transition moment angle analyses can be performed, where discrimination occurs via polarization effects as a strong electric DC field is applied.^{237,241}

The ultracold conditions of superfluid He droplets were already applied to perform studies on UV excitations of amino acids like Trp, Tyr^{231,236}, protected amino acids like Ac-Trp-NH₂ or model systems like tryptamine^{233,236}. The EI detection scheme was also used to record the IR spectrum in the OH-stretching region for glycine²³² and its dimer²³⁴. Additionally, the N-acetylglycine methylamide dipeptide model was investigated by IR spectroscopic method to analyze its (gas phase) thermochemistry with regard to isomerizations between different conformers²⁴¹. A neutral system investigated in helium droplets even larger than the model dipeptide is the hetero dimer between histidine and tryptophan. Nevertheless, a detailed spectroscopic investigation is missing here and the aggregates were analyzed by EI giving hints on the structural arrangement.³⁰⁴ Meanwhile the embedding of charged proteins could be demonstrated,²³⁹ as well as their ejection from the droplet by UV/VIS light. In that context the hemin⁺ UV/VIS spectrum²⁴⁰ and the IR spectra of the leu-enkephalin and its 18-crown-6 complex could for example be measured³⁰⁵.

4.2.8. Laser systems

The spectroscopic methods explained above require light sources in the UV/VIS and IR regions. Without going into details, some laser systems should be briefly mentioned with further reference to literature. In most of the experiments, the wavelength tuneable UV radiation is generated from the frequency doubling of a dye laser output, which can be pumped by a Nd:YAG laser (cf. e.g.^{134,216,266,306} or an excimer laser (cf. e.g.²¹⁹). Typical absorption regions of the UV chromophore of Phe, Tyr and Trp, based on efficient π - π^* transitions are found between about 37,400 – 38,200, 35,300 – 37,000 and 34,500 – 35,000 cm⁻¹, respectively (cf. e.g.^{134,167,307,308}).

Regarding the generation of IR light, mainly table top laser systems and free electron lasers (FEL) must be distinguished. FEL lasers have some advantageous characteristics, e.g. a high average power and high peak power (cf. e.g.³⁰⁹⁻³¹¹), pulse durations from quasi continuous to sub-ps-range (cf. e.g.^{309,310}), repetition rates up into the kHz region (cf. e.g.³¹⁰). A typical frequency region can start around 10 cm⁻¹ (cf. e.g.³¹²) up to typically about 2000 cm⁻¹, and with much lower intensity partly also in the IR region up to about 3300 cm⁻¹ (cf. e.g.³¹⁰); in some FEL facilities the spectral range is further extended via the far IR region down to the THz region (cf. e.g.³¹³). The far IR region below approximately 800 cm⁻¹ still remains the domain of the FEL lasers, since this region cannot sufficiently be covered by table top lasers (see below). Though this region is not the standard region to be explored in context with peptides (cf. e.g.^{222,286,314-320}), it can reveal characteristic vibrational signatures as out-of-plane NH-bending or water modes in peptide hydrates (cf. e.g.^{222,318} and cf. Section 6.2). The decisive disadvantage of the FEL systems is the partly low spectral resolution usually ranging between 0.3% and 1%, especially for higher frequencies as the NH- or OH-stretching.

The successfully developed table top laser systems for the generation of IR light are based on the combination of different non-linear optical processes also depending on the spectral region to be covered: optical parametric oscillator (abbrev. OPO cf. e.g.³²¹⁻³²⁴) or difference frequency mixing (abbrev. DFG) between dye laser radiation and YAG fundamental, followed by OPA (optical parametric amplification) and eventually further DFG (cf. e.g.^{285,325}). The table top IR systems generate sufficient energy for IR/UV spectroscopic techniques in a spectral range, in which structurally important modes are present (OH-stretching, NH-stretching (amide A), CO-stretching (amide I), NH- and OH-bending (amide II and III), cf. Sections 6.1 and 6.2). The OPO systems are widely used also in context with spectroscopic peptide analysis (e.g.^{80,218,266,306}). In applications of the Gerhards group (cf. e.g.¹⁴³), it was demonstrated that dye laser/DFG based systems²⁸⁵ are robust light sources with high energy and high spectral resolution (for further details cf. ^{143,285} and for applications from other groups cf. e.g.^{162,270,326}).

4.3. Assignment strategy: principle and potential pitfalls

The above described combined IR/UV laser spectroscopic methods enable experimentalists to gather multidimensional spectroscopic data, whose interpretation requires a careful examination and a comparison with theory in order to derive consistent and convincing structural assignments.

4.3.1. UV spectroscopy

The mass selectivity of the above presented IR methods makes use of the electronic properties of UV chromophores of the amino acid side chains or protection groups via electronic excitation and ionization; the isomer selectivity is based on the isomer selective excitation of the UV chromophore. Thus, the electronic properties play a decisive role for the characteristics of the IR spectroscopic methods. In context with the spectroscopy of low frequencies modes by dispersed fluorescence (cf. e.g. ¹⁶⁸), electronic spectroscopy can partly be applied to draw conclusions for structural determinations. Since the electronic molecular spectroscopy is partly more easily accessible than IR spectroscopic techniques, which are always an at least double resonance method, the first reported molecular beam spectroscopic experiments on amino acids were based on LIF and REMPI spectroscopy (cf. e.g. ^{130,211,212}) as well as dispersed fluorescence (cf. e.g. ^{132,168}). The UV methods can help to reveal the number of conformers, e.g. by power dependent measurements (cf. e.g. ^{132,167}) or UV/UV hole burning experiments (cf. e.g. ^{214,215}). However, on the sole basis of UV spectroscopy, invaluable information can already be gained. UV chromophores, indeed, are sensitive to the structure of the molecule studied. First, cap chromophores (such as carboxybenzyl or benzylamide caps) may in principle provide such a structural information. Nevertheless, some specific aspects must be taken into account, in particular their poor sensitivity to backbone structural changes due to their remote location, and their manifold of rotamers. The conformational population is indeed spread among cap rotamers, which contribute to make absorption weaker and spectral congestion worse than already expected from the remote location of the chromophore. Experiments based on double-resonance techniques like IR/UV may be penalized by this situation. Conversely, chromophores embedded in the sequence are more prone to provide structural information, even if, as already mentioned earlier, they influence the structure, e.g. by forming π H-bonds. The series of origin electronic transitions collected over the years for aromatic residues³²⁷ provide useful guidelines to confirm assignments derived most of the time from IR spectroscopy. The sensitivity of electronic states to the structure became clear on the example of the L_a and L_b states of capped tryptophan (cf. e.g. ¹³³), where not only direct interactions (e.g. with NH amide groups) but also the electric field created by the electric dipole moments on the backbone contribute to shape the electronic spectrum. The sensitivity of the origin band position with the nature and the number of neighboring amino acids (cf. e.g. ^{142,328} and Figure 10) can also be used as an assignment guideline, as soon as the characteristic signatures of some secondary structure motifs have been recognized.¹⁴²

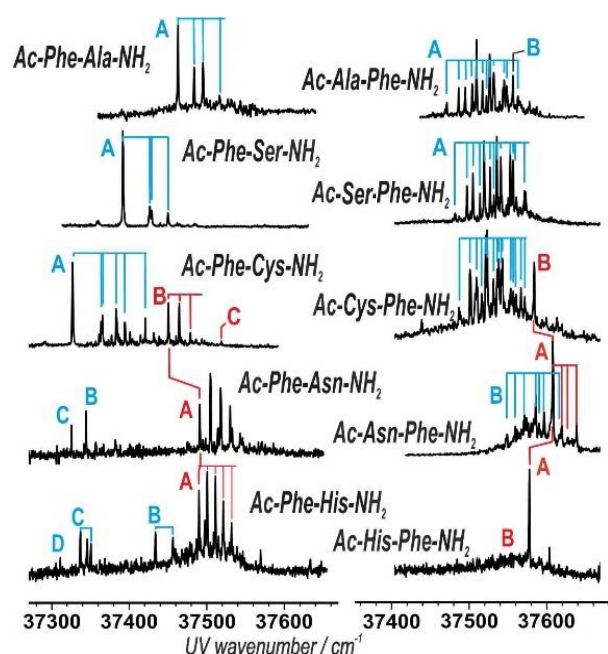


Figure 10: UV spectra of selected capped dipeptides previously studied,⁸⁰⁻⁸² interpreted in terms of conformational content (conformers labelled A-D, in decreasing population order) as obtained from IR/UV double resonance spectroscopy. The UV

bands assigned to β -turns (in red) appear in similar spectral ranges, due to comparable environments of the phenyl chromophore in these systems.

Beside the scalar nature of the electronic transition frequency, the Franck-Condon vibronic activity also brings complementary information about the geometry changes between ground and excited states. In the case of indole-containing peptides²⁶⁹ and the related molecule tryptamine³²⁹, the low frequency modes, through both their frequency and their dramatic FC progression, have been informative due to the large structural change in the indole L_b excited state. With the Phe residue, the FC activity is of lower intensity in general, but noticeable exceptions reveal significant geometry changes between ground and excited state due to interactions involving the phenyl ring of Phe with a neighboring extended residue, like another Phe²⁹², His⁸¹, or with another part of the molecule.⁷⁵ The very low frequency (<30 cm⁻¹) modes observed in the UV spectra are also potentially useful assignment tools, since this range depends upon the overall folding of the molecule. In this case, the ground state calculations can be taken as reasonable estimates of the excited state counterpart, and these low frequency modes can be used to distinguish among several conformational candidates,³³⁰ providing that the density of these modes remains low in the molecules considered (a few residue molecules). More rare is the use of the Franck-Condon activity intrinsic to the chromophore, but in a simple case such as Phe, the 6a/6b ring vibrations are found to be sensitive to the phenyl environment and hence the peptide structure.³³¹

4.3.2 IR spectroscopy

As already addressed in the introduction molecular vibrations can directly probe intra- and intermolecular interactions and can reveal information by their number, band position, band shape and relative intensities. The latter can allow to draw some conclusion on the isomer or conformer distribution found in the measurement (cf. e.g.²⁴¹ and Section 9), but often more sophisticated methods must be applied for this (cf. populations transfer methods in section 4.2). The significance of the individual IR spectroscopic regions for the structural determination of amino acids and peptides is further described in detail in Section 6, so that only basic aspects, including representative references and pioneering works, should be pointed out here. NH stretch oscillators are known to have a remarkable sensitivity for their environment and the associated interactions like H-bonds. Since they are frequently uncoupled from other NH groups, the number of measured NH stretching vibrations in the so-called amide A region can give first hints about the number of NH groups and thus about the isomer-selectivity of the measured IR spectrum. Beyond, the band position and line shapes can also give information about their involvement in an H-bond and, therefore, provide hints about the possible secondary structure motifs the system adopts. In addition to the NH stretching vibrations of the amide backbone, the physically coupled NH vibrations within a non-protected N-terminus (cf. e.g.²⁰⁵) or those in a NH₂ capped C-terminus can give further valuable structural hints (cf. e.g.^{60,136}). NH groups can further be found in side chains having very characteristic vibrational frequencies (like the indole NH in Trp, cf. e.g.¹³¹ or in histidine, cf. e.g.⁸¹), providing an indicator of involvement of the side chain in H-bonding (e.g.³³²). Further sensitive H-bonding indicators used for structural assignments are the OH stretching vibrations either of the carboxyl group of an unprotected C terminus (cf. e.g.²⁰⁵), of side chains (cf. e.g. serine⁸³), or of aggregates with water (cf. e.g.¹⁵⁸). Going further down in the frequency region, CH stretching vibrations follow. However, they are rarely used for structure determination of amino acids and peptides since band broadening and coupling effects often make an interpretability difficult (cf. e.g.¹³⁴). In comparison, CO stretching (around 1700 cm⁻¹), NH bending (around 1500 cm⁻¹) and CN stretching (around 1250 cm⁻¹), denoted as amide I, II and III regions respectively, provide much more specific probes, especially for the backbone structure (cf. e.g.^{134,222,286} and sections 6, 7). Nevertheless, the interpretation of this spectral region is slightly more complicated due to vibrational couplings and low bandwidth, which can be a problem if the spectral resolution is limited as in case of FEL systems. Despite this disadvantage, regions below 1000 cm⁻¹, including the far IR region (cf. section 6.2), remains the exclusive domain of FEL lasers with regard to the accessibility provided by IR/UV laser

spectroscopy. Throughout the last years, an increasing attention has been paid to this spectral region and the associated vibrational modes (e.g. collective backbone motions, cf. section 6.2). One should keep further in mind that these low frequency modes are also accessible via other spectroscopic methods like dispersed fluorescence (cf. e.g. ¹⁶⁸) or Raman (cf. e.g. ³²).

Finally, one can mention that the comparison between the electronic ground state IR/UV spectra and those after $\pi\text{-}\pi^*$ excitation of a UV side chain chromophore (UV/IR/UV) also provides an additional information. Resulting from such a $\pi\text{-}\pi^*$ labelling, only those NH groups which interact with the π system will have their frequency significant shifted in the excited state IR spectrum, compared to the ground state; this provides further support to the vibrational band assignment in the electronic ground state (cf. e.g. ³³³, ³³⁴). In some respect this can be compared to the deuteration strategy of NH groups, whose changes on UV spectra provide hints about the interaction between the substituted group and the UV chromophore (cf. supplementary information of ¹⁸¹).

4.3.3. Assignment

The structural assignment of the isomers, whose UV and IR signatures have been selectively recorded, stems from a close comparison of these experimental data with relevant spectroscopic-grade theoretical counterpart, in practice quantum chemistry calculations (cf. Section 5). The assignment is based on the ability of theoretical IR spectra, calculated for a set of low-energy forms, to best fit experimental spectra. This should be the case, in several spectral ranges when available, with an agreement usually considered as satisfactory when the individual frequency error remains below the 20 cm^{-1} range (cf. Section 5), as illustrated in Figure 11. Additional hints issued by UV spectroscopy features and excited state properties (cf. Sections 4.3.1, 4.3.2) are then often used to corroborate the IR-based assignment proposed.

However, one should mention that several issues potentially affect the assignment principle and should be accounted for.

- First, the final isomer distribution is of course reflected, to some extent, in the relative intensities in the electronic (R2PI) spectrum. However, the relative intensities resulting from the integration over the vibronic activities of each isomer remains only indicative since the intensity of electronic transitions also depends on the absorption and ionization cross section of each individual isomer (cf. e.g. ¹³³). In the worst cases, a too short excited lifetime might hamper or even forbid the detection, as already mentioned in section 4.2. The excited state lifetime, indeed, is a decisive aspect for the ns R2PI spectroscopy and can strongly depend on the isomer

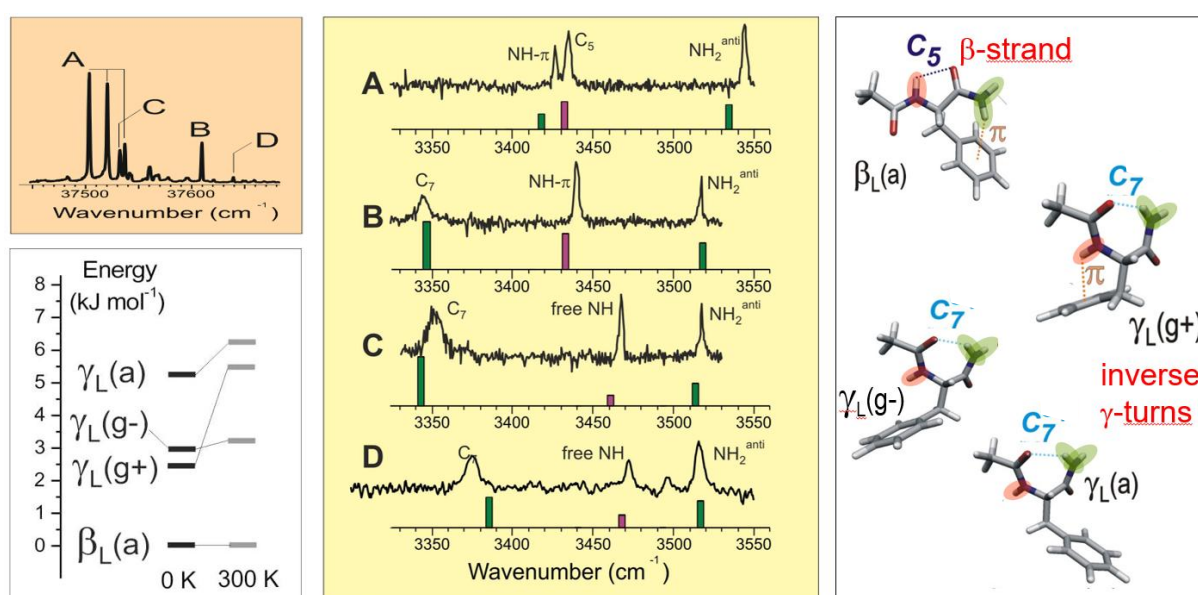


Figure 11: top left panel: UV spectroscopy of Ac-Phe-NH₂ in the origin region of the $\pi\pi^*$ transition of the phenyl chromophore; central: IR/UV spectra of the 4 conformers detected A-D; right and bottom left:

corresponding B97-D3/TZVPP structures and energetics, respectively. Band assignment is color-coded (central and right panel).

(cf. e.g. Phe¹⁷⁴, capped Phe¹⁸¹, Tyr²⁷⁰). Note that fluorescence-based detection is affected by the same drawbacks. Such a failure would result in a 'missing conformer' in the distribution observed, a reason previously evoked for the absence of certain conformers (cf. e.g.^{177,266,267}).

- Second, the set of observable conformers/isomers is ill defined, since it depends upon the isomerization and relaxation processes which can take place during the expansion (cf. Section 4.1). These processes depend drastically upon i) the large barrier height between topologic families of isomers and ii) the relatively smaller barrier height between isomers within the same family. As a result, some isomers stable at high temperatures can be observed (kinetic trapping), whereas other much more stable are not. Related to this issue, in the case of complexes or clusters, the formation process can be strongly influenced by the monomer distribution in the expansion, which can for example hamper or forbid the formation of specific species, e.g., insertion complexes, which requires a monomer intramolecular interaction to be broken for insertion to take place.

5. Introduction to theory

As shown in the previous section, experiments can provide measurements of several observables characterizing peptide folding in the gas phase. Although interpretations can be conducted by internal comparisons within a set of experiments or using well-known general principles, comparisons of experimental results with theory have rapidly proven to be so fruitful that they became essential. The main reason of such a success is the isolated conditions of the gas phase, where the issue of theoretically describing a complex environment vanishes in contrast to more classic investigations in solution. Theoretical and experimental results in the gas phase are thus more readily comparable. In addition, calculations of isolated peptides at a quantitative level of theory are affordable, and allows to fully exploit the high spectral resolution specific to gas phase investigations. Several benefits arise from the possibility to compare accurately measured and calculated observables. On the one hand, calculations are of great assistance to interpret experiments and unambiguously identify spectroscopic transitions, molecular structures, conformational distributions, relaxation mechanisms or any other intrinsic peptide property revealed by spectroscopy. On the other hand, experiments are useful to characterize the typical error made by a given level of theory on the observables, pinpoint its strengths and weaknesses, or guide the attention of theoreticians to a peculiar effect observed on a specific system. This interplay between experiment and theory was early recognized as an essential driving force of detailed peptide investigations, and contributed to make dual approaches attractive and popular.

The first task in gas phase peptide investigations consists of unambiguously identifying the molecular objects observed in the experiment. Among all the observables sensitive to the peptide structure, vibrational frequencies in the ground state are the most useful. Despite the measurement of a few experimental frequencies cannot pretend to exhaustively document the structure of a system made of several tens of atoms, it nevertheless often provides enough hints, e.g. by characterizing the H-bonding content, to sketch the structure. To go further, one seeks a good theoretical prediction of these few critical observables, which is taken as an indication that the whole theoretical structure fairly describes the molecular object considered, and moreover legitimates the level of theory chosen. Some vibrational modes involve a few atoms (like NH or OH stretches) and act as local probes of their environment, particularly sensitive to intramolecular interactions (cf. Section 6.1). Some other modes are more delocalized and provide a characterization of large structural motifs (cf. Section 6.2). Several approaches were thus designed to provide quantitative theoretical frequencies that can be compared to experimental IR spectra. The case of peptides is challenging for two reasons. First, peptides are relatively large molecules for which quantitative calculations can rapidly become unaffordable. Second, peptides are flexible molecules with a complex conformational landscape made of numerous minima, which need to be explored. The situation even becomes worse in peptide aggregates, in which the presence of various binding sites for the aggregation partner leading to different isomers should also be taken into account. This conformational exploration demands numerous energy calculations, which are affordable only at a

qualitative level of calculation. This is why two-step strategies were developed and are still in use today.^{31,79,257,319,333-336}

In the first step, the exploration of the minima of the potential energy surface (PES) can be carried out using either Monte-Carlo or molecular dynamics (MD) simulations, where peptides are usually described by a force field. This force field is expected to depict the PES well enough to select a reasonable number of lowest-energy structures, which will be considered in the second step where heavier quantitative calculations are targeted. In particular, it is expected from the exploration that (i) all low-energy conformations are found, and (ii) structures and relative energetics of the minima are sufficiently reliable. The choice of the force field then results from a compromise between the time dedicated to the exploration and the accuracy desired to minimize the computational efforts of the second step. Several classical force fields were originally designed to be applied on macromolecules in solution, like AMBER^{337,338} or CHARMM,^{339,340} and proved to be convenient for conformational explorations of peptides in the gas phase. Their latest versions are still routinely used.^{79,336} Other classical force field like OPLS,³⁴¹ or second generation force field like CFF³⁴² or MMFF^{343,344}, were designed to have a larger range of applicability, and were also used on peptides.^{79,334,335} Whatever the force field used, significant deviations from the correct structure are frequently observed, and a few conformations may be missing in the worst cases. This issue is generally solved by employing several force fields^{79,219} which provide complementary conformational landscapes. The more accurate polarizable force fields could also provide an interesting solution to address this problem, but are still not preferred to the more traditional approaches. In contrast, semi-empirical quantum chemical methods³⁴⁵ recently demonstrated their ability to explore the conformations of a dipeptide.²⁵⁷ With a claimed accuracy of ~ 4 kJ mol⁻¹, these methods may provide a valuable alternative to force field approaches, where conformations of relatively large energies (typically ~ 50 kJ mol⁻¹)⁷⁹ must still be considered as potential candidates for being the main conformation of the experimental distribution, whereas the observation window lies typically in the 0-10 kJ mol⁻¹ range.

Once the lowest-energy structures are identified by the conformational exploration, they are treated at a quantitative quantum chemistry level. The most used strategy consists of first optimizing the geometry, and then calculate vibrational frequencies. Getting a correct structure in these systems can be challenging. Indeed, equilibrium geometries in these flexible systems result from a subtle balance between several interactions of different nature, *e.g.* H-bonds involving more or less polarizable acceptors, dispersion between π clouds, or steric clashes, just to mention some of them. It is then mandatory to use a combination of theoretical methods and basis sets that is capable to describe correctly all these interactions. The treatment of dispersion is a long-standing issue since DFT methods underestimate it, whereas MP2 methods overestimate it.³⁴⁶ Several DFT methods corrected for dispersion addressed this issue quite efficiently,^{346,347} and were systematically used on peptides. Functionals such as B3LYP,³⁴⁸ or B97³⁴⁹ combined with the third version of dispersion corrections (D3)³⁵⁰ have proven to be successful for a decade. Additional refinements, such as the Becke-Johnson (BJ) damping aiming at better describing dispersion and correlation at short distances,³⁵¹ were used more recently, increasing the description accuracy of the structure. The functional ω B97X specifically designed to treat long range interactions and short range exchange can also be used with dispersion corrections.³⁵² A recent publication comparing several methods found that this ω B97X-D functional provided the most reliable structures for a dipeptide.²⁵⁷ In parallel, a fourth version of dispersion corrections (D4) is expected to improve the accuracy of this type of approach.¹⁴⁸ All these functionals are typically used with triple zeta basis sets and at least the addition of polarization functions.

Frequencies are usually calculated at the same level of theory as the geometry optimization. The harmonic approximation provides a fast way to proceed, however harmonic frequencies need to be further corrected to be compared to the experimental ones. The simplest approach consists of applying an empirical correction through a single scaling factor. A scaling factor can also be defined for each spectral domain in order to improve the accuracy of the corrected frequencies (*cf.* *e.g.* Ref.⁷⁹). In the case of non-coupled vibrational modes, mode-dependent scaling factors can also be defined,^{353,354} and in the most documented cases such as NH, OH, NH₂ and CO₂⁻ stretches, it is even possible to define linear scaling functions. These sophisticated approaches can typically reach an accuracy of 20 cm⁻¹ and sometimes down to 5 cm⁻¹ for dipeptides.^{73,219,355} For coupled modes, it is not possible to define mode-dependent scaling factors (*e.g.* multiple OH stretch modes),¹⁴² and more refined anharmonic calculations become necessary to describe vibrational resonances or simply have

access to intensities of overtones and combination bands, and thus increase prediction accuracy. The vibrational self-consistent field (VSCF) approximation and/or the second order vibrational perturbation theory (VPT2)³⁵⁶ and their extensions^{357,358} can be applied to polypeptides and compared with experimental spectra.^{257,336} Localized-mode approaches are also now available and applied to peptides.^{359,360}

While this two-step strategy (geometry optimizations followed by frequency calculations) is the most popular, an alternative approach relying on Born-Oppenheimer molecular dynamics (BOMD) simulations at a DFT level (DFT-MD)³⁶¹ has proven to be successful in reproducing IR spectra of peptides, especially in the far-IR domain.^{314,319,320,362,363} Basically, the nuclei are treated classically whereas the electrons are treated at a DFT-D level, and IR spectra result from the Fourier transform calculation of the time correlation functions of the fluctuating dipoles.^{314,320} Such a strategy includes anharmonicity, and is especially useful to interpret the far-IR domain with a remarkable standard deviation of 6 cm⁻¹.^{314,319,363}

Despite the valuable information provided by vibrational frequencies in the ground state, other observables can be useful to identify unambiguously each conformer of the conformational distribution, or simply to further characterize their properties. The weight of each conformation in the distribution can often be roughly estimated by experiments, and even sometimes measured (cf. population transfer methods, Section 4.2). If the experimental conformational distribution reflects an equilibrium, like after the pick-up of gas phase molecules by He droplets where a fast kinetic trapping occurs,²⁴¹ then Gibbs relative energies at the relevant temperature are totally appropriate to compare with experiment. In molecular beam experiments, kinetic trapping also occurs, but at a rate similar to that of conformational isomerization (cf. section 4.1). Final populations then also depends on other parameters like isomerization barrier heights.³⁶⁴ In a few cases, disconnectivity diagrams were calculated at the force field level,¹³³ and used to characterize conformational distributions. At best, molecular dynamics simulations of the cooling process in a molecular beam can be achieved to compare theoretical distributions with experiments.³⁶⁴ However, for most of peptides, Gibbs energy still provides a good indication of the conformational distribution in molecular beam experiments.¹⁰³ This is not true in the case of clusters, as they are usually formed once each partner is already cooled. Their conformation and isomer distribution is then expected to be out of equilibrium, and kinetic aspects must be taken into account in the conformational analysis.²¹⁹

Several types of calculations in the electronic excited states were developed in order to interpret IR spectra of S₁ states,^{75,179,333} rationalize the relative position of S₀->S₁ transitions of each conformer^{180,181,183,365} and sometimes their Franck-Condon activity,¹⁷⁹ or explain S₁ lifetime variations with the conformation,¹⁸¹⁻¹⁸³ including ultrafast processes responsible for experimentally missing conformers when using R2PI techniques.^{177,178} When excited and ground state properties must be compared, *e.g.* for excitation energies or shifts between S₀ and S₁ IR spectra, the approximate second-order coupled cluster method CC2³⁶⁶ is mostly preferred for capped amino acids by comparison with multireference methods.³⁶⁷ Excited state modelling is still a difficult matter, since the precision achieved on the electronic energies is typically of the order of ~1000 cm⁻¹ for the low lying excited states,^{367,368} which is far behind the experimental requirements for spectroscopic assignment owing to the modest spectral shifts between conformers (typically 100 cm⁻¹ at most). However, CC2 methods has recently proven to provide valuable benchmarks on relatively large species.³⁶⁹ Beyond transition energies, the same approach can also simulate Franck-Condon activity of electronic transitions and thus provide additional assignment information. Although popularized by recent simulations of vibronic spectra of protonated species,³⁷⁰ its use in assigning UV spectra of neutrals remains widely unexploited. Lifetimes are usually even more complex to explain¹⁸³ and may require an in-depth exploration of the possible relaxation paths at a non-adiabatic time-dependent DFT (NA-TDDFT) level.¹⁸¹

Finally, theoretical tools are useful to understand better the nature of the shaping interactions at play in peptides. Natural Bond Orbital (NBO)³⁷¹ analysis has recently been used to investigate the nature of NH- π interactions in peptides,³³³ and is appropriate to rationalize NH amide spectral shifts.³⁷² Non-Covalent Interaction (NCI) plots,³⁷³ an extension of the Atoms-In-Molecules (AIM) analysis,³⁷⁴ was shown to provide useful information on the location and nature of intramolecular interactions in large systems based on a topological analysis of the electron density.³⁷⁵ Although this tool has its own limitations,³⁷⁶ it is convenient to support the existence of significant interactions,³⁷⁷ compare their strength,^{80,333} and give an overview of the

subtle balance between all the interactions at play in peptides beyond those that can be directly probed in experiments.³⁷⁸

6. Optical probes of H-bonds and other structuring intramolecular interactions in peptides

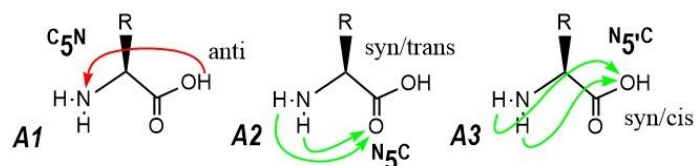
6.1. The stretching motion of the amide NH covalent bonds and other hydrides: The amide A region

The stretching modes of hydrides (XH), such as the polar NH bonds of the amide groups or the OH bonds of carboxylic acids, exhibit a significant transition moment for IR absorption, allowing spectroscopists to use their absorption signatures to probe these chemical groups. The exquisite sensitivity of the stretching mode frequency to the environment of hydrides, together with the local character of the NH stretch modes, provides an elegant way to assess the H-bonding pattern of a molecule. Furthermore, those modes are poorly coupled to each other as well as to the other molecular modes (in contrast to the CO stretches or NH bends; cf. section 6.2.). Each individual XH covalent bond usually gives rise to a well-defined absorption band, whose spectral position is the main source of structural assignments in gas phase studies. Other spectral features, i.e. broadening, increased intensity and anharmonicity in the case of H-bonded hydrides provide additional information.³⁷⁹ The spectral sensitivity stems from the dependence of the XH stretching frequency resulting from the electronic density of the covalent XH σ bond. This dependence can be interpreted as an effect of electron delocalization due to H-bonding in the Natural Bond Orbital (NBO) framework.³⁷¹ To a lesser extent it arises from hyperconjugative interactions with vicinal covalent σ bonds.³⁷² As far as linewidths and intensities are concerned, free XH groups exhibit weak and sharp lines (typical widths of a few cm^{-1}), whereas weakly H-bonded XH are more intense, but keep a sharp linewidth controlled by the rotational contour of the transition. For strongly hydrogen-bonded NH-groups, a broadening of up to several tens of cm^{-1} can be observed, presumably due to a larger coupling between the initially excited NH stretching mode and the manifold of low frequency modes of the molecule. However, these broadenings often remain modest and enable the recording of vibrationally resolved spectra for small peptides, in contrast with the bonded NH groups in uncapped peptides characterized by $\sim 100 \text{ cm}^{-1}$ broadened lines.³⁸⁰ Anharmonicity of the NH stretching modes is significant in H-bonded amides; the phenomenon is usually taken into account using specific, sometimes mode-selective scaling factors (cf. Section 5 and e.g.^{142,219,353,354}).

By collecting spectral features recorded for individual hydrogen-bonds, which are as isolated as possible from the rest of the molecule, typical frequencies and intensities have been extracted for amide NH stretching modes in various environments and secondary structures (cf. subsections in the present chapter). Of course, these features are at the heart of labelling techniques such as isotopic labelling (^{15}N in particular) or π -labelling, which will be discussed here as well. Cooperative effects in presence of other bonds or general perturbations induced by a molecular environment (e.g. by steric constraints) will be discussed in more detail in Section 8.

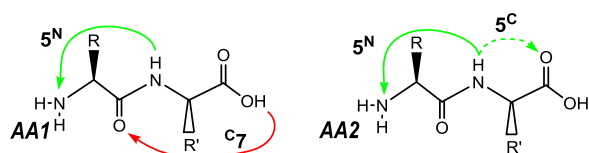
6.1.1. Spectroscopic probe of backbone-backbone interactions specific to uncapped peptides (COOH/NH₂): OH/NH/NH₂ hydride stretches

The mid IR-spectroscopy (3 μm range) provides invaluable direct information, such as the carboxylic acid OH stretch absorption, at least as long as this one remains in its neutral form. Despite their weaker absorption, the antisymmetric and symmetric components of the NH stretches of the N terminal NH₂ group are often observable and provide an additional information (cf. Table 4). Most of the IR/UV studies on the gas phase aromatic amino acids (AAs) Trp, Tyr and Phe indicate the presence of three types of conformers, here labelled A1, A2 and A3 (cf. Scheme 1).



Scheme 1: H-bonding patterns observed in unprotected amino acids.

In conformers A2 or A3, the OH group is either not involved in H-bonding or only as H-bond acceptor, which gives rise to a free OH stretch mode, whose frequency is close to 3600 cm^{-1} . In contrast, in the A1 conformer, the H-bonded OH (through a 5^N bond) leads to a strongly red-shifted, broadened band in the $3200\text{--}3300\text{ cm}^{-1}$ region. Further assignment in terms of type A2/A3 relies on the comparison with calculations especially for the NH_2 stretches with 5^C and 5^N bonds, whose frequencies present slight but significant differences (cf. 2).



Scheme 2: H-bonding patterns observed in dipeptides with unprotected N- and C-termini.

Larger uncapped peptides are interesting with respect to the simultaneous presence of uncapped N and C terminals together with peptide bonds, which increases the number of combined interactions and provides the opportunity to document the role of emerging secondary structures as stabilizing features. Table 4 presents two typical additional interactions relevant for the description of the H-bonding network, namely the 5^N and $c7$ H-bonds. Concerning conformer-selective IR spectroscopy of dipeptides, only the Tyr-Gly, Trp-Gly and Gly-Trp sequences have been reported experimentally and interpreted using quantum chemistry calculations. H-Gly-Trp-OH²⁶⁹ is found to exhibit two conformers, assigned to different H-bonding patterns (labelled AA1 and AA2, cf. Scheme 2). Both structures are stabilized by a N-terminal, local, $\text{NH} \rightarrow \text{NH}_2$ H-bond (5^N) accompanied by a C-terminal localized $\text{OH} \rightarrow \text{OC}(1)$ bond $c7$ (bridging the acidic OH to the Gly amide) in AA1 and possibly by a weaker 5^C interaction in AA2. In contrast, the reversed sequence, Trp-Gly²⁶⁹, and its Tyr counterpart, Tyr-Gly³⁸⁰, exhibit only AA1 type conformers, in which the intra-residue 5^N interaction is made easier by the absence of a side chain on the Gly residue. In all these cases, the aromatic side chain is too rigid to establish any interaction with the backbone, as testified again by the free OH/ NH side chain stretching bands.

Table 4: Stretching vibrations of H-bonded OH/NH/NH₂ hydrides: a spectroscopic probe of C-terminal/N-terminal and terminal-backbone interactions in neutral amino acids and uncapped dipeptides. For H-bond labelling, see Schemes 1 and 2.

H-bond type	remark	band intensity	range/cm ⁻¹	References
Free carboxylic OH		strong	3570-3593	36,37,131,205,231,270,380,381
aminoNH ₂ <i>i</i> → OH <i>i</i> N ₅ ^C	antisymm	very weak	3430-3440	205
	symm.	weak	3340-3350	
aminoNH ₂ <i>i</i> → OC <i>i</i> N ₅ ^C	antisymm.	weak	3405-3410	131,205,269,270,380,381
	symm	very weak	not obsv	
aminoNH ₂ <i>i</i> ← NH <i>i</i> +1 5 ^N		strong	3390-3420	269,270,326,380-382
	in combination with C ₇		3304-3370	
OH <i>i</i> +1 → aminoNH ₂ <i>i</i> C ₅ ^N		strong, broad	3200-3300	131,205,269,380
OH <i>i</i> +1 → OC <i>i</i> C ₇		very strong	<3200	269,380

6.1.2. Spectroscopic probe of backbone-backbone interactions: NH stretches in models of a protein chain

The basic backbone-backbone H-bonding structures (cf. schemes of Table 5) bridging an amide NH and an amide CO in a protein chain have been obtained from the study of model molecules investigated in the 2000's using IR/UV techniques using capped aromatic amino acids (Trp, O-methylated Tyr and Phe, cf. Section 2.3). O-alkyl C-terminal caps allow focussing on extended conformations (Phe^{134,284} and Trp³³² chromophores). N- and C-terminal ends capped with acetyl and amide/methyl-amide respectively provide relevance to the description of basic protein secondary structures by keeping the amide groups in the molecule intact (cf. Section 2.3): Studies have been performed on capped amino acids such as Trp^{133,203,296,332,364} or Phe^{60,135,219,383}, on di- and tripeptides containing a modified tyrosine^{102,157,384,385} or a Phe residue^{60,75,217,328,386-389}. Chromophore-containing caps (e.g. Z-caps; benzyloxycarbonyl) have also been used but remain less popular.^{61,74,76,316,390}

References for free NH stretches can be deduced from the spectroscopy of *trans*-methylacetamide, a minimalist model for a peptide bond in a protein chain (3508 cm⁻¹)^{31,38}, as well as from a few peptides in which a NH bond was found to be free from any H-bonding interaction: 3492-95 cm⁻¹⁷⁵ for a Gly residue in a β-turn, 3469 and 3472 cm⁻¹ for Ser/Cys¹⁵⁶ and Phe (cf. Figure 10) resp. in a γ-turn. The significant difference between these references is indicative of hyperconjugative effects within the peptide chain, between the NH bond considered and vicinal covalent σ bonds, such as the C^αH bond of the same residue.³⁷²

The spectral signatures of gas phase isolated 5, 7 and 10 H-bonds have been determined early in the 2000 decade (cf. Table 5), together with their combinations with other bonds. It leads to an increasing H-bond strength in the following order: 5, 10, 7, which is corroborated by NBO analyses,³⁷² from which frustration effects are found to be ubiquitous. For example, the 5 bond is strongly non linear, since the NH and CO bonds of the same residue are nearly parallel, due to the backbone extended arrangement, locally stabilized by hyperconjugation effects. The 10 bond is frustrated by the β-turn/helical backbone, which impedes both amide groups to come closer. The backbone of the inverse γ-turn is constrained by hyperconjugative interactions, which tend to align the CO and NH covalent bonds of the residue and therefore oppose to the formation of a strong 7 H-bond.

Table 5: Stretching vibrations of backbone NH/NH₂ hydrides: a spectroscopic probe of backbone → backbone H-bonding interactions in linear protein chains.

	H-bond type	remark	band intensity	range/cm ⁻¹	references
	free NH	in methylacetamide	Weak	3508	31
	free NH	in peptides	Weak	3472-3495	75
	NH <i>i</i> → OC <i>i</i> 5	in comb. with other 5 bonds	Weak	3435-3455 3405-3445	60,133-135,332 75
	NH <i>i</i> +1 → OC <i>i</i> -1 7	in comb. with other HBs (2 ₇ ribbons, 7-10) ^a	Strong	3340-3380 3310-3420	60,133,135,386 60,385,386
	NH <i>i</i> +2 → OC <i>i</i> -1 10		strong	3380-3415	141,330,387

a) H-bonds shifting the NH stretches below 3300 cm⁻¹ are observed in some cyclic (tetra)peptides^{335,391}

Specific case of NH₂ in a C-terminal carboxamide termination

In some model peptides, simple amide caps are chosen instead of methylamides, despite the latter are more qualified as model terminations since the methyl group provides a minimalist mimicking of the rest of the protein chain. However, the carboxamide termination provides an invaluable piece of spectroscopic information, which originates from the coupling existing between the symmetric and antisymmetric components of the carboxamide NH₂ moiety (in the following, NH₂ will refer to the terminal part of the carboxamide group considered). This coupling basically results from the fact that both NH stretch oscillators share the same N atom. If one of these NH modes is involved in an H-bond, its frequency should be red-shifted. However, this structural coupling also perturbs the frequency of the other oscillator in a way, which can be described by a two level model. At the limit of weak H-bonding, both oscillators are free: the coupling gives rise to a splitting, with both a symmetric and antisymmetric component, with an average frequency being that of the free NH oscillator. In the limit of strong H-bonds the coupling becomes negligible, the symmetric component tends to a purely H-bonded oscillator whereas the antisymmetric approaches the free oscillator frequency. Such a model remains an approximation, since it does account for anharmonicity effects, but experimental data proves its validation within a very reasonable margin of error (cf. Figure 12). The great interest of the model is that the frequency of the antisymmetric component bears an indication about the existence of the H-bond originating from the NH₂ group, together with an estimate of its strength. In the context of a C-terminal amide, this provides the H-bonding status of this end of the molecule, which is a crucial information regarding the structural assignment of the studied conformations,^{60,136,142} even in absence of quantum chemistry calculations.

It should be noted that the same spectroscopic trick applies to the carboxamide groups of the asparagine and glutamine side chains^{77,78,82}, as well as to the N-terminal amino groups of uncapped peptides, although less used in this latter case.

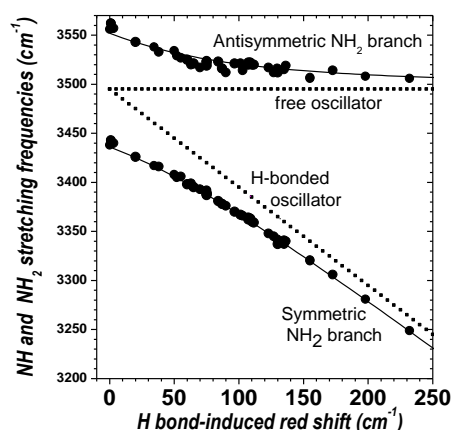
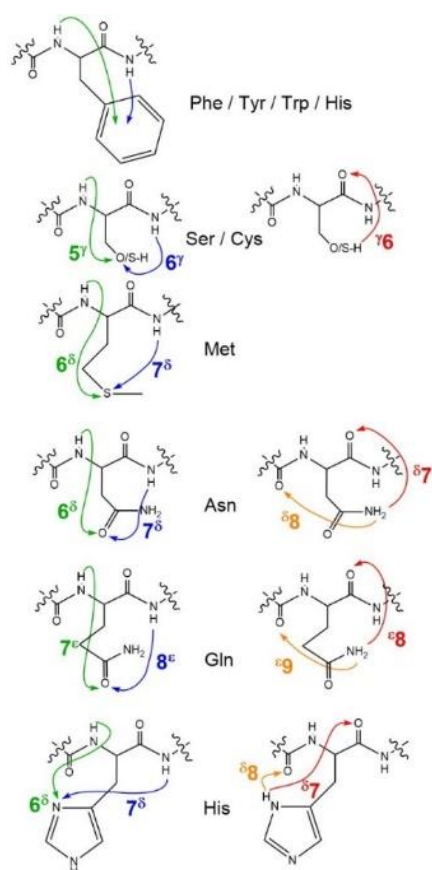


Figure 12: Experimental symmetric and antisymmetric stretching modes of H-bonded carboxamide (-CO-NH₂) groups within a series of capped peptides reported in the literature.^{60,136,142} The frequencies fit well a simple coupling model (lines), in which two oscillators, one free (fixed frequency at 3495 cm⁻¹) and one H-bonded, red-shifted (the redshift being taken as a measure of the H-bond strength) are coupled according to a coupling constant independent of the H-bond.

6.1.3. Spectroscopic probe of local backbone-side chain interactions in neutral residues: backbone NH \rightarrow side chain acceptors

Local NH - π interactions, where a backbone NH interacts with a nearby aromatic ring, which then plays an acceptor role, are often detected in sequences made of non-polar amino acids. The presence of an aromatic ring in the model molecule is indeed imposed by the IR/UV double resonance technique. These interactions form spontaneously as soon as they are topologically allowed by the backbone flexibility, due to the significant enthalpic gain they represent in the gas phase and the moderate entropic penalty associated to a weak bond. They are consequently ubiquitous in the isolated model systems studied, either as intra- or inter-residue bonds. Despite being relatively weak, with modest red shifts, they have been clearly identified as such in amino acids^{131,205,380}, uncapped peptides³⁸² and protein chain models,^{60,135,296,377,384} and even characterized in the excited state.³³³ Their opportunist behavior sometimes can even be hampering, when the aromatic moiety does not belong to the molecule of interest and for instance is part of the cap used for IR/UV spectroscopy (benzyloxycarbonyl-, Z- or benzylamide -NH-Bn groups). They tend to form spontaneously between the cap and the backbone^{77-79,103}, or a side chain donor site,^{77-79,103} often additionally stabilizing the conformation. One of the drawbacks is their ability, through both enthalpic and entropic effects, to shift the conformational equilibrium towards structures in which they occur (cf. Section 9 for examples and discussion).

Other residues possessing an H-bond acceptor site potentially lead to a NH \rightarrow side chain H-bond and are often characterized by typically red-shifted IR signatures (Table 6). Depending on the side chain length and on the upstream or downstream position of the donor along the sequence, the local H-bond can be designated as being intra- or inter-residue (cf. left panel of Scheme 3). Backbone NH \rightarrow side chain acceptor H-bonds are observed concomitantly with backbone-backbone H-bonds (cf. Section 7). However, when the side chain is short enough, the compactness of the backbone-residue system allows the simultaneous presence of three types of H-bonds: the basic backbone-backbone H-bonds and two H-bonds where the side chain is both donor to and acceptor from the backbone. This is the case for instance with the Ser, His, Asn and Gln side chains, where an extended locking through multiple bonds occurs between the backbone and the side chain. This leads to more or less severe constraints and cooperative effects, which can affect the H-bond strengths observed and should be considered when consulting the NH stretch frequency data of Table 6. Nevertheless, one can conclude from the red shift ranges observed (from ~ 30 to ~ 300 cm^{-1}) that Ser and Cys behave as poor local acceptors, followed by Met and Asn, Gln and His (in its ϵ tautomeric form, where the mobile H atom of the imidazole ring is localized on the N^{ϵ} atom). The red shifts show a significant dependence with respect to the type of hydrogen bond and the backbone arrangement.



Scheme 3: Backbone-side chain local H-bonding for neutral residues in a protein chain. *Left panel* : side chain is acting as an H-bond acceptor ; *right panel*, as a donor. The H-bond terminology adopted accounts for the position and the role of the heteroatom playing the acceptor role or bearing the bridging H-atom (greek superscript) as well as for the size of the ring formed at the H-bond formation (cf. Section 2.1). Intraresidue H-bonds are marked in green and orange; interresidue in blue and red.

Table 6: Stretching vibrations of H-bonded backbone NH hydrides: a spectroscopic probe of backbone – side chain H-bonding in protein chains.

Donor → Acceptor	Type	Residue/ Conformation	NH stretch frequency/cm ⁻¹	Reference
NH → π <i>i</i> / <i>i</i> +1 → <i>i</i> <i>i</i> & <i>i</i> +1 → <i>i</i>	π	Phe, Tyr, Trp NH between rings	3415-3450 3370-3380	135,296,60,333 81,377
NH → OH <i>i</i> → <i>i</i>	5 ^γ	Ser γ-turn 5 ^γ (^γ 6)-7	3455	80
NH → SH <i>i</i> → <i>i</i> <i>i</i> → <i>i</i> +1	5 ^γ 6 ^γ	Cys γ- or β-turns 5-6 ^γ extended	3415-3435 3370	80,83,156,390 390
NH → SeH <i>i</i> → <i>i</i>	5 ^γ	γ- or β-turns	3400-3415	156
NH → SMe <i>i</i> → <i>i</i> <i>i</i> +1 → <i>i</i>	6 ^δ 7 ^δ	Met β-turn γ-turn	3360-3362 3340	392 392
NH → O=C (carbonyl/amide) <i>i</i> → <i>i</i> <i>i</i> +1 → <i>i</i> <i>i</i> → <i>i</i> <i>i</i> +1 → <i>i</i>	6 ^δ 7 ^δ 7 ^ε C ^{8ε} 8 ^ε	Asn γ-turn 6 ^δ (^δ 7)-7 extended 5-7 ^δ (^δ 8) Gln γ-turn 7 ^ε (^ε 8)-7 β-turn 7 ^ε -7 ^ε (^ε π)-10 C ^{8ε} ; OH C-term extended 5-8 ^ε (^ε f)	3353-3363 3305 3343 3320-3550 3140 3308-3350	79,82 82 78 77 78 78
NH → N <i>i</i> → <i>i</i> <i>i</i> +1 → <i>i</i>	6 ^δ 7 ^δ	His γ-turn 6 ^δ (^ε f)-7 β-turn extended 5(^ε f)-7 ^δ	3333 3355-57 3172	82 82 82

6.1.4. Spectroscopic probe of local backbone-side chain interactions in neutral residues: side chain donor → backbone CO

The presence of local H-bonds is greatly influenced by the length of the side chain. As mentioned for side chain acceptor H-bonds, the H-bond strength is presumably affected by constraints and cooperative effects if the side chain is also an H-bond acceptor. Nevertheless, apart from the Ser with its strongly red-shifted OH stretch, the red shifts of the H-bonded side chain NHs remain modest in the 100 cm⁻¹ range (cf. Table 7).

NH or OH groups of Trp and Tyr are sometimes involved in interactions with H-bond accepting groups providing that the molecule is long enough for an end-to-end folding to occur. This has been reported for Trp, in

uncapped peptides with a backbone carbonyl acceptor (H-Trp-Ser-OH³²⁶, H-Tyr-Gly-Gly³⁸⁰) and in capped peptides with the π ring of a neighboring other aromatic residue residue (Ac-Trp-Tyr-NH₂³⁷⁷). The measured shifts remain modest because the formed H-bonds are hampered by the combined rigidity of the side-chain itself, and that of the backbone.

Interestingly, Asn/Gln containing species show a red shift of the antisymmetric NH₂ amide frequency below the free oscillator frequency ($\sim 3500\text{ cm}^{-1}$), which indicates doubly bonded amides. In this case the *trans* NH is involved in an H-bond with the backbone and the *cis* NH in a ${}^{\epsilon}\pi$ H-bond to either an aromatic residue of the sequence (cf. Supplementary information of ref³⁶⁹) or to a -NH-Bn benzylamide cap.^{78,79} This type of doubly bonded amide structure was also observed in a conformer of capped phenylalanine monohydrate.²¹⁹

Table 7: Stretching vibrations of side chain OH/NH hydrides: a spectroscopic probe of intramolecular side chain \rightarrow backbone H-bonding in protein chains

Donor / residue	Type	Conformation	NH stretch frequency/cm ⁻¹	Reference
OH Tyr $i \rightarrow i+2$	free OH-O	\rightarrow OC of C-term	3593 3400-3530	380 380
OH Ser $\rightarrow i$	free γ_6 $\gamma_6^{O'}$	methanol π -5 ^{(γ_6)-10 C-7^{($\gamma_6^{O'}$) C-term}}	3681 3450 3585	393 80,83 326
NH Trp $i \rightarrow i+1$	free NH-O	\rightarrow OC of C-term / stacking	3520 3503^a	326,382 326,382
NH His $i \rightarrow i$ $i 1 \rightarrow i$	free δ_7 δ_8	γ -turn $\pi^H(\delta_7)$ -7 extended 5 ^{(δ_8)-8δ}	3512 3384-3398 not observed	81 81 81
NH Asn/Gln Asn $i \rightarrow i$ $i + 1 \rightarrow i$	free δ_7 δ_8	from Gln γ -turn 6 ^{(δ_7)-7 extended 5^{(δ_8)-7δ}}	3442/3562 3380-3395/3505-3515 3400/3515	78 79,82 82
Gln $i \rightarrow i$ $i+1 \rightarrow i$	free π ϵ_8 ϵ_9	5(stacked+ π) ^C COOH C-term γ -turn in 7 ^{(ϵ_8/ϵ_9)-7 ext. 5^{(ϵ_9)^Cfree uncapped peptide}}	3442/3562 \sim3400/3520 3400 / 3510* 3370 / 3510	78 78 here doubt about π double donor binding 78 * = NH ₂ double donor (ϵ_8/ϵ_9) 78

a) for interstrand bonds cf. Ac-Trp-OMe dimer³³²

6.2. The spectral region below 2000 cm⁻¹

6.2.1. Some general aspects

Beyond the region of N-H stretching frequencies (denoted as the amide A region) further regions of the IR spectrum yield valuable information on the structure via characteristic vibrations. A brief tabular overview (cf. Table 8) of these regions is presented here, whose divisions are not considered to be strict, especially in the lower energy region. The important regions important for the structure determination of amino acids and peptides are described in more detail in the following section 6.2.2.

Since the carbonyl groups play an important role as H-bond acceptor within an amino acid or peptide, the amide I region can be essential for structural assignments. This region mainly comprises the C=O stretching motions of the amide backbone, the C terminus but also of amino acid side chains. In comparison to the N-H

and O-H stretching modes, the C=O stretching vibrations (with their mainly double bonding character) are also quite localized modes. However, they exhibit a slightly less anharmonic character than the amide A modes, which is also revealed in the higher scaling factor used in the amide I region^{74,79,135,157,160,250,284,335,383,394}. Additionally, the C=O stretching modes are less influenced by H-bonding, leading to lower (absolute and relative) red-shifts of the carbonyl stretching frequencies than in the amide A region; free and H-bonded CO groups often exhibit a quite small but still characteristic red shift (sometimes only about 10 cm⁻¹). A further main aspect is the usually strong coupling of the amide I vibrations. It leads to a specific frequency and intensity pattern, which is greatly dependent upon the relative orientation of the carbonyl groups and hence upon the overall molecular shape. Due to these effects, the vibrational pattern of a conformer in the C=O region is frequently very characteristic. Finally, being vibrations of high intensity, the C=O stretching modes can also influence the amide A region, e.g. as overtones, which can couple with fundamentals of N-H stretching modes to Fermi resonances.

Table 8: Main, structurally relevant IR regions below 2000 cm⁻¹

spectral region / cm ⁻¹	region denoted as	main vibrations	further remarks/vibrations
1800 – 1600	amide I	C=O stretching	C=O stretching COOH: ≈ 1790 cm ⁻¹ C=O stretching amide backbone: ≈ 1650 – 1730 cm ⁻¹
1600 – 1400	amide II	N-H bending (in plane) O-H bending (in plane)	C-N-H bending amide backbone combined with CN stretch: ≈ 1510 – 1570 cm ⁻¹ bending vibration of water in hydrates ¹⁶⁰ (free water: 1595 cm ⁻¹) COH bending of strongly H-bonded COOH group C-H deformation modes (CH ₂) C=C stretching
1400 - 1000	Amide III (upper fingerprint region)	C-O-H bending C-O stretch C-N stretch C-H bending	C-N stretching + C-C stretch + NH bending secondary amides C-H deformation modes (CH ₃) =C-H in plane bending
1000 - 800	lower fingerprint region	O-H out of plane deformation C-H out of plane vibrations aromatic chromophores	
< 800	far IR region	N-H wagging C-H wagging delocalized collective backbone bending modes	

The so-called amide II region comprises N-H bending modes of the amide backbone groups and the unprotected C-terminus as well as the O-H bending modes of water molecules in hydrates. All of these vibrations exhibit an even stronger coupling behaviour than amide I modes. Both kinds of bending vibrations are blue-shifted when involved in H-bonding. Though the anharmonicity of in plane N-H bending modes is slightly higher than for C=O stretching modes,³⁹⁴ it is frequently a satisfying approach to use the same scaling factor as in the amide I region^{74,135,153,157,160,250,335,395,396}. Occasionally the difference in anharmonicity is taken into account by using a scaling factor in between the amide A and I scaling factors^{79,217,250}.

Further enhancement of vibrational coupling is found in the region below 1400 cm⁻¹ to about 1000 cm⁻¹, which is occasionally denoted as amide III (cf. e.g.¹⁴²) or as 'fingerprint region' (cf. e.g.¹⁹⁶). The expression fingerprint region is very flexibly used and partly even comprises the amide I and II regions as well as the vibrations below

1000 cm^{-1} , cf. e.g. ^{153,222,286,394}. The region 1000-1400 cm^{-1} comprises the C-H deformation/bending modes of saturated alkyl groups, in plane =C-H bending of aromatic systems, C-O stretching modes often coupled with the C-O-H bending vibration. The region below 1000 cm^{-1} down to the far IR region is characterized by =C-H out of plane vibrations of aromatic side chains as well as the C-O-H out of plane vibrations. Where the so-called far IR region begins is as ambiguously defined as the use of the term 'fingerprint region': authors working in the field of molecular beam spectroscopy denote the upper limit to be 800 cm^{-1} , 700 cm^{-1} , 500 cm^{-1} or even around 200 cm^{-1} (cf. ^{222,314,318,320,363}). In the region around 800-600 cm^{-1} , intense out of plane deformation (wagging) vibrations of the hydrogen atoms of the phenyl ring (cf. e.g. ³¹⁸⁻³²⁰) are found along with alkyl deformation (cf. e.g. ³²⁰) modes. In case of hydrates, also water (out of plane) libration modes can be found down to about 500 cm^{-1} , corresponding in plane modes around 400 cm^{-1} (cf. e.g. ³¹⁸). The spectral region 400-550 cm^{-1} comprises out of plane N-H bending and NH_2 inversion modes (cf. e.g. ³¹⁸); partly, blue shifts above 600 cm^{-1} are possible if the NH group is involved in H-bonding (cf. e.g. ³¹⁹). Delocalized, collective backbone bending modes can be found between about 400 cm^{-1} down to around 200 or 100 cm^{-1} (cf. e.g. ^{319,320}), followed by torsional backbone motions (cf. e.g. ³¹⁹) in the region lower than 100 cm^{-1} . This spectral range is described with more details in the dedicated review of the present issue ³⁶².

6.2.2. The spectral region below 2000 cm^{-1} regarding the structural analysis of peptides

Which of these spectral regions is finally measured does not only depend on the scientific question but also on the precise experiment and its instrumental equipment as well as (with regard to the interpretability) on the possibility to compare with diagnostically valuable calculations.

With regard to FTIR spectroscopy, the vibrational ground state spectra in the mid and far IR region usually down to about 400 cm^{-1} are accessible depending on the light source (globars, Nernst lamps, mercury lamps, the latter especially for regions lower than 200 cm^{-1}) and the detector (often pyroelectric detectors or photodetectors). Nevertheless, the region below 1000 cm^{-1} is rarely used in gas cell or jet FTIR for structure analysis in context with amino acids or peptides (cf. e.g. ^{36-38,40}). This is partly due to a missing adequate theoretical description by standard DFT methods, especially for larger systems (cf. following sections), and due to the fact that major structural motifs (H-bonding patterns) can already be analyzed in the amide A,I,II regions.

For molecular beam IR spectroscopy, the region from the mid IR to the far IR is hardly accessible by using one optical source. Nowadays, table top systems are able to cover the mid IR region down to about 600 cm^{-1} (cf. e.g. ^{285,316,325,397}). The region below 600 cm^{-1} and more generally the region below 2000 cm^{-1} is a domain of the FEL lasers (cf. e.g. ^{310,312,313}). This is sometimes the reason why publications split up on those investigating the amide A, I, II (cf. e.g. ^{74,79,102,134,135,160,217,250,284,316,335,382,391,395,396,398,399}) and partly III (cf. e.g. ^{316,397}) regions, and others focusing on the amide I-III (cf. e.g. ¹⁹⁶) and (cf. e.g. ^{137,153,217,286,318,394,396})/or (cf. e.g. ^{314,318-320}) far IR regions.

With regard to the C=O stretching and N-H bending regions, it has been demonstrated that the amide I, II region comprises valuable structural information. Nevertheless, to have an additional support for the interpretation, the amide I,II region is often analyzed in combination with further spectral regions as the N-H and O-H stretching regions where amino acids up to pentapeptides have been investigated (cf. e.g. ^{74,79,102,134,135,160,217,250,284,316,335,382,391,395,396,398,399}) or with the region below 1400 cm^{-1} (cf. ^{196,397}) and the far IR region (cf. e.g. ^{137,153,286,314,318-320,394,396}).

The characteristic differences in the amide I,II region for free and H-bonded CO and NH groups can be very sensitive towards the H-bonding pattern and the general peptide backbone structure. This is not only true for isolated peptides but especially for hydrates as the mono- up to triply hydrated Ac-Phe-OME¹⁶⁰, in which the carbonyl groups are the most important H-bond accepting partners for the attached water. Additionally, the experimental knowledge about amide I, II modes can help to decide whether additional bands in the amide A region can be attributed to overtones and Fermi resonances or to the presence of more than one isomer in the corresponding IR/R2PI spectrum (cf. e.g. ^{335,398}). In many cases, a first comparison with amino acid or peptide systems whose structural preferences were already successfully analyzed often allows to draw principle structural conclusions (cf. e.g. ^{102,160}) from the experimental data. A more detailed analysis in comparison with calculations frequently supports and further refines the conformational assignments based on the amide A

region (cf. e.g.^{79,102,134,135,160,217,250,284,316,335,391,395,396,398,399}). How valuable the amide I,II region is of course depends on the individual system (cf. e.g.^{74,382}).

Beyond, for structurally unambiguously assigned systems, the amide I,II region can present a further benchmarking system to validate theoretical methods. The strongest deviations between harmonic frequency calculations and experimental data are normally found for the N-H bending modes (cf. e.g.^{217,399}). This is due to coupling effects, which can lead to a broadening of the experimental bands, making them more difficult to interpret. Additionally, the coupling in extended chains with sequential C5 interactions effects a large intensity enhancement of the in-phase bending motions (cf. e.g.^{74,399}). These coupling effects in the amide I,II region were analyzed in more detail in the Zwier group by Hessian reconstruction and a modified procedure of it; by this site frequencies as well as nearest neighbor and next-nearest neighbor coupling constants (cf.³⁹⁹) were extracted. In that context, a potential energy distribution analysis for a combination of NH bend and CN stretch modes showed that those are less localized than the CO stretching modes. Beyond, the analysis of the coupling constants revealed strong indications that the main mechanism by which two carbonyl stretching vibrations couple is the NH...CO H-bond connecting the two different backbone amide groups. This picture differs from the mechanisms proposed by TDC (transition dipole coupling) or TCC (transition charge coupling), which explains CO coupling by the electrostatic coupling of the oscillation dipoles (with TCC including higher order multiple terms). Some general conclusions were drawn from this analysis: In both regions (amide I and II) coupling constants are only large (with the largest ones found for amide II/II couplings) if the amide groups are connected by an H-bond and the value of the coupling constant is characteristic for the type of H-bond formed.

Though the O-H stretching, amide A, I and II already exhibit a very comprehensive picture of amino acid or peptide structure, especially with regard to H-bonding pattern and backbone structure, more detailed structural aspects sometimes remain unclear (cf. e.g.^{134,284,382}). A typical example in which the region below 1400 cm⁻¹ becomes of interest are the OH in plane bending vibrations of uncapped peptides³⁹⁶. In their free or only weakly H-bonded form they can be located below 1400 cm⁻¹, whereas they are measured between 1400-1500 cm⁻¹ when they are involved in a strong H-bond. Further typical examples are side chain orientations^{134,284,397} or orientations of chromophores in caps^{137,153}. Thus, the significance of the region between about 1400 and 1000 cm⁻¹ for assigning structural details was realized; nevertheless, measurements in the amide I-III^{222,286,316,317,335,394,396} regions were often still combined with amide A measurements^{131,158,205,316,335,396}.

In many cases, harmonic, DFT/B3LYP-based calculations give (as for the amide I and II vibrations) an adequate description of the experimental data between 1400 and 1000 cm⁻¹, including (cf. e.g.^{137,153,196,222,286,396} 222) scaling to account for the anharmonicity (cf. e.g.^{153,196,396,397}). Occasionally, unscaled frequencies are used especially when the spectral region below 1000 cm⁻¹ is analyzed. Though some deviations from the absolute positions can occur, especially in the amide I and II region, the vibrational patterns are still characteristic^{137,222,286}. Special care must be taken if dispersion interactions play a role as shown by Jaexq et al. on the examples of Z-Glu-OH and Z-Arg-OH¹⁹⁶: for conformations stabilized by dispersion interactions, the region 1400-1000 cm⁻¹ was better described by DFT calculations including dispersion (via e.g. the M05-2X functional) than without dispersion (e.g. B3LYP functional).

Throughout the last years, increasing attention has been paid to the region below 1000 cm⁻¹ and especially the far IR region (cf. e.g.^{314,318-320,362}), in which different out-of-plane deformation modes as well as collective backbone vibrations are localized. Though our contribution is focused on IR spectroscopic investigations, one should bear in mind that especially the far IR region is in principle also the domain of Raman spectroscopy, which, in combination with the low sample concentration of the molecular beam, of course requires high sensitive Raman set-ups³²⁻³⁵. In that context, Balabin analyzed small amino acids without an aromatic chromophore as Gly^{32,35}, its hydrate³³ as well as Ala³⁴ by jet cooled spontaneous Raman-spectroscopy combined with MP2 and DFT-based theory. For some cases he could show, in comparison with microwave spectroscopy, that further conformers^{32,34} could be identified by Raman spectroscopy below 500 cm⁻¹.

The light sources applied in context with amide III measurements already mentioned above (cf. e.g.^{137,222,286,317}) already allowed measurements in the region lower than 1000 cm⁻¹ and in the far IR region. In these quite early publications (covering a time span between 2004 and 2008) the deviations between DFT-

based harmonic description and the experimental spectra were obvious, especially in the far IR region. As reason the anharmonicity of the corresponding vibrations, which can hardly be approximated by scaling (cf. Section 5), was identified. This e.g. leads (in some of the publications) to a complete neglect of scaling in this spectral region (cf. e.g.^{137,286}) and a comparison between experiment and theory mainly based on vibrational patterns. In that context calculated out-of-plane NH₂ vibrations partly showed the strongest deviations from the experiment (cf. e.g.^{137,394}) since this motion can be compared to the NH₃ umbrella motion, taking place in a symmetrical but anharmonic double minimum potential.³¹⁷ In 2012 the Mons group investigated the spectral region between 140 and 800 cm⁻¹ for the monomer and the two most abundant isomers of the monohydrated Ac-Phe-NH₂ (based on their former analysis in the amide A region cf.²¹⁹). By this, access to intermolecular vibrations as the in-plane and out-of-plane librations of the water molecule and additionally the wagging mode of the free OH bond of water was offered. It (once again) became obvious that, due to the moderate agreement between the experiment and current DFT(-D) based methods, an identification of these two isomers would have hardly been possible without the results of the amide A region.

In literature a few examples exist for which the pure mid IR region (mainly the amide A, I and II with quite localized modes) is not sufficient to provide a definitive structural assignment (cf. e.g.^{314,319}), especially with regard to structural details like side chain arrangements. Thus, the characteristics of further modes must be taken into account: The 'soft', partly strongly delocalized modes in the region below 500 cm⁻¹ are expected to be very sensitive to detailed backbone conformations (cf. e.g.^{314,320,362}) and H-bonded networks (cf.⁸³). Additionally it can occur that, in larger peptides, the number of localized vibrational motions can lead to overlap phenomena and increasing spectral congestion in the amide A, I and II regions, and thus to a complicated interpretation. In contrast, the far IR region can still show quite well-resolved spectra (cf. e.g.^{314,362}). As a consequence, the far IR region is not simply a complement to the other spectral regions but it yields structural information not accessible by e.g. O-H, N-H, C=O stretching or N-H (in plane) bending modes. However, its interpretation is not straightforward and requires a strong theoretical effort. In cooperation with experimentalists (cf. e.g.^{314,319,320,362}), Gaigeot proposed as approach to describe the vibrations in the far IR region, the BOMD (Born-Oppenheimer molecular dynamics) simulations at the DFT level (DFT-MD) which are able to directly provide anharmonic spectra (cf. e.g.^{314,319,320} also cf. section 5 and the review in the present issue³⁶²). To establish and further benchmark this method, a variety of dipeptide systems (Ac-Phe-XX-NH₂^{314,319,320}) were investigated (also in comparison with the amide A region^{80,83,387}). An excellent agreement between experiment and theory especially in the region below 500 cm⁻¹ was found; in the region between 500 and 800 cm⁻¹, the deviation was slightly larger with up to 20 cm⁻¹. For the amide I and II region the match between experiment and theory is found to be less good with discrepancies of about 70-80 cm⁻¹ and 30-40 cm⁻¹, respectively. The fact that strongly localized modes such as CO stretches are possibly quite sensitive to local deviations of the PES, whereas the delocalized far IR modes characterized by quite global motions over the PES react less sensitively to them, can explain the better match to the dynamically calculated spectra (cf. e.g.³¹⁴).

With regard to the most sensitive vibrations, (out-of-plane) wagging motions proved to be highly diagnostic. However, the strongest conformer selectivity is shown by backbone vibrations in the region 240-400 cm⁻¹, whose conformation-dependent coupling, make them a direct probe of backbone conformation (cf. e.g.^{319,320,362}). The investigations in the far IR region demonstrated that they could distinguish different (cf. e.g.^{320,387}) and even sometimes isoenergetic (cf. e.g.³²⁰) secondary structure motifs and help to perform unambiguous structural assignments, which were not possible on the amide A basis. In a later publication³⁶³, far IR spectroscopy was further applied to Ac-Phe-OMe and its dimer. These analyses confirmed the $\beta_1(g+)$ monomer conformation but found indications especially in the 100-400 cm⁻¹ region that the side chain conformation in the dimer is not identical in the two monomeric strands, but rather of the $\beta_1(g+)$ - $\beta_1(g-)$ type. This finding is in contrast to a previous assignment based on amide III measurements.³⁹⁷

The summarized aspects of the investigations on peptide systems performed in different spectral regions reveal the value of each of them for the structural analysis. The fact that certain regions as the far IR region have been investigated less frequently is of due to experimental equipment required for these measurements and due to a relative lack of adequate theoretical description. With regard to reliable structural assignments future developments will show to what extent the spectral information gained in the far IR region can become independent from additional information of other spectral regions.

7. Probing biological structures

The driving force to analyze peptide structures, namely the aim to understand and systematically influence their structure-functionality correlation, was already addressed in preceding sections. In Chapter 2.1 typical secondary structures and their characteristics were illustrated. In the following chapter the focus is laid on examples of archetypal, biologically relevant secondary structure motifs and their investigation by molecular beam spectroscopy (cf. Figure 13). The issue at stake is the existence of intrinsic forces, capable of driving the formation of these secondary structure binding motifs and backbone peptide folding in a molecular beam expansion, even in the absence of any molecular environment.

7.1. β -strands

The β -strand with its stretched structure (cf. Section 2) has its importance as unit of larger secondary structures as β -sheets or β -helices, with the first being further addressed in the following section.

Stretched β -strands are stabilized by weak C5 H-bonds between the NH and CO groups of the same amino acid in the sequence. This C5 interaction is intrinsically weak due to its non-linearity between H-bond donor and acceptor and the relatively large distance (about 230 pm in molecular beam investigations, e.g.^{142,372}). Therefore the C5 interaction always competes with stronger intramolecular hydrogen-bonding interactions like C7 H-bonds (H-bond distance around 200 pm, e.g.^{142,372}, further e.g.^{60,133,135,138,383} and following sections) or intermolecular interactions leading to aggregation. In contrast to the strongly H-bonded NH groups in e.g. γ -turns with frequencies below 3400 cm^{-1} the weakness of an isolated C5 interaction leads to an NH stretching frequency above 3430 cm^{-1} ; in combination with other C5 interactions values below 3430 cm^{-1} (starting at around 3405 cm^{-1}) are possible (cf. 6.1, 7.3). The capping of the polar N- and C-terminus (cf. Section 2.3 and 6.1) with protection groups can partly drive the structural preferences of short peptide systems towards stretched arrangements, especially if the N terminus is esterified and not amidated (cf. e.g.^{102,103,398}). A further factor that can decrease the preference of folded structures is their unfavourable entropic effect and the associated lower proportion of low frequency modes (compared to stretched isomers). This is especially true if the unfavourable entropic effects are not sufficiently compensated for by the enthalpic gain due to H-bond formation (cf. Section 9).

With the examples of Ac-Phe-OMe, Ac-Trp-OMe and Ac-Val-Phe-OMe prototypes of protected amino acids and small peptides with esterification on the N terminus were investigated in the Gerhards group (e.g.^{134,284,332,397,398}). For all of them a stretched β -strand arrangement was assigned. Ac-Phe-OMe was the most extensively investigated system, being analyzed not only in the amide A but also in the amide I-III region, allowing a detailed structural analysis even of the side chain orientation ($\beta_1(\text{g}^+)$)^{134,284,397}. Later on investigations were also performed in the far IR region.^{362,363} Beyond the monomer the homo dimer was investigated^{134,284,362,363,397} (cf. Section 12) as well as the aggregation with water as the most important biological solvent¹⁶⁰ (cf. Section 11). In case of Ac-Trp-OMe, the structural influence of the unprotected NH group in the indole side chain should be analyzed, which turned out to be important for the aggregation (cf. Section 12). In contrast, a $\beta_1(\text{g}^-)$ arrangement was found for the monomer. With Ac-Val-Phe-OMe the first IR/UV spectroscopic analysis on a peptide under isolated molecular beam conditions was performed, leading to the assignment of a $\beta_1(\text{g}^-)$ - $\beta_1(\text{g}^+)$ arrangement.³⁹⁸

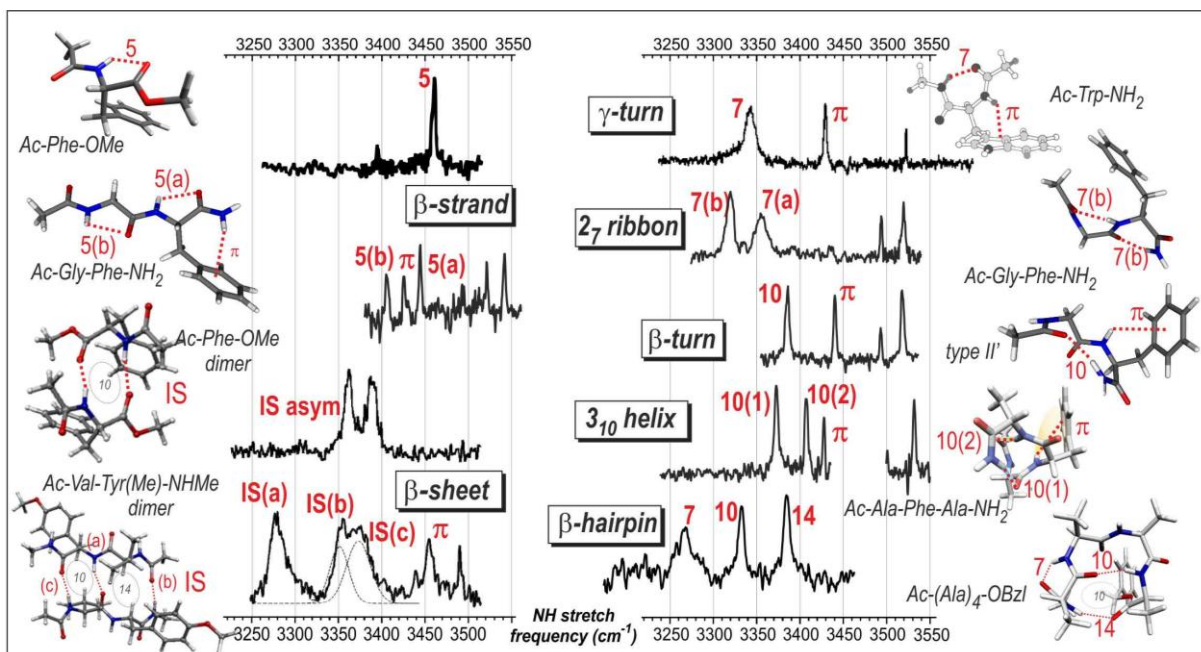


Figure 13: Representative examples of remarkable secondary structures of proteins observed in the gas phase from model molecules identified by their NH stretch region IR spectrum and the corresponding H-bonding content (in red). In the β -sheet and hairpin models, IS stands for interstrand HB and the rings formed by the interstrand HBs are indicated in grey. IR spectra are taken from the following references : Ac-Phe-OMe and its dimer¹³⁴; Ac-Gly-Phe-NH₂⁷⁵; Ac-Val-Tyr(Me)-NHMe dimer¹⁵⁷; Ac-Trp-NH₂¹³³; Ac-Ala-Phe-Ala-NH₂¹⁴¹. Other remarkable secondary structures (and partly their IR spectra) are illustrated in the corresponding subsections of this section. Ac-Trp-NH₂ spectrum reprinted with permission from Ref. ¹³³, copyright (2202) AIP Publishing. Ac-Phe-OMe dimer spectrum reprinted with permission from Ref. ¹³⁴, copyright (2002) PCCP Owner Societies.

By introducing a secondary amide group at the N-terminus of the protected amino acid phenylalanine the dipeptide model Ac-Phe-NHMe is created¹³⁵. The second amide group introduces the possibility for further structural isomers. This was confirmed by the measurements in the amide A and I,II region in which three conformers were assigned in comparison with DFT calculations. Though the $\beta_L(a)$ was the most dominant one, two γ -turn isomers, being close in energy (with about 250 cm⁻¹ relative to $\beta_L(a)$), were found as well. The different options for the monomer raised the question about the structural behaviour in case of aggregation either as a dimer¹³⁵ (cf. Section 12) or with water²¹⁹ (cf. Section 11).

Instead of using a secondary amide group the C-terminus can be protected with a primary one as in Ac-Phe-NH₂³⁸³. Comparable to Ac-Phe-NHMe the most stable conformer exhibits a β_L arrangement, followed by two γ -turns differing in the side chain orientation. The analysis of the Mons group also paid attention to NH $\cdots\pi$ interactions, which seemed to have a stabilizing effect in the most abundant stretched conformer. It was assumed that this interaction also had an impact on the photophysics of the conformers, which was later on analyzed by R2PI, LIF and pump-probe spectroscopy partly with ps-laser systems (details cf. ¹⁸¹). Ac-Phe-NH₂ was additionally investigated in its hydrated form²¹⁹ (cf. Section 11).

Basically the same structural behaviour as for the protected amino acid phenylalanine was also found for tryptophan: In analyses already performed in 2002, the Zwier group demonstrated for Ac-Trp-NH₂ and Ac-Trp-NHMe that for both substances stretched C5 structures as well hydrogen-bonded γ -turns (C7) were formed, being nearly isoenergetic (with regard to the accuracy of the performed DFT calculations)¹³³. In contrast, the absence of the second amide group and the replacement by an ester group in Ac-Trp-OMe leads to a complete stretched arrangement³³². For Ac-Trp-NH₂ and Ac-Trp-NHMe Zwier and coworkers observed a quite strong correlation between conformation and photophysical behaviour, which was further investigated^{169,203,296,364}. In that context it is important to mention that the IR-PTS as well as the HFS techniques (cf. Section 4.2) were both introduced on the example of Ac-Trp-NHMe^{203,296}.

The protected tyrosine has been investigated much less intensively. Ac-Tyr-NHMe was analysed in context with its aggregation to monosaccharides⁴⁰⁰. For the monomeric protected tyrosine conformer-selective IR/R2PI spectra revealed (in comparison with dispersion corrected calculation) a β_L and a γ -turn arrangement.

Ac-Gly-Phe-NH₂ and Ac-Gly-Phe-NHMe⁷⁵ have been part of a series of investigations^{60,75,217,386,387} on dipeptides in the form of Ac-Xxx-Phe-NH₂, Ac-Phe-Xxx-NH₂ and partly Ac-Xxx-Phe-NHMe. The structural flexibility of these systems of course increases enormously with the three amide groups leading to several conformers, with double γ -turn and β -turn structures. Nevertheless, a stretched arrangement with two C5 interactions as well as with an additionally stabilizing interaction between the π -system of the Phe ring and the NH₂ or NHMe group respectively (5-5- π) was found as a minor conformer. Regarding energy aspects (especially the Gibbs energy) the stretched arrangement can still compete with the folded structures.⁷⁵

As illustrated by the Ac-Xxx-Phe-NH₂ and Ac-Phe-Xxx-NH₂ dipeptides, the extension of the peptide backbone and the associated increasing structural flexibility lead to competitive situations between different conformers, making a final assignment sometimes difficult. This has been the case for the tripeptide model Ac-Val-Tyr(Me)-NHMe for which the existence of either a stretched β -strand or a β -turn was discussed^{102,388,401} (cf. Section 7.4.).

7.2. β -sheet-structures

The special interest in β -sheet structures as secondary structure originates from their medical relevance: pathogenic β -sheet structures are suspected to be responsible for a variety of infectious and non-infectious neurodegenerative diseases, among them BSE (bovine spongiform encephalopathy) of cattle, Scrapie of sheep and the Creutzfeldt-Jakob disease or the Alzheimer's and Parkinson's diseases (cf. Section 1 and 12).

On the molecular level, viewed by spectroscopy in molecular beams, the C5 interactions in β -strands are relatively weak, as already mentioned in the preceding section. They are therefore expected not only to compete with intramolecular H-bonding and thus other secondary structure motifs like turns (cf. Section 9) but also with intermolecular H-bonding to aggregation partners. The detailed discussion about the IR/UV laser spectroscopic molecular beam investigations on the aggregation behaviour of neutral amino acids and peptides, which are only performed by a few groups, is given in Section 12.

Among them the Gerhards group started with aggregates of protected amino acids, already having a certain preference for β -strand structures in their monomeric form, and continued up to whole β -sheet unit cells^{134,135,157,284,332,397}. Additionally a heterodimer composed of two different peptides was investigated¹⁴³. Later on the homo aggregation behavior was further analyzed in the far IR region, also with regard to small systems having the UV chromophore in the cap of N terminus.³⁶² The remarkable result with regard to these aggregates was the observation of naturally occurring secondary structure motifs without the influence of a biological environment.

7.3. γ -turns

Turns as structural elements mainly serve to change the direction in a polypeptide chain. By this, they make secondary structure units more compact and can also connect peptide units of different secondary structure.

The γ -turn is the smallest of all possible turns, forming an H-bond between the NH(*i*+2) and the CO(*i*) moieties within the peptide backbone leading to a seven-membered ring (C7 or just 7). The C7 structure unit is chiral, but independent of the chirality of the α -C-atom, in principle two kinds of turns are possible (cf. Figure 14): inverse γ_L and direct γ_D turns (sometimes denoted as 7_L and 7_D , respectively), which differ in backbone Ramachandran dihedral angles (cf. Section 2). For chiral residues one form is energetically strongly preferred, for L-configured α -C-atoms the γ_L structure, for D-configured α -C-atoms the γ_D structure. In amino acids with the naturally most abundant L-configuration the side chain is in an equatorial position relative to the C7 ring (C7eq) in a γ_L and in an axial position in the γ_D conformer (C7ax). Though hardly adapted in L-configured amino acids, the C7ax turn exhibits the stronger hydrogen bond with a NH...CO distance lower than 200 pm (e.g. ≈ 189 pm^{142,372}) in comparison to the corresponding C7eq turn with a value about 200 pm (e.g. ≈ 206 pm^{142,372}).

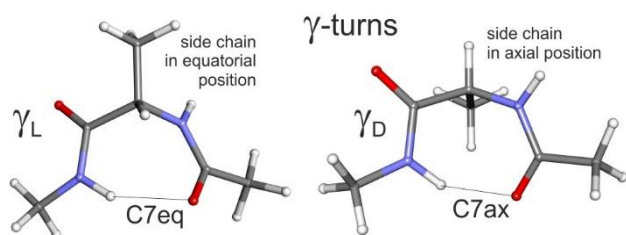


Figure 14: Scheme of the two types of γ -turns: the inverse (γ_L , left) and direct (γ_D , right) turns.

Among the intramolecular interactions in a peptide, C7 H-bonds are of significant strength leading to the strongly red-shifted, broadened NH-stretch vibration of the involved NH group below 3400 cm^{-1} . The exact frequency is sensitive to the individual amino acid being part of the C7 ring (cf. Section 6.1). For an L-configured amino acid forming an energetically highly preferred γ_L turn, it was demonstrated that sterically demanding side chains in equatorial position or strongly sterically constrained ones like Pro effect a relatively larger red-shift (cf. e.g. systematic measurements on Ac-Phe-Xxx-NH₂ peptide³⁸⁶). Red-shifts are found between about 3380 cm^{-1} for sterically less demanding side chains like Gly³⁸⁶ and 3330 cm^{-1} for Pro. For cases in which a γ_D position is possible with an axial side chain, red-shifts are found in that lower region around 3340 cm^{-1} (cf. systematic studies on the dipeptide Ac-Phe-Aib-NH₂ containing the achiral, non-natural α -amino-isobutyric acid³²⁸).

That γ -turns can become of relevance, as soon as a second amide group is present, was already mentioned in the preceding section for the amino acids protected with an amide group at the C-terminus (cf. Ac-Phe-NHMe¹³⁵). When the backbone is further extended γ -turns gain increasing importance as demonstrated in the series^{60,75,217,386,387} of Ac-Xxx-Phe-NH₂, Ac-Phe-Xxx-NH₂ (and partly Ac-Xxx-Phe-NHMe) peptides. For the Ac-Phe-Xxx-NH₂ peptides a preference for a β_L - γ_L conformation (towards a minor populated β -turn) was found (cf. e.g.³⁸⁶). If the amino acid sequence is reversed double γ -turns (2_7 ribbon structure) are revealed.^{387,388} They can be close in energy to the β_L - γ_L conformations so that sidechain-backbone interactions can decisively influence structural preferences for these two energetically close lying, competing secondary structure motifs³⁸⁷. Beyond, β_L - γ_L conformations 2_7 ribbon structures also compete with β -turns (cf. e.g.^{75,217,387} Section 9).

The 2_7 ribbon structure motif was even further extended in the tripeptide (tetrapeptide model) Ac-Leu-Val-Tyr(Me)-NHMe, which was analyzed with regard to protein aggregation in neurodegenerative diseases³⁸⁵ (cf. Section 1). A triple γ -turn (cf. Figure 15) was found to be less stable of the two conformers, with the middle γ -turn having a very weak hydrogen bond so that the corresponding NH stretching vibration is shifted above 3400 cm^{-1} . This example also showed with its most stable assigned structure that a γ -turn can also be combined with a β -turn.

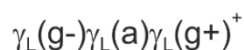
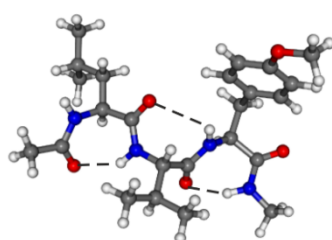
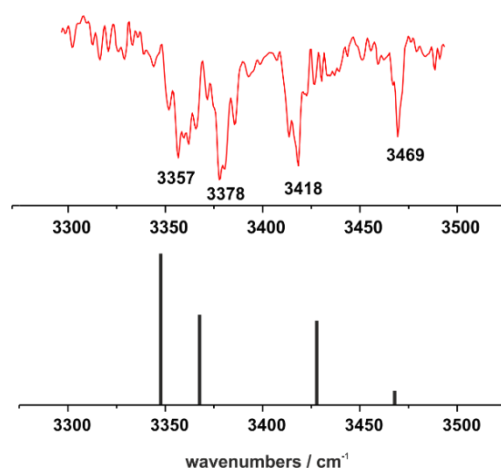


Figure 15: IR/R2PI spectrum and stick spectrum of the 2, ribbon isomer of the tetrapeptide model Ac-Leu-Val-Tyr(Me)-NHMe calculated at the B3LYP/6-31+G(d) level. Spectrum reprinted with permission from Ref. ³⁸⁵. Copyright (2007) PCCP Owner Societies.

7.4. β -turn

In a β -turn the hydrogen bond is formed between the amino acid i and $i+3$ in the backbone sequence leading to a ten-membered ring (C10 structures with $\text{NH}\cdots\text{CO}$ distance around 210-220 pm^{142,372}).

Four major types of β -turns exist denoted as I, II and I', II' (cf. Table 1 Section 2 and Figure 16), which are of special importance for peptide secondary structures since they can reverse the direction within a β -strand, so that the formation of an antiparallel β -sheet structure from a single peptide strand is possible^{68,100,388}. Types I and II mainly differ in a 180° reverse of the central amide bond. Type I' and II' can be considered as backbone mirror images of type I and II, respectively (the chirality of the α -C-atoms is preserved). The type I turns are the most abundant ones in peptides.

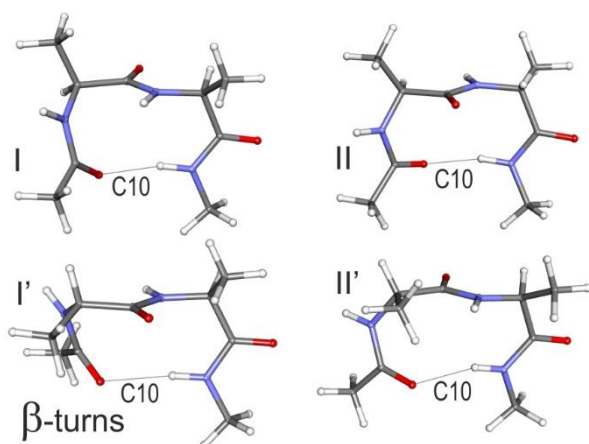


Figure 16: Scheme of the four types (I-II, I'-II') of β -turns: In the figure the acceptor carbonyl groups are pointing backwards for I and II, and forwards for I' and II'. Primed backbones are mirror images of the corresponding I and II backbones, with the chirality of the amino acids being preserved.

With regard to molecular beam investigations a series of studies with Phe-containing dipeptides forming β -turns exist^{217,292,383,384,387,389,392}. The stability of the different types of turns sensitively depends on the chirality of the amino acid residues within the C10 ring³⁸⁹. On the example of N-Ac-Xxx-L-Phe-NH₂ (Xxx = L- and D-Ala or Aib) it could for example be demonstrated that the heterochiral species shows a strong preference for a certain type of turn (here: type II'), differing from the type I of the homochiral species. However, the turn motif still competes with open, strand-like structures. Regarding the type of β -turn it was found that the amide A region, though being very sensitive to the H-bond strength, is not such a good sensor for the precise assignment in terms of type. In contrast, the amide I and II region seems to be more characteristic for the individual type of turns^{399,402}.

These structural motifs of β -turns have a weaker H-bond than the γ -turns, which is testified by a lower red shift of the corresponding NH stretching vibration, typically located in the region around 3400 cm⁻¹ (also cf. Section 6.1). Due to this intrinsic weakness β -turns always compete with other structural motifs (details cf. section 9): among them conformers having multiple H-bonds like double γ -turns (e.g. Ac-Xxx-Phe-NH₂ cf. e.g.^{75,217,387}) or with C5 and C7 interactions additionally stabilized by interactions with the aromatic side chain (e.g. Ac-Phe-Xxx-NH₂ peptides³⁸⁶). However, in comparison with these structural motifs, the β -turns can profit from the lower backbone strain within a C10 ring^{75,387}. Additionally, β -turns are frequently stabilized by further interactions arising from the side chain H-bond acceptor groups (e.g. NH \cdots S H-bond in Ac-Phe-Met-NH₂ and Ac-Met-Phe-NH₂⁴⁰³ or NH \cdots π interactions, cf. e.g.^{377,384,387,389,392,404}). Furthermore, strong side chain-side chain interactions, like dispersions dominated $\pi\cdots\pi$ interactions between neighboring aromatic chromophores, play a decisive role in stabilizing a β -turn backbone conformation (cf. e.g.^{292,377,384}).

Nevertheless, it sometimes happens that not only the determination between different types of turns but even between different conformers is delicate: Occasionally, different structural motifs (accidentally) lead to enormously similar IR spectra as this has been the case for Ac-Val-Tyr(Me)-NHMe (cf. Figure 17). Since in the R2PI spectrum only the electronic origin as prominent transition was observed the presence of one dominant conformer was assumed and the existence of either a stretched β -strand or a β -turn was discussed^{102,388,401} partly

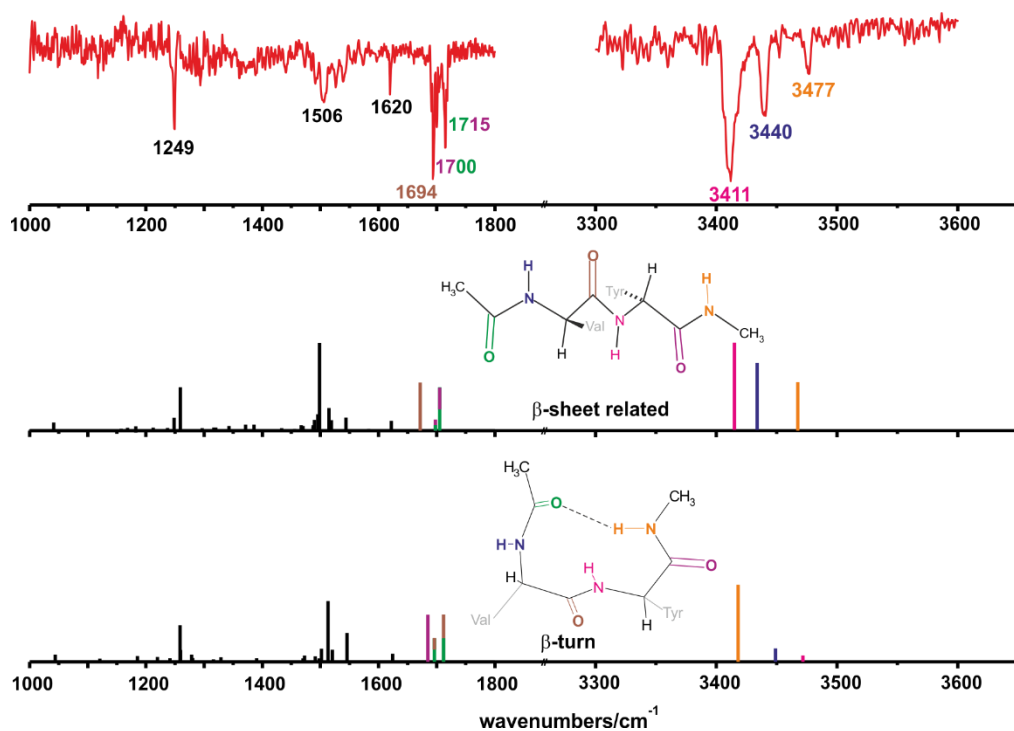


Figure 17: IR/R2PI spectrum of Ac-Val-Tyr(Me)-NHMe in the amide A, CO stretching¹⁰² and fingerprint region.⁴⁰¹ Direct comparison of the calculated stick spectra (B3LYP/6-31+G(d)) for a β_1 and β -turn conformer exhibiting their resemblance; the vibrational assignments are colour-coded. The CO-stretching vibrations are stronger coupled here than the NH oscillators and even in the harmonic approach it is partly difficult to

assign vibrations in the amide I region to only one CO oscillator leading to the partly mixed colour coding of the vibrations.

also in comparison with Ac-Val-Phe-NHMe³⁸⁸. Though the experimental IR spectra of the latter exhibited a spectral gap between about 3460-3510 cm⁻¹, in which one NH stretching mode was calculated for the β -turn conformers, the remaining calculated vibrations of the β -turn and β -strand motifs still differed sufficiently. As a consequence a clear discrimination could be performed and the assignment of a β -turn instead of a stretched arrangement was unambiguous for the Phe containing dipeptide. In contrast, the calculated IR spectra of the tyrosine-containing dipeptide were very similar for the β -turn and β -strand conformer. This was the case for the whole experimentally measured region, reaching from the amide A (without a gap), via the amide I, II region finally down to 1000 cm⁻¹ (cf. ^{102,401}). A slightly better fit to the experimental data might be seen for the β -turn in the calculated vibrational pattern of CO stretching modes. However, an unambiguous decision for one of the two structures remains difficult. Thus, Ac-Val(Tyr)-Me-NHMe could be one of the examples, in which the far IR region might help to finally decide between these two structures (also cf. Section 6.2).

When the backbone chain is further extended to 4 amide groups a double β -turn can be formed with the 3_{10} helix motif consisting of two identical β -turns (type III - type III¹⁴¹ or very close to type III⁷⁶). A first double β -turn was found for Ac-Phe-Gly-Gly-NH₂, being the most dominant isomer among five. It showed a distinctively different IR spectrum in the amide A region compared to the other isomers also forming extended H-bonds but containing at least one γ -turn¹⁴⁰. To further discriminate it from combined β - γ -turns and distinguish the different double β -turns, the amide I and II regions were measured allowing the assignment of a type II – type I' conformer. A further double β -turn (type III – type I) was revealed for the neutral tetrapeptide model Ac-Ala-Phe-Ala-NH₂¹⁴¹. As characteristics (in comparison with a normal type I turn) the NH₂ group was involved in a quite weak H-bond leading to a blue shift of the associated antisymmetric stretching mode, which was considered to be a signature of the helical form. The helical arrangement was found to be additionally stabilized by NH \cdots π interactions. Two years later, Ac-Aib-Phe-Aib-NH₂ with the synthetic amino acid aminoisobutyric acid, known to prefer 3_{10} helical structures in condensed phase, was analyzed in comparison³³⁰. The preference for a type III – type III arrangement could be demonstrated for the gas phase measurements. The tendency of the Aib amino acid to support 3_{10} helix formation was further analyzed in the Zwier group⁷⁶. Even in Z-Aib-OH and in Z-(Aib)₂-OH, which are too short to form a β -turn with a C10 H-bond, the assigned conformers exhibit dihedral angles close to those of the 3_{10} helix. When further Aib moieties are added (Z-(Aib)₄-OH) the most abundant conformer is a 3_{10} helix with two free and two NH groups H-bonded in a C10 ring (f-f-10-10). What is remarkable about the helical arrangement is the large dipole moment (13.7 D) in the gas phase, despite the absence of a stabilizing polar (solvent) environment. Other examples in literature are known like Z-(Gly)₅-OH and Z-(Gly)₅-NHMe⁷⁴ preferring helical structures in the gas phase (so called C₁₄/C₁₆ helices formed of alternating C14 and C16 hydrogen-bonded rings) with a quite small overall dipole moment. The minimization of the dipole moment (under isolated molecular beam conditions) was seen as the driving force to form these helices with mixed ring size, which had not been observed before for pure α -peptides⁷⁴. Therefore, the question arises if the tendency for 3_{10} helix formation can be further retained in the Aib-peptides when the backbone is further elongated effecting a further increase of the overall dipole moment⁷⁶. That the stabilization of the macrodipole created by the alignment of amide groups in a helix is a central issue under isolated conditions was also realized for charged peptide systems. Rizzo and coworkers analyzed a series of alanine polypeptides⁴⁰⁵⁻⁴⁰⁸, known to be good α -helix formers. These systems contained a phenylalanine as UV chromophore and a lysine at the C-terminus, whose protonated ammonium group helped to stabilize the overall dipole moment⁴⁰⁵.

A further aspect to be pointed out is the possibility to combine different turns in a direct sequence. This was already mentioned above for the tetrapeptide model Ac-Leu-Val-Tyr(Me)-NHMe, whose most stable assigned isomer presented a γ - β conformation³⁸⁵. A β - γ conformation was further found for Z-Pro-Leu-Gly-NH₂, which was analyzed in comparison with Z-Pro-Leu-Gly-OH⁶¹. With an additionally NH \cdots π stabilized double γ -turn the latter preferred a different structure. Especially the free carboxyl group of this structure offers a binding site for aggregation giving an idea why Pro-Leu-Gly sequences with different end groups at the C terminus exhibit different inhibition activities toward the human skin collagenase.^{61,409,410}

7.5. α -turn

α -turns, in which 5 amino acid residues are involved, have rarely been reported for molecular beam spectroscopy. The only known example in literature is the pentapeptide Phe-Asp-Ala-Ser-Val which was investigated by de Vries and coworkers applying IR/UV hole burning spectroscopy⁴¹¹. Independent from the UV transition, several identical IR spectra were measured indicating the formation of only one conformer or conformer family in the jet. The experimental IR data already allowed the conclusion that the hydroxyl group of the serine side chain must be hydrogen-bonded whereas the OH groups of the two carboxyl units (terminal one and Asp side chain) are free. The best description of the measured IR spectrum is finally given by an α -turn having free COOH groups and a hydrogen-bonded serine side chain. The (tentative) assignment was based on the best match between experimental and calculated frequencies though the α -turn did not belong to the most stable structures.

7.6. The Asx turn

A quite special turn, since the hydrogen bonds are not formed between two amide groups of the backbone, but a side chain amide group participates instead, is the so called Asx turn¹⁶². This turn is found in condensed phase measurements (IR, NMR, crystallography) for a special peptide sequence Asn-Xxx-Ser/Thr (with Xxx \neq Pro) in which the amide CO group of the Asn side chain forms an H-bond to the NH backbone group of the Ser (or Thr respectively). By this a ten-membered ring is formed somehow comparable to a kind of backbone β -turn. This peptide sequence gained scientific attention since in eukaryotic N-linked glycoproteins it was found that a certain glycan (Glc₃Man₉GlcNAc₂, Glc: glucose, Man: mannose) was always (enzymatically) attached to the NH₂ group of the Asn in this Asn-Xxx-Ser/Thr motif. Thus the question emerged in how far the preferred structure of that peptide sequence could influence reactivity of the Asn side chain towards glycosylation. In that context the already mentioned condensed phase measurements but also spectroscopic investigations under isolated molecular beam conditions were performed by Cocinero et al.¹⁶². The gas phase studies included Ac-Asn-Gly-Ser-NH-Bzl (Bzl: benzyl) as well as two 'mutants' of this sequence namely Ac-Gln-Gly-Ser-NH-Bzl (with Gln also having an amide side chain) and Ac-Asn-Pro-Ser-NH-Bzl (with Pro normally excluded from the naturally occurring Asx sequence). The gas phase global minima structures of these three peptide systems differ distinctively from each other. One of the main aspects was that (in contrast to the condensed phase) the Asx turn could not be found for Ac-Asn-Gly-Ser-NHBzl, but an open, S-shaped backbone structure was assigned instead. This discrepancy was explained by the high dipole moment of the Asx turn motif that could be well stabilized by polar solvents but not under isolated gas phase conditions. As for the helical arrangements referred to above we again have to keep in mind the more difficult stabilization of polar structures under isolated conditions, when eventual differences between condensed phase and gas phase are discussed.

7.7. β -hairpins

A β -hairpin is defined as a structural motif in which two adjacent β -strands oriented in an antiparallel direction are linked by a short loop of two to five amino acids. They belong to the larger peptide structural motifs making them more sophisticated to be studied by molecular beam spectroscopy. Nevertheless, Mons and coworkers could reveal β -hairpin conformers for tetra- and pentapeptide systems. Investigations on the structural behaviour of protected alanine containing peptides were performed, among them Ac-(Ala)₄-O-Bzl⁷² (Bzl: benzyl) and Ac-(Ala)₅-O-Bzl, Ac-(Ala)₃-Phe-NH₂ and Ac-D-Ala-Phe-Gly-D-Ala-NH₂.⁷³ The experimental IR spectra were analysed in comparison with structures calculated at the DFT-level including dispersion corrections⁷². All of the analyzed peptides exhibit at least one conformer with a β -hairpin arrangement including three⁷² or four hydrogen bonds: a C14 and a C10 hydrogen bond and additionally one^{72,73} or two⁷³ C7 H-bonds being located 'outside' of the β -hairpin structure. For Ac-(Ala)₄-O-Bzl three conformers with β -hairpin structures are assigned which differ in the orientation of the OBzl group⁷² (with the most stable one dispersion stabilized by contacts between the Phe ring and methyl groups). In case of Ac-(Ala)₅-O-Bzl two such structures are found⁷³. For Ac-(Ala)₃-Phe-NH₂⁷³ only one β -hairpin structure was found, whose mirror image represents the (β -hairpin) backbone structure assigned to Ac-D-Ala-Phe-Gly-D-Ala-NH₂.⁷³ Nevertheless, among the four investigated peptide systems, Ac-D-Ala-Phe-Gly-D-Ala-NH₂ is the only peptide which exhibits a second conformer not presenting a hairpin⁷³. It is composed of a C14 interaction, two 'crossing' C10 H-bonds within the C14 ring, one

γ -turn out of this C14 ring and a stabilizing NH $\cdots\pi$ interaction. During the studies of all of these peptide systems the authors realized that the conformational distribution at 0 K is not reflected in their experiment,⁷³ in which the sample molecules were evaporated by laser desorption. Instead, conformers being energetically and entropically preferred at higher temperatures (e.g. 300 K) are finally assigned in comparison to the measured IR spectra. Thus, the conclusion was drawn that conformational preferences are ‘frozen out’ in the molecular beam expansion and again peptides with a large conformational space relax to a few global minima. As already briefly mentioned before, Rizzo and coworkers found helical structures for Ala-rich oligopeptides, charged in the form of a protonated lysine side chain at one end⁴⁰⁵⁻⁴⁰⁸. This is in contrast with the findings in the neutral systems but it illustrates once again the structural flexibility of even small polypeptides and their capacity to adapt to the given requirements, like charge or dipole moment stabilization.

8. Probing the changes induced by specific residues on the local conformation



8.1. Documenting the effect of specific residues on the secondary structure through the NH stretch probe

Structural details of the remarkable conformations described in Section 7 depend upon the residues present in the sequence, which justifies the diversity of the proteinogenic amino acids introduced by nature. Gas phase studies have contributed to document this issue, especially on three structures: β -strand-like extended forms, γ - and β -turns. Most of the time, changes on the backbone structure remain modest, which justifies to keep an outline based on backbone secondary structures.

8.1.1. β -strand-like extended forms

Aromatic residues

The NH- π interactions, in which a NH moiety points towards a π ring of an aromatic residue, with NH- C distances of the order of 250 pm,³³³ are ubiquitous in gas phase peptides. In practice, if their formation requires a limited backbone torsion, they will form spontaneously due to the enthalpic gain they provide under an isolated environment. In non-covalently bound species, they enable anchoring a peptide to an aromatic moiety, which can thus serve as a UV chromophore.¹⁶⁴ In chain models, they are already present in the capped aromatic amino acids, where they contribute to control the rotamer distribution. Thus extended backbone conformations are greatly stabilized by an aromatic side chain adopting an *anti* conformation, which enables an interresidue NH $i+1 \rightarrow \pi$ H-bond formation.^{60,133,135,333} It is the most stable structure of these capped amino acids. Even structural details such as conformations differing by the flip of the aromatic side chain, when this latter is not symmetric (Trp), can be distinguished by small spectral shifts.¹³³ These gas phase observations echo protein structural data extracted from crystallized protein surveys, which provide evidence for a significant prevalence of these interresidue bonds between an aromatic residue i and its next neighbor $i+1$.⁴¹² The extended local structure is often retained in capped dipeptides containing an aromatic amino acid, where it acts as a scaffolding on which other secondary structures can be grafted.^{81,82,328,386} In this line, fully extended backbones of the type 5-5- π were observed in capped Ala-Phe and Gly-Phe sequences.⁷⁵ In these latter conformations, the frequency of the 5 band depends on the position of the NH concerned (1st or 2nd residue), without any clear interpretation so far.

Owing to the important dispersive contribution in these interactions, they also tend to be stronger when the aromatic moiety is excited in its $\pi\pi^*$ state: the corresponding red shift upon electronic excitation thus provides an elegant assignment tool when excited state IR spectroscopy is also measured.³³³

Methionine : 7 δ interresidue backbone \rightarrow SC interaction

Methionine, with its long side-chain having a proton acceptor S atom in δ -position, is prone to form local bb-SC 7 δ interactions with the NH $i+1$ group of the next residue (interresidue HB, cf. Scheme 3). The Z- and amide capped Met amino-acid gives rise to an extended 5 backbone combined with a 7 δ interaction (unpublished

results in Mons group). In the Ac-Met-Phe-NH₂ dipeptide analogue, one of the conformations (B) initially assigned to a 5-7^δ-7eq form,³⁹² has finally recently been reassigned to a 5-7^δ-7ax conformation (unpublished results in Mons group). In this conformation, the backbone is locally extended, with a 7^δ H-bond in the 3340 cm⁻¹ frequency range, which additionally stabilizes the extended conformation.

Cysteine residue: 6^γ interresidue backbone → SC interaction

The shorter side chain of cysteine, compared to Met, gives rise to a shorter 6^γ interresidue H-bond. This was observed in the capped (Z/-NH₂) amino acid Cys in combination with an extended 5 backbone (5-^γ6 form), the SH group not being an H-bond donor (cf. Figure 18.a).³⁹⁰ The corresponding 5 interaction is found to be stronger as the same form in the Ala residue, objectifying cooperative effects between both interactions.

With serine, this extended backbone form is not observed,⁴⁹ presumably because of a weaker NH...O interresidue interaction due to the shorter van der Waals radius of the O acceptor. As a result, the extended backbone form is disfavoured compared to the folded one.^{80,83,156}

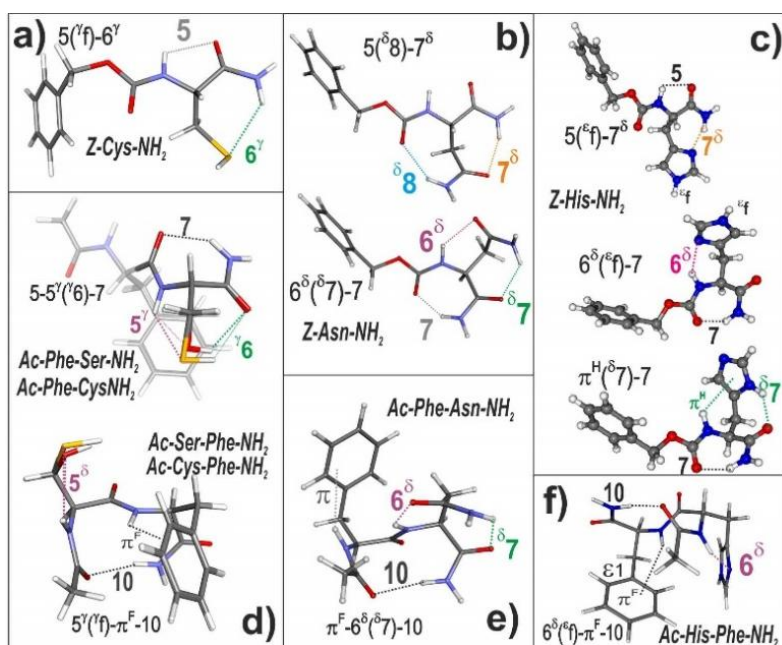


Figure 18 Conformational H-bonding networks in selected polar residues in capped peptides mimicking a protein chain. The conformations depicted have been described experimentally and their chemistry obtained by quantum chemistry. The corresponding structures are taken from Ref. a) ³⁹⁰; b) and e) ⁸²; c) and f) ⁸¹; d) ⁸⁰. Conformations are identified by the sequential list of H-bonds, in which the backbone NH groups are involved, together with, between brackets, the SC→bb H-bonds on the His residue.

Asparagine residue: conformational locking with simultaneous inter- (8^δ) and intra-residue (7^δ) bb-SC HBs.

With its short side chain bearing a terminal carboxamide group, asparagine (Asn) gives rise to intricate H-bonding pattern involving both side chain and local backbone. The small size of the Asn side chain matches the local H-bonding network of an extended backbone and noticeably provides a strong anchoring of the side chain to the local backbone structure, with the formation of a 5(8^δ)-7^δ local H-bonding network, forming a continuous chain of HBs, where each amide bond is both donor and acceptor, and where the extended backbone feature is preserved (cf. Scheme 3 and Figure 18.b). The carboxamide group being a better H-bond acceptor than donor, the bb→SC H-bond (7^δ) is the strongest (see Sections 6.1.3 and 6.1.4), in agreement with both the spectral shifts⁸² and the calculated H-bonding distances.^{79,82} It should however be noticed that the distances calculated for such an intricate pattern should be taken with caution owing to the somewhat disappointing agreement found for the frequency predictions using methods, which usually provide satisfactory results. This illustrates the challenging character of the description of these intertwined bonds.

Glutamine residue : intra-residue (8^δ) bb-SC HB

With the longer side chain of glutamine, the same types of side chain donor and acceptor H-bonds as previously could be expected, with HB lengths incremented by one unit (cf. Scheme 3). However, optimized side chain donor and acceptor H-bonds can no longer occur simultaneously, leading to H-bond strengths different from those of Asn: only extended backbones stabilized by strongly red shifted (by $\sim 350\text{ cm}^{-1}$) 8^δ bonds are mainly observed ($5^{(\epsilon f)}$ - 8^δ forms) with (Z-, -NHMe) caps.⁷⁸ The use of partly capped models (Z-) with a C terminal COOH leads to an acidic OH bound to the side chain through an OH – O_{GluSC} H-bond irrelevant to the description of a protein chain fragment. A second conformer, however, provides an example of $5^{(\epsilon 9)}$ Glu local H-bonding.

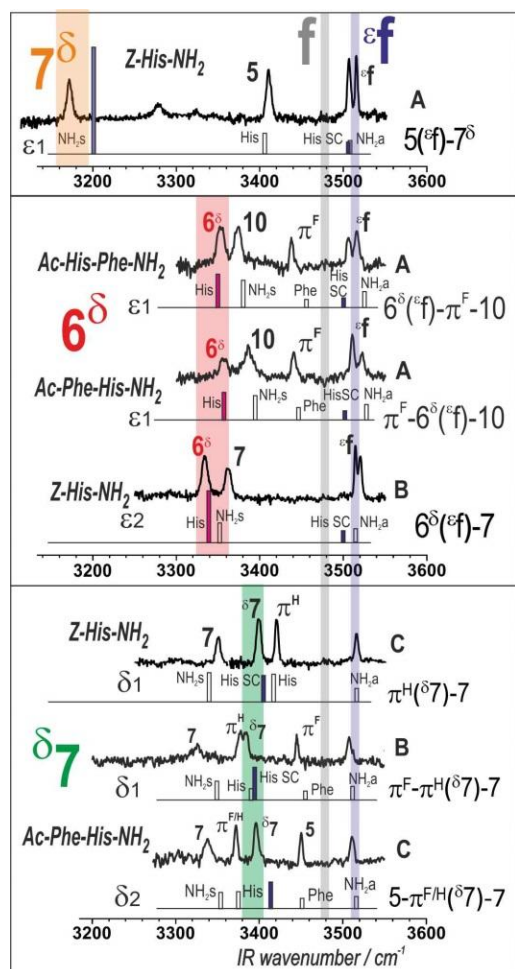


Figure 19: Conformer-selective IR spectroscopy of a His residue in several model molecules. Conformational H-bonding networks in selected polar residues in capped peptides mimicking a protein chain. Conformations are identified by the sequential list of H-bonds, in which the backbone NH groups are involved, together with, between brackets, the SC→bb H-bonds on the His residue. The theoretical NH stretch IR absorptions (B97-D3 level of theory) are depicted as stick spectra, labelled by the corresponding NH bond. Cf. Figure 18 and section 2 for the H-bonding terminology. Reprinted with permission from Ref. ⁸¹. Copyright (2017) PCCP Owner Societies.

Histidine: inter- (8^δ) / intra-residue (7^δ) and tautomerism

Histidine shares many features with the Asn residue, namely the size/length/polar character of its imidazole side chain, with both donor and acceptor sites. It also exhibits additional complexity, due to the existence of two tautomeric neutral forms, analogs to the 4- and 5-methylimidazole molecules. The main difference with Asn, however, stems from the facts that i) the side chain cannot act simultaneously as H-bond donor and acceptor (if one excludes the presence of π H-bonds), and ii) the local donor/acceptor characters depend on the tautomeric form adopted by the side chain. As a result, tautomerism strongly controls the H-bond network due to the much stronger proton acceptor character of the imidazole ring nitrogen, that bears the N lone pair.

Among the stable local networks expected, besides the most stable, γ -turn folded structures (see Section 8.1.2 below), a unique extended form $5^{(\epsilon f)}$ - 7^δ is observed (ϵ tautomer; cf. Figure 18.c)⁸¹; its counterpart with the other imidazole tautomer (δ) being much higher in energy. In strong similarity with the 8^δ bond of the extended

capped Gln, IR spectroscopy (cf. Figure 19) indicates that the 7^δ H-bond is also one of the strongest ever observed in these systems, with a red shift of the order of 350 cm⁻¹.

It should be noted that in all these extended forms, as a consequence of the constraints exerted by the side chain on the backbone, the 5 interaction is stronger than its counterpart in apolar residues, such as Ala, as evidenced by its NH stretch frequency found in the 3400-3430 cm⁻¹ range.

8.1.2. γ -turns

The 7 H-bonds in inverse and direct γ -turns have been widely documented in the gas phase, in particular through the IR NH stretch diagnostics together with quantum chemistry calculations.

Alkyl residues

Its dependence on the nature of the alkyl side chain has been early investigated from a series of capped dipeptides, where a Phe residue plays the role of a scaffolding from which an inverse γ -turn develops.³⁸⁶ In the non-cyclic side chain residues (Gly, Ala, Val), the HB is found to depend modestly upon the SC size, with HB red shifts in the 110-120 cm⁻¹ range; these slight differences are assigned to close contact interactions between SC and backbone, which distort the backbone, and correlate to changes in the HB distance, as illustrated by the two SC rotamers observed with valine.³⁸⁶ In the case of the proline residue, the red shift is larger and reaches 150 cm⁻¹, due to the stronger constraint imposed by the cyclic pyrrolidine ring.

Aromatic residues

In inverse γ -turns characterized by 7eq HBs, the forms observed exhibit most of the time an intraresidue NH- π HB made possible by a suitable orientation of the aromatic SC (N-C ^{α} -C ^{β} -C ^{γ} χ_1 dihedral), a single *gauche+* form with capped Trp,¹³³ *gauche+* and *gauche-* (*g+* and *g-*, in short) conformers with capped Phe^{60,135,333}. Most recently, a very minor *anti* conformer of a capped Phe (Ac-Phe-NH₂) has eventually been found (cf. Figure 10). The strength of the 7eq HB is found to depend significantly upon the residue and on the SC orientation, e.g. the frequencies of the *g+*, *g-* and Phe conformers are found at 3345, 3353 and 3374 cm⁻¹, respectively. (cf. Figure 10) In connection to this, direct γ -turns (characterized by 7ax HBs) also seem to exhibit a singular behavior, since despite their backbone is a mirror image of that of the inverse turns, they systematically exhibit a more red shifted NH stretch frequency (by ~35 cm⁻¹), as testified by spectroscopic data on the Aib residue.³²⁸ A very recent theoretical analysis of the HBs in peptides, carried out using the NBO diagnostics,³⁷² has rationalized these observations. Whereas all these turns correspond to the same approach of the NH donor amide to the acceptor, the intrinsic backbone flexibility (controlled by hyperconjugative effects - HC) and side chain-backbone interactions (through close contacts and steric hindrances) are crucial in determining the HB distance and hence the strength of the 7 HB. In particular the weaker HB in 7eq (compared to the 7ax) is assigned to the presence of intrabackbone HC effects, which tend to keep the NH and CO bonds of the 7 bond parallel to the C ^{α} H bond in axial position, and therefore opposes the formation of a strong 7 HB. The absence of such an interaction in direct γ -turns, where the C ^{α} H bond is in an equatorial position (or absent, like in residues with disubstituted α carbons, e.g., the aminoisobutyric acid) leads to a stronger 7 bond.³²⁸

Serine, Cysteine, Selenocysteine

Both serine and cysteine exhibit a short polar side chain (CH₂-OH and CH₂-SH respectively), with both, a donor and acceptor character, potentially giving rise to simultaneous bb \leftrightarrow SC local intraresidue interactions stabilizing an inverse γ -turn (5 ^{γ} (γ 6)-7 local form), in contrast to extended forms, where the absence of folding hampers the simultaneity of bb-SC interactions (cf. Figure 18.d). Serine acts as a donor with a significant γ 6 H-bond to the carbonyl of the same residue, whereas one of the Ser O lone pairs acts as a weak acceptor for a 5 ^{γ} H-bond, as evidenced from IR spectroscopy of capped Phe-Ser and Ser-Phe sequences.^{80,83} This subtle balance is reversed for cysteine (capped Cys³⁹⁰ and capped Phe-Cys and Cys-Phe sequences^{80,83}), due to the weaker donor character of the SH group : the resulting stronger 5 ^{γ} H-bond is testified by the larger red shift of the Cys NH stretch frequency (cf. Table 6, Section 6). The SH donor character is only documented by quantum chemistry, due to the difficult spectral range in which the SH stretch frequency falls (2600-2700 cm⁻¹). Large

changes, up to 40 cm^{-1} ,⁸⁰ in the NH stretch frequencies of the 7 HBs compared to simpler residues (Gly or Ala) indicate that significant geometry changes occur upon formation of the 5^{γ} H-bond. In cysteine, substitution of sulfur by a selenium atom comforts the interaction balance present in Cys, with a still stronger 5^{γ} interaction, even if the strength remains quite modest (red shift $\sim 55\text{ cm}^{-1}$), in comparison with other bonds.¹⁵⁶

Asparagine, Glutamine and Histidine residues

As with extended backbones, the Asn side chain also matches the local H-bonding network of inverse γ -turns leading to a remarkable, strong anchoring of the side chain to the local backbone structure, with a $6^{\delta}(\delta^{\delta})$ -7 local H-bonding pattern (found in capped (Z;-NH₂)⁸² and (Ac;-NHBn)⁷⁹ Asn – cf. Figure 18.b - and in the capped PheAsn sequence⁸²). The bb \rightarrow SC H-bonds (6^{δ}) are found to be stronger than the SC \rightarrow bb bonds (cf. Table 6, Section 6), in agreement with both the spectral shifts⁸² and the calculated H-bonding distances.^{79,82} With the longer side chain of glutamine, γ -type folding appears as an exception favoured by extra interactions: in one of the conformers of the Ac-Gln-NHBn molecule, a π H-bond occurring between the Gln side chain amide and the NHBn cap enables the formation of a compact $7^{\delta}(\delta^{\delta}-\pi^{\text{Bn}})$ -7 network.⁷⁸ Likewise, several conformations observed are additionally stabilized by opportunist Gln amide- π interactions, made possible by an aromatic environment.^{77,78} As in extended backbones, the histidine side chain proton acceptor and/or donor sites match the γ -turn structure, whatever the His tautomer considered. In capped His as well as in the capped (Ac;-NH₂) Phe-His sequence one observes, in the order of decreasing stability, two inverse γ -turns, $\pi^{\text{H}}(\delta^{\delta})$ -7 and $6^{\delta}(\epsilon^{\text{f}})$ -7, due to different imidazole tautomers (δ and ϵ resp.).⁸¹ IR spectroscopy however indicates that the 6^{δ} H-bonds are the strongest H-bonds as expected from the presence of the imidazole N lone pair, followed by the alternative intraresidue 7^{δ} bond, present in the other tautomer (cf. Figure 19). In both cases, the 7 H-bond is found to be enhanced compared to the same backbone in the Ala residue.

8.1.3. β -turns

Aromatic residues

In large peptides, NH- π H-bonds of various strengths can be observed depending on the NH environment, especially with β -turn backbones where an aromatic residue occupies the second central position ($i+2$ position in biochemistry terminology), due to a favorable orientation provided by type I conformations.^{333,384,387,389} Especially red shifted bands are found for a backbone NH sandwiched between two aromatic groups; the corresponding stabilization contributes to the occurrence of high energy conformations.³⁷⁷

Proton acceptor and donor side chain residues

The local fold at the residue scale in both the central positions of a type I β -turn remains qualitatively close to that of a γ -turn. In the same way as the γ -turn is able to accommodate one or two local bb-SC bonds due to the presence of proton donor/acceptor residues, gas phase β -turns with such a residue also exhibit moderate distortions of their backbone geometry. This illustrates the robustness of this secondary structure, in line with the detection of similar bb-SC local bonds in the protein β -turn structures in presence of such residues, as well as the relevance of gas phase data to account for structures in the inner core of proteins.^{81,82}

Cysteine

The local 5^{δ} H-bonds are observed in capped dipeptides in β -turn secondary structures, whatever the central position (first or second) occupied by the residue in the turn (cf. Figure 18.d).⁸⁰ The insensitivity of the IR spectral signature of the 10 bond suggests that the turn backbone is not significantly affected by the presence of these bb-SC interactions. Like in the case of extended backbones, the β -turn arrangement forbids the formation of a secondary $^{\gamma}6$ H-bond.

Histidine and methionine

In His-containing chain model dipeptides (cf. Figure 18.f), the same intraresidue 6^δ bonds as in γ -turns are present and contribute to stabilize the β -turn, with moderate changes in the 10 HB strength (cf. Figure 19) ; they occur with ϵ -type tautomers of the imidazole ring.⁸¹ A survey of the angular distribution of His residues in γ - and β -turn structures of crystallized protein structures reveals that these local interactions persist in compact hydrophobic regions of proteins, whereas, alternatively, distortions from the gas phase structures can be interpreted by a water-mediated local anchoring of the His side chain to the turn backbone.⁸¹

With methionine, the 6^δ H-bonds, which are not strong enough to enable γ -turns to challenge extended forms in capped Met (unpublished results from Mons group), are present in capped dipeptides and contribute to stabilize the β -turns.³⁹²

Asparagine and glutamine

The anchoring structure of the Asn with its two (6^δ and 7^δ) bb-SC bridges observed in γ -turns is at least partially retained when Asn occupies the first or the second central part of a β -turn ($i+1$ and $i+2$ positions), the strongest SC-bb bond (6^δ) being preserved whereas the weaker 7^δ adapts itself to the conformation or vanishes.^{79,82} As far as the biological pertinence is concerned, these intrinsic anchoring structures are observed in crystallized proteins when Asn is located in a turn embedded in a hydrophobic environment.⁸²

A similar observation is made in the capped Ala-Gln sequence. An intraresidue 7^δ HB stabilizes the turn,⁷⁸ with however two major differences with Asn: the strength of the 10 HB is strongly enhanced by ca. 50 cm^{-1} and the Gln SC NH_2 group, not properly oriented to establish a 8^δ HB, does not interact with the backbone, but gives rise to a π HB with the nearby aromatic cap of the model molecule studied. The same type of local structures is observed, but repeated, in Gln-Gln sequences, related to the polyglutamine sequences involved in the Huntington's disease, without direct interactions between the Gln side chains but again with a stabilizing π HB with the cap.⁷⁷ As for Asn, examples of protein sequences sharing the same 7^δ HB feature on the Gln residue as the gas phase structures could also be found.⁷⁸

8.1.4. Uncapped peptides

The intricate H-bonding pattern induced by the presence of polar short side chains in amino acids, observed in microwave experiments, is similar to that previously described on capped peptides. For example, a locking effect has been reported for Asn⁴¹³, which shows a unique $^{\text{C}}\text{S}^{\text{N}}$ folded (A1) conformer, accompanied by 6^δ and 7^δ SC-BB H-bonds. As a matter of fact, the HB distance obtained from calculations (supported by the high-resolution experiment) confirms a shrinkage of the $^{\text{C}}\text{S}^{\text{N}}$ H-bond distance from 196 pm in Ala⁴¹⁴ to 186 pm in Asn. No direct evidence for the HB strength dependence with the residue could be obtained so far from IR spectroscopy.

8.2. Documenting the effect of specific residues from the low frequency spectral region below 1800 cm^{-1}

As already described in Section 6.2, the structural influence of specific amino acid residues on preferred secondary structures is also reflected in the spectral region below 2000 cm^{-1} . Examples in which the C terminal carboxyl group is involved was Trp-Gly, Gly-Trp and Trp-Gly-Gly³⁹⁶. For Trp-Gly only stretched conformers were found, in contrast to Gly-Trp and Trp-Gly-Gly, for which also structures with an H-bonded COOH group were reported. The remarkable features were the in-plane OH bending vibrations shifted above 1400 cm^{-1} for the H-bonded conformers, whereas the free ones were detected below 1400 cm^{-1} . A further example with regard to uncapped peptides are the prominent forms of the Gly-Gly²⁵⁷ and Ala-Ala²⁵⁸ dipeptides in a supersonic expansion which were recently investigated using a non-selective VUV detection scheme coupled with an IRMPD excitation in the $700\text{-}1850\text{ cm}^{-1}$ range. Only the extended form (cf. AA2 in Scheme 1) could be conclusively observed in both cases, despite not being the most stable form of Ala-Ala at 0 K; the global minimum being a folded form (cf. AA1 in Scheme 2). The Ala-Ala species thus provides a peptide example of kinetic trapping of a high energy species favoured by entropic effects in the early times of expansion, followed by subsequent conformational relaxation and cooling. It also provides a structural reference, against which the role of specific residues in the sequence can be analyzed. In this respect the folded conformers reported in the

conformer-selective studies of Xxx-Gly (Xxx=Tyr, Trp) and Gly-Trp, discussed in Section 6.1 and above, can be seen as examples of residue effects on the sequence.

In the context of semi-capped models, the polar residues Glu and Arg were also investigated in this spectral range using the neutral Z-Glu-OH¹⁹⁶ and Z-Arg-OH models.¹⁹⁶ Experimental IR spectroscopy combined with calculations revealed that the structures of the former species are dominated by stacking or NH- π interactions between the side chain and the Z-tail, hampering the documentation of the interaction between this specific SC and uncapped terminals. The situation is more positive with arginine, however, where SC-bb H-bonds stabilize efficiently the conformers observed: depending on the tautomer, the conformer is either of 7^e(ⁿ π) type, i.e. stabilized by NH_{Arg} \rightarrow N^e (7^e) and NⁿH \rightarrow π_z (ⁿ π) HB interactions (canonical tautomer), or of 5-^c8^e (f) type, stabilized by a OH_{carboxyl} \rightarrow N^e bond. As dispersion interactions play a large role in these systems,¹⁹⁶ the region of 1400-1000 cm⁻¹ was better described by DFT calculations including dispersion (via e.g. the M05-2X functional) than without dispersion interaction (e.g. B3LYP functional).

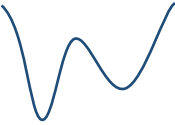
On the examples of the capped Z-Pro-NHMe¹³⁷ and Z-Aib-Pro-NHMe¹⁵³ Compagnon et al. demonstrated that structural assignments can be performed from IR spectroscopy in the regions between 500-1800 cm⁻¹ and 900-1800 cm⁻¹, respectively, without further information from the amide A region. For the protected amino acid, a γ -turn was found, whose characteristics were mainly found in the amide I, II region; the modes in the region between about 1500 cm⁻¹ down to 1000 cm⁻¹ (mainly C-H bending) even allowed the authors to determine the orientation of the chromophore in the protection group. This was also true for the dipeptide system, in which the γ -turn was conserved, despite the propensity of the Aib residue to induce 3₁₀ helical structures.¹⁵³

9. Competition between secondary structures; sequence-induced changes

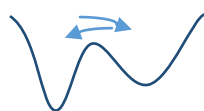
The competition between secondary structures is at the heart of the folding process. The balance between the several structural motifs is quite sensitive to the presence of specific residues and to the interactions they can establish with their environment. In absence of a structured environment, like a solvent, isolated structures as observed in the gas phase usually exhibit an optimum number of stabilizing interactions, in particular hydrogen bonds. They constitute therefore good models for the archetypical structures found in inner cores of proteins, i.e., resulting from a folding process, through which the protein backbone is gradually dehydrated. This echoes the general considerations, used in protein structure, where backbone NH donor sites are supposed to satisfy their propensity to form H-bonds by seeking an acceptor partner CO site leading to intramolecular H-bonding,⁴¹⁵⁻⁴¹⁸ and where the energetics of the corresponding backbone dehydration is even sometimes considered as the main driving force of protein folding.^{419,420} In uncapped peptides, the role of the side chains is a much less addressed issue, in particular because many of the gas phase model residues chosen as references were very flexible (Gly), which contributed to blur the specific effects of the side chains.

9.1. In protein chain fragment models

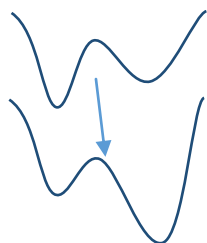
9.1.1. At the local scale: competition between extended (5) and folded (7eq) forms in capped amino acids and dipeptides

 The coexistence in a supersonic expansion of two conformational families, with extended and folded backbones, has been evidenced very early from the study of the capped aromatic residues, Trp,¹³³ Phe^{60,135}, whatever the C-terminal cap used, amide or methylamide. The number of conformations within each family and the detail of their structure (e.g. flip of the Trp side chain, number of rotamers, etc...) is found to depend upon the residue and cap used. In all cases, π H-bonds play a significant role in the structure of these two families: in extended forms it originates from the NH(*i*+1) amide group whereas in folded 7eq forms (of 7_L type in chiral L-residues), it is an intraresidue NH- π interaction. From an energetic point of view, these H-bonds can play a significant stabilizing role, which can blur the intrinsic extended vs. folded competition. More recently the conformational competition was also investigated on more simple capped Gly and Ala residues using techniques, which did not

rely on IR/UV spectroscopy. Microwave high resolution experiments proved the simultaneous presence of 5 and 7eq forms of Ac-Ala-NH₂ in a supersonic expansion by comparison of the rotational constants measured with quantum chemistry predictions.¹³⁸ Alternatively, the sudden cooling provided by He droplets during a collisional pick-up process enabled spectroscopists to freeze the gas phase conformational distribution, which is further probed by IR spectroscopy of the embedded molecules.²⁴¹ By varying the temperature of the pick-up oven, a van't Hoff analysis enabled the authors to derive precise thermochemistry data, namely the enthalpy and entropy of interconversion from 5 to 7eq forms (-4.5 kJ/mol and -12.4 J/(mol K)) at 500 K demonstrating both the enthalpy stabilization of the folded form together with the entropic stabilization of the extended form. By fixing the temperature control issue, the He-droplet procedure enables a more precise measurement of the relative energies of two species than in a supersonic expansion. In this latter case, the final conformational population, which results from the cumulative effects of conformational interconversions, relaxations and kinetic trapping phenomena along the expansion (cf. Section 4.1), can be used to estimate the free enthalpy difference between conformers, at an intermediate temperature, between initial vaporization conditions (thermal or laser-desorption) and final cooling.^{103,258,421} In practice, the simultaneous observation of two conformers with comparable apparent intensities suggests Gibbs energies differing by much less than 10 kJ/mol.



The kinetic trapping phenomena discussed above naturally introduce the issue of the barrier which separates the conformers. Vibrational excitations using lasers in the early times of a supersonic expansion followed by convenient collisional relaxations (cf. Section 4) was elegantly used to trigger population transfers in the Ac-Trp-NHMe species and related species through isomerization in the expansion, helping to document the vibrational energy flow in large molecules.^{203,296,297,364 297,300} Somewhat disappointingly, these experiments did not end up with the stabilization of new conformers. However, the potential observation of a threshold for the population transfers enabled the direct measurement of the barrier to isomerization and comparison with the reverse measurement provided access to energetic data.^{298,422} Similarly, a same IR-induced isomerization process between conformers was also observed on a depsipeptide by the Gerhards group in their IR/IR/UV experiments, designed to recover conformational selectivity (cf. Section 4.2.).¹⁴⁹



Investigating the role of the residue in the competition between 5 and 7 forms requires the use of model residues, either with a UV chromophore embedded in a cap (Z-⁸² or -NHbn⁷⁹), attached to it¹⁶⁴ or contained in the sequence (Phe), with potential perturbations due to it. IR/UV experiments on these model systems sometimes observe the conformer populations that significantly differ from those of microwave experiments. For example Ac-Phe-Xxx-NH₂ models, which capitalize on a backbone scaffold provided by the local extended form on the Phe residue,³⁸⁶ provide evidence for the formation of a local γ -turn on the Xxx residue but do not exhibit any fully extended form (with a 5 interaction on the Xxx residue). Likewise, complexation of the Ac-Ala-NH₂ peptide with toluene leads to an inverse γ -turn attached to it.¹⁶⁴ Conversely, the Ac-Ala₂-O-Bzl species exhibits both extended and folded forms.¹⁰³ These data emphasize the extreme sensitivity of the 5 / 7eq competition to the environment, broadly speaking.

Apart from the proline case, whose pyrrolidine ring forbids the formation of an extended form as testified by the γ -turn detected for capped Pro from microwave⁵⁰ or optical¹³⁷ spectroscopy, the 5 vs. 7eq competition is always expected. Beyond the Ala case discussed above and which can serve as reference, the influence of a bulky alkyl group (valine) has been investigated¹³⁹: structural data showed that the voluminous isopropyl group is not able to prevent the less stable 5 conformer from forming but it destabilizes the NH *i*+1 \rightarrow OC *i*-1 interaction of the 7 form. Interestingly IR/UV spectroscopy of Ac-Phe-Val-NH₂³⁸⁶, for which no extended Val backbone could be observed, was nevertheless able to distinguish two Val γ -turns, which correspond to rotamers of the valine side chain and differ by the strength, and the distances, of their H-bonds.

More interesting from a chemical point of view are the polar side chain residues. With cysteine, both 5 and 7 forms are observed, specifically stabilized by additional SC-bb HBs, leading to 5-6 γ and 5 γ (6)-7 structures respectively, as testified by the IR/UV spectroscopy of Z-Cys-NH₂.³⁹⁰ With serine (Ac-Ser-NH₂), only the 7 backbone was detected by microwave study⁴⁹: it exhibits a local locking of the structure, with a 5 γ (6)-7 conformation; the γ 6 bond being much stronger than the 5 γ one, according to the H-bonding distances

calculated and NBO analysis.³⁹⁰ This point is confirmed by IR/UV spectroscopy of Ac-Phe-Ser-NH₂ and Ac-Ser-Phe-NH₂, where the NH stretch signatures of 5^γ and 7^δ bonds are observed in both γ- and β-turns.^{80 83}

A less strict conformational preference is observed for the other short, polar side chain residues asparagine^{79,82} and histidine⁸¹ (for both tautomeric forms in the latter case), since the additional H-bonds turn out to nicely match both 7 / 5 backbones and contribute to stabilize them, leading to a local locking of the side chain: with extended 5(^δ8)-7^δ Asn and 5(^εf)-7^δ His forms and folded Asn 6(^δ7)-7 and His 6(^δεf)-7 or π^H(^δ7)-7 forms (cf. Figure 18).

In the polar glutamine, whose carboxamide side chain is also both donor and acceptor, the longer chain is mainly favorable to extended backbone conformations (5(^εf)-8^ε forms).⁷⁸ Interestingly, methionine, the other long polar neutral residue, exhibits such a comparable selectivity with an extended 5-7^δ form, suggesting that this specific conformational preference could derive from the length of the side chain.

In the above mentioned chiral residues, the side chain in the inverse γ-turn 7 form (cf. Section 7) lies in an equatorial position (7eq, also designated as a 7_L form for a L residue); the isolated 7_D direct γ-turn, higher in energy, is never observed in the gas phase due to the energetic destabilization induced by SC-BB close contacts when the side chain is in an axial position (despite 7ax is a stronger H-bond than 7eq).^{372,375} In achiral isolated residues (capped or not), like Gly or the unnatural Aib, both folds are isoenergetic. They are observed simultaneously, but are undistinguishable by absorption spectroscopy with linearly polarized light when isolated. In presence of a neighbor chiral residue (L-Phe), specific UV spectroscopic signatures for the phenyl absorption enables the recognition of the Aib fold handedness, despite very similar structures as illustrated by the IR spectra.³²⁸ In the case of Gly (Ac-L-Phe-Gly-NH₂), however, no experimental evidence for the simultaneous presence of two γ-fold forms of Gly could be obtained, despite similar energetics³⁸⁶, suggesting the occurrence of an efficient conformational relaxation process, due to a low isomerization barrier.

9.1.2. In capped dipeptides, competition between β-turns, 2₇ ribbons and β-strand like extended forms

Evidence for this competition, as a general feature of dipeptide chains isolated in the gas phase, is provided by the emergence of β-turn structures,^{60,102,387,388} besides conformations essentially consisting of a juxtaposition of local features, namely double γ-turns,¹⁴⁰ combinations of γ-turns or extended forms,³⁸⁶ sometimes favored by an aromatic residue in the sequence. The Ala-Phe and Gly-Phe sequences (with Ac-, -NHMe and -NH₂ caps) epitomize this competition, with the involvement of three backbone families: x-7-7 double γ-turns (or 2₇ ribbons), x-y-10 β-turns (with different types depending on the first residue) and 5-5-x fully extended β-strand-like forms.⁷⁵ In these systems, 2₇ ribbons seem to be the most populated conformers, followed by the β-turns. The extended forms appear as minor conformers; their intrinsic high energy being partly compensated by a strong entropic stabilization due to the flexibility of the 5-5 backbone.⁷⁵

In β-turns, the type of turn observed is controlled by the close contacts, which can form between the folded backbone and the residue side chain and eventually destabilize the structure.⁶⁸ These depend upon the existence of a side chain (Gly vs. other natural residues) in one of the central positions of the turn as well as upon the chirality of these residues (L vs. D). In the above mentioned sequence example, Gly as a first residue gives rise to both I and II' types while L-Ala is restricted to type I.⁷⁵ A D-Ala residue instead leads to a type II' β-turn due to a folding rearrangement centered on the first residue.³⁸⁹ Like with Gly, both types I and II' appear in presence of the achiral residue Aib (which presents two methyl side chains). A third type (II) has also been evidenced from IR/UV spectroscopy: it occurs exclusively when Gly occupies the second turn position,³⁸⁷ for the same steric reasons: it is not observed with achiral residues (having a side chain).³⁸⁶

In the reference species described above, β-turns are generally not the most populated conformer. The large variety of capped dipeptides studied so far allows us to illustrate the role of additional interactions, most of the time involving one of the side chains, into the conformational competition.

The formation of a π H-bond between the central NH of a capped dipeptide and an aromatic residue located in second position hampers the involvement of this NH bond into a 7-7 backbone structure and is compatible with

the formation of a 10 H-bond, which eventually favors the turn formation (blue labeled populations in Figure 20 right).^{102,217,389} The effect is enhanced by side chain-side chain dispersive interactions between two aromatic residues e.g. in Phe-Phe^{292,377} and Phe-Tyr(Me)³⁸⁴ sequences, or between an aromatic and a bulky alkyl group, e.g., in Val-Tyr(Me)¹⁰² and Val-Phe²¹⁷ sequences. In most of these cases^{217,292,377,384,389} the β -turn becomes the most prominent conformer or becomes at least a serious competitor.^{102,388} A similar mechanism is at play with polar residues, whose side chain, acting as a proton acceptor, is able to establish intrasidue local H-bonds, like Asn (6^δ),^{79,82} Met (6^δ),³⁹² Gln (7^ϵ),^{77,78} and His (6^δ),⁸¹ cited in the order of increasing bond strength, as assessed from their spectral shift. Such a strong local bonding to the SC of the second central residue fulfills the H-bonding requirement of the central NH donor and stabilizes the β -turn, which can become a prominent conformer (red labels in Figure 20). One notices that this effect is much weaker with Cys, which gives rise to a weakly stabilizing 5^γ intrasidue H-bond.^{80,390} It is even absent with Ser, whose local bonding preference goes to a 7^6 H-bond, where the SC OH plays a donor role, which fits best to a local γ -turn structure.⁸⁰

In contrast, in the reverse Phe-Xxx model chain sequences, $5-\pi-7$ patterns form spontaneously with the weakly polar Ala, Val,³⁸⁶ Ser or Cys^{80,83} residues and no or weak β -turn populations are observed. With the Phe, Asn, His and Met residues,^{81,82,292,384,392} however, the efficient proton acceptor site of the side chain takes over for the solvation of the central amide NH, resulting in the enhancement of the β -turn population (red labeled populations in Figure 20), at the expense of the $5-\pi-7$ patterns (in grey); the strong intrasidue H-bond in these residues provides an additional stability to the turn structure.

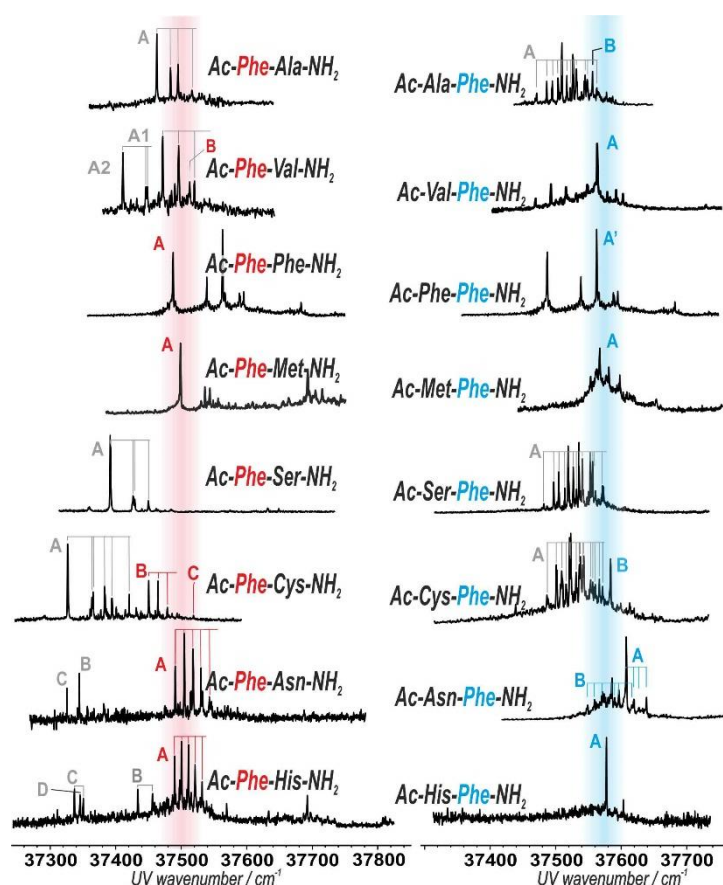


Figure 20: Evolution of a Phe residue near UV spectroscopy, along a series of capped dipeptides of the form Ac-Phe-Xxx-NH₂ (left panel) and Ac-Phe-Xxx-NH₂ (right panel) with the nature of the neighbor residue Xxx. Labels A, B, C ... refer to identified conformers (from IR/UV double resonance spectroscopy) in the order of decreasing populations. β -turn signatures (indicated by colored labels) appear in the same spectral range, whatever the Xxx neighbor residue along the series (when observed), due to the weak sensitivity of the Phe environment (mainly a π H-bond) to the Xxx residue in these structures. The spectral range, however, depends upon the position of Phe in the turn sequence (red vs. blue color), since the corresponding environment changes accordingly. This synthesis figure is built up from spectra published in References^{80-82,217,292,386,387} Reprinted from²¹⁷ and³⁸⁶, with the permission of AIP Publishing. Spectra reprinted with permission from Ref.⁸⁰⁻⁸². Copyright (2015, 2017, 2018) PCCP Owner Societies.

It should be noted that, as expected from gas phase structures, the most stable conformations are often opportunist structures, whose geometry allows them to maximize the number of interactions present, including weaker ones like π H-bonds. As an example, the 7^e - 7^e -10 conformation of the Gln-Gln sequence⁷⁷ with its successive, non-interacting 7^e is widely stabilized by additional π interactions between the second SC and the Bn cap. The same remark holds for the Ala-Gln sequence.⁷⁸

Finally, as far as Asx turns are concerned, one can notice that the gas phase experiments reported about the tripeptide models in Section 7.6., studied for their ability to mimic N-glycosylation sites of proteins,¹⁶² also provide a good example of sequence-mediated structural competition, in which the Asn side chain does form an Asx turn in the isolated Asn-Pro-Ser sequence, but not in Asn-Gly-Ser, in contrast to condensed phase conditions.

9.1.3. Emergence of helices: Competitions in capped trimers f-f-10-10

Acetyl/(methyl)amide capped trimers or partially capped tetramers are minimalistic species on which incipient helices can be detected; these latter being defined as the shortest species exhibiting at least one example of the series of H-bonds, which define the helix. Incipient 3_{10} helices have been reported as main conformers in Ac-Ala-Phe-Ala-NH₂¹⁴¹, Ac-Aib-Phe-Aib-NH₂³³⁰ and capped poly Aib peptides.⁷⁶ These conformations exhibit two nearly parallel 10 H-bonds between NH_{*i*} and CO_{*i*-1} sites. In the two first species, helices are challenged by minor, unassigned conformations, for which calculations suggest that several candidate competitors, such as a succession of β -turns of different nature or an inverse γ -turn accompanied by an antiparallel 13 H-bond between both ends of the molecule, both giving rise to compact structures.³³⁰ In the polyPhe capped peptide³⁷⁷ a strongly distorted helix constitutes the most stable form, accompanied with minor forms combining an inverse γ -turn and a β -turn. Such a f-7-f-10 backbone structure was reported for similar sequences such as Ala-Ala-Phe,¹⁴¹ or Leu-Val-Tyr(Me)³⁸⁵, with the presence of a π HB to the aromatic ring. Alternatively the presence of an aromatic residue at the first position favours structures mixing extended backbone and 2-7 ribbons (5- π -7-7).¹⁴¹ Again, these data support the idea that minor interactions play a decisive role in orienting the formation of specific structures such as helices. In the poly-Aib species,⁷⁶ the two remaining minor conformers observed are assigned to a distorted helix family (f-f-10-7 backbone), in which the second 10 HB is distorted into a 7 bond, and to a compact 11/14-7-7-f network, with a N \rightarrow C 14 HB, respectively. This result echoes the outcomes of a study on capped polymers based on the other achiral, but much more flexible Gly residue.⁷⁴ From a certain length, these species, namely Z-(Gly)₄-OH and Z-(Gly)₅-NHMe, exhibit stable conformations characterized by antiparallel 14 and 16 H-bonds, which form in the latter case an incipient H_{14/16} mixed helix. Incipient 3_{10} helices are not observed and calculations on Z-(Gly)₄-OMe, directly comparable to Z-(Aib)₄-OMe, confirm the trend of the flexible Gly to form 14 H-bonds compatible with a H_{14/16} mixed helix rather than the 3_{10} . This general trend of the Gly residue is interpreted by the authors as a consequence of the smaller macrodipole of the mixed helix, electrostatically more favorable in the solvent-free gas phase experiments.⁷⁴

9.1.4. Diversity in β -sheet model dimers

In peptide dimers, a variety of isomers are in principle possible, including different orientations of the two monomeric units (e.g. parallel, antiparallel) as well as the competition between inter- and intrastrand hydrogen bonds. Even on the early examples of relatively small systems like the dimers of the capped phenylalanine, (Ac-Phe-OMe)₂ (cf. ^{134,284,397} and Section 12) and (Ac-Phe-NHMe)₂ (cf. ¹³⁵ and Section 12), and later on for larger systems allowing to form a whole β -sheet unit cell (cf. (Ac-Val-Tyr(Me)-NHMe)₂¹⁵⁷ in Section 12) or mixed peptide dimers (cf. ¹⁴³ and Section 12), the preference of antiparallel and parallel β -sheet arrangements already became obvious in the MD simulations (cf. e.g. ^{135,157}). The possibility to form several (in the mentioned examples up to three) interstrand hydrogen bonds without generating remarkable backbone tension in the corresponding monomers results in a strong energetic preference of β -sheet structures. The interpretable systems investigated so far all exhibit a preference for antiparallel (*ap*) β -sheets. No parallel (*p*) could unambiguously be assigned yet. A reason for this partly originates from the intrastrand hydrogen-bonds, which are often stronger (shorter H-bonding distances, stronger red-shifts of NH stretching frequencies) than in the parallel arrangements (cf. e.g. ¹⁵⁷). Thus, in parallel β -sheet isomers (*pgt*), which can energetically compete with

the antiparallel ones, additional intrastrand H-bonds, like γ -turns, appear quite often. For the dimer of Ac-Val-Tyr(Me)-NHMe (cf.¹⁵⁷ and Section 12) as well as the mixed dimer of Ac-Val-Tyr(Me)-NHMe/Ac-Ala-Ala-Ala-OMe (cf.¹⁴³ and Section 12)), these arrangements (antiparallel and parallel with γ -turn) are nearly isoenergetic, regarding the computational accuracy. The remarkable aspect about the mixed dimer was the fact that a purely parallel β -sheet (without any additional intrastrand hydrogen bonds) was in the energetic range of the *ap* and *pgt* isomer. The inclusion of dispersion interactions turned the *p* structure to a *pgt*, which became by far the most stable arrangement with the *ap* arrangements being about 12 kJ·mol⁻¹ and 25 kJ·mol⁻¹ less stable. In this specific example the enormous stabilization of the *pgt* was due to the interaction of the tyrosine chromophore with the Ala chain. Nevertheless, the calculated frequencies could not describe the experimental data and an antiparallel arrangement was assigned again. The example showed that dispersion can play a decisive role in the energetic relations of different arrangements and (at the time of investigation) could not be taken into account for the early examples of peptide dimers, but the influence of dispersion must already be treated with care. A further aspect, which of course should not change the principle assignment based on the best fit of the calculated and measured frequencies, is the inclusion of entropic aspects. For future investigations, attention must also be paid to that point since the formation of the peptide dimers during molecular beam expansion of course generates aggregates with a quite high temperature compared to corresponding monomeric species.

An aspect that was further remarkable in context with the mixed peptide dimer was the fact that the Ac-Val-Tyr(Me)-NHMe sequence seems to have the intrinsic driving force to form β -sheet arrangements. This has even been observed though neither the tripeptide model itself nor its aggregation partner (Ac-(Ala)₃-OMe) in the heterodimer do necessarily have an exclusive preference for stretched monomeric arrangements; for both, the formation of folded structures must be considered (cf.^{102,143,388} in Section 7 and 12).

How an unprotected side chain could disturb the preference of β -sheet arrangements became obvious on the example of the Ac-Trp-OMe dimer with the NH group of the indole side chain being a potential H-bonding donor. Though the indole side chain did not have an influence on the stretched monomeric structure, both indole NH groups were unambiguously involved in interstrand H-bonding with backbone CO groups in the Ac-Trp-OMe dimer finally leading to an asymmetric non- β -sheet dimer (cf.³³² and Section 12). An H-bonding interaction of an unprotected side chain within a peptide aggregate was also found for the dimer of the hexapeptide Ac-Val-Gln-Ile-Val-Tyr-Lys-NHMe (cf.⁴²³ and Section 12). However, the presence of either parallel or antiparallel β -sheets was proposed but a final structural assignment was not possible, so that the influence of the side chain was difficult to estimate. Thus, it could also be probable that the possibility to form up to seven stabilizing intrastrand H-bonds drives the formation of β -sheet arrangements in which the unprotected side chains are involved in intrastrand H-bonding.

The influence of side chains with either protected H-bonding groups (like Tyr(Me)) or without any strong H-bonding groups on the principle arrangements in dimer structures are normally less strong and mainly include stabilizing dispersion interactions (cf. e.g. mixed dimer¹⁴³). For an unambiguous assignment of e.g. the side chain orientation in the dimer, measurements of the amide A, I and II region are not necessarily sufficient. Thus measurements for Ac-Phe-OMe in the region down to 1000 cm⁻¹ finally lead to the unambiguous assignment of $\beta_1(g+)$;³⁶³ for the dimer structure these measurements were less unambiguous but a *gauche(+)* side chain orientation in both strands (cf.³⁹⁷ and Section 12) was proposed. Later investigations in the far IR region, interpreted with calculations also taking dispersion interactions into account, confirmed the $\beta_1(g+)$ conformation of the monomer but gave preference to a $\beta_1(g+) - \beta_1(g-)$ dimer structure.³⁶³ In cases like (Ac-Phe-NHMe)₂ for which only the amide A, I and II regions were measured, principle discriminations between inner and outer bound isomers (via the NH and CO group of the amino acid or the protection groups, cf.¹³⁵ and Section 12) could be made based on the frequency patterns. However, the decision for an outer bound isomer with side changing from anti in the monomer to *gauche(+)* in the dimer was (at these early beginnings of dimer investigations) based on simple calculations without any dispersion interaction. Nowadays, the awareness about the influence of dispersion interactions on structure exists but one should keep in mind that especially for smaller dimer systems the intrastrand, predominantly electrostatically dominated H-bonds might be the main shaping force whereas dispersion interactions, whose quite small single contributions sum up in large systems, gain influence in larger aggregates.

9.1.5. Probing new secondary structures arising from specific residues in capped and uncapped dipeptides

In capped di- or tri-peptides, conformations not assigned to a juxtaposition of typical secondary structures can arise from the existence of specific SC-SC or SC-bb HBs. An example is provided by the Phe-Phe sequence, whose main conformer is a β -turn (cf. Figure 20).³⁷⁷ Under strong cooling conditions, in which high energy conformers can be trapped in the jet, a $\pi_1/\pi_2-\pi_2-7eq$ conformation was observed, where the two first and consecutive NHs are not paired to a backbone carbonyl but instead contribute, through NH- π HBs, to stabilize a SC conformation where both Phe rings interact with each other, eventually leading to a non-standard $\delta_L-\gamma_L$ secondary structure (cf. Figure 21).

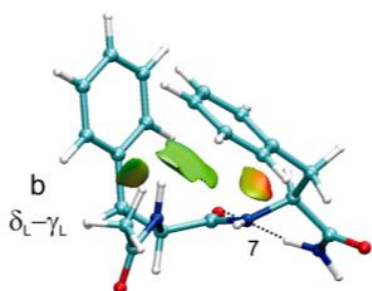


Figure 21: Example of a non-standard $\delta_L-\gamma_L$ secondary structure, experimentally revealed by kinetic trapping of the Ac-Phe-Phe-NH₂ model, reprinted with permission from Ref. ³⁷⁷. Copyright (2013) American Chemical Society.

9.2. Uncapped and partially capped peptides

In partially capped peptides, competition occurs between backbone-backbone H-bonds and those involving the COOH or NH₂ terminal ends. As an example, the Z-Gly-OH molecule⁷⁴ and its dimethylated counterpart Z-Aib-OH⁷⁶ exhibit a 5-^Cf preferred backbone, which is challenged by a simply folded structure devoid of any H-bond, presumably stabilized by electrostatic interactions. With the polar residue glutamine, the extended form 5 is retained⁷⁸; however, the side chain interacts either with the C-terminal acid OH as an H-bond acceptor (^Cg⁶), with the CO of the N-side cap (⁶9) or with the backbone amide group through a stacking interaction. Similarly, the partially capped dipeptide Z-Gly-Pro-OH, whose C-terminal structure is greatly shaped by the constraints of the pyrrolidine ring, also exhibits two extended conformations stabilized by a 5 H-bond, capable of challenging overall folded structures, where the carboxylic OH bounds to the Z-cap through a π H-bond.⁴²⁴

In (uncapped) amino acids, only aromatic residues have been investigated using IR/UV techniques. The presence of a free OH stretch mode close to 3600 cm⁻¹ is the signature of a type A2/A3 conformer (for types and H-bond labelling, see Schemes 1), in contrast to the A1 type, whose H-bonded OH (through a ^C5^N bond) leads to a strongly red shifted, broaden band in the 3200-3300 cm⁻¹ region. Further assignment in terms of A2/A3 types relies on the comparison with calculations especially for the NH₂ involving ^N5^C and ^N5^C bonds.

In most of the cases, several conformers are observed (6 for Trp¹³¹, 7 for Tyr³⁸⁰ and 6 for Phe^{174,205}), with various population panels (A1/A2/A3/not H-bonded conformations) obtained : 2/2/2/0 for Trp, 3/4-x-y/x/y (x, y = 0 or 2) for Tyr and 2/2/1/0 for Phe). The distribution is widely influenced by the presence of additional interactions between the SC and the NH₂ group, especially NH- π interactions, which together with cooperative effects, participate in a fine-tuning of the structure.

A precise structural assignment, especially in terms of H-bonding, is however strongly dependent upon the quality of the quantum chemistry methods used for structure and frequency calculations, making further assignment merely tentative. For example it is difficult to distinguish conformations which differ by a flip of their side chain, whose NH/OH side chain substituents (Trp and Tyr cases resp.) remain free as evidenced by the typical free hydride bands (at 3522 and 3669 cm⁻¹, respectively). Likewise, the Phe assignments were later partially revised in the light of rotational contour measurements of the 6 conformers.¹⁷⁰ These conformer-selective experiments nevertheless constitute a much richer source of data compared to classical gas phase FT-IR absorption experiments, which could not detect the Phe H-bonded conformers at 570 K. Interestingly, the

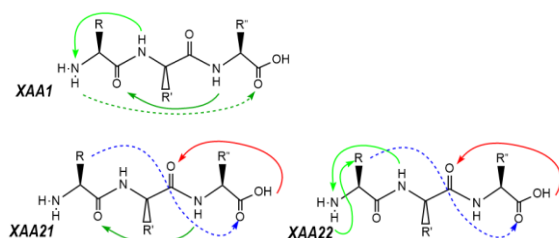
conformational distribution of Trp and Tyr in He droplets²³¹ differs significantly from that measured in a jet, as can be expected from a very different cooling process (see Section 4.1.), with the vanishing of one conformer in Trp¹³¹ and of three in Tyr³⁸⁰. The conformer that vanishes in the LIF spectrum of Trp in He droplets (labelled A in¹³¹) is of A1 type (cf. Scheme 1), whereas a side chain rotamer, labelled F, also of A1 type, is observed. Surprisingly enough, the Tyr conformers that vanish in the absorption spectra in droplets, labelled B, C, F in³⁸⁰, all belong to different phenolic OH rotamer pairs: A-C; B-D; F-G; each pair corresponding to the same structure apart from opposite orientations of the OH group in the phenyl ring plane. In other words, only one member within each OH rotamer pair (A, D, G) is observed in He droplets. No clear-cut explanation could be proposed so far to account for these puzzling specificities. Both a conformer-selective excited state dynamics, due to a selective coupling with the He matrix and a significant inter-OH rotamer relaxation during the pick-up process were tentatively evoked.²³¹

The gas phase results above fit to the observations of the most simple amino acids Gly in millimetric or microwave experiments, i.e., first a major conformer of type A2^{125,126} and then a less populated one of type A1⁴²⁵ with a reverse H-bonding pattern, namely conformers I and II in the recent review on the subject.⁴³ Precise H-bonding patterns were eventually obtained thanks to high resolution scans of the hyperfine pattern in specific isotopologues.^{426,427} The absence of higher energy conformers, in particular of A3 type, expected from calculations was assigned to conformational relaxation in the supersonic expansions. Some of them were eventually detected from their OH stretch IR absorption spectroscopy in He-droplets for Gly²³² and from their low frequency modes detected by Raman absorption spectroscopy in a jet for both Gly³² and Ala³⁴. The Ala structure was also obtained in high resolution experiments,^{414,428} which demonstrated the presence of both type I and II conformers. Interestingly the microwave spectrum of Phe was carried out thanks to a laser desorption set-up combined to a Fourier transform microwave spectrometer.⁴²⁹ The authors detected only the two A2 type conformers (B and X in²⁰⁵), in sharp contrast with the large conformational panel in the laser studies. This was assigned to the difference in the vaporizing conditions between thermal and laser desorption conditions. Alternatively, the hyperfine resolution, which is strongly dependent upon the orientation of the amino group, confirmed the initial tentative assignment based on IR spectra of B and X species²⁰⁵ as well as the unambiguous one based on rotational contours.¹⁷⁰

In the uncapped peptides, the role of the sequence has not been investigated in a systematic way. Two effects can nevertheless be mentioned.

- NH or OH groups of Trp and Tyr are often involved in interactions with proton accepting groups providing that the molecule is long enough for an end-to-end folding to occur. This has been reported for Trp, in peptides with a backbone carbonyl acceptor (H-Trp-Ser-OH³²⁶, H-Tyr-Gly-Gly³⁸⁰) and in capped peptides with the π ring of a neighboring Tyr residue (AcTrp Tyr NH₂³⁷⁷). The shifts measured remain modest because the HBs formed are hampered by the overall rigidity of the molecule.

- The role of flexible Gly residues: Among the few tripeptides documented so far, most of them comprise Gly-based flexible sequences (H-Xxx-Gly-Gly-OH), in which one of the residues Xxx is aromatic, as well as the H-Gly-Phe-Ala-OH system. Several conformations exhibiting different H-bonding networks are observed simultaneously. Again, apart from the status of the acidic OH and that of the side chain OH/NH in Tyr/Trp, the absorption bands in the region 3380-3430 cm⁻¹ testify medium strength H-bonds assigned to either C7 or C5 (5^N) interactions, but assignment remains a challenging task, made difficult by several issues. First, because of the flexibility of the systems considered, especially those containing the achiral Gly residue and large side chain aromatic residues as well. Second, the fact that dispersive interactions were not properly accounted for in the interpretation of these early experiments,²⁶⁹ with consequences on both the energetics and the vibrational spectrum (especially the NH/OH stretch region)^{228,267,346,347,430}. Third, the fact that differential entropic effects between folded vs. extended conformations are important, requiring finite temperature energetics^{228,266,267} or, better, free energy landscape²⁶⁶ to be considered in order to capture relevant conformations.



Scheme 4: H-bonding patterns observed in tripeptides with unprotected N- and C-termini.

IR spectroscopy of Xxx-Gly-Gly sequences shows that specific H-bonds such as NH(2)→N(1) (3380-3430 cm^{-1}) and NH(3) → OC(1) (3320-3390 cm^{-1}) **7** H-bonds are common in the conformations observed (cf. Scheme 4, type XAA1), indicating i) the robustness of the N-terminal local folding and ii) the emergence of a central γ -turn secondary structure in the molecule, eventually completed by an end-to-end H-bond between the N-terminal NH_2 and the C-terminal carbonyl group (antiparallel to the γ -turn HB), leaving the acidic OH free. Occurrence of bound carboxylic OH groups remains indeed seldom.^{228,269,380} They are only observed concomitantly with a bound NH/OH side chain donor, with Trp and Tyr, but not with Phe, suggesting that, in this case, the local folding structures along the chain can accommodate this SB-bb H-bonding (type XAA22). Interestingly, the Gly-Phe-Ala sequence behaves differently and emphasizes the scaffolding properties of a Phe residue, which favours either a locally extended structure or a central γ -turn (types XAA22 and XAA21 resp.).²⁶⁶

10. Modified peptides : Homo amino acids, β - and γ -peptides

Among modified α -amino acids and peptides, those differing by the insertion of a methylene group either within the side chain (homo amino acids) or of several methylene groups with the backbone (β -, γ -, etc... amino acids), are interesting classes of molecules, e.g., for their use as intermediates in the synthesis of drugs,¹⁵⁴ and as building blocks of foldamers,^{431,432} i.e., synthetic polymers synthesized for their unique specific structural features. Representatives of these two classes have been studied under isolated conditions using laser spectroscopy.

10.1 Homo amino acids

In homophenylalanine (HPhe) an additional methylene group is included in the side chain compared to the corresponding α -amino acid (cf. Figure 22).¹⁵⁴ Fujii and coworkers analyzed the HPhe by UV-UV hole burning and IR ion dip spectroscopy in comparison with dispersion corrected DFT calculations¹⁵⁴. The experimental data revealed 10 conformers to be present in the molecular beam, 4 isomers more than for phenylalanine^{132,173,174,205,243,433,434}, which is not surprising due to the higher flexibility of the elongated side chain. All the 10 conformers exhibit interactions between the COOH and NH_2 moiety. In such a relatively small system like HPhe the quite high number of conformers leads to many, slightly different structures, difficult to assign precisely due to too similar IR spectra. Interestingly, UV spectroscopy, in particular differences in excitations energies and Franck-Condon activities, turned out to be useful tool providing alternative and complementary additional source of conformational assignment.

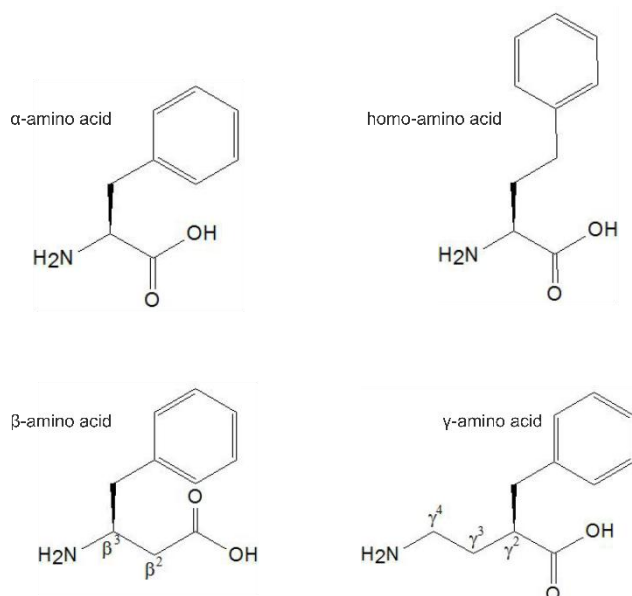


Figure 22: Different types of amino acids.

The β -homotryptophan was also studied by Fujii and coworkers¹⁵⁵, who demonstrated the flexibility of the molecule, again illustrated by large number of conformers (14) observed. They classified them into three distinct groups according to the status of the termini regarding H-bonding: i) free OH and NH- π bond, ii) free OH and NH₂ and iii) C₆N bond (following the terminology of Tables 2 and 4). Despite the third group exhibits the strongest H-bond, unfavorable entropic effects and/or backbone flexibility were supposed to be the reason why the most abundant form belongs to the second group.

10.2 Capped β - and γ -amino acids

The addition of methylene groups within the backbone of α -amino acids gives rise to β - or γ -amino acids and by condensation to β - and γ -peptides (cf. Table 9). These synthetic building blocks are at the heart of the notion of foldamers,⁴³² which, in comparison to natural α -peptides, can exhibit further structural motifs and thus interesting chemical or biological features, thanks either to the enhanced flexibility provided by the methylene group, or, conversely, to the rigidity caused by the involvement of the additional methylene group into a cyclic structure spanning over the backbone and connecting different backbone sites along the linear sequence (cf. Section 10.3 and Figure 23).

Laser spectroscopy has been used to investigate capped β -peptides, either devoid of any strong structural constrain (case of the β^3 -hPhe amino acid, where the Phenyl residue plays the role of UV chromophore^{150,151,290}) or containing constrains of different natures, including a covalent ring as described above (also cf. Section 10.3 and Figure 23).⁴³⁵⁻⁴³⁷ In the absence of covalent constrain several conformations are observed³⁷²: characterized by different approaches of the donor to the acceptor CO, they are stabilized by intraresidue 6 or interresidue 8 H-bonds and (cf. Table 9), the former constituting the most abundant family. These two forms are the counterparts of the 5 and 7 forms encountered in α -peptides (cf. Table 5). In large pure β - or mixed α - β / β - α peptides,^{150,290} the 6 bond is barely influenced by the molecular H-bonding network, despite the donor or acceptor amide of the 6 bond are also engaged into another H-bond. In contrast the 8 bonds exhibit a much greater diversity of strengths, depending on the nature (H-bond type, backbone folding type) of its environment, in a way comparable to observations on α -peptides.³⁸⁶ The accuracy of the frequency prediction using the

Table 9: H-bonding in β -peptide chains, with corresponding NH stretch frequencies observed.

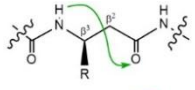
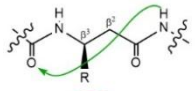
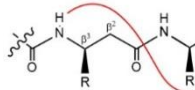
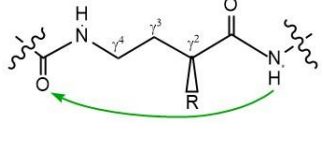
H-bond type	frequency/cm ⁻¹	Environment	Reference	
	6, NH _i →CO _i	3400	isolated intraresidue	150
		3378-3415	6-6 combin. in β - β peptides	151
		3400-3410	5-6 or 6-5 combin. in α - β peptides	290
	8, CO _i ←NH _{i+2}	3417	Interresidue	150
		3339-3369	8-7 or 7-8 combin. in β - β peptides	151
		3275-3380	5-8 combin. in α - β peptides	290
	10, NH _i →CO _{i+1}	3381- 3390	in β - β peptides	151

Table 10: H-bonding in γ -peptide chains, with corresponding NH stretch frequencies observed.

H-bond type	frequency /cm ⁻¹	Reference
-------------	-----------------------------	-----------

	9, $CO_i \leftarrow NH_{i+2}$	3350-3380	152
	amide stacked conformation	> 3465	152

standard quantum chemistry methods, however, is significantly lower than in α -peptides, making the assignment sometimes more difficult. Capped γ -peptides^{152,438-441} are featured by a large predilection for 9 interactions (Table 10), whose strength turns out to be significantly dependent upon the backbone conformation.¹⁵² Interestingly, in capped γ -amino acids the backbone is flexible enough for amide stacked structures to be detected as a secondary conformer, from their original signature of virtually free NH bonds;¹⁵² these structures become the exclusive conformation when N-methylations are carried out on the C-terminal.⁴⁴⁰

10.3 Influence of cyclic structures in β - and γ -peptide chains

Cyclic building blocks, where the side chain is covalently bound to the backbone, in a way comparable to proline, are widely used in foldamer science in order to control or at least limit the flexibility of β - or γ -peptides.⁴³² Some of these cyclic structures have been investigated using laser spectroscopy.

In capped β -peptides, whereas the conformational preference usually goes to a 6 intrasidue H-bonding in absence of constrain,¹⁵⁰ a capped cyclic β -amino acid constrained by a four-membered ring⁴³⁶ (2-aminocyclobutanecarboxylic acid ; ACBC in short, cf. Figure 32) exhibits a predilection for the alternative 8 H-bonding arrangement, whatever the stereochemistry of the substituted cyclobutane, i.e. either with amides in a *trans*- or *cis*- disposition. However, due to the very different geometries, the H-bond approaches and the corresponding strengths, as revealed by IR spectroscopy, are radically different between both conformations, with a red shift more pronounced by ca. 100 cm^{-1} in favor of the *trans*-form (at 3320 cm^{-1}). In the same line, replacement of the β^3 carbon atom of the ring by a nitrogen atom stabilizes still more strongly the folded structure due to the simultaneous engagement of the NH donor into the 8 bond and a 5 interaction with the nitrogen lone pair, epitomizing the notion of hydrazino-turn.⁴³⁶ The similar use of a five-membered building block, the *trans*-2-aminocyclopentanecarboxylic acid (ACPC), in capped dipeptides⁴³⁵ leads to a comparable behavior at the level of the ACPC residue, where 6 bonding arrangements are banished.

A comparable strategy, carried out on a γ -peptide (γ -ACHC, in short, cf. Figure 32) endowed with two constrains,⁴⁴¹ i.e., a six-membered ring with a *trans*-disposition of the γ^3 and γ^4 carbons and an ethyl side chain on the γ^2 carbon, has led to a strong backbone constrain enabling the formation of a strong 9 H-bond, having a NH stretch frequency in the 3300 cm^{-1} energy range, the most red-shifted band for an isolated intramolecular H-bond in a capped linear peptide. The conformational analysis of the 9 structures giving rise to large red shifts has been correlated to the presence of a pivot H atom borne by the γ^4 atom, which controls the orientation of the N-terminal amide relative to the other end of the molecule and secures an efficient approach of the donor NH to the N-terminal amide carbonyl.³⁷²

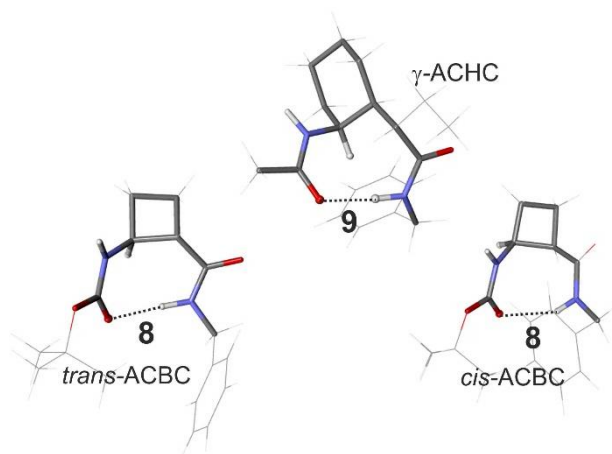


Figure 23: Examples of 8 and 9 H-bonds in main conformations of cyclicly constrained β - (bottom: *trans*- and *cis*-ACBC⁴³⁶) and γ -peptides (top, γ -ACHC⁴⁴¹), calculated at the B97-D3 level of theory.

10.4 Competition between secondary structures in larger β - and γ -peptide chains

Larger peptide chains enables spectroscopist to address the emergence of secondary structures, on which oligomers can build up to adopt original conformational designs, one of the goals of foldamer science. The need for a precise description of the conformations available, not directly at hand with classical conformational identification techniques, triggered a series of gas phase studies on synthetic peptomimetics.

The conformational structure of capped di- β -peptides (Ac- β^3 -hPhe- β^3 -hAla-NHMe and the reversed sequence) has been analyzed in great details by the Zwier group,¹⁵¹ who determined that the *a priori* expected succession of local preferences (6 bonds) are challenged by overall folded 10-stabilized conformations, which exhibit the same H-bonding orientation ($\text{NH}_i \rightarrow \text{CO}_{i+1}$) as the 6 bonds ($\text{NH}_i \rightarrow \text{CO}_i$), with the donor amide located on the N-terminal side, i.e., before the acceptor amide in the sequence of the chain. Despite this network orientation, which is just the opposite to that in the 10 H-bonds of β -turns in α -peptides, the same kind of backbone reversal is obtained. Interestingly, a structure analogous to the β -turn fold of α -peptides would have to be stabilized by a $\text{CO}_i \leftarrow \text{NH}_{i+3}$ 12 interaction in β -peptides, which is not observed. Conversely the fold of α -peptides, that is equivalent to the present 10 interaction and would be stabilized by a 8 interaction ($\text{NH}_i \rightarrow \text{CO}_{i+1}$), is not observed either due to marked steric effects into the α -backbone.

In mixed α - β peptide chains,²⁹⁰ the situation is more contrasted since the α -residue is inclined to keep its local preference, i.e., most of the time a 7eq fold or an extended 5 form, forcing the β -peptide to a 6 or 8 conformation. The notable exception is encountered with a D-Phe α -residue,²⁹⁰ which gives rise to a 11 interaction, the equivalent of the 10 of β -turns in α -peptides. Its specific occurrence with this latter α -D-residue was assigned to an avoided steric effect compared to its L-counterpart. The observation of similar conformational preferences in related compounds, however, suggests an alternative interpretation in terms of intrabackbone hyperconjugative effects.³⁷² With the cyclically constrained *trans*-2-aminocyclopentanecarboxylic acid (ACPC) β -residue,⁴³⁵ competition between double rings (7 vs. 8, since the 6 bonds are sterically forbidden) and 11 bonds are also observed, whatever the stereochemistry of the α -residue.

Capped γ -dipeptides have been investigated with unconstrained (γ^2 -hAla, γ^2 -hPhe⁴³⁸) and constrained (γ -ACHC^{441,442}) γ -residues. In the first case, compact structures with a 7/7/14 network could be formed efficiently due to the flexible backbone, satisfying the donor properties of all the amide groups. In contrast, the γ -ACHC residue, in α - γ dipeptides,⁴⁴² is found to impose its large propensity to form 9 bonds, including in a bifurcated H-bonded form, where the same carbonyl group plays the role of an acceptor for both a 9 and a 12 bond, suggesting the preorienting property of the specific γ -ACHC residue facilitating the formation of C12 in α - γ oligomers.

Advantage has been taken from the rigidity of such cyclically constrained β - and γ -backbones to counterbalance the local propensity to form 6/8 and 9 bonds respectively and eventually build up larger secondary structures like incipient helices. Two γ -ACHC residues have been found to form an isolated 14 bond, constituting the first turn of a 2.6₁₄ helix, one of the most constrained helical structure.⁴⁴¹ Noticeably, this $\text{NH}_i \rightarrow \text{CO}_{i-3}$ 14 H-bond is strong, with a NH stretch frequency in the 3320 cm^{-1} range, among the most red ones within isolated amide-amide H-bonds (cf. Table 4). Mixed β - γ peptides, made of the cyclically constrained β -ACPC and γ -ACHC residues,⁴⁴³ form bifurcated H-bonds : one of the components being the local preference of the first residue and the second one being a $\text{NH}_i \rightarrow \text{CO}_{i-3}$ 13 H-bond, similar to that of the α -helices in natural peptides. Interestingly, the 13 bond exhibits a medium range strength (NH stretch at 3360-3370 cm^{-1}), but the amide disposition in the turn is favorable to the formation of a periodic helical structure, found in crystals of larger oligomers. β -ACHC, when embedded in a capped α - β - α tripeptide,⁴³⁷ is also able to promote incipient mixed C11-C9 helices, such as those observed in the solid phase, but these forms are strongly challenged by compact structures, in which the system optimizes the number of H-bonds present in the molecule.

11. Microsolvation experiments: a detailed view of peptide solvation

One common criticism against gas phase studies of biomolecular objects is that isolated conditions are too different from a real biological environment to provide results capable to address biological issues. As mentioned in the introduction, several arguments can be opposed to such a statement, and plead in favor of gas phase investigations. The first one is trivial, but deserves to be repeated: the role of the environment on molecular folding, or any other molecular property, can be deduced from the comparison between measurements in the gas and condensed phases. This is illustrated by recent articles which analyzed the side chain folding of histidine⁸¹ and asparagine residues.⁸² It was explained that the environment found in crystallized proteins, including water molecules, may have either very little impact on the gas phase structures, like in the histidine case, or may completely change the conformational distribution through specific H-bonding networks including water molecules, making the gas phase structure non-representative of the condensed phase, like for asparagine. An additional argument in favor of gas phase studies comes from the possibility to carry out microsolvation experiments, where the environment of the biomolecule can be made increasingly more complex by adding solvent molecules one by one in a controlled manner (Section 4.2). One natural motivation for such experiments could be to bridge the gap between gas and condensed phase experiments, but this objective is barely reached in general. This is especially true in the case of neutral species for which large heterogeneous clusters are always relatively difficult to form in a molecular beam, and an amino acid solvated by a complete first solvation shell still remains to be investigated. The significance of microsolvation experiments lies elsewhere. Of course, microsolvated peptides provide benchmarks quite useful when it comes to model the protein-solvent interface, but more importantly, these experiments shed light on the active role played by the very first solvent molecules in peptide folding. While several basic properties can be investigated by microsolvation experiments, like e.g. the influence of solvation on the photophysics of residues containing a UV-chromophore, this section focuses on structural issues.

Heterogeneous clusters made of a small biomolecule and a few solvent molecules combine several advantages. Their conformational landscape is often simple enough to be rationalized, and their limited size makes an unambiguous structure elucidation accessible. Being the minimal system capable to model the biomolecule-solvent interface, they are ideal to provide benchmarks and find concepts useful to build a theoretical description of phenomena occurring at the surface of proteins. While it is relatively easy to produce these small heterogeneous clusters in a molecular beam experiment, it is however difficult to reach experimental conditions that enable their full characterization by spectroscopic techniques. This is one of the reasons why the number of study satisfactorily addressing microsolvation is not as large as one could expect from the significance of the question. Several peptide bond models^{107,109,111,113,115,117-119} were first investigated by vibrational spectroscopy, as well as uncapped^{33,158,159,222,229} and capped α -^{160,164,219} and γ -^{440,441} amino acids. Microsolvation of a few polypeptides^{102,161} was also investigated, up to a cyclic tetrapeptide.³⁹¹ Different types of solvent molecules were used: water,^{33,102,107,109,111,113,115,117-119,158-160,219,222,229,440,441} ammonia,¹¹⁹ methanol^{159,161} or toluene.¹⁶⁴ The latter can be also regarded as a way to investigate the self-solvation of the protein backbone by a remote phenylalanine side chain.

One of the first questions to answer in a microsolvation experiment is about the preferred solvation site(s) of the model molecule. While this question is trivial for the monohydrates of cis-amides where the H-bond donor NH and acceptor CO groups provide a natural solvation site for one doubly H-bonded water molecule,¹¹⁷ it becomes rapidly more difficult to find the answer for other systems without a detailed conformational analysis. In trans-amides, where the NH and CO groups make two distinct solvation sites, the question of the preferred location of the first water molecule arises, and was addressed by several studies.^{107,109,111,113} Remarkably, isomerization experiments could be conducted on the trans-formanilide monohydrates, and successfully measured the energy barrier between these two solvation sites, and thus their relative energy.¹¹³ In polyamides, the complexity increases with new types of solvation sites bridging both amide groups, making the number of possible monohydrates already quite large, but still manageable.^{161,219} Increasing the number of solvent molecules is also a source of rapid complication of the structure elucidation process. Interestingly, experiments with multiple solvent molecules shed light on bridges made of up to four solvent molecules, mostly water but also methanol¹⁶¹ and ammonia,¹¹⁹ formed around polar groups such as cis-amides,^{109,115,117-119} trans-amides,^{107,160,161} or carboxylic acid and amino groups.^{158,159,222,229} While it is difficult to fully elucidate

the structure for systems with more than four solvent molecules, the determination of the minimum number of water or methanol molecules (typically 5) necessary to stabilize the zwitterionic form of tryptophan constitutes a noticeable achievement.¹⁵⁹ These microsolvation experiments conducted with up to nine solvent molecules are among the very few that can actually claim to significantly bridge the gap between gas and solution phases.

The sensitivity of vibrational probes to structural changes, together with the accuracy of theoretical quantum chemistry methods, enabled several teams to report how biomolecular structures are affected in the stepwise microsolvation process. One can distinguish three different cases (cf. Figure 24). First, the gas phase structure is found to resist upon microsolvation by the first water molecule(s). This observation has often been made in structures where a water molecule binds to a peptide with a single H-bond. Several examples of structures resisting upon microsolvation can be found in the literature: monohydrates of β -strands,^{102,219} a β_L -backbone conformation up to two water molecules,¹⁶⁰ a monohydrate of a γ -turn²¹⁹ and the C9 structure of a γ -peptide monohydrate.⁴⁴⁰ In the second case, microsolvated structures are found similar to the isolated ones, *i.e.* with the same intramolecular H-bond network, the same torsional angle orientations... but deformations can be observed. A prototypical example of such an adaptation of the peptide backbone to microsolvation is a doubly H-bonded monohydrate of a γ -turn of a capped phenylalanine (cf. Figure 24 right).²¹⁹ While the γ -turn structure is preserved, the water bridge between both amide groups induces a rearrangement of the peptide backbone accompanied by the C7 H-bond lengthening by ~ 20 -30 pm as compared to the isolated structure. In general, such deformations are observed when a water molecule bridges two ends of a molecule, like two amide groups,^{219,440,441} or one amide and one phenyl ring. The third case corresponds to microsolvation-induced conformational isomerizations. For uncapped amino acids, where numerous conformations are usually observed in the isolated system, only a few of them are detected after addition of one water molecule, revealing that microsolvation-induced conformational isomerization of the carboxylic acid and amino groups are common in these systems.^{33,158,159,222,229} In larger systems, more complex isomerizations occur where the secondary structure is strongly affected by microsolvation. The folding of a β -strand into a γ -turn structure was reported in a monohydrate of a capped phenylalanine,²¹⁹ and in capped alanine-toluene complexes,¹⁶⁴ illustrating that microsolvation may have a strong impact on peptide folding from the very first solvent molecule. This has even been found to be true for larger systems like a cyclotetrapeptide, where a single water molecule is enough to disrupt the intramolecular H-bond network.³⁹¹ In contrast, β -strands of another capped phenylalanine, which were found to be resistant to the first microsolvation step, can isomerize as the number solvent molecules is increased.¹⁶⁰ In this case, isomerization leads to a conformation, where a three-water bridge stabilizes a ϵ_L backbone structure. Similarly, two methanol molecules were needed to trigger the isomerization of a γ -turn into a β -turn in a capped dipeptide.¹⁶¹ Finally, not only associating but also dissociating solvent molecules can trigger a backbone isomerization, which has been observed for a γ -peptide in an IR-induced photodissociation experiment.⁴⁴⁰ In conclusion, microsolvation-induced isomerizations demonstrate the significant role played by a single solvent molecule in controlling the conformational distribution of relatively large portions of peptide sequences. These types of experiments give a remarkable stepwise picture of how solvent molecules shape a peptide, sometimes showing just a direction towards full solvation,²¹⁹ sometimes demonstrating that only a few solvent molecules are needed to obtain the secondary structure observed in solution.¹⁶¹

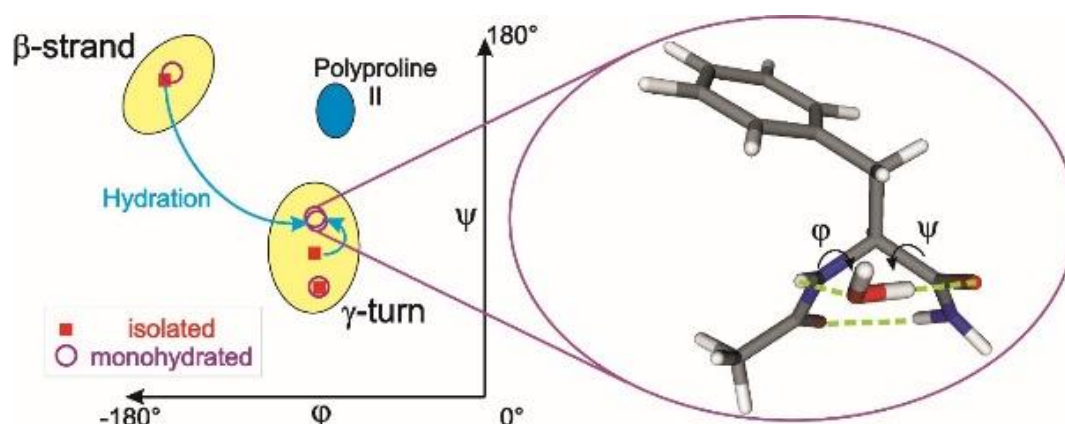


Figure 24: Shaping of a peptide chain by a single water molecule reported on a Ramachandran map (left) for a capped phenylalanine with two amide bonds (right).²¹⁹ This system gathers the three different outcomes of a microsolvation : (i) the structure is largely unchanged by microsolvation (squares and circles are in the same region of the map); (ii) the microsolvated structure is distorted as compared to the isolated one (short blue arrow); (iii) a microsolvation-induced isomerization occurs (long blue arrow). Polyproline II, the structure expected for small peptide chains in aqueous solution, is also shown.

12. Specific peptides and aggregates

12.1. Cyclic peptides and depsipeptides

Cyclic peptides are ubiquitous substances in nature, which are frequently present in plants, fungi, bacteria and lower sea organisms (cf. e.g. ^{444,445}). Many cyclopeptides exhibit cytotoxic properties (cf. e.g. phallotoxin⁴⁴⁶), act as antibiotics (cf. e.g. valinomycin⁵⁹), neuropeptides (cf. e.g. vasopressin⁴⁴⁷) or iron chelators (cf. e.g. ferrichrome⁴⁴⁸). These properties originate from their ability to form bioactive conformations, which can either be substrate molecules for larger peptides (cf. e.g. ⁴⁴⁹) or act as cyclic ligands for embedded guest molecules or ions. Their high biological effectiveness is partly due to the ring closure, which (in comparison to linear peptides) makes them more resistant towards decomposition by proteases (cf. e.g. ⁴⁵⁰). Additionally, a lower entropic barrier for the complexation of molecules or ions is advantageous ⁴⁵⁰. Taking nature as model, synthetic cyclopeptides have gained importance as artificial receptors (e.g. ⁴⁵⁰⁻⁴⁵²), partly including rigid non-natural amino acid subunits (cf. e.g. ⁴⁵⁰). For these sequences made of natural and non-natural amino acids, the analysis of molecular recognition abilities always requires a detailed conformational investigation. Therefore, molecular beam spectroscopy can offer valuable results regarding intrinsic structural properties and structural behaviour during a stepwise addition of solvent molecules and aggregation partners.

Among cyclopeptides, some naturally relevant ones belong to the class of depsipeptides, in which at least one amide group is replaced by an ester group. A famous, medically relevant example is the bacterially synthesized valinomycin, whose antibiotic effects are based on the complexation and transport of potassium ions through the cell membrane of pathogenic bacteria leading to a breakdown of the membrane potential and finally the death of the bacterium (e.g. ^{453,454}). Beyond the cyclic representatives, linear depsipeptides with a high biological activity exist, e.g. dolastatin, a cytostatic anticancer agent (cf. e.g. ⁴⁵⁵). The introduction of an ester group in the sequence can affect different H-bonding patterns, trigger a different folding behavior^{456,457} and thus probably leads to a different biological activity.

In comparison to linear α -peptides, depsipeptides and cyclic (depsi)peptides have been less investigated spectroscopically under isolated conditions, but especially cyclic systems have gained increasing attention throughout the last years.

12.1.1 Depsipeptides

Spectroscopic molecular beam investigations on depsipeptides started in the Gerhards group with the linear MOC system ([1-[(2-methoxyphenyl)amino]-1-oxopropane-2-yl]2-(cyclohexanecarbonyl-amino)acetate (or cyclohexylcarbonyl-glycine-lactate-2-anisidine, abbrev. CyCO-Gly-Lac-NH-PhOMe, in the peptide nomenclature)³⁰¹. It contains a glycine and a lactic acid (Lac) moiety as well as a suitable UV chromophore in the protection group and a cyclohexyl ring at the other protecting group (cf. Figure 25). Up to that point only some theoretical studies on Gly and Lac containing oligopeptides could be referred to^{457,458} as well as IR investigations in solution^{456,459}. In case of e.g. *t*-Bu-Gly-Lac-NH-Me, which shares the same amino acid blocks as MOC, a β -turn structure was found⁴⁵⁹ by IR spectroscopic analysis. However, the missing ester group in the backbone effects a quite limited comparability.

From the experimental point of view, R2PI spectra combined with IR/R2PI and IR/IR/R2PI measurements revealed three isomers. For DFT calculations including Grimme dispersion (D3)³⁵⁰, folded structures turned out to be energetically favored. They are mainly stabilized by strong dispersion interactions between the cyclohexyl and the phenyl residue, rather than by H-bonds. The most stable isomer with a folded $\alpha_D\delta_D$ arrangement (cf. Figure 25), exclusively stabilized by dispersion (thus not found by dispersion-excluding calculations) showed an excellent agreement with the experimental IR data. In addition, two further folded isomers could be identified with the H-bonded arrangement being the least stable one among the three assigned isomers. The excellent agreement with the experiment illustrated the capacity of DFT-D methods to properly account for dispersive interactions as well as the necessity to include them especially in systems in which $\text{CH}\cdots\pi$ interactions can form (a feature that is shared by various peptide systems containing at least one aromatic chromophore but especially in case of neighboring aromatic groups, cf. e.g. Section 12.1.2 and^{64,65} or²⁹²).

A further striking point with regard to the performed IR/IR/R2PI experiments on MOC is a possible IR-initiated rearrangement of one isomer into the other two isomers observed³⁰¹. Thus, these results are a motivating basis for further investigations on linear and particularly cyclic depsipeptides with a special focus on their aggregation behavior.

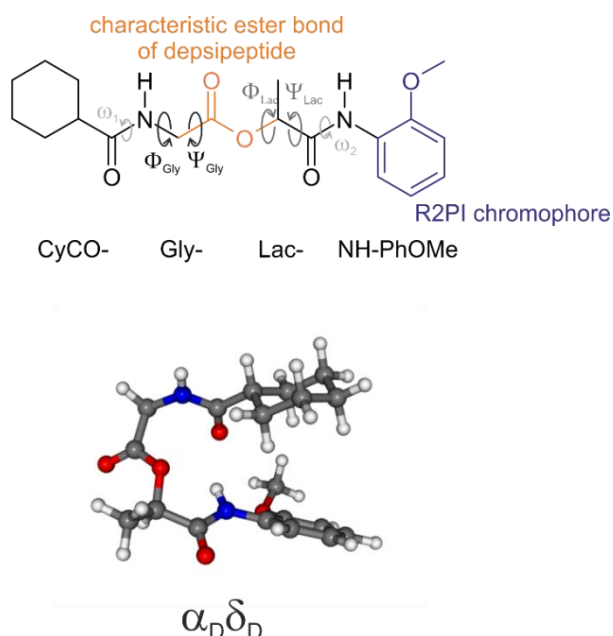


Figure 25: Schematic illustration of the linear depsipeptide MOC (top) along with the most stable assigned isomer (bottom), whose stability is due to dispersion interactions (cf. text).

12.1.2. Cyclopeptides

Despite the high biologic relevance, only a few spectroscopic studies on isolated (neutral) cyclopeptides have been performed so far. Investigations on cyclic dipeptides and tetrapeptides will be presented in the following

sections. The largest cyclic peptide analyzed so far is Gramicidin S which will be addressed in context with other non-cyclic gramicidin peptides (cf. Chapter 12.2).

Cyclic dipeptides

Though cyclic dipeptides were the first cyclopeptides to be investigated^{62,63} by molecular beam spectroscopy, the latest studies are less than two years old^{64,65}. Beyond interesting stereochemical effects specifically due to ring closure, cyclodipeptides also attract attention for their potential pharmacological activity, which might involve interactions between aromatic amino side chains and receptors⁶⁴.

The first to analyze a cyclic dipeptide, cyclo(Gly-Trp), by R2PI, UV/UV hole burning and photoelectron spectroscopy were Weinkauff and coworkers.⁶² The experimental data allowed the conclusion that only one isomer with an ionization energy higher than that of pure 3-methylindole is present, which indirectly indicated a strong geometry change upon ionization. In DFT calculations, the three most stable structures showed attractive interactions between the peptide ring and the Trp side chain (NH $\cdots\pi$, CH $\cdots\pi$). These interactions become repulsive in the cationic form of all three conformers, resulting into the geometry change upon ionization. Though a final assignment to one of these calculated structures was not possible in comparison to the performed experiments, the authors tentatively proposed the most stable isomer with NH $\cdots\pi$ interaction in the S_0 state to be formed in their molecular beam experiments.⁶²

Another cyclic dipeptide, cyclo(Phe-Ser) was studied by R2PI, UV/UV hole burning and structurally more sensitive IR/R2PI measurements in the de Vries group⁶³. Five conformers were assigned from comparison with DFT calculations. In two of them a strong H-bond between the hydroxyl group of the serine side chain and CO of Ser is formed. In a third one the H-bond is weak whereas in the other two remaining isomers the OH group is completely free. For two of the structures additional CH $\cdots\pi$ interactions are observed. Despite the stronger rigidity of the system, the number of conformers was not reduced for cyclo(Phe-Ser) in comparison with the linear Phe-Ser but the intensity of torsional vibrations was reduced. A remarkable feature for the cyclo(Gly-Trp) as well as for the cyclo(Phe-Ser) is the cis orientation of the amide bonds which is usually unfavorable in linear peptides.

In 2018, Zehnacker and coworkers studied the cyclo(Phe-Phe) in its L-L and its L-D configuration also in comparison with their linear analogues⁶⁵, already analyzed before⁴⁶⁰. The Phe-Phe sequence is supposed to play a role in the formation of amyloid fibres⁴⁶¹ but sequences with more than one (and even neighboring) aromatic side chains are always of interest with regard to the influence of dispersion onto structural preferences. R2PI and IR-UV hole burning were applied in comparison with dispersion corrected DFT calculations. Anharmonic frequencies were calculated by variational perturbation theory for the most stable cyclic structures. Furthermore, optimization and frequency calculations in the S_1 state and the visualization of the intramolecular interactions were performed by the non-covalent interaction plot. Due to the rigidity of the ring as well as the interactions involving the Phe side chains only one conformer was found in the molecular beam. The influence of chirality was found to be small for the two cyclic diastereomers: Hardly any differences were observed in the electronic spectra and the assigned conformation was similar. It is characterized by one of the side chains in a flagpole position with the aromatic ring folded over the peptide backbone ring, whereas the second Phe chromophore extends out of the backbone ring. Stabilizing CH $\cdots\pi$ and NH $\cdots\pi$ interactions occur but their nature and strength in the two diastereomers differ which leads to differences in the NH stretching region. A special importance for shaping the cyclic dipeptide is ascribed to the CH $\cdots\pi$ interactions. Conformers having a stacked conformation of the Phe rings could not be found under experimental conditions. In the DFT-D3 calculations a stacked conformer was only found for the L-L configured cyclopeptide, whose Phe side chains can both be in equatorial position, which reduces their repulsive interaction. This is not possible in the L-D configuration.

In a next step of their investigations the Zehnacker group analyzed the two diastereomers (L-L and L-D) of cyclo(Tyr-Tyr)⁶⁴, with the unprotected hydroxyl group of the Tyr side chain having a remarkable influence on the conformation. For both diastereomers, a similar family of structures exists, with comparable features as in cyclo(Phe-Phe). Again stabilizing CH $\cdots\pi$ and NH $\cdots\pi$ interactions occur which differ in strength for the diastereomeric cyclo(Tyr-Tyr). However, in contrast to cyclo(Phe-Phe), a stacked structure was now observed and assigned in the L-L species (cf. Figure 26), due to the possible formation of an H-bond between the side

chain OH groups, a feature not allowed in the L-D species. The OH groups thus act as a kind of anchoring side in the L-L diastereomere finally making the stacked structure the most stable isomer. For the L-D peptide the most stable conformer is the one comparable to the structure found for the corresponding cyclo(Phe-Phe). Taking the results for cyclo(Phe-Phe) and cyclo(Tyr-Tyr) into account the question arises how the cyclo(Phe-Tyr) would structurally behave under isolated molecular beam conditions especially with regard to the fact that for the L-L diastereomer NMR solution measurements suggest a structure similar to the stacked one found for L-L configured cyclo(Tyr-Tyr)⁶⁴.

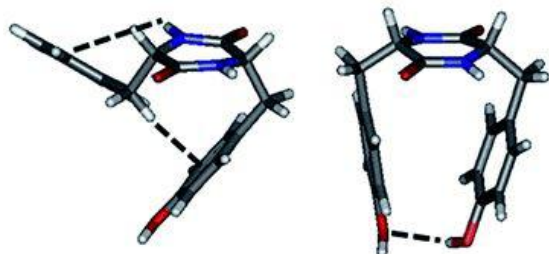


Figure 26: The two assigned structures (non-stacked and stacked) assigned for the L-L cyclo(Tyr-Tyr). The non-stacked structure presents the most stable isomer, with the stacked structure being only 0.2 kcal/mol higher in Gibbs energy (B3LYP-D3/6-3111++G(d,p)). Reprinted with permission from Ref. ⁶⁴. Copyright (2018) The Royal Society of Chemistry.

Cyclic tetrapeptides

The Gerhards group studied the first cyclic tetrapeptide cyclo[L-Tyr(Me)-D-Pro]₂ (abbrev.: CP_{Tyr}) and its monohydrate by applying IR/R2PI spectroscopy in the amide A/OH stretching and partly in the amide I/II region³⁹¹. The secondary amide groups of the proline residues reduced the number of NH groups to two instead of four, but the IR/R2PI spectrum finally only exhibits one slightly asymmetric band at 3276 cm⁻¹ (cf. Figure 27). This can be a hint that both NH groups are H-bonded in a quite similar binding environment. The B3LYP calculations predicted three basic types of conformers: those with two internal H-bonds, one H-bond or without any H-bond. The most stable structure with two strong H-bonds between the NH and CO groups of the two opposite Tyr residues could best explain the experimental IR data. This is true with regard to the amide I/II region and with regard to the two NH stretching vibrations calculated to be nearly identical (cf. Figure 27). In contrast, the other structural types of conformers all exhibit split NH vibrations, partly in the free NH stretching region remarkably above 3400 cm⁻¹.

Though the assignment of the most stable doubly H-bonded isomer was unambiguous, the strength of the two H-bonds was underestimated in the calculations so that even the scaled NH-stretching modes were located above 3300 cm⁻¹. Experimental data could partly be better predicted by applying a more mode specific scaling factor derived from reference calculations with the Ac-Phe-NHMe dimer. Thus, the necessity to apply mode specific scaling became obvious again^{353,354}.

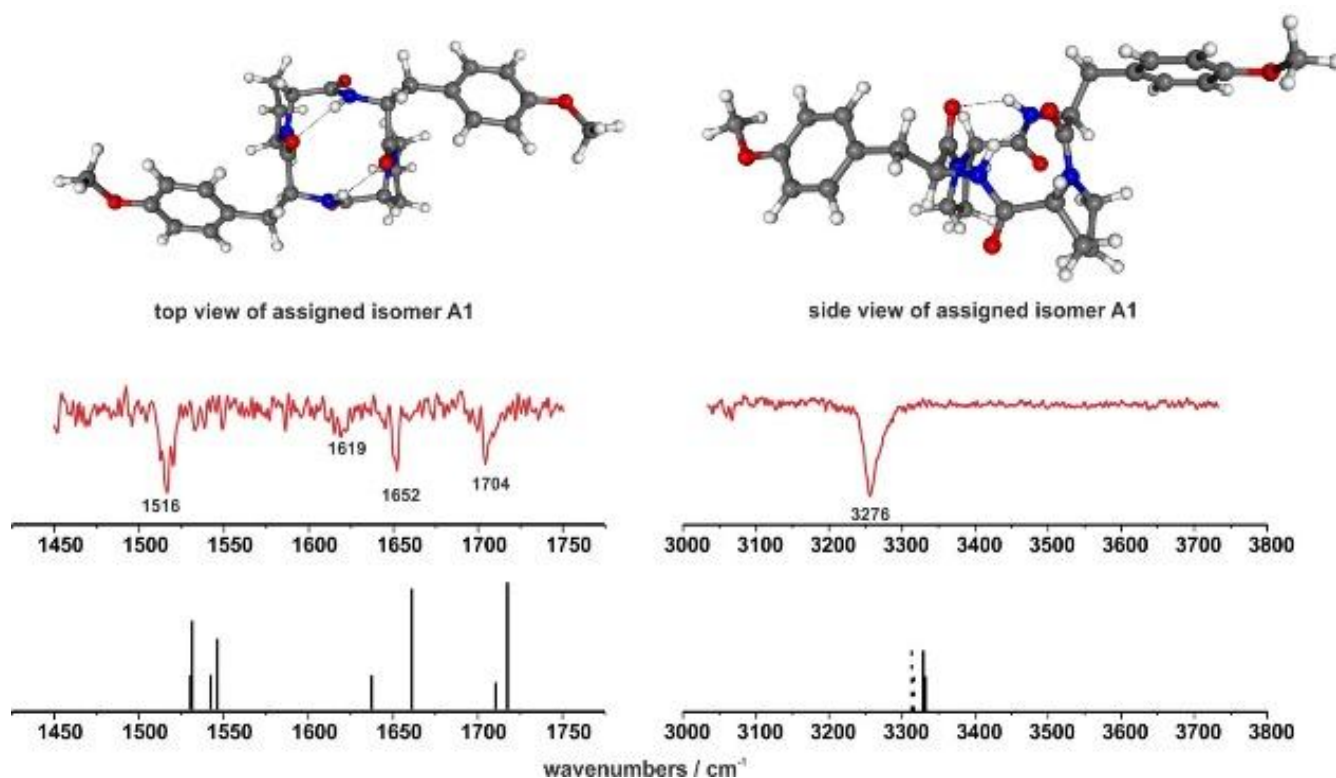


Figure 27: Experimental IR/R2PI spectra in comparison with calculated stick spectra (DFT/B3LYP/TZVP) of the assigned conformer for cyclo[L-Tyr(Me)-D-Pro]₂. The dotted lines depict the calculated NH modes scaled by a more mode specific scaling factor (see text). Spectra reprinted with permission from Ref. ³⁹¹. Copyright (2011) John Wiley and Sons.

For the monohydrate, not only the structure of the cyclic peptide backbone (doubly, singly or non-H-bonded) but also the different binding motifs for the water molecule must be taken into account: single or double H-bond donor or acceptor, H-bond donor and acceptor (bridging NH and CO) or even in a triple function. Additionally, interactions with the π -system of the aromatic side chains can occur. Since the experimental spectrum contained one band more than expected (five instead of four, cf. Figure 28) and UV-generated fragmentation of larger clusters or Fermi resonances could be excluded, two isomers, having the same UV excitation energy, were taken into account. The most stable calculated isomer can be derived from the monomeric structure by attaching water as an H-bonding donor to a proline CO group. This structural motif is the one which can be unambiguously assigned (cf. Figure 28). As further tentative assignment, explaining the band around 3400 cm^{-1} , a second binding motif with one internal H-bond and water in a bridging function between a CO and a NH group (cf. Figure 28) was given. Thus, the first molecular beam investigations on a cyclic tetrapeptide were performed and structural assignments for the monomer and monohydrate could be given.

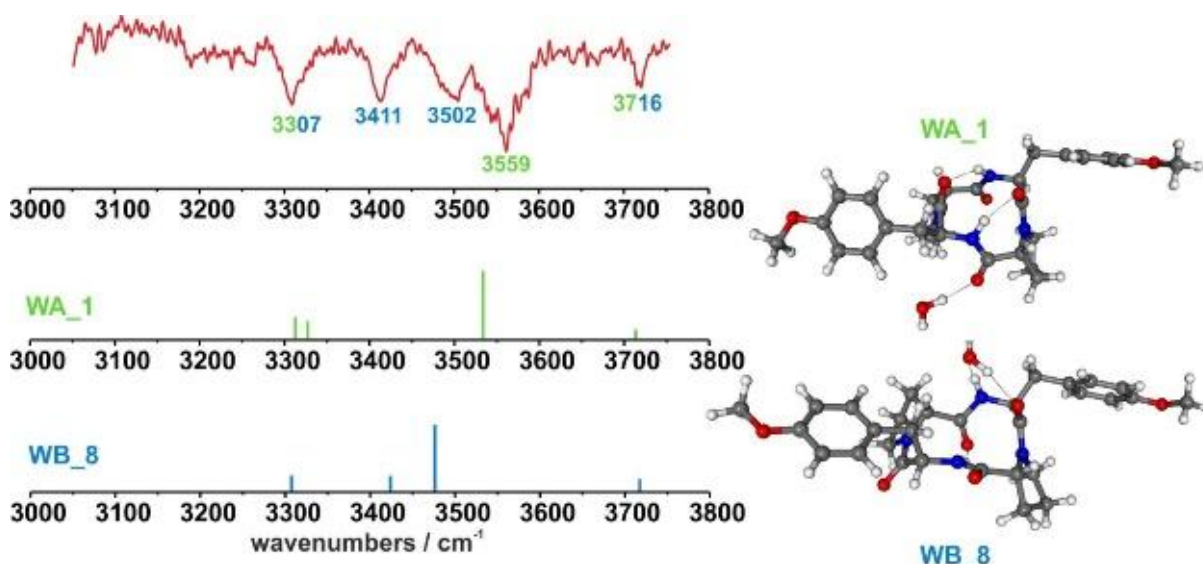


Figure 28: The experimental IR/R2PI spectrum in comparison with the calculated stick spectra (DFT/B3LYP/TZVP) of the assigned conformer WA_1 for the monohydrated cyclo[L-Tyr(Me)-D-Pro]₂ as well as for a second isomer, tentatively assigned. Spectrum reprinted with permission from Ref. ³⁹¹. Copyright (2011) John Wiley and Sons.

To analyze the influence of an asymmetric amino acid constitution the investigations on cyclic tetrapeptides were further extended by replacing one of the tyrosine units with a sterically less demanding alanine moiety (cyclo[L-Tyr(Me)-D-Pro-L-Ala-D-Pro], abbrev.: CP_{Ala}) or with a sterically more demanding glutamic acid, protected by a methyl ester at its acidic end (cyclo[L-Tyr(Me)-D-Pro-L-Glu(Me)-D-Pro], abbrev.: CP_{Glu})³³⁵. In the IR/R2PI measurements an asymmetric or partly slightly split band around 3275 cm⁻¹ is again visible, giving a first hint for a similar binding motif as found for CP_{Tyr}. In addition, the CP_{Glu} IR/R2PI spectrum exhibits a further band of low intensity around 3330 cm⁻¹. In the DFT(-D3) calculations, the most stable structure is doubly hydrogen-bonded for CP_{Ala} and CP_{Glu}, comparable to CP_{Tyr}. Additionally, further structural binding motifs similar to those of CP_{Tyr} were found (with two, one or no H-bond). The side chain of the glutamic acid in CP_{Glu} with its CO group allowing interactions with the peptide backbone offers more structural flexibility so that more conformers must be taken into account. A comparison of the calculated and experimental IR spectra for CP_{Ala} and CP_{Glu} allowed the unambiguous assignment of the doubly H-bonded structure in both cases (cf. Figure 29). For CP_{Glu} a second conformer with a doubly H-bonded structure and a further H-bond between the carbonyl group of the Glu side chain and its NH group in the backbone, being remarkably less stable, is proposed (cf. Figure 29). The additional H-bond does not seem to compensate the backbone deformation necessary to allow the Glu side chain to fold back onto the backbone. Furthermore the CO_{Tyr} and the CO_{Glu,sidechain} share the same H-bond donor (NH_{Glu}), leading to two comparatively weak H-bonds and a calculated NH vibration above 3300 cm⁻¹.

Solvation effects on both cyclic tetrapeptides were estimated by the polarized continuum model (PCM): For CP_{Ala} the originally assigned doubly H-bonded structure is conserved in the presence of a first solvation shell in contrast to CP_{Glu} for which a singly H-bonded structure was found. The missing internal H-bond was compensated by the efficient solvation of the carbonyl group of the Glu side chain.

The comparative analysis of these three cyclic tetrapeptides indicates further investigations of these systems including a variation in amino acid constitution and ring size, also with regard to the binding ability for other binding partners like solvent molecules or metal cations.

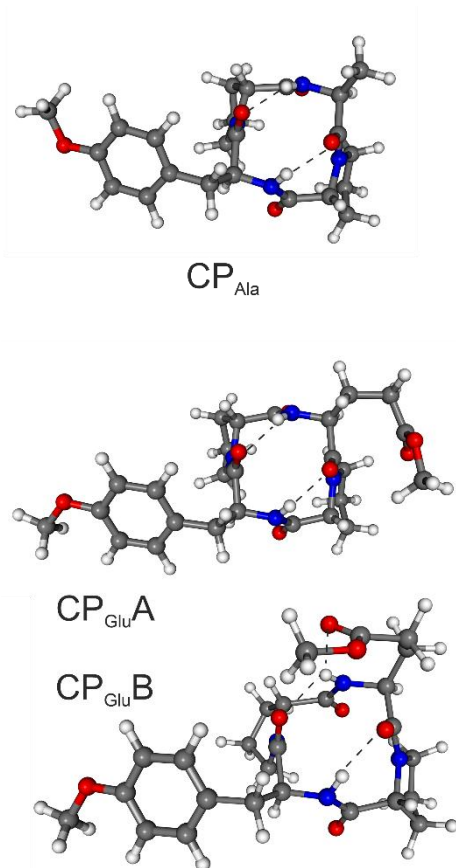


Figure 29: DFT-D3/B3LYP/TZVP structure of the assigned conformer for the cyclo[L-Tyr(Me)-D-Pro-L-Ala-D-Pro] (top) and of the two conformers assigned for the cyclo[L-Tyr(Me)-D-Pro-L-Glu(Me)-D-Pro] (in the central and bottom). Structures reprinted with permission from Ref. ³³⁵. Copyright (2017) PCCP Owner Societies.

12.2. Naturally relevant peptides or sequences/chain fragments

Gramicidin peptides

Gramicidin peptides can be obtained from the bacterium *Bacillus brevis*^{146,462} and they are well known for their antibiotic effects, which are based on the selective transport of potassium ions through cell membranes resulting in the death of the targeted cell^{146,463}. They can be subdivided in a family of linear 15-residue peptides with subgroups (e.g. A, B, C cf. Table 11) which differ in one (aromatic) amino acid and the cyclic gramicidin S, a decapeptide built of two identical pentapeptide units (cf. Figure 30).

Gramicidin	X	Y
A1	Val	Trp
B1	Val	Phe
C1	Val	Tyr

Table 11: Sequence of the different gramicidin peptides HCO-X-Gly-Ala-D-Leu-Ala-D-Val-Val-D-Val-Trp-D-Leu-Y-D-Leu-Trp-D-Leu-Trp-NHCH₂CH₂OH, with those investigated by de Vries and coworkers⁴⁶⁴.

The OH-, NH- and CH-stretching region of gramicidin peptides was first spectroscopically investigated under isolated molecular beam conditions by de Vries and coworkers in 2006¹⁴⁶ who analyzed linear forms as well as

the cyclic one. These first, purely experimental results already suggested a helical arrangement for the investigated linear gramicidin peptides and a β -sheet like structure for the cyclic one. The presence of only one dominant conformer in a helical conformation was later on confirmed for the linear gramicidin A1 and C1 by further expanding the spectra to the region of 1800 to 1000 cm^{-1} and comparing them with calculations. The latter gave a better description of the experimental data if dispersion was taken into account⁴⁶².

With regard to the structure of cyclic gramicidin S, the doubly protonated, thus ionic form was also investigated⁴⁶⁵⁻⁴⁶⁹. The main finding of a β -sheet like arrangement comparable to the neutral form was confirmed. Overall, three isomers were identified with two of them having a similar structure, whereas the structure for the third one is still pending.

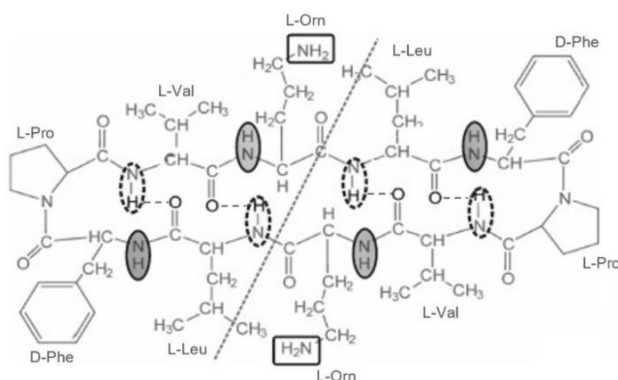


Figure 30: The principle composition and structure of the gramicidin S peptide, adapted with permission from Ref. ¹⁴⁶. Copyright (2006) John Wiley and Sons.

Forbidden Sequences

In nature, several sequences seem to be absent from all known protein primary structures and were thus named 'forbidden sequences'. This singularity can be tentatively explained by the fact that these sequences might disturb the formation of functional protein secondary structures. In 2009, Vaden et al.³⁰⁶ analyzed such forbidden sequences in two pentapeptides: Phe-Phe-Met-Cys-Thr and Trp-Cys-Phe-Asn-Leu. IR/R2PI measurements in comparison with DFT calculations (using B3LYP or the dispersion including M05-2X functional) assigned one isomer for each pentapeptide. In the case of Phe-Phe-Met-Cys-Thr, the formation of a β -turn motif was proposed, probably additionally stabilized by side chain-backbone as well as $\text{OH} \cdots \pi$ interactions, whereas interactions between adjacent Phe chromophores do not seem to play a significant role. For Trp-Cys-Phe-Asn-Leu a 3_{10} helical structure is the most dominant (and on the M05-2X level the most stable) isomer but the presence of a second helical arrangement was assumed. The authors argue that the bulky side chains arranged in a sterically demanding way could e.g. disturb the formation of functional protein secondary and tertiary structures. Nevertheless, the authors concede that the analysis of these peptides can only be a first step in understanding these forbidden sequences and that further variations, including capped peptide sequences, must be investigated. The latter aspect is especially true since a segment of a natural peptide backbone can better be imitated by capped peptides in which the probability for interactions between the N- and C-terminus is reduced.

Ser-Ile-Val-Ser-Phe-NH₂

The Ser-Ile-Val-Ser-Phe peptide³³⁴ represents a partial sequence of the so-called β_2 -adrenaline receptor protein (β_2 AR) binding the catecholamin neurotransmitter adrenaline. Though a crystal structure of the adrenaline- β_2 AR complex is known, it still cannot reveal the origin of molecular recognition why adrenaline is recognized whereas other molecules are not bound. Thus, Fujii and coworkers³³⁴ drew on the bottom-up approach to analyze the Ser-Ile-Val-Ser-Phe-NH₂ sequence by REMPI, UV-UV hole burning as well as by IR ion dip spectroscopy in comparison with dispersion corrected DFT-calculations. The experimental data already revealed that only one dominant isomer is present in the molecular beam. Comparing the calculated IR spectra

of different isomers with the experimental IR/UV hole burning spectra, two structures were found to be possible, the most stable as well as the second most stable conformer. The decision was finally made on the basis of the frequencies calculated for the first electronically excited state: for the most stable isomer, they could better describe the low-frequency vibronic modes found in the UV-UV hole burning spectrum. This global minimum isomer is characterized by a distorted β -hairpin structure.

Hexapeptide sequence of the tau protein

The tau protein of neurons is suspected to be responsible for the formation of intracellular neurofibrillary aggregates associated with neurodegenerative diseases like the Alzheimer's disease (cf. Section 1 and 7). In 2008, Snoek and coworkers¹⁴⁵ investigated a hexapeptide sequence of this protein, namely Ac-Val-Gln-Ile-Val-Tyr-Lys-NHMe in its neutral as well as in its charged form with the lysine side chain being protonated ($-\text{NH}_3^+$).

For the neutral hexapeptide investigated by IR/UV hole burning the structure observed was assigned to a β -turn motif with two stretched halves, despite this was not the most stable conformer calculated. The β -turn contained an additional C7 interaction in the turn and interactions between the Lys and Asn NH_2 groups with CO backbone groups, but a non-H-bonded OH in the Tyr side chain. However, a minor population in the global minimum structure (a distorted β -turn) could not be excluded.

In comparison, the charged species studied by IRMPD in an ESI-FTICR set-up, was analyzed in the CO-stretching and NH-bending region but the structural assignment turned out to be even more ambiguous. A tentative assignment was given to the most stable, almost helical, but quite coiled structure in which the enormous distortion of the backbone is compensated by the interaction of the lysine NH_3^+ group with the CO backbone groups. The presence of further isomers and even an interconversion between them at room temperature could not be excluded.

Though unambiguous structural assignments were not possible in case of the charged species, reasonable structural proposals were found exhibiting the possibly strong influence the charge can have on structural preferences. The general experimental and computational challenges (which increase with the size of the system) became even more evident when the dimer of the hexapeptide was investigated⁴²³ (cf. Section 12.4.1).

Delta-Sleep inducing peptide

Bakker et al.³⁹⁶ tried to analyze the nonapeptide Trp-Ala-Gly-Gly-Asp-Ala-Ser-Gly-Glu, known as delta sleep-inducing peptide (a neuropeptide)^{470,471}. The IR spectrum was measured in the region of $600 - 1800 \text{ cm}^{-1}$, characterized by broad bands due to an overlap of CO-stretching, NH- and OH-bending modes. However, this probably also partly originates from insufficient cooling of the large peptide. In 2005, calculations for such a big system were enormously challenging and thus only two structures were calculated on the semi-empirical AM1 level, a stretched and a helical one. Nevertheless, an assignment was not possible at that point. To go further, a proposal of the authors was to improve the cooling efficiency for such larger systems so that the spectral congestion is reduced which should increase the interpretability of the spectra.

12.3. Zwitterions

At the physiologically important pH of ~ 7 , most amino acids or peptides appear in their zwitterionic form. Under isolated conditions, those are usually only observed if the charges can be additionally stabilized by e.g. polar solvent molecules or metal cations (cf. e.g. references in ¹⁴⁴). With the focus on the formation of zwitterionic structures, Rijs et al.¹⁴⁴ investigated the hexapeptide model Ac-Glu-Ala-Phe-Ala-Arg-NHMe by IR/UV hole burning spectroscopy in the of $1000 - 1850 \text{ cm}^{-1}$ region (cf. Figure 31). The middle sequence Ala-Phe-Ala was chosen since it exhibits a certain preference for 3_{10} helical structures³⁸⁷ bringing the basic arginine and the acidic glutamic acid side chain into close spatial proximity. In comparison with calculations but also with data of other, smaller Glu containing systems a 3_{10} helical structure was assigned, in which a proton transfer between the side chains of Arg and Glu occurred. The structure was characterized by a salt bridge additionally stabilized by two H-bonds between the protonated and deprotonated side chains. This result demonstrates that zwitterionic forms can be observed in neutral peptides when the formation of a salt bridge is made possible by the structure.

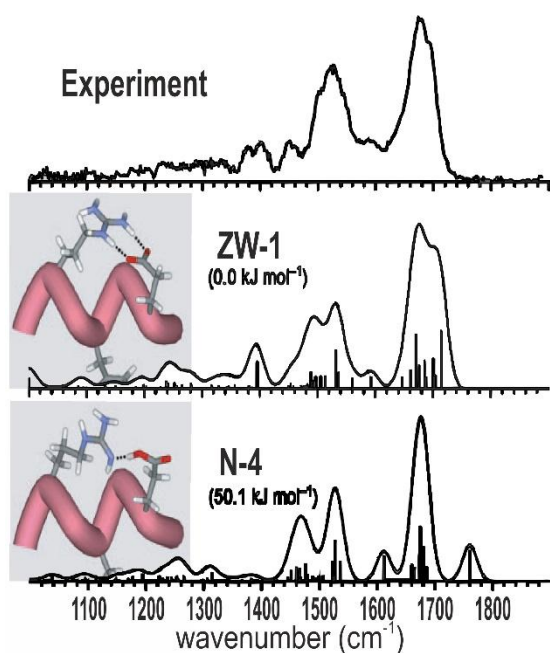


Figure 31: Representative illustration of a calculated zwitterionic and non-zwitterionic structure (energies MP2 level) and their calculated IR spectra (B3LYP/6-31+G(d)) in comparison with the experimental one (upper trace).¹⁴⁴ The backbone conformation is schematically sketched by the pink tube (see details in Ref.¹⁴⁴). Adapted with permission from Ref.¹⁴⁴. Copyright (2010) John Wiley and Sons.

12.4. Aggregates

The biological environment of peptides is manifold so that potential aggregation partners can for example be other peptide sequences (cf. following section) or water as the biologically most relevant solvent (cf. Section 11), but also non-peptide molecules (cf. Section 12.4.2). Molecular beam investigations always offer the option to successively add these aggregation partners. The aggregates are usually not present in the original sample but the binding partners are co-expanded in the molecular beam. Hence, they aggregate by collisions in the warm part of the molecular beam (cf. Section 4.1) before the formed aggregate is spectroscopically investigated in the cold part of the beam.

12.4.1. Peptide-peptide aggregates

As already explained in the introductory section and section 7, the interest in peptide aggregates and especially in potential β -sheet models arises from the role they play in infectious diseases like BSE, Scrapies and Creutzfeldt-Jakob (cf. e.g.⁸⁹⁻⁹¹) or non-infectious neurodegenerative diseases like Alzheimer and Parkinson (cf. e.g.⁹²⁻⁹⁵). Without going into details, it is assumed for both cases (infectious and non-infectious) that a pathogenic secondary structure change towards β -strand dominated forms occurs for certain brain proteins. Those can autocatalytically induce the formation of further pathogenic structures, finally leading to fibrils and plaques in the brain tissue.

For both, infectious and non-infectious diseases, not only the suppression of the outbreak but also the prevention of the progress and thus of the autocatalytical fibril formation is the main goal. In the past, a quite 'chemical' approach was the application of template molecules, binding to formed β -strands, or -sheets so that the growth of β -sheets up to fibrils is interrupted.

The following sections focus on the structural investigations of neutral amino acid and peptide aggregates (with at least one aromatic moiety) using combined IR/UV laser spectroscopic molecular beam methods.

Nevertheless, we want to briefly mention examples of aggregates of non-aromatic amino acids (Gly, Ala, Val), which were analyzed by Suhm and coworkers applying FTIR and Raman spectroscopy in a jet expansion^{30,40}. Furthermore, Hu and Bernstein studied higher aggregates of valine in a supersonic expansion by IR/VUV spectroscopy²⁵⁴. Beyond, also charged proton-bound amino acid dimers (cf. e.g.⁴⁷²⁻⁴⁷⁶) and dimers of polypeptides (cf. e.g.⁴⁷⁷⁻⁴⁷⁹) exist.

(Ac-Phe-OMe)₂

In addition to the monomeric Ac-Phe-OMe and Ac-Phe-NHMe, the homo dimers of the two protected amino acids were detected in the molecular beam expansion and were spectroscopically investigated. The R2PI and IR/R2PI spectra of (Ac-Phe-OMe)₂ indicated the presence of only one isomer with two H-bonded NH modes (frequencies below 3400 cm⁻¹)¹³⁴. Further measurements in the CO-stretching region and the comparison with calculations supported the assumption of a very symmetric β -sheet like arrangement composed of two monomers having the same side chain orientation ($\beta_i(g+)$ - $\beta_i(g+)$ or $\beta_i(a)$ - $\beta_i(a)$)²⁸⁴. The analysis in the upper fingerprint region³⁹⁷ revealed some characteristics, which were better reflected in the calculated spectra of $\beta_i(g+)$ - $\beta_i(g+)$ (also energetically preferred by MP2 calculations on DFT optimized structures). In the assigned structure, the intermolecular H-bonds between both β -strands form a ten-membered ring representing the smaller part of the unit cell within a β -sheet (cf. Section 2 and Figure 32). Later investigations in the far-IR (100-800 cm⁻¹), in comparison with anharmonically calculated modes from DFT-based molecular dynamics simulations (supported by graph theory), also discussed a β -sheet arrangement. However, their interpretation, mainly based on the 100-400 cm⁻¹ spectral region, suggests the monomers to have different side chain orientations, namely $\beta_i(g+)$ - $\beta_i(g-)$.³⁶³

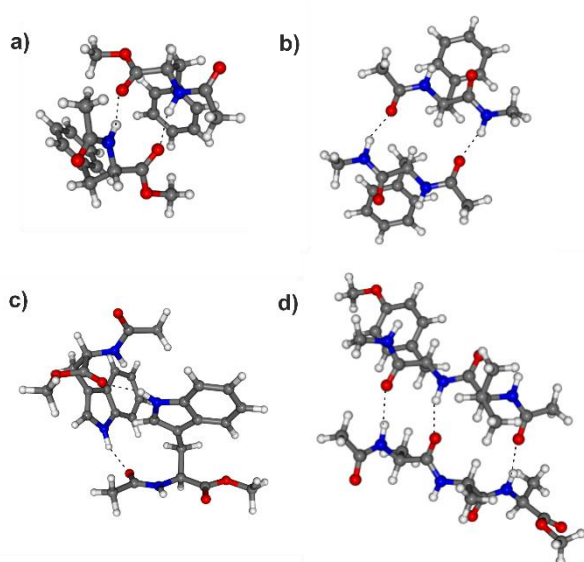


Figure 32: Assigned structures of the different peptide dimers: a) (Ac-Phe-OMe)₂ forming the ten-membered ring of a β -sheet unit cell, here with both side chain in a g(+) orientation^{134,284,397}, b) (Ac-Phe-NHMe)₂ forming the fourteen-membered ring of a β -sheet unit cell¹³⁵, c) dimer of Ac-Trp-OMe³³², d) the mixed dimer of Ac-Val-Tyr(Me)-NHMe and Ac-Ala-Ala-Ala-OMe¹⁴³.

(Ac-Phe-NHMe)₂

As next step, the dimer of the dipeptide model Ac-Phe-NHMe¹³⁵ was analyzed for which additional binding motifs originate due to the second amide group. Comparable to (Ac-Phe-OMe)₂ the reduced number of IR bands in the amide A and amide I/II region already implies a structure of high symmetry. Taking the calculated IR spectra into account, a parallel arrangement of the peptide strands could be excluded. With regard to an antiparallel motif two different arrangements can be formed: in the 'inner bound' isomer, intermolecular H-bonds are formed between the CO and NH groups of the phenyl residues (comparable to (Ac-Phe-OMe)₂); in the 'outer bound' isomer, H-bonds are formed between the CO and NH groups of the protection groups, cf. Figure 32. The latter one gives the best description for the experimental IR spectrum and is additionally the most stable isomer. This outer bound arrangement with its fourteen-membered interstrand ring represents the larger part of a β -sheet cell.

(Ac-Trp-OMe)₂

As mentioned before, the unprotected, polar NH group in the indole side chain does not have a direct impact on the backbone structure of the Ac-Trp-OMe monomer. However, the influence of the NH indole group becomes evident in the dimerization³³²: Beyond β -sheet-like arrangements structures must be taken into account in which the NH indole group participates in H-bonds. A free NH indole-stretching vibration around 3520 cm^{-1} would give an indication for a β -sheet arrangement but was not found in the experimental spectrum. In case of a symmetric arrangement involving the CO ester and NH indole groups in H-bonds only half of the expected vibrations (4 NH, 4 CO) should be observed. Since this was not found in the experimental spectra, a symmetric dimer could be excluded. Finally, the best fit between experimental data and theory was found for an asymmetric arrangement having one intermolecular H-bond between an NH indole and CO ester group and the second H-bond between the other NH indole group and the CO amide group (cf. Figure 32).

(Ac-Val-Tyr(Me)-NHMe)₂

The (Ac-Phe-OMe)₂ dimer revealed a ten-membered 'interstrand' ring, whereas in (Ac-Phe-NHMe)₂ a fourteen-membered ring is formed, both being binding motifs within an antiparallel β -sheet. Nevertheless, a complete β -sheet unit cell is composed of a ten- and fourteen-membered ring formed by three interstrand H-bonds. Thus, such a unit cell requires three amide bonds per strand which is for example fulfilled by the tripeptide model Ac-Val-Tyr(Me)-NHMe¹⁵⁷ studied in the Gerhards group. MD simulations, HF and subsequent DFT calculations predicted β -sheet arrangements to be the most favoured structures. On the DFT-level an antiparallel β -sheet and a parallel one with a γ -turn were calculated to be the most stable ones, with pure parallel β -sheets being more than 1100 cm^{-1} higher in energy. The structure of the most stable antiparallel β -sheet was characterized by three strong H-bonds being all of similar length; in comparison, the inner H-bond of the parallel β -sheet was longer than the outer ones and, in the parallel β -sheet with the γ -turn, the inner H-bond length was strongly decreased. Therefore, these structures should exhibit characteristic, distinguishable frequencies. The behavior of the IR/R2PI spectrum via different UV excitation energies as well the detected number of transitions (three above 3400 cm^{-1} and three below) indicated the presence of one dominant isomer. The excellent fit between experimentally observed and calculated frequencies finally allowed to assign the observations to the most stable calculated antiparallel β -sheet (cf. Figure 33) and to unambiguously exclude other structural motifs.

With the investigation of the Ac-Val-Tyr(Me)-NHMe dimer the first formation of a secondary structure unit cell under isolated molecular beam conditions was demonstrated. Against the background of the discussion about a β -strand or β -turn preference of the monomer,^{102,388,401} one should be aware that the dimerization process occurs in the early stage of the molecular beam expansion between (relatively 'hot') monomers. Therefore, remarkable structural changes are possible until the final dimer structure is frozen out. Thus, these investigations reveal the strong intrinsic driving forces of peptide sequences to adopt defined naturally relevant structures without a solvent or peptide environment.

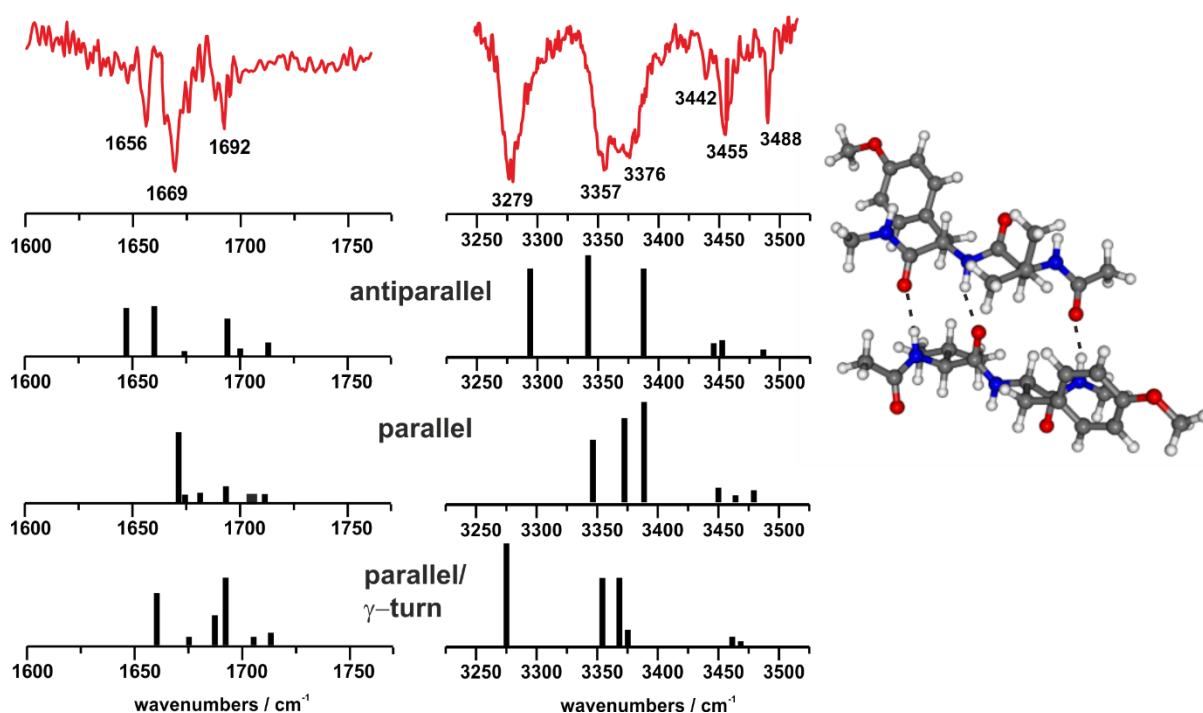


Figure 33: IR/RPI spectra of the $(\text{Ac-Val-Tyr(Me)-NHMe})_2$ in comparison with calculated stick spectra (B3LYP/cc-pVDZ). At the right hand side: structure of the assigned β -sheet unit cell (details cf. ¹⁵⁷). Experimental spectrum reprinted with permission from Ref. ¹⁵⁷. Copyright (2008) American Chemical Society.

A hetero dimer of Ac-Val-Tyr(Me)-NHMe and Ac-Ala-Ala-Ala-OMe

The question if peptide systems are able to form special (naturally relevant) secondary structures during molecular beam expansion was further addressed with the investigation of the dimerization between Ac-Val-Tyr(Me)-NHMe and Ac-Ala-Ala-Ala-OMe.¹⁴³ Additionally, it should be evaluated if the observed formation of (antiparallel) β -sheet(-like) arrangements is only possible for two identical monomeric units or if hetero dimers can also be formed from monomers with potentially different structural preferences.

For the monomeric Ac-Val-Tyr(Me)-NHMe (cf. Section 7.4), a β -strand was originally assigned though a β -turn could also be discussed^{102,388,401}. In contrast, the structure of Ac-Ala-Ala-Ala-OMe was not analyzed so far. The results from literature indicated that a C-terminal lysine protonated at its side chain can drive the formation of helical arrangements^{405,406,477,480}, whereas an N-terminal tryptophan supports the formation of antiparallel β -sheet-like structures⁴⁸¹. Investigations of the Mons group on Ala₅ with either a Phe moiety or a OBz protection group revealed a preference for β -hairpin structures or further strongly H-bonded arrangements^{72,73}.

Due to the missing UV chromophore, the analysis of Ac-Ala-Ala-Ala-OMe was performed along with investigations on further protected alanine peptides of increasing chain length (Ac-Ala_n-OMe, $n = 1 - 4$) by FT-IR spectroscopy in a gas cell (cf. ¹⁴³). For structural assignments, the experimental data were compared to DFT- and DFT-D3 calculations, which (especially the latter) predicted folded structures to gain importance in the tri- (and tetra) peptide compared to the monomer or dimer. In case of the tripeptide, DFT-D3 calculations at 0 K clearly favor a folded double γ -turn structure, which becomes entropically disfavoured (but not irrelevant) at higher temperatures. These theoretical predictions are in consistence with the FTIR measurements having gas cell temperatures above 500 K: Here the stretched conformations still dominate the spectrum but H-bonded conformations are also remarkably populated. These gas cell conditions are of course not directly comparable to molecular beam expansion: Here the two peptides Ac-Val-Tyr(Me)-NHMe and Ac-Ala-Ala-Ala-OMe are

brought into the carrier gas stream by being heated in two sequential but separated sample reservoirs (about 400 K). The dimerization occurs during coexpansion in the molecular beam. Though the remaining internal energy of the two monomers before dimerization (as well as the final temperature of the formed dimers) is difficult to estimate in the molecular beam. Nevertheless, the gas phase FT-IR spectroscopic investigations revealed that structural preferences of Ac-Ala-Ala-Ala-OMe are not exclusively stretched conformers.

MD and DFT-D calculations were performed on the hetero dimer and revealed that, as in case of the homodimer (Ac-Val-Tyr(Me)-NHMe)₂, β -sheet arrangements are preferentially formed. In comparison with the experimental IR/R2PI spectrum an antiparallel β -sheet structure was assigned again (cf. Figure 32). Therefore, these first studies on a hetero dimer demonstrated, that the co-expansion of two independent and different molecules can lead to the formation of a β -sheet model under isolated molecular beam conditions.

The results for (Ac-Val-Tyr(Me)-NHMe)₂ as well as for the self-assembled heterodimer might indicate that peptides containing a Val-Tyr sequence can show an intrinsic template behavior: other peptide binding partners are forced to form a dimer with a certain secondary structure like an antiparallel β -sheet arrangement.

Dimer of the tau-peptide

Beyond the monomeric hexapeptide Ac-Val-Gln-Ile-Val-Tyr-Lys-NHMe (cf. section 12.2)¹⁴⁵ also the dimer was investigated by Vaden et al.⁴²³. In comparison to the monomer, the dimer spectrum shows more red-shifted features, which could indicate the presence of stronger H-bonds than in the monomer species. Based on a comparison between (DFT-) calculated and experimental spectra tentative assignments were proposed excluding coiled structures and leading to partly opened β -sheets. However, the final discrimination between an antiparallel and a parallel β -sheet was not possible. Nevertheless, the principle presence of such β -sheet arrangements was supported by a comparative energetic estimation. In that procedure the energy required to unfold the monomeric structure and the binding energy of the dimer were taken into account. It revealed that the stronger H-bonds in the dimer could overcompensate the unfolding energy of the monomer.

12.4.2 Non-peptide aggregates

Beyond peptide-peptide and peptide-water aggregation (cf. Section 11), also sugars, nucleobases or potentially β -sheet blocking agents are of biological interest as peptide binding partner, which are further addressed in the following sections. In addition, metal peptide interactions of course play an important biological role in ion channels (cf. e.g.⁴⁸²), in (redox) active centers of proteins (cf. e.g.^{483,484}) or in antibiotic depsipeptides acting as ion transporters through cell membranes (cf. e.g.^{453,454}).

Nevertheless, as this review focuses on neutral systems, aggregates with metals should not be addressed here in detail and only exemplary references are given for the interested reader: Binding energies and binding properties of aggregates between metal cations and amino acids or small peptides are analyzed by CID (cf. e.g.^{485,486}) or ECD experiments (cf. e.g.⁴⁸⁷⁻⁴⁸⁹). For structural investigations, IRMPD measurements are frequently performed (cf. e.g.^{165,490-495}), mostly in non-cooled ion traps, less frequently in cooled ion traps.⁴⁹⁶ Quite rare are studies which investigate metal-amino acid/peptide aggregates under jet-cooled conditions (cf. ⁴⁹⁷⁻⁵⁰¹). Beyond IRMPD measurements^{500,501}, also an IR+UV photodissociation method was established⁵⁰¹ on the example of [Al-AcPheOMe]³⁺.

Pyrazole-based template molecules as potential β -sheet blockers

The knowledge about the correlation between the formation of pathogenic β -sheet structures with autocatalytic behavior and (un)infectious neurodegenerative diseases (cf. chapter 1, 7, 12.4.1) effected the development of different approaches for treatment: One of them consists in deactivating the (autocatalytically active) aggregation sites of β -sheets using template molecules⁵⁰²⁻⁵⁰⁵.

Pyrazole and pyrazole derivatives were investigated as template molecules by aggregating them with protected amino acids and small protected peptides^{163,506}. In a first publication, the aggregation between the well-analyzed protected amino acid Ac-Phe-OMe and pyrazole (Py) or 5-amino-3-methylpyrazole (MAP) (cf. Figure

34) was analyzed⁵⁰⁶. For the Ac-Phe-OMe...pyrazole cluster, the comparison between the IR/R2PI spectrum and DFT-calculations allowed the assignment of a doubly H-bonded aggregate ($\text{CO}_{\text{Phe}} \cdots \text{NH}_{\text{Py}}$ and $\text{NH}_{\text{Phe}} \cdots \text{N}_{\text{Py}}$). In this aggregate the β_{L} conformation of Ac-Phe-OMe is conserved but the side chain orientation changes from gauche(+) in the monomer to anti. Furthermore, the red-shift of the NH_{Phe} stretching mode (compared to the Ac-Phe-OMe monomer) is larger than for the Ac-Phe-OMe dimer, which indicates a stronger H-bonding and a higher stabilization energy in the Ac-Phe-OMe...pyrazole cluster. In case of the aggregate with MAP it must be additionally taken into account that MAP has two tautomeric forms (cf. Figure 34). According to *ab initio* and DFT calculations, the aggregates with the MAP(1) form are more stable than those with MAP(2). Nevertheless, in comparison with the IR/R2PI spectra a tentative assignment for both aggregates is performed with the MAP(2) tautomer and Ac-Phe-OMe having a $\beta_{\text{L}}(\text{g}+)$ or $\beta_{\text{L}}(\text{a})$ structure (cf. Figure 35). The deviations between the two IR/R2PI spectra are supposed to originate from differences in backbone conformation of the protected amino acid rather than from different tautomer forms of MAP.

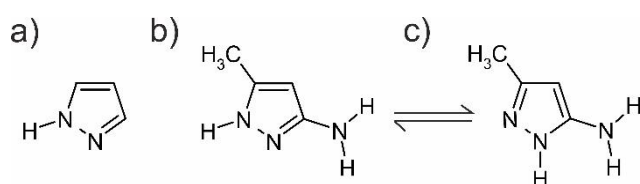


Figure 34: Principle structures of the template molecules a) pyrazole and b), c) 5-methyl-3-aminopyrazole in its two tautomeric forms b) MAP(1), c) MAP(2).

In a further step, the aggregates of aminopyrazole derivatives with the already investigated Ac-Val-Phe-OMe and Ac-Val-Tyr(Me)-NHMe were analyzed¹⁶³. Both peptide sequences are models for an extraction from the KLVFF sequences, which are assumed to be involved in the formation of pathogenic β -sheets of the Alzheimer's disease. MAP and 5-methyl-3-trifluoroacetylpyrazole (tf-MAP) were chosen as template molecules. The measured IR/R2PI spectrum of the Ac-Val-Phe-OMe...MAP aggregate in the NH stretching region already gives clear hints towards a triply H-bonded structure. Since in Ac-Val-Phe-OMe H-bonding acceptors (CO) and H-bonding donors follow in the sequence, an aggregation of MAP in its tautomeric form 1 is probable. A final unambiguous assignment can be given in comparison to DFT calculations (cf. Figure 35). It turns out that two of the three H-bonds are strong but the one between the Ac protection group and the NH_2 MAP moiety is quite weak and could be broken in favor of a stronger binding partner (e.g. a peptide).

In case of the Ac-Val-Tyr(Me)-NHMe...MAP aggregate, the IR/R2PI spectrum of the cluster exhibits characteristics for a free NH_2 MAP, a further free NH, as well as three H-bonded NH groups with one H-bond of a γ -turn. The comparison with calculations confirmed this assumption and the match between experimental and calculated frequencies was found for an aggregate with a γ -turn in the peptide backbone ($\text{NH}_{\text{Me}} \cdots \text{CO}_{\text{Val}}$) and with CO_{Ac} and NH_{Tyr} being involved in intermolecular H-bonds with the N-atom and NH group of the MAP(2) tautomer (structure cf. Figure 35). This example illustrates the fact that the formation of an intramolecular H-bond can win over a third intermolecular H-bond. To yield an effective template molecule, the binding strength had to be improved. Thus, attempts were made to increase the H-bonding strength of MAP by a trifluoroacetylation of the NH_2 which was expected to effect a significant rise in the acidity of the remaining NH group. In the Ac-Val-Tyr(Me)-NHMe ... tf-MAP IR/R2PI spectrum, the five expected vibrations were detected but only one free vibration above 3400 cm^{-1} . Taking calculations into account, an arrangement was assigned in which the γ -turn Ac-Val-Tyr(Me)-NHMe structure of the MAP cluster was conserved. However, three instead of only two intermolecular H-bonds were formed now with the acidified $\text{NH}_{\text{tf-MAP}}$ group being now involved (cf. Figure 35). The red-shift of this corresponding NH vibration furthermore revealed that the H-bond between the $\text{NH}_{\text{tf-MAP}}$ and the CO_{Ac} is the strongest one within the aggregate.

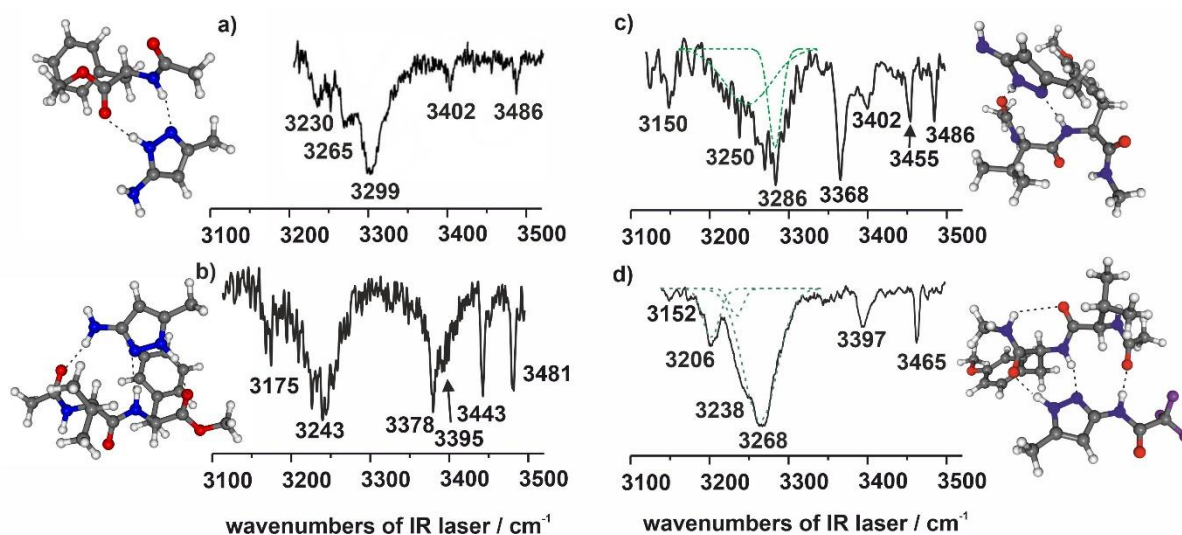


Figure 35: Overview of the IR/R2PI spectra of clusters between different protected amino acids up to tripeptide models with aminopyrazole based template molecules and their calculated assigned structures. a) Ac-Phe-OMe in a $\beta_1(a)$ conformation and the MAP in its tautomeric form 2 (B3LYP/6-31G(d)). The second isomer of the cluster differs in the orientation of the side chain (g+). b) Ac-Val-Phe-OMe...MAP cluster, (B3LYP/6-31+G(d)). c) Ac-Val-Tyr(Me)-NHMe...MAP cluster with the assigned structure (B3LYP/6-31+G(d)). d) IR/R2PI spectrum of Ac-Val-Tyr(Me)-NHMe...tf-MAP and the assigned calculated structure (B3LYP/6-31+G(d)). Spectrum in a) reprinted with permission from Ref. ⁵⁰⁶, copyright (2002) Springer Nature. Spectra b) to d) reprinted with permission from Ref. ¹⁶³, copyright (2009) John Wiley and Sons.

Aggregates between peptides and monosaccharides

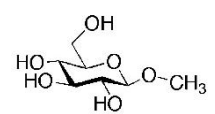
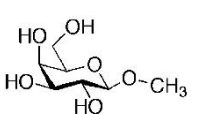
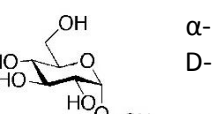
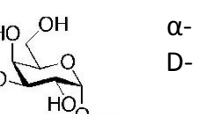
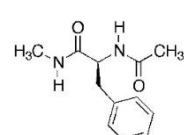
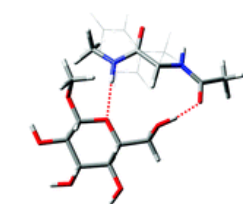

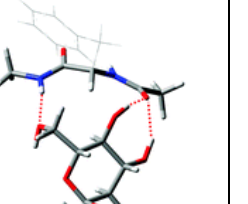
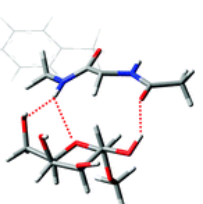
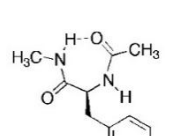
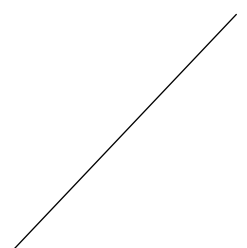
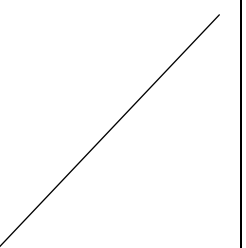
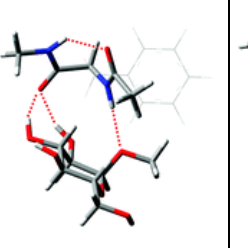

In biological processes, carbohydrate-protein interactions play an important role, e.g. in cellular recognition in context with inflammation processes (cf. e.g. ^{291,400} and references therein). From the spectroscopic point of view, carbohydrate-protein interactions were already analyzed from crystal structures as well as by NMR spectroscopy in solid and liquid state. Against this background, Simons and coworkers investigated aggregates between monosaccharides and peptide systems in the solvent-free, especially water-free environment of the molecular beam ^{162,218,291,400,507,508}.

Cocinero et al. ²¹⁸ analyzed the complex between D-galactose, methylated at the anomeric OH group, and the stretched conformer of Ac-Phe-NHMe ¹³⁵ with regard to the anomeric effect. The principle H-bonding pattern in the sugar-amino acid aggregate was the same for the α - and β -anomeric species of galactose. Nevertheless, the IR/R2PI spectra showed differences. Thus, the Ac-Phe-NHMe can act as a kind of sensor for the aggregated anomeric sugar form, since characteristic vibrational shifts of certain stretching vibrations occurred. Theoretical investigations also including an NBO analysis tried to analyze the influence of the endo- and exo-anomeric effect and postulated the dominance of the exo-anomeric effect for both galactose anomers within the hetero cluster. Later on Wang et al. performed further theoretical studies on this sugar-amino acid aggregate. ⁵⁰⁹ In the D-galactose they replaced the endocyclic oxygen by a methylene group, thus eliminating the endo- and exo-anomeric effect. Nevertheless, they found calculated vibrational shifts for the corresponding sugar amino acid cluster, which were comparable to those measured by Cocinero et al.. Thus, Wang and his co-authors concluded that the spectral differences found for the aggregates of Ac-Phe-NHMe with the α - and β -anomeric galactose in reference ²¹⁸ were due to the conformational differences of the two anomers rather than truly based on anomeric effects.

However, not only the aggregation behavior of the stretched but also of the γ -turn isomer of Ac-Phe-NHMe ¹³⁵ was investigated. The aggregation partners investigated were methylated D-galactopyranose ²¹⁸ and the methylated epimer D-glucopyranose ²⁹¹ in which the configuration of the OH group in the 4 position is

equatorial instead of axial. R2PI and IR/R2PI measurements revealed six complexes: the α - and β -anomer of both sugars aggregate with the stretched isomer of the protected Phe but only the α -anomers of both sugars bind to the γ -turn conformer, making a sum of six complex structures in total (cf. Table 12). In contrast to crystalline structures²⁹¹ and molecular beam investigations on aggregates between sugars and aromatic compounds⁵⁰⁷ no stacked structures were found. Instead, Ac-Phe-NHMe...monosaccharide dimers were dominated by H-bonding. The absence of stacked arrangements was proposed to be due to the formation of hydrophobic regions in a natural aqueous environment, a situation which is not provided in the molecular beam. Moreover, it was observed that monosaccharides always attach to the 'outer' H-bonding sites¹³⁵ of the stretched isomer and to the 'inner side' H-bonding sites¹³⁵ (cf. Section 12.4.1) in the γ -turn structure. The precise H-bonding pattern within the complexes strongly depends on the configuration and conformation of the sugar, the D-glucopyranose leading to quite different arrangements than the D-galactopyranose. Nevertheless, a certain selectivity towards β -strands was revealed making the authors think about the therapeutic potential in context with neurodegenerative diseases (cf. Sections 1, 7, 12.4.1). Since stacked carbohydrate-protein interactions preferentially occur at peptide binding sites containing tyrosine and tryptophan, further studies were performed on aggregates of p-hydroxytoluene with α,β -methyl D-galactopyranose, α,β -methyl D-glucopyranose and α,β -methyl D-fucopyranose as well as on Ac-Tyr-NHMe... α,β -methyl D-galactopyranose complexes⁴⁰⁰. For p-hydroxytoluene combined with D-galactopyranose only singly H-bonded motifs were found but with additional CH... π interactions leading to stabilized stacked structures. In the aggregate between Ac-Tyr-NHMe and α,β -methyl D-galactopyranose, an H-bond between the OH in the tyrosine side chain and the monosaccharide (O6) is found in the most stable arrangements which are additionally stabilized by OH...O, NH...OH and CH... π interactions. The OH group in the aromatic side chain was considered to act like a kind of anchor, which enables the CH... π interactions. Thus, its absence in the Phe side chain was proposed to be the reason for the lack of stacked arrangements in the Ac-Phe-NHMe... α,β -methyl D-galactopyranose complex²⁹¹.

Table 12: Combinations found between the conformers of Ac-Phe-NHMe and the different anomers of D-galactopyranose (MeGal) and D-glucopyranose (MeGlc) (DFT/M05-2x/6-31+G level of theory).**^{218,291} Figures reprinted with permission from Ref. ²¹⁸, copyright (2011) Springer Nature; further figures reprinted with permission from Ref. ²⁹¹, copyright (2008) American Chemical Society.

	 β -D-MeGlc	 β -D-MeGal	 MeGlc	 α -D-MeGal
 extended backbone				
 C ₇ folded backbone				

Aggregates between nucleobases and amino acids

Interactions between DNA and proteins belong to the most important regulatory processes in a cell. As an example, gene expression and the whole cell cycle are controlled by protein-DNA interactions. Nevertheless, details of these interactions and the associated recognition mechanisms are not well understood yet. This was the motivation of de Vries and coworkers to analyze the aggregate between guanine and aspartic acid by R2PI and IR/UV hole burning spectroscopy in a molecular beam expansion,⁵¹⁰ with guanine providing the necessary UV chromophore. The tautomer diversity of the guanine nucleobase and some derivatives was investigated by R2PI, UV/UV and IR/UV hole burning (cf. e.g. ^{264,511-514}) as well as by using helium droplet experiments²³⁷ or microwave spectroscopy⁵¹⁵ (for the principally possible tautomers and their nomenclature cf. Figure 36). For the guanine-aspartic acid complex, five isomers were found in comparison with theory at the MP2 level employing harmonic and one-dimensional anharmonic approximations. Regarding the tautomeric form of the nucleobase, the complexes with the 7-keto and 7-enol tautomers always turned out to be several $\text{kJ}\cdot\text{mol}^{-1}$ higher in energy than the corresponding 9H-tautomers. Among the 9H-aggregates, those with guanine in the keto form were calculated to be more stable. Though the enol and keto forms show characteristic IR frequencies, the tautomers only differing in the 7 and 9 position are hardly distinguishable (7H-keto and 9H-keto or 7H-enol and 9H-enol). For the first (probably most stable) dimer, a triply H-bonded structure with guanine in the 9-keto form was assigned (cf. 9KN in Figure 37). The authors describe this binding motif to be comparable to the guanine-cytosine Watson-Crick arrangement. Based on the extremely broad signature of this isomer in the R2PI spectrum, the authors do not exclude the presence of more weakly populated isomers, with either minimal differences in the amino acid conformation or a 7H guanine tautomer. The following three dimers are assigned to structures with the 9H-enol form of the nucleobase (among them 9E1 cf. Figure 37). Finally, a fifth one is observed, but the assignment is difficult since it appears as protonated aspartic acid fragment. Interestingly, whereas the 9-keto guanine tautomer was not observed in R2PI experiments on the monomer due to its short-lived excited state^{264,512} the perturbation induced by the aspartic acid, like in the case of the guanine-cytosine Watson-Crick pair,⁵¹⁶ is strong enough to inhibit the ultrafast deactivation and allow the complex of the keto guanine to be observed by R2PI.

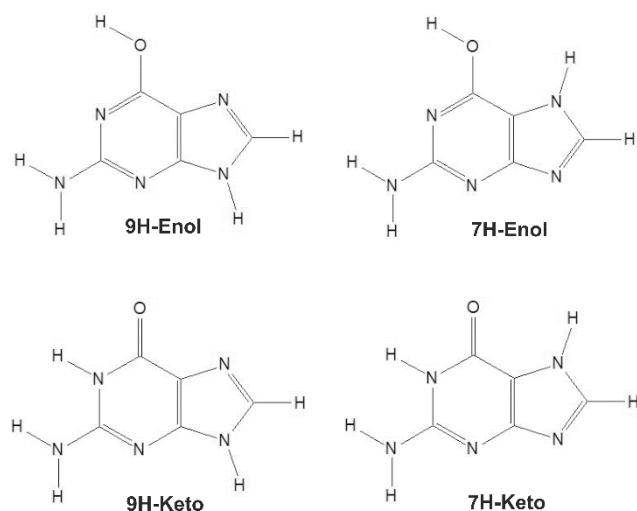


Figure 36: Scheme of the most stable tautomers of guanine in the gas phase.

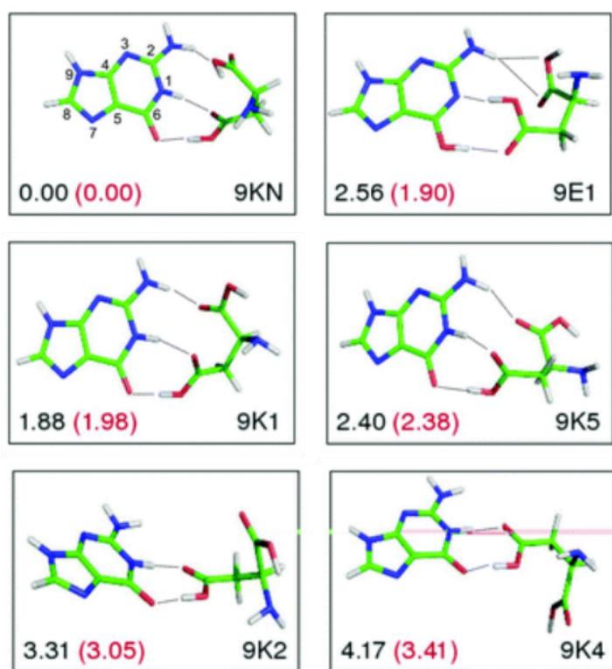


Figure 37: Representative low energy structures of 9-keto and 9-enol guanine-aspartic acid clusters (MP2/cc-pVTZ) with 9KN and 9E1 being assigned. Relative interaction energies (in black) and enthalpies (in red) are both BSSE corrected and given in kcal·mol⁻¹ (details cf. ⁵¹⁰). Reprinted in part with permission from Ref. ⁵¹⁰. Copyright (2010) PCCP Owner Societies.

13. Conclusions and perspectives

Experimental data vs. theoretical predictions

During the past two decades, laser spectroscopy has proven to be the most fruitful method to document isolated neutral biomolecules and especially peptides. By preparing these molecules in the gas phase, soft vaporization techniques combined to molecular beam expansion are able to bring them in a cooled state, well suited to laser investigations. In their most sophisticated variants, spectroscopic techniques provide a unique isomer- and conformer-selective characterization of these flexible neutral systems. It took a couple of decades before the experimental outcome, namely the individual molecular structures and conformational populations, as revealed by vibrational spectroscopy, could be compared to reliable theoretical descriptions, which eventually has enabled an efficient cross-fertilization of the two approaches.

Comparison between experiments and theory is not only mandatory for proposing a basic interpretation, but is also at the heart of several of the most outstanding outcomes in the field.^{72,74,103,113,133,134,141,144,150,152,153,157-160,162,163,181,203,218,219,241,284,301,314,334,387,391,423,517}

Nowadays, quantum chemistry suites are often sophisticated black boxes: even if an in-depth rationalization of the underlying phenomena is not easy to extract from calculations, they provide experimentalists with a reliable and relevant prediction of some of the experimental observables in the ground electronic state, like vibrational modes. The situation is more contrasted as far as the electronic structure and dynamical properties of the excited states of aromatic residues are concerned. This field remains a challenge, especially in the context of systems of increasing size, but recent new approaches appear promising.³⁶⁹

Underlying physical foundations

A generalized use of theoretical rationalization tools, such as the NBO analysis^{518,519} or the NCI-plot suite,³⁷³ enable a better understanding of the interactions in biomolecules and peptides in particular. Among other outcomes, it has been shown that spectral vibrational red shifts, whose interpretation in terms of H-bond strength is often taken for granted, turns out to actually also depend upon the intrinsic backbone structures³⁷² and not only upon the H-bonds, as ubiquitous as they are. Despite the numerous pairwise interactions already experimentally documented so far (cf. Sections 7 and 8), comparing experimental data with such newly available theoretical diagnostics will undoubtedly continue to be a fruitful approach that will allow researchers to go beyond the simple description of systems and to grasp the underlying physics and chemistry of the observed phenomena.

Interface with biochemistry

The classical structures of proteins have been demonstrated to form spontaneously under isolated conditions in the gas phase (cf. Section 7), suggesting that desolvation can be one of the driving forces at play in the folding process.⁴¹⁹ Comparison between protein structures, such as derived from X-ray crystallography or NMR studies, and simple gas phase structures of model systems brings direct information onto the respective role of intramolecular H-bonding and intermolecular interactions with the solvent.^{81,82,160} This kind of approach, applied to specific folding structures, such as β -turns, Asx turns or β -bulges, could probably provide interesting hints about the enthalpic role of H-bonds on the formation of these structures. Gas phase spectroscopy of biologically relevant model molecules can also provide biochemists with guidelines about various other physical chemistry phenomena, such as e.g. the electronic and vibrational Stark effect induced by a nearby electric field on a molecular probe.⁵²⁰ The corresponding spectral displacements indeed are widely used as a structural diagnostics of the protein structure, whose physical foundations and experimental calibration remain poorly investigated. Beyond these general phenomena, several systems were designed to uniquely address particular biochemical issues by sophisticated gas phase investigations, i.e. a detailed analysis on a molecular level can be an interesting approach to understand fundamental biochemically relevant mechanisms. This includes e.g. the mechanism of peptide aggregation^{143,157,423,521}, and the complexation with template/blocking molecules¹⁶³ relevant for important diseases like Alzheimer (for further aggregations see also section 12). Additionally, antibiotic effects are of high medical relevance, making the structural investigation of antibiotic agents like the (partly cyclic) gramicidin peptides^{146,466} or substances based on cyclic peptides³⁹¹ essential. All these examples illustrate the connections between gas phase investigations and biochemical issues, although we believe that this interface is still underdeveloped, and should be extended in the future, in line with its tremendous potential.

Future directions

The modest size of the objects studied so far enabled their complete structural characterization, though in some cases it was limited by their mode of preparation, i.e. vaporization within the supersonic expansion, and the cooling required as well as, especially in the early studies, by the lack of an adequate theoretical description. The degree of success of future gas phase works will also depend on critical instrumental improvements. One of them consists of being able to investigate larger systems and address supramolecular issues by studying molecular complexes capable to model more and more relevant environments for condensed phase issues. However, a gain in size would occur at the expense of spectral resolution and complete structural characterization; the labelling and multiple laser spectroscopic techniques being important tools in this context (Section 4). Increasing the size can be achieved by significantly improving the desorption sources or by searching for different strategies. In this context, it will be of interest to see how far laser spectroscopic investigations of neutral species in helium droplets, which have only been performed up to the size of dipeptide models so far (cf. Section 4.2.7), can be further developed and compared to molecular beam investigations.

As mentioned above, investigations on model systems to describe biomolecular interactions should be continued, e.g. by analyzing aggregates between peptides and template molecules relevant for Alzheimer and

Parkinson diseases. Furthermore, capitalizing on the expertise gained on natural biomolecules, laser spectroscopic studies also target bio-inspired systems, like synthetic peptides built from originally designed building blocks. This comprises β - and γ -peptides (Section 11) as well as synthetic cyclo- and depsipeptides (Section 12). The degree of details reached by gas phase investigations on natural biomolecules and synthetic peptides can help organic chemists and biochemists to characterize the folding capabilities of these objects and then orient their research towards the most promising building blocks through a fine-tuning of molecular structural design. Consortiums gathering organic chemists and gas phase spectroscopists already showed the way ^{163,224,391,436,437,443} towards an interdisciplinary research ranging from pure fundamental up to applied research, including pharmaceutical or medical aspects.

Author Information

Corresponding Authors

*E-mail: michel.mons@cea.fr Tel. No.: +33 (0)1-6908-2001.

*E-mail: gerhards@chemie.uni-kl.de Tel. No.: +49 631 205 2537

ORCID

Eric Gloaguen: 0000-0002-1023-2791

Michel Mons: 0000-0001-9930-831X

Kirsten Schwing : 0000-0003-1037-7170

Markus Gerhards: 0000-0002-8748-2940

Notes

The authors declare no competing financial interest.

Biographies

Eric Gloaguen is a researcher at the Institute of Physics of CNRS in France. He obtained his PhD in Chemical Physics in 2005 under the supervision of Dr Benoit Soep at University Paris-Sud, where he studied the ultrafast relaxation of ethylenics by photoelectron imaging, as well as the transition state spectroscopy of van der Waals clusters. Then, he has been a postdoctoral fellow in the group of Pr. Stephen R. Leone at the Advanced Light Source synchrotron (Berkeley, California), where he investigated aerosol chemistry by VUV photoionization at the Chemical Dynamics Beamline. Since 2006, he is working at CNRS on isomer-selective vibrational and electronic spectroscopies of neutral peptides and their complexes in the gas phase in order to rationalize molecular folding and supramolecular organization with the help of quantum chemistry studies. More recently, he also pioneered the laser vaporization of salts with the aim to record IR and UV spectra of isolated ion pairs and thus document conformational issues in complexes between molecular ions of opposite charge.

Michel Mons, is a Senior Researcher at CEA (French Atomic Energy Agency), where he leads the ‘BioMolecular Structures’ group at LIDYL (Laboratoire Interactions, Dynamique et Lasers) of the Paris-Saclay CEA Center (France). He graduated in Physics from the Paris-Sud University (Orsay) in 1983 and then received his PhD in Physical Chemistry (Thèse d’Etat) in 1988, under the supervision of Dr Iliana Dimicoli, with a work focused on probing of the photofragments of NO₂. He then pursued his experimental research at CEA, on the laser probing of interactions in molecular clusters, targeting models of biomolecules. During a sabbatical year in 1998-99, at the PTCL, Oxford (Physical and Theoretical Chemistry Laboratory, headed by J.P. Simons), he implemented the IR/UV double resonance technique in the group. Back to Saclay, he applied it to laser-desorbed molecules of biological interest, in particular flexible biomolecules, like peptides, following a strategy based on a strong synergy between conformation-resolved spectroscopy and quantum chemistry modelling. His current interests range from fundamental aspects of intra- and inter-molecular interactions, especially H-bonding, in peptides and proteins, to applications of these interactions in bioinspired systems, targeting innovative foldamer structures.

Kirsten Schwing graduated in 2007 at the TU Kaiserslautern in chemistry (Diplom). During the last phase of her studies she did research projects in physical chemistry (second harmonic generation of chromophores (Prof. Wortmann, TU Kaiserslautern) and in inorganic chemistry (University of Edinburgh, Prof. Tasker). Within her diploma thesis in physical chemistry (Prof. Gerhard, University of Düsseldorf) she performed spectroscopic investigations on systems showing excited state proton transfer by combined IR/UV spectroscopy in molecular beams. In her PhD thesis she switched to peptide systems including cyclopeptides, aggregates with water and peptide-peptide aggregates (Prof. Gerhards, TU Kaiserslautern). She received her PhD in 2011. Her work is

focused on peptides, aggregation, cyclic peptides, depsipeptides, analyses in gas cells as well as photoreactive systems like coumarins and chromones.

Markus Gerhards is a Professor in Physical Chemistry at the TU Kaiserslautern since 2006. He graduated in chemistry at the HHU Düsseldorf in 1991 (with a topic on Resonance Raman Spectroscopy in his diploma thesis). In 1995 he received his PhD in Physical Chemistry (group of Prof. Kleinermanns). In his thesis he built up a molecular beam apparatus and investigated hydrogen-bonded clusters. His habilitation was on IR/UV double resonance investigations with respect to ions, especially by using the MATI technique and by developing combinations with IR spectroscopy. In 2001 photo electron spectroscopy on isolated anions (metal/benzene cluster) was performed in the Bowen group (Johns Hopkins Baltimore) continued by IR investigations on metal/alcohol aggregates in Kaiserslautern. Around 2000 he started with IR/UV investigation on neutral protected amino acids and peptides, especially with a focus on aggregation with solvents, template molecules and other peptides, partly also the attachment of ions has been analyzed. The investigations include further methodical developments (e.g. quadruple resonance methods) as well as laser system developments. Beside studies on peptides with a focus on interactions in aggregations another focus of his research is on photophysical and photochemical processes, dispersion controlled aggregations. Beyond laser spectroscopy in molecular beams also condensed phase analyses via time-resolved FTIR and luminescence spectroscopy is applied.

Conflicts of interest

There are no conflicts of interest to declare

Acknowledgements

EG and MM wish to thank their close colleagues V. Brenner and B. Tardivel, and the former group members I. Dimicoli and F. Piuze. They also acknowledge financial support from the French National Research Agency (ANR) (Grants ANR-08-BLAN-0158-01-LASIHMODo; ANR-14-CE06-0019-01-ESBODYR; ANR-16-CE29-0017-IONPAIRS; ANR-17-CE29-0008-TUNIFOLDS) and from the French 'Investissement d'Avenir' funding scheme LabEx PALM (ANR-10-LABX-0039-PALM) in Paris-Saclay. M.G. and K.S. especially thank the Deutsche Forschungsgemeinschaft (DFG) who supported and supports most parts of the work financially within different projects (GE 961/3-1,2,3 and 7-1,2).

We also would like to thank all the post-docs, PhD and master students, who contributed to the success of these projects (see co-authors of the references that refer to our groups).

References

- (1) Tzeng, S. R.; Kalodimos, C. G. Protein Activity Regulation by Conformational Entropy. *Nature* **2012**, *488*, 236-240.
- (2) Ramachandran, G.; Kartha, G. Structure of Collagen. *Nature* **1954**, *174*, 269-270.
- (3) Agre, P. Aquaporin Water Channels (Nobel Lecture). *Angew. Chem. Int. Ed.* **2004**, *43*, 4278-4290.
- (4) MacKinnon, R. Potassium Channels and the Atomic Basis of Selective Ion Conduction (Nobel Lecture). *Angew. Chem. Int. Ed.* **2004**, *43*, 4265-4277.
- (5) Feixas, F.; Lindert, S.; Sinko, W.; McCammon, J. A. Exploring the Role of Receptor Flexibility in Structure-Based Drug Discovery. *Biophys. Chem.* **2014**, *186*, 31-45.
- (6) Fischer, E. Einfluss Der Configuration auf die Wirkung der Enzyme. *Berichte der deutschen chemischen Gesellschaft* **1894**, *27*, 2985-2993.
- (7) Fuxreiter, M.; Simon, I.; Bondos, S. Dynamic Protein-DNA Recognition: Beyond What Can Be Seen. *Trends Biochem. Sci.* **2011**, *36*, 415-423.
- (8) Mittag, T.; Kay, L. E.; Forman-Kay, J. D. Protein Dynamics and Conformational Disorder in Molecular Recognition. *J. Mol. Recognit.* **2010**, *23*, 105-116.

- (9) Butterfield, D. Brain Protein Oxidation in Age-Related Neurodegenerative Disorders That Are Associated with Aggregated Proteins. *Mechanisms Ageing Dev.* **2001**, *122*, 945–962.
- (10) Brown, D. R.; Kozlowski, H. Biological Inorganic and Bioinorganic Chemistry of Neurodegeneration Based on Prion and Alzheimer Diseases. *Dalton Trans.* **2004**, *13*, 1907–1917.
- (11) Kendrew, J. C.; Dickerson, R. E.; Strandberg, B. E.; Hart, R. G.; Davies, D. R.; Phillips, D. C.; Shore, V. C. Structure of Myoglobin: A Three-Dimensional Fourier Synthesis at 2 Å Resolution. *Nature* **1960**, *185*, 422–427.
- (12) Watson, J. D.; Crick, F. H. C. Genetical Implications of the Structure of Deoxyribonucleic Acid. *Nature* **1953**, *171*, 964–967.
- (13) Wuthrich, K. Protein Structure Determination in Solution by Nuclear Magnetic Resonance Spectroscopy. *Science* **1989**, *243*, 45–50.
- (14) Tzakos, A. G.; Grace, C. R. R.; Lukavsky, P. J.; Riek, R. NMR Techniques for Very Large Proteins and RNAs in Solution. *Annu. Rev. Biophys. Biomol. Struct.* **2006**, *35*, 319–342.
- (15) Raman, S.; Lange, O. F.; Rossi, P.; Tyka, M.; Wang, X.; Aramini, J.; Liu, G.; Ramelot, T. A.; Eletsky, A.; Szyperski, T.; Kennedy, M. A.; Prestegard, J.; Montelione, G. T.; Baker, D. NMR Structure Determination for Larger Proteins Using Backbone-Only Data. *Science* **2010**, *327*, 1014–1018.
- (16) Stryer, L. Fluorescence Energy Transfer as a Spectroscopic Ruler. *Ann. Rev. Biochem.* **1978**, *47*, 819–846.
- (17) Nie, S.; Zare, R. N. Optical Detection of Single Molecules. *Annu. Rev. Biophys. Biomol. Struct.* **1997**, *26*, 567–596.
- (18) Beychok, S. Rotatory Dispersion and Circular Dichroism. *Ann. Rev. Biochem.* **1968**, *37*, 437–462.
- (19) Wen, Y.-X.; Chen, E.; Lewis, J. W.; Kliger, D. S. Nanosecond Time-Resolved Circular Dichroism Measurements Using an Upconverted Ti:Sapphire Laser. *Rev. Sci. Instrum.* **1996**, *67*, 3010.
- (20) Suenram, R. D.; Grabow, J. U.; Zuban, A.; Leonov, I. A Portable, Pulsed-Molecular-Beam, Fourier-Transform Microwave Spectrometer Designed for Chemical Analysis. *Rev. Sci. Instrum.* **1999**, *70*, 2127.
- (21) Lesarri, A.; Mata, S.; López, J. C.; Alonso, J. L. A Laser-Ablation Molecular-Beam Fourier-Transform Microwave Spectrometer: The Rotational Spectrum of Organic Solids. *Rev. Sci. Instrum.* **2003**, *74*, 4799.
- (22) Felker, P. M. Rotational Coherence Spectroscopy: Studies of the Geometries of Large Gas-Phase Species by Picosecond Time-Domain Methods. *J. Chem. Phys.* **1992**, *96*, 7844–7857.
- (23) Weichert, A.; Riehn, C.; Barth, H.-D.; Lembach, G.; Zimmermann, M.; Brutschy, B.; Podénas, D. Implementation of a High-Resolution Two-Color Spectrometer for Rotational Coherence Spectroscopy in the Picosecond Time Domain. *Rev. Sci. Instrum.* **2001**, *72*, 2697.
- (24) Caminati, W.; Melandri, S.; Schnell, M.; Banser, D.; Grabow, J.-U.; Alonso, J. L. The Fourier Transform Rotational Spectrum of Difluoromethane–Water: Internal Motion of Water. *J. Mol. Struct.* **2005**, *742*, 87–90.
- (25) Thomas, J.; Sukhorukov, O.; Jäger, W.; Xu, Y. Direct Spectroscopic Detection of the Orientation of Free OH Groups in Methyl Lactate-(Water)_{1,2} Clusters: Hydration of a Chiral Hydroxy Ester. *Angew. Chem. Int. Ed.* **2014**, *53*, 1156–1159.
- (26) Kannengießer, R.; Klahm, S.; Nguyen, H. V. L.; Lüchow, A.; Stahl, W. The Effects of Methyl Internal Rotation and ¹⁴N Quadrupole Coupling in the Microwave Spectra of Two Conformers of *N,N*-Diethylacetamide. *J. Chem. Phys.* **2014**, *141*, 204308.
- (27) Braiman, M. S.; Rothschild, K. J. Fourier Transform Infrared Techniques for Probing Membrane Protein Structure. *Annu. Rev. Biophys. Biomol. Struct.* **1988**, *17*, 541–570.
- (28) Manning, M. C. Use of Infrared Spectroscopy to Monitor Protein Structure and Stability. *Expert Rev. Proteomic* **2005**, *2*, 731–743.
- (29) Carbonaro, M.; Nucara, A. Secondary Structure of Food Proteins by Fourier Transform Spectroscopy in the Mid-Infrared Region. *Amino acids* **2010**, *38*, 679–690.
- (30) Otto, K. E.; Hesse, S.; Wassermann, T. N.; Rice, C. A.; Suhm, M. A.; Stafforstz, T.; Diederichsen, U. Temperature-Dependent Intensity Anomalies in Amino Acid Esters: Weak Hydrogen Bonds in Protected Glycine, Alanine and Valine. *Phys. Chem. Chem. Phys.* **2011**, *13*, 14119–14130.
- (31) Forsting, T.; Gottschalk, H. C.; Hartwig, B.; Mons, M.; Suhm, M. A. Correcting the Record: The Dimers and Trimers of *trans-N*-Methylacetamide. *Phys. Chem. Chem. Phys.* **2017**, *19*, 10727–10737.
- (32) Balabin, R. M. Conformational Equilibrium in Glycine: Experimental Jet-Cooled Raman Spectrum. *J. Phys. Chem. Lett.* **2010**, *1*, 20–23.

- (33) Balabin, R. M. The First Step in Glycine Solvation: The Glycine-Water Complex. *J. Phys. Chem. B* **2010**, *114*, 15075-15078.
- (34) Balabin, R. M. The Identification of the Two Missing Conformers of Gas-Phase Alanine: A Jet-Cooled Raman Spectroscopy Study. *Phys. Chem. Chem. Phys.* **2010**, *12*, 5980-5982.
- (35) Balabin, R. M. Experimental Thermodynamics of Free Glycine Conformations: The First Raman Experiment after Twenty Years of Calculations. *Phys. Chem. Chem. Phys.* **2012**, *14*, 99-103.
- (36) Linder, R.; Nispel, M.; Häber, T.; Kleineremanns, K. Gas-Phase FT-IR Spectra of Natural Amino Acids. *Chem. Phys. Lett.* **2005**, *409*, 260-264.
- (37) Linder, R.; Seefeld, K.; Vavra, A.; Kleineremanns, K. Gas Phase Infrared Spectra of Nonaromatic Amino Acids. *Chem. Phys. Lett.* **2008**, *453*, 1-6.
- (38) Albrecht, M.; Rice, C. A.; Suhm, M. A. Elementary Peptide Motifs in the Gas Phase: FTIR Aggregation Study of Formamide, Acetamide, *N*-Methylformamide, and *N*-Methylacetamide. *J. Phys. Chem. A* **2008**, *112*, 7530-7542.
- (39) Häber, T.; Schmitt, U.; Suhm, M. A. Ftir-Spectroscopy of Molecular Clusters in Pulsed Supersonic Slit-Jet Expansions. *Phys. Chem. Chem. Phys.* **1999**, *1*, 5573-5582.
- (40) Lee, J. J.; Albrecht, M.; Rice, C. A.; Suhm, M. A.; Stamm, A.; Zimmer, M.; Gerhards, M. Adaptive Aggregation of Peptide Model Systems. *J. Phys. Chem. A* **2013**, *117*, 7050-7063.
- (41) Hesse, S.; Suhm, M. A. Conformation and Aggregation of Proline Esters and Their Aromatic Homologs: Pyramidal vs. Planar RR'N-H in Hydrogen Bonds. *Zeitschrift für Physikalische Chemie* **2009**, *223*, 579-604.
- (42) Steber, A. L.; Neill, J. L.; Zaleski, D. P.; Pate, B. H.; Lesarri, A.; Bird, R. G.; Vaquero-Vara, V.; Pratt, D. W. Structural Studies of Biomolecules in the Gas Phase by Chirped-Pulse Fourier Transform Microwave Spectroscopy. *Faraday Discuss.* **2011**, *150*, 227.
- (43) Alonso, J. L.; Lopez, J. C. Microwave Spectroscopy of Biomolecular Building Blocks. *Gas-Phase IR Spectroscopy and Structure of Biological Molecules* **2015**, *364*, 335-401.
- (44) Connell, L. L.; Corcoran, T. C.; Joireman, P. W.; Felker, P. M. Conformational Analysis of Jet-Cooled Tryptophan Analogs by Rotational Coherence Spectroscopy. *Chem. Phys. Lett.* **1990**, *166*, 510-516.
- (45) Calabrese, C.; Uriarte, I.; Insausti, A.; Vallejo-López, M., J. Basterretxea; Cochrane, S. A.; Corzana, F.; Cocinero, E. J. Observation of the Unbiased Conformers of Putative DNA-Scaffold Ribosugars. *ACS Cent. Sci.* **2020**, *6*, 293-303.
- (46) Cocinero, E. J.; Lesarri, A.; Grabow, J.-U.; López, J. C.; Alonso, J. L. The Shape of Leucine in the Gas Phase. *Chemphyschem* **2007**, *8*, 599-604.
- (47) Sanz, M. E.; Lesarri, A.; Peña, M. I.; Vaquero, V.; Cortijo, V.; López, J. C.; Alonso, J. L. The Shape of β -Alanine. *J. Am. Chem. Soc.* **2006**, *128*, 3812-3817.
- (48) Vaquero, V.; Sanz, M. E.; Peña, I.; Mata, S.; Cabezas, C.; López, J. C.; Alonso, J. L. Alanine Water Complexes. *J. Chem. Phys. A* **2014**, *118*, 2584-2590.
- (49) Cabezas, C.; Robben, M. A. T.; Rijs, A. M.; Peña, I.; Alonso, J. L. Fourier Transform Microwave Spectroscopy of Ac-Ser-NH₂: The Role of Side Chain Interactions in Peptide Folding. *Phys. Chem. Chem. Phys.* **2015**, *17*, 20274-20280.
- (50) Cabezas, C.; Varela, M.; Alonso, J. L. Probing the γ -Turn in a Short Proline Dipeptide Chain. *Chemphyschem* **2013**, *14*, 2539-2543.
- (51) Gazit, E. A Possible Role for π -Stacking in the Self-Assembly of Amyloid Fibrils. *FASEB J.* **2002**, *16*, 77-83.
- (52) Chelli, R.; Gervasio, F. L.; Procacci, P.; Schettino, V. Stacking and T-Shape Competition in Aromatic-Aromatic Amino Acid Interactions. *J. Am. Chem. Soc.* **2002**, *124*, 6133-6143.
- (53) Tatko, C. D.; Waters, M. L. Selective Aromatic Interactions in β -Hairpin Peptides. *J. Am. Chem. Soc.* **2002**, *124*, 9372-9373.
- (54) Meyer, E. A.; Castellano, R. K.; Diederich, F. Interactions with Aromatic Rings in Chemical and Biological Recognition. *Angew. Chem. Int. Ed.* **2003**, *42*, 1210-1250.
- (55) Butterfield, S. M.; Cooper, W. J.; Waters, M. L. Minimalist Protein Design: A β -Hairpin Peptide That Binds SSDNA. *J. Am. Chem. Soc.* **2005**, *127*, 24-25.
- (56) Mahalakshmi, R.; Raghothama, S.; Balaram, P. NMR Analysis of Aromatic Interactions in Designed Peptide β -Hairpins. *J. Am. Chem. Soc.* **2006**, *128*, 1125-1138.

- (57) Eidenschink, L.; Kier, B. L.; Huggins, K. N. L.; Andersen, N. H. Very Short Peptides with Stable Folds: Building on the Interrelationship of Trp/Trp, Trp/Cation, and Trp/Backbone-Amide Interaction Geometries. *Proteins* **2009**, *75*, 308–322.
- (58) Wu, L.; McElheny, D.; Takekiyo, T.; Keiderling, T. A. Geometry and Efficacy of Cross-Strand Trp/Trp, Trp/Tyr, and Tyr/Tyr Aromatic Interaction in a β -Hairpin Peptide. *Biochemistry* **2010**, *49*, 4705–4714.
- (59) Pressman, B. C. Biological Applications of Ionophores. *Ann. Rev. Biochem.* **1976**, *45*, 501–530.
- (60) Chin, W.; Mons, M.; Dognon, J.-P.; Piuze, F.; Tardivel, B.; Dimicoli, I. Competition between Local Conformational Preferences and Secondary Structures in Gas-Phase Model Tripeptides as Revealed by Laser Spectroscopy and Theoretical Chemistry. *Phys. Chem. Chem. Phys.* **2004**, *6*, 2700–2709.
- (61) Chakraborty, S.; Yamada, K.; Ishiuchi, S.-i.; Fujii, M. Gas Phase IR Spectra of Tri-Peptide Z-Pro-Leu-Gly: Effect of C-Terminal Amide Capping on Secondary Structure. *Chem. Phys. Lett.* **2012**, *531*, 41–45.
- (62) Wiedemann, S.; Metsala, A.; Nolting, D.; Weinkauff, R. The Dipeptide Cyclic(Glycyltryptophanyl) in the Gas Phase: A Concerted Action of Density Functional Calculations, S_0 - S_1 Two-Photon Ionization, Spectral UV/UV Hole Burning and Laser Photoelectron Spectroscopy. *Phys. Chem. Chem. Phys.* **2004**, *6*, 2641–2649.
- (63) Abo-Riziq, A. G.; Crews, B.; Bushnell, J. E.; Callahan, M. P.; de Vries, M. S. Conformational Analysis of Cyclo(Phe-Ser) by UV-UV and IR-UV Double Resonance Spectroscopy and *Ab Initio* Calculations. *Mol. Phys.* **2005**, *103*, 1491–1495.
- (64) BenNasr, F.; Perez-Mellor, A.; Alata, I.; Lepère, V.; Jaidane, N. E.; Zehnacker, A. Stereochemistry-Dependent Hydrogen Bonds Stabilise Stacked Conformations in Jet-Cooled Cyclic Dipeptides: (LD) vs. (LL) Cyclo Tyrosine-Tyrosine. *Faraday Discuss.* **2018**, *212*, 399–419.
- (65) Perez-Mellor, A.; Alata, I.; Lepère, V.; Zehnacker, A. Chirality Effects in the Structures of Jet-Cooled Bichromophoric Dipeptides. *J. Mol. Spec.* **2018**, *349*, 71–84.
- (66) Ramachandran, G. N.; Sasisekharan, V.; Ramakrishnan, C. Molecular Structure of Polyglycine II. *Biochim. Biophys. Acta* **1966**, *112*, 168–170.
- (67) Perczel, A.; Angyan, J. G.; Kajtar, M.; Viviani, W.; Rivail, J. L.; Marcocchia, J. F.; Csizmadia, I. G. Peptide Models. 1. Topology of Selected Peptide Conformational Potential-Energy Surfaces (Glycine and Alanine Derivatives). *J. Am. Chem. Soc.* **1991**, *113*, 6256–6265.
- (68) Hutchinson, E. G.; Thornton, J. M. A Revised Set of Potentials for β -Turns Formation in Proteins. *Protein Science* **1994**, *3*, 2207–2216.
- (69) Richardson, J. S. The Anatomy and Taxonomy of Protein Structure. *Advances in Protein Chemistry* **1981**, *34*, 167–339.
- (70) Andersen, C. A. F.; Rost, B. In *Structural Bioinformatics*; ed.; Bourne, P. E.; Weissig, H., Eds.; Wiley: Hoboken, NJ, 2005; DOI:10.1002/0471721204.ch17 10.1002/0471721204.ch17; p 339–363.
- (71) Toniolo, C.; Benedetti, E. The Polypeptide 3_{10} -Helix. *Trends Biochem. Sci.* **1991**, *16*, 350–353.
- (72) Gloaguen, E.; Pollet, R.; Piuze, F.; Tardivel, B.; Mons, M. Gas Phase Folding of an (Ala)₄ Neutral Peptide Chain: Spectroscopic Evidence for the Formation of a β -Hairpin H-Bonding Pattern. *Phys. Chem. Chem. Phys.* **2009**, *11*, 11385–11388.
- (73) Plowright, R. J.; Gloaguen, E.; Mons, M. Compact Folding of Isolated Four-Residue Neutral Peptide Chains: H-Bonding Patterns and Entropy Effects. *Chemphyschem* **2011**, *12*, 1889–1899.
- (74) Dean, J. C.; Buchanan, E. G.; Zwier, T. S. Mixed 14/16 Helices in the Gas Phase: Conformation-Specific Spectroscopy of Z-(Gly)_N, N=1, 3, 5. *J. Am. Chem. Soc.* **2012**, *134*, 17186–17201.
- (75) Loquais, Y.; Gloaguen, E.; Habka, S.; Vaquero-Vara, V.; Brenner, V.; Tardivel, B.; Mons, M. Secondary Structures in Phe-Containing Isolated Dipeptide Chains: Laser Spectroscopy Vs Quantum Chemistry. *J. Phys. Chem. A* **2015**, *119*, 5932–5941.
- (76) Gord, J. R.; Hewett, D. M.; Hernandez-Castillo, A. O.; Blodgett, K. N.; Rotondaro, M. C.; Varuolo, A.; Kubasik, M. A.; Zwier, T. S. Conformation-Specific Spectroscopy of Capped, Gas-Phase Aib Oligomers: Tests of the Aib Residue as a 3(10)-Helix Former. *Phys. Chem. Chem. Phys.* **2016**, *18*, 25512–25527.
- (77) Walsh, P. S.; Blodgett, K. N.; McBurney, C.; Gellman, S. H.; Zwier, T. S. Inherent Conformational Preferences of Ac-Gln-Gln-NHBn: Sidechain Hydrogen Bonding Supports a β -Turn in the Gas Phase. *Angew. Chem. Int. Ed.* **2016**, *55*, 14618–14622.

- (78) Walsh, P. S.; Dean, J. C.; McBurney, C.; Kang, H.; Gellman, S. H.; Zwier, T. S. Conformation-Specific Spectroscopy of Capped Glutamine-Containing Peptides: Role of a Single Glutamine Residue on Peptide Backbone Preferences. *Phys. Chem. Chem. Phys.* **2016**, *18*, 11306-11322.
- (79) Blodgett, K. N.; Fischer, J. L.; Lee, J.; Choi, S. H.; Zwier, T. S. Conformation-Specific Spectroscopy of Asparagine-Containing Peptides: Influence of Single and Adjacent Asn Residues on Inherent Conformational Preferences. *J. Phys. Chem. A* **2018**, *122*, 8762-8775.
- (80) Alauddin, M.; Biswal, H. S.; Gloaguen, E.; Mons, M. Intra-Residue Interactions in Proteins: Interplay between Serine or Cysteine Side Chains and Backbone Conformations, Revealed by Laser Spectroscopy of Isolated Model Peptides. *Phys. Chem. Chem. Phys.* **2015**, *17*, 2169-2178.
- (81) Sohn, W. Y.; Habka, S.; Gloaguen, E.; Mons, M. Unifying the Microscopic Picture of His-Containing Turns: From Gas Phase Model Peptides to Crystallized Proteins. *Phys. Chem. Chem. Phys.* **2017**, *19*, 17128-17142.
- (82) Habka, S.; Sohn, W. Y.; Vaquero-Vara, V.; Géléoc, M.; Tardivel, B.; Brenner, V.; Gloaguen, E.; Mons, M. On the Turn-Inducing Properties of Asparagine: The Structuring Role of the Amide Side Chain, from Isolated Model Peptides to Crystallized Proteins. *Phys. Chem. Chem. Phys.* **2018**, *20*, 3411-3423.
- (83) Yan, B.; Jaeqx, S.; van der Zande, W. J.; Rijs, A. M. A Conformation-Selective Ir-Uv Study of the Dipeptides Ac-Phe-Ser-NH₂ and Ac-Phe-Cys-NH₂: Probing the SH...O and OH...O Hydrogen Bond Interactions. *Phys. Chem. Chem. Phys.* **2014**, *16*, 10770-10778.
- (84) Pauling, L.; Corey, R. B.; Branson, H. R. The Structure of Proteins: Two Hydrogen-Bonded Helical Configurations of the Polypeptide Chain. *PNAS* **1951**, *37*, 205-211.
- (85) Fodje, M. N.; Al-Karadaghi, S. Occurrence, Conformational Features and Amino Acid Propensities for the α -Helix. *Protein Engineering Design and Selection* **2002**, *15*, 353-358.
- (86) Pauling, L.; Corey, R. B. The Pleated Sheet, a New Layer Configuration of Polypeptide Chains. *PNAS* **1951**, *37*, 251-256.
- (87) Lefevre, T.; Rousseau, M. E.; Pezolet, M. Protein Secondary Structure and Orientation in Silk as Revealed by Raman Spectromicroscopy. *Biophysical Journal* **2007**, *92*, 2885-2895.
- (88) Buijs, J.; Norde, W.; Lichtenbelt, J. W. T. Changes in the Secondary Structure of Adsorbed IgG and F(ab')(2) Studied by FTIR Spectroscopy. *Langmuir* **1996**, *12*, 1605-1613.
- (89) Bolton, D.; McKinley, M.; Prusiner, S. Identification of a Protein That Purifies with the Scrapie Prion. *Science* **1982**, *218*, 1309-1311.
- (90) Prusiner, S. B. Nobel Lecture: Prions. *PNAS* **1998**, *95*, 13363-13383.
- (91) Colby, D. W.; Prusiner, S. B. De Novo Generation of Prion Strains. *Nat. Rev. Microbiol.* **2011**, *9*, 771-777.
- (92) Tjernberg, L. O.; Naslund, J.; Lindqvist, F.; Johansson, J.; Karlstrom, A. R.; Thyberg, J.; Terenius, L.; Nordstedt, C. Arrest of β -Amyloid Fibril Formation by a Pentapeptide Ligand. *J. Biol. Chem.* **1996**, *271*, 8545-8548.
- (93) LaFerla, F. M.; Green, K. N.; Oddo, S. Intracellular Amyloid- β in Alzheimer's Disease. *Nat. Rev. Neurosci.* **2007**, *8*, 499-509.
- (94) Ittner, L. M.; Götz, J. Amyloid- β and Tau - A Toxic Pas De Deux in Alzheimer's Disease. *Nat. Rev. Neurosci.* **2011**, *12*, 65-72.
- (95) Goedert, M. Neurodegeneration. Alzheimer's and Parkinson's Diseases: The Prion Concept in Relation to Assembled Amyloid- β , Tau, and α -Synuclein. *Science* **2015**, *349*, 1255-1255.
- (96) Fitzpatrick, A. W. P.; Falcon, B.; He, S.; Murzin, A. G.; Murshudov, G.; Garringer, H. J.; Crowther, R. A.; Ghetti, B.; Goedert, M.; Scheres, S. H. W. Cryo-EM Structures of Tau Filaments from Alzheimer's Disease. *Nature* **2017**, *547*, 185-190.
- (97) Rajashankar, K. R.; Ramakumar, S. π -Turns in Proteins and Peptides: Classification, Conformation, Occurrence, Hydration and Sequence. *Protein Sci.* **1996**, *5*, 932-946.
- (98) Pavone, V.; Gaeta, G.; Lombardi, A.; Nastri, F.; Maglio, O.; Isernia, C.; Saviano, M. Discovering Protein Secondary Structures: Classification and Description of Isolated α -Turns. *Biopolymers* **1996**, *38*, 705-721.
- (99) Wilmot, C. M.; Thornton, J. M. Analysis and Prediction of the Different Types of β -Turn in Proteins. *J. Mol. Biol.* **1988**, *203*, 221-232.
- (100) Venkatachalam, C. M. Stereochemical Criteria for Polypeptides and Proteins. V. Conformation of a System of Three Linked Peptide Units. *Biopolymers* **1968**, *6*, 1425-1436.

- (101) Milner-White, E. J. Situations of Γ -Turns in Proteins. Their Relation to α -Helices, β -Sheets and Ligand Binding Sites. *J. Mol. Biol.* **1990**, *216*, 386–397.
- (102) Fricke, H.; Gerlach, A.; Unterberg, C.; Rzepecki, P.; Schrader, T.; Gerhards, M. Structure of the Tripeptide Model Ac-Val-Tyr(Me)-NHMe and Its Cluster with Water Investigated by IR/UV Double Resonance Spectroscopy. *Phys. Chem. Chem. Phys.* **2004**, *6*, 4636-4641.
- (103) Gloaguen, E.; de Courcy, B.; Piquemal, J. P.; Pilmé, J.; Parisel, O.; Pollet, R.; Biswal, H. S.; Piuze, F.; Tardivel, B.; Broquier, M.; Mons, M. Gas-Phase Folding of a Two-Residue Model Peptide Chain: On the Importance of an Interplay between Experiment and Theory. *J. Am. Chem. Soc.* **2010**, *132*, 11860-11863.
- (104) Blanco, S.; Lopez, J. C.; Lesarri, A.; Alonso, J. L. Microsolvation of Formamide: A Rotational Study. *J. Am. Chem. Soc.* **2006**, *128*, 12111-12121.
- (105) Manea, V. P.; Wilson, K. J.; Cable, J. R. Conformations and Relative Stabilities of the Cis and Trans Isomers in a Series of Isolated *N*-Phenylamides. *J. Am. Chem. Soc.* **1997**, *119*, 2033-2039.
- (106) Dickinson, J. A.; Hockridge, M. R.; Robertson, E. G.; Simons, J. P. Molecular and Supramolecular Structures of *N*-Phenyl Formamide and Its Hydrated Clusters. *J. Phys. Chem. A* **1999**, *103*, 6938-6949.
- (107) Robertson, E. G. Ir-Uv Ion-Dip Spectroscopy of *N*-Phenyl Formamide, and Its Hydrated Clusters. *Chem. Phys. Lett.* **2000**, *325*, 299-307.
- (108) Fedorov, A. V.; Cable, J. R. Spectroscopy of Hydrogen-Bonded Formanilide Clusters in a Supersonic Jet: Solvation of a Model Trans Amide. *J. Phys. Chem. A* **2000**, *104*, 4943-4952.
- (109) Robertson, E. G.; Hockridge, M. R.; Jelfs, P. D.; Simons, J. P. IR-UV Ion-Dip Spectroscopy of *N*-Benzylformamide Clusters: Stepwise Hydration of a Model Peptide. *J. Phys. Chem. A* **2000**, *104*, 11714-11724.
- (110) Ottaviani, P.; Melandri, S.; Maris, A.; Favero, P. G.; Caminati, W. Free-Jet Rotational Spectrum and Ab Initio Calculations of Formanilide. *J. Mol. Spec.* **2001**, *205*, 173-176.
- (111) Mons, M.; Dimicoli, I.; Tardivel, B.; Piuze, F.; Robertson, E. G.; Simons, J. P. Energetics of the Gas Phase Hydrates of Trans-Formanilide: A Microscopic Approach to the Hydration Sites of the Peptide Bond. *J. Phys. Chem. A* **2001**, *105*, 969-973.
- (112) Ohba, K.; Usami, T.; Kawashima, Y.; Hirota, E. Fourier Transform Microwave Spectra and Ab Initio Calculation of *N*-Ethylformamide. *J. Mol. Struct.* **2005**, *744-747*, 815–819.
- (113) Clarkson, J. R.; Baquero, E.; Shubert, V. A.; Myshakin, E. M.; Jordan, K. D.; Zwier, T. S. Laser-Initiated Shuttling of a Water Molecule between H-Bonding Sites. *Science* **2005**, *307*, 1443-1446.
- (114) Caminati, W.; Lopez, J. C.; Blanco, S.; Mata, S.; Alonso, J. L. How Water Links to Cis and Trans Peptidic Groups: The Rotational Spectrum of *N*-Methylformamide-Water. *Phys. Chem. Chem. Phys.* **2010**, *12*, 10230-10234.
- (115) Robertson, E. G.; Hockridge, M. R.; Jelfs, P. D.; Simons, J. P. IR-UV Ion-Depletion and Fluorescence Spectroscopy of 2-Phenylacetamide Clusters: Hydration of a Primary Amide. *Phys. Chem. Chem. Phys.* **2001**, *3*, 786-795.
- (116) Cabezas, C.; Varela, M.; Caminati, W.; Mata, S.; Lopez, J. C.; Alonso, J. L. The Two Conformers of Acetanilide Unraveled Using LA-MB-FTMW Spectroscopy. *J. Mol. Spec.* **2011**, *268*, 42-46.
- (117) Florio, G. M.; Gruenloh, C. J.; Quimpo, R. C.; Zwier, T. S. The Infrared Spectroscopy of Hydrogen-Bonded Bridges: 2-Pyridone-(Water)_n and 2-Hydroxypyridine-(Water)_n Clusters, n=1,2. *J. Chem. Phys.* **2000**, *113*, 11143.
- (118) Carney, J. R.; Fedorov, A. V.; Cable, J. R.; Zwier, T. S. Infrared Spectroscopy of H-Bonded Bridges Stretched across the Cis-Amide Group: I. Water Bridges. *J. Chem. Phys. A* **2001**, *105*, 3487–3497.
- (119) Fedorov, A. V.; Cable, J. R.; Carney, J. R.; Zwier, T. S. Infrared Spectroscopy of H-Bonded Bridges Stretched across the Cis -Amide Group: II. Ammonia and Mixed Ammonia/Water Bridges. *J. Chem. Phys. A* **2001**, *105*, 8162–8175.
- (120) Blanco, S.; Lopez, J. C.; Lesarri, A.; Caminati, W.; Alonso, J. L. Conformational Equilibrium of Formanilide: Detection of the Pure Rotational Spectrum of the Tunnelling Cis Conformer. *Mol. Phys.* **2005**, *103*, 1473-1479.
- (121) López, J. C.; Sánchez, R.; Blanco, S.; Alonso, J. L. Microsolvation of 2-Azetidinone: A Model for the Peptide Group-Water Interactions. *Phys. Chem. Chem. Phys.* **2015**, *17*, 2054-2066.
- (122) Vaquero-Vara, V.; Alstadt, V.; Sewatsky, T. P.; Claughton, J. L.; Finneran, I. A.; Shipman, S. T.; Pate, B. H.; Pratt, D. W. *N*-Ethylformamide Dimer. A β -Turn Model Peptide in the Gas Phase. *J. Mol. Spec.* **2017**, *335*, 102–107.
- (123) Yatsyna, V.; Bakker, D. J.; Feifel, R.; Rijs, A. M.; Zhaunerchyk, V. Far-Infrared Amide IV-VI Spectroscopy of Isolated 2- and 4-Methylacetanilide. *J. Chem. Phys.* **2016**, *145*.
- (124) Yatsyna, V.; Bakker, D. J.; Salén, P.; Feifel, R.; Rijs, A. M.; Zhaunerchyk, V. Infrared Action Spectroscopy of Low-Temperature Neutral Gas-Phase Molecules of Arbitrary Structure. *Phys. Rev. Lett.* **2016**, *117*, 118101.

- (125) Brown, R. D.; Godfrey, P. D.; Storey, J. W. V.; Bassez, M. P. Microwave-Spectrum and Conformation of Glycine. *J. Chem. Soc.-Chem. Commun.* **1978**, 547-548.
- (126) Suenram, R. D.; Lovas, F. J. Millimeter Wave Spectrum of Glycine. *J. Mol. Spec.* **1978**, *72*, 372-382.
- (127) Lesarri, A.; Cocinero, E. J.; López, J. C.; Alonso, J. L. The Shape of Neutral Valine. *Angew. Chem. Int. Ed.* **2004**, *43*, 605-610.
- (128) Lesarri, A.; Sánchez, R.; Cocinero, E. J.; López, J. C.; Alonso, J. L. Coded Amino Acids in Gas Phase: The Shape of Isoleucine. *J. Am. Chem. Soc.* **2005**, *127*, 12952-12956.
- (129) Bermúdez, C.; Mata, S.; Cabezas, C.; Alonso, J. L. Tautomerism in Neutral Histidine. *Angew. Chem. Int. Ed.* **2014**, *53*, 11015-11018.
- (130) Rizzo, T. R.; Park, Y. D.; Peteanu, L. A.; Levy, D. H. The Electronic Spectrum of the Amino Acid Tryptophan in the Gas Phase. *J. Chem. Phys.* **1986**, *84*, 2534-2541.
- (131) Snoek, L. C.; Kroemer, R. T.; Hockridge, M. R.; Simons, J. P. Conformational Landscapes of Aromatic Amino Acids in the Gas Phase: Infrared and Ultraviolet Ion Dip Spectroscopy of Tryptophan. *Phys. Chem. Chem. Phys.* **2001**, *3*, 1819-1826.
- (132) Martinez III, S. J.; Alfano, J. C.; Levy, D. H. The Electronic Spectroscopy of the Amino Acids Tyrosine and Phenylalanine in a Supersonic Jet. *J. Mol. Spec.* **1992**, *156*, 421.
- (133) Dian, B. C.; Longarte, A.; Mercier, S.; Evans, D. A.; Wales, D. J.; Zwier, T. S. The Infrared and Ultraviolet Spectra of Single Conformations of Methyl-Capped Dipeptides: *N*-Acetyl Tryptophan Amide and *N*-Acetyl Tryptophan Methyl Amide. *J. Chem. Phys.* **2002**, *117*, 10688-10702.
- (134) Gerhards, M.; Unterberg, C. Structures of the Protected Amino Acid Ac-Phe-Ome and Its Dimer: A β -Sheet Model System in the Gas Phase. *Phys. Chem. Chem. Phys.* **2002**, *4*, 1760-1765.
- (135) Gerhards, M.; Unterberg, C.; Gerlach, A.; Jansen, A. β -Sheet Model Systems in the Gas Phase: Structures and Vibrations of Ac-Phe-Nhme and Its Dimer (Ac-Phe-Nhme)₂. *Phys. Chem. Chem. Phys.* **2004**, *6*, 2682-2690.
- (136) Chin, W.; Piuzzi, F.; Dimicoli, I.; Mons, M. Probing the Competition between Secondary Structures and Local Preferences in Gas Phase Isolated Peptide Backbones. *Phys. Chem. Chem. Phys.* **2006**, *8*, 1033-1048.
- (137) Compagnon, I.; Oomens, J.; Bakker, J.; Meijer, G.; Helden, G. v. Vibrational Spectroscopy of a Non-Aromatic Amino Acid-Based Model Peptide: Identification of the γ -Turn Motif of the Peptide Backbone. *Phys. Chem. Chem. Phys.* **2005**, *7*, 13-15.
- (138) Cabezas, C.; Varela, M.; Cortijo, V.; Jiménez, A. I.; Peña, I.; Daly, A. M.; López, J. C.; Cativiela, C.; Alonso, J. L. The Alanine Model Dipeptide Ac-Ala-NH₂ Exists as a Mixture of C₇^{eq} and C₅ Conformers. *Phys. Chem. Chem. Phys.* **2013**, *15*, 2580-2585.
- (139) León, I.; Alonso, E. R.; Mata, S.; Cabezas, C.; Rodríguez, M. A.; Grabow, J.-U.; Alonso, J. L. The Role of Amino Acid Side Chains in Stabilizing Dipeptides: The Laser Ablation Fourier Transform Microwave Spectrum of Ac-Val-NH₂. *Phys. Chem. Chem. Phys.* **2017**, *19*, 24985-24990.
- (140) Chin, W.; Compagnon, I.; Dognon, J. P.; Canuel, C.; Piuzzi, F.; Dimicoli, I.; von Helden, G.; Meijer, G.; Mons, M. Spectroscopic Evidence for Gas-Phase Formation of Successive β -Turns in a Three-Residue Peptide Chain. *J. Am. Chem. Soc.* **2005**, *127*, 1388-1389.
- (141) Chin, W.; Piuzzi, F.; Dognon, J.-P.; Dimicoli, I.; Tardivel, B.; Mons, M. Gas Phase Formation of a ₃₁₀-Helix in a Three-Residue Peptide Chain: Role of Side Chain-Backbone Interactions as Evidenced by IR-UV Double Resonance Experiments. *J. Am. Chem. Soc.* **2005**, *127*, 11900-11901.
- (142) Gloaguen, E.; Mons, M. In *Gas-Phase IR Spectroscopy and Structure of Biological Molecules*; Rijs, A. M.; Oomens, J., Eds., 2015; Vol. 364; p 225-270.
- (143) Schwing, K.; Gerhards, M. Investigations on Isolated Peptides by Combined IR/UV Spectroscopy in a Molecular Beam - Structure, Aggregation, Solvation and Molecular Recognition. *Int. Rev. Phys. Chem.* **2016**, *35*, 569-677.
- (144) Rijs, A. M.; Ohanessian, G.; Oomens, J.; Meijer, G.; von Helden, G.; Compagnon, I. Internal Proton Transfer Leading to Stable Zwitterionic Structures in a Neutral Isolated Peptide. *Angew. Chem. Int. Ed.* **2010**, *49*, 2332-2335.
- (145) Vaden, T. D.; Gowers, S. A. N.; de Boer, T. S. J. A.; Steill, J. D.; Oomens, J.; Snoek, L. C. Conformational Preferences of an Amyloidogenic Peptide: IR Spectroscopy of Ac-VQIVYK-NHMe. *J. Am. Chem. Soc.* **2008**, *130*, 14640-14650.
- (146) Abo-Riziq, A. G.; Crews, B. O.; Callahan, M. P.; Grace, L.; de Vries, M. S. Spectroscopy of Isolated Gramicidin Peptides. *Angew. Chem. Int. Ed.* **2006**, *45*, 5166-5169.

- (147) Oomens, J.; Polfer, N.; Moore, D. T.; van der Meer, L.; Marshall, A. G.; Eyler, J. R.; Meijer, G.; von Helden, G. Charge-State Resolved Mid-Infrared Spectroscopy of a Gas-Phase Protein. *Phys. Chem. Chem. Phys.* **2005**, *7*, 1345-1348.
- (148) Cabezas, C.; Varela, M.; Alonso, J. L. The Structure of the Elusive Simplest Dipeptide Gly-Gly. *Angew. Chem. Int. Ed.* **2017**, *56*, 6420-6425.
- (149) Stamm, A.; Bernhard, D.; Gerhards, M. Structural Investigations on a Linear Isolated Depsipeptide: The Importance of Dispersion Interactions. *Phys. Chem. Chem. Phys.* **2016**, *18*, 15327-15336.
- (150) Baquero, E. E.; James III, W. H.; Choi, S. H.; Gellman, S. H.; Zwier, T. S. Single-Conformation Ultraviolet and Infrared Spectroscopy of Model Synthetic Foldamers: β -Peptides Ac- β^3 -hPhe-NHMe and Ac- β^3 -hTyr-NHMe. *J. Am. Chem. Soc.* **2008**, *130*, 4784-4794.
- (151) Baquero, E. E.; James, W. H.; Choi, S. H.; Gellman, S. H.; Zwier, T. S. Single-Conformation Ultraviolet and Infrared Spectroscopy of Model Synthetic Foldamers: β -Peptides Ac- β^3 -hPhe- β^3 -hAla-NHMe and Ac- β^3 -hAla- β^3 -hPhe-NHMe. *J. Am. Chem. Soc.* **2008**, *130*, 4795-4807.
- (152) James III, W. H.; Müller, C. W.; Buchanan, E. G.; Nix, M. G. D.; Guo, L.; Roskop, L.; Gordon, M. S.; Slipchenko, L. V.; Gellman, S. H.; Zwier, T. S. Intramolecular Amide Stacking and Its Competition with Hydrogen Bonding in a Small Foldamer. *J. Am. Chem. Soc.* **2009**, *131*, 14243-14245.
- (153) Compagnon, I.; Oomens, J.; Meijer, G.; Helden, G. v. Mid-Infrared Spectroscopy of Protected Peptides in the Gas Phase: A Probe of the Backbone Conformation. *J. Am. Chem. Soc.* **2006**, *128*, 3592-3597.
- (154) Sohn, W. Y.; Ishiuchi, S. I.; Çarçabal, P.; Oba, H.; Fujii, M. UV-UV Hole Burning and IR Dip Spectroscopy of Homophenylalanine by Laser Desorption Supersonic Jet Technique. *Chem. Phys.* **2014**, *445*, 21-30.
- (155) Sohn, W. Y.; Kim, J. J.; Jeon, M.; Aoki, T.; Ishiuchi, S. I.; Fujii, M.; Kang, H. Entropic Effects Make a More Tightly Folded Conformer of α -Amino Acid Less Stable: UV-UV Hole Burning and IR Dip Spectroscopy of L- β^3 -Homotryptophan Using a Laser Desorption Supersonic Jet Technique. *Phys. Chem. Chem. Phys.* **2018**, *20*, 19979-19986.
- (156) Goldsztejn, G.; Mundlapati, V.; Donon, J.; Tardivel, B.; Brenner, V.; Gloaguen, E.; Mons, M. Intraresidue H-Bonding Motifs in Selenocysteine and Cysteine: Role of the Chalcogen Heteroatoms Revealed by Gas Phase Laser Spectroscopy and Quantum Chemistry Study of Isolated Dipeptides. *Phys. Chem. Chem. Phys.* *accepted*.
- (157) Fricke, H.; Funk, A.; Schrader, T.; Gerhards, M. Investigation of Secondary Structure Elements by IR/UV Double Resonance Spectroscopy: Analysis of an Isolated β -Sheet Model System. *J. Am. Chem. Soc.* **2008**, *130*, 4692-4698.
- (158) Snoek, L. C.; Kroemer, R. T.; Simons, J. P. A Spectroscopic and Computational Exploration of Tryptophan-Water Cluster Structures in the Gas Phase. *Phys. Chem. Chem. Phys.* **2002**, *4*, 2130-2139.
- (159) Blom, M. N.; Compagnon, I.; Polfer, N. C.; Helden, G. v.; Meijer, G.; Suhai, S.; Paizs, B.; Oomens, J. Stepwise Solvation of an Amino Acid: The Appearance of Zwitterionic Structures. *J. Phys. Chem. A* **2007**, *111*, 7309-7316.
- (160) Fricke, H.; Schwing, K.; Gerlach, A.; Unterberg, C.; Gerhards, M. Investigations of the Water Clusters of the Protected Amino Acid Ac-Phe-OMe by Applying IR/UV Double Resonance Spectroscopy: Microsolvation of the Backbone. *Phys. Chem. Chem. Phys.* **2010**, *12*, 3511-3521.
- (161) Zhu, H.; Blom, M.; Compagnon, I.; Rijs, A. M.; Roy, S.; Helden, G. v.; Schmidt, B. Conformations and Vibrational Spectra of a Model Tripeptide: Change of Secondary Structure Upon Micro-Solvation. *Phys. Chem. Chem. Phys.* **2010**, *12*, 3415-3425.
- (162) Cocinero, E. J.; Stanca-Kaposta, E. C.; Gamblin, D. P.; Davis, B. G.; Simons, J. P. Peptide Secondary Structures in the Gas Phase: Consensus Motif of N-Linked Glycoproteins. *J. Am. Chem. Soc.* **2009**, *131*, 1282-1287.
- (163) Fricke, H.; Gerlach, A.; Unterberg, C.; Wehner, M.; Schrader, T.; Gerhards, M. Interactions of Small Protected Peptides with Aminopyrazole Derivatives: The Efficiency of Blocking a β -Sheet Model in the Gas Phase. *Angew. Chem. Int. Ed.* **2009**, *48*, 900-904.
- (164) Gloaguen, E.; Tardivel, B.; Mons, M. Gas Phase Double-Resonance IR/UV Spectroscopy of an Alanine Dipeptide Analogue Using a Non-Covalently Bound UV-Tag: Observation of a Folded Peptide Conformation in the Ac-Ala-NH₂-Toluene Complex. *Structural Chemistry* **2016**, *27*, 225-230.
- (165) Kapota, C.; Lemaire, J.; Maître, P.; Ohanessian, G. Vibrational Signature of Charge Solvation vs. Salt Bridge Isomers of Sodiated Amino Acids in the Gas Phase. *J. Am. Chem. Soc.* **2004**, *126*, 1836-1842.
- (166) Dunbar, R. C. Spectroscopy of Metal-Ion Complexes with Peptide-Related Ligands. *Gas-Phase IR Spectroscopy and Structure of Biological Molecules* **2015**, *364*, 183-223.

- (167) Rizzo, T. R.; Park, Y. D.; Peteanu, L.; Levy, D. H. Electron Spectrum of the Amino Acid Tryptophan Cooled in a Supersonic Molecular Beam. *J. Chem. Phys.* **1985**, *83*, 4819-4820.
- (168) Rizzo, T. R.; Park, Y. D.; Levy, D. H. Dispersed Fluorescence of Jet-Cooled Tryptophan: Excited State Conformers and Intramolecular Exciplex Formation. *J. Chem. Phys.* **1986**, *85*, 6945-6951.
- (169) Dian, B. C.; Longarte, A.; Zwier, T. S. Hydride Stretch Infrared Spectra in the Excited Electronic States of Indole and Its Derivatives: Direct Evidence for the $^1\pi\sigma^*$ State. *J. Chem. Phys.* **2003**, *118*, 2696-2706.
- (170) Lee, Y.; Jung, J.; Kim, B.; Butz, P.; Snoek, L. C.; Kroemer, R. T.; Simons, J. P. Alanyl Side Chain Folding in Phenylalanine: Conformational Assignments through Ultraviolet Rotational Band Contour Analysis. *J. Phys. Chem. A* **2004**, *108*, 69-73.
- (171) Tubergen, M. J.; Cable, J. R.; Levy, D. H. Substituent Effects on the Electronic Spectroscopy of Tryptophan Derivatives in Jet Expansions. *J. Chem. Phys.* **1990**, *92*, 51-60.
- (172) Sobolewski, A. L.; Domcke, W.; Dedonder-Lardeux, C.; Juvet, C. Excited-State Hydrogen Detachment and Hydrogen Transfer Driven by Repulsive $^1\pi\sigma^*$ States: A New Paradigm for Nonradiative Decay in Aromatic Biomolecules. *Phys. Chem. Chem. Phys.* **2002**, *4*, 1093-1100.
- (173) Lee, Y. H.; Jung, J. W.; Kim, B.; Butz, P.; Snoek, L. C.; Kroemer, R. T.; Simons, J. P. Alanyl Side Chain Folding in Phenylalanine: Conformational Assignments through Ultraviolet Rotational Band Contour Analysis. *J. Phys. Chem. A* **2004**, *108*, 69-73.
- (174) Hashimoto, T.; Takasu, Y.; Yamada, Y.; Ebata, T. Anomalous Conformer Dependent S_1 Lifetime of L-Phenylalanine. *Chem. Phys. Lett.* **2006**, *421*, 227-231.
- (175) Sobolewski, A. L.; Domcke, W. Relevance of Electron-Driven Proton-Transfer Processes for the Photostability of Proteins. *Chemphyschem* **2006**, *7*, 561-564.
- (176) Sobolewski, A. L.; Shemesh, D.; Domcke, W. Computational Studies of the Photophysics of Neutral and Zwitterionic Amino Acids in an Aqueous Environment: Tyrosine-(H_2O)₂ and Tryptophan-(H_2O)₂ Clusters. *J. Phys. Chem. A* **2009**, *113*, 542-550.
- (177) Shemesh, D.; Hättig, C.; Domcke, W. Photophysics of the Trp-Gly Dipeptide: Role of Electron and Proton Transfer Processes for Efficient Excited-State Deactivation. *Chem. Phys. Lett.* **2009**, *482*, 38-43.
- (178) Shemesh, D.; Sobolewski, A. L.; Domcke, W. Efficient Excited-State Deactivation of the Gly-Phe-Ala Tripeptide Via an Electron-Driven Proton-Transfer Process. *J. Am. Chem. Soc.* **2009**, *131*, 1374-1375.
- (179) Shemesh, D.; Sobolewski, A. L.; Domcke, W. Role of Excited-State Hydrogen Detachment and Hydrogen-Transfer Processes for the Excited-State Deactivation of an Aromatic Dipeptide: *N*-Acetyl Tryptophan Methyl Amide. *Phys. Chem. Chem. Phys.* **2010**, *12*, 4899-4905.
- (180) Shemesh, D.; Domcke, W. Effect of the Chirality of Residues and γ -Turns on the Electronic Excitation Spectra, Excited-State Reaction Paths and Conical Intersections of Capped Phenylalanine-Alanine Dipeptides. *Chemphyschem* **2011**, *12*, 1833-1840.
- (181) Mališ, M.; Loquais, Y.; Gloaguen, E.; Biswal, H. S.; Piuze, F.; Tardivel, B.; Brenner, V.; Broquier, M.; Juvet, C.; Mons, M.; Došlić, N.; Ljubić, I. Unraveling the Mechanisms of Nonradiative Deactivation in Model Peptides Following Photoexcitation of a Phenylalanine Residue. *J. Am. Chem. Soc.* **2012**, *134*, 20340-20351.
- (182) Domcke, W.; Sobolewski, A. L. Peptide Deactivation: Spectroscopy Meets Theory. *Nature Chemistry* **2013**, *5*, 257-258.
- (183) Mališ, M.; Loquais, Y.; Gloaguen, E.; Juvet, C.; Brenner, V.; Mons, M.; Ljubić, I.; Došlić, N. Non-Radiative Deactivation of Electronically Excited Phenylalanine in Model Peptides: Quenching Properties of a Primary Amide Group. *Phys. Chem. Chem. Phys.* **2014**, *16*, 2285-2288.
- (184) Loquais, Y.; Gloaguen, E.; Alauddin, M.; Brenner, V.; Tardivel, B.; Mons, M. On the near Uv Photophysics of a Phenylalanine Residue: Conformation-Dependent $\pi\pi^*$ State Deactivation Revealed by Laser Spectroscopy of Isolated Neutral Dipeptides. *Phys. Chem. Chem. Phys.* **2014**, *16*, 22192-22200.
- (185) Malis, M.; Doslic, N. Nonradiative Relaxation Mechanisms of UV Excited Phenylalanine Residues: A Comparative Computational Study. *Molecules* **2017**, *22*, 24.
- (186) Soorkia, S.; Juvet, C.; Grégoire, G. UV Photoinduced Dynamics of Conformer-Resolved Aromatic Peptides. *Chem. Rev.* **2020**, doi/10.1021/acs.chemrev.1029b00316.
- (187) Nosenko, Y.; Kunitski, M.; Thummel, R. P.; Kyrychenko, A.; Herbich, J.; Waluk, J.; Riehn, C.; Brutschy, B. Detection and Structural Characterization of Clusters with Ultrashort-Lived Electronically Excited States: IR Absorption Detected by Femtosecond Multiphoton Ionization. *J. Am. Chem. Soc.* **2006**, *128*, 10000-10001.

- (188) León, I.; Montero, R.; Castaño, F.; Longarte, A.; Fernández, J. A. Mass-Resolved Infrared Spectroscopy of Complexes without Chromophore by Nonresonant Femtosecond Ionization Detection. *J. Phys. Chem. A* **2012**, *116*, 6798-6803.
- (189) Schwing, K.; Gerhards, M. Combined Infrared/Ultraviolet Spectroscopy in Molecular Beam Experiments. *Bunsenmagazin* **2014**, *3*, 116–131.
- (190) Rijs, A. M.; Oomens, J. In *Gas-Phase IR Spectroscopy and Structure of Biological Molecules*; Rijs, A. M.; Oomens, J., Eds., 2015; Vol. 364; p 1-42.
- (191) Miller, R. D. In *Atomic and Molecular Beam Methods*; Scoles, G., Ed.; Oxford University Press: New York, 1988; Vol. 1; p 14-53.
- (192) Levy, D. H. Laser Spectroscopy of Cold Gas-Phase Molecules. *Annu. Rev. Phys. Chem.* **1980**, *31*, 197–225.
- (193) Smalley, R. E.; Wharton, L.; Levy, D. H. Molecular Optical Spectroscopy with Supersonic Beams and Jets *Acc. Chem. Res.* **1977**, *10*, 139-145.
- (194) Meijer, G.; de Vries, M.; Hunziker, H. E.; Wendt, H. R. Laser Desorption Jet-Cooling of Organic-Molecules - Cooling Characteristics and Detection Sensitivity. *Applied Physics B* **1990**, *51*, 395-403.
- (195) Miller, T. A. Chemistry and Chemical Intermediates in Supersonic Free Jet Expansions. *Science* **1984**, *223*, 545-553.
- (196) Jaeqx, S.; Du, W.; Meijer, E. J.; Oomens, J.; Rijs, A. M. Conformational Study of Z-Glu-OH and Z-Arg-OH: Dispersion Interactions Versus Conventional Hydrogen Bonding. *J. Phys. Chem. A* **2013**, *117*, 1216-1227.
- (197) Wiley, W. C.; McLaren, I. H. Time-of-Flight Mass Spectrometer with Improved Resolution. *Rev. Sci. Instrum.* **1955**, *26*, 1150-1157.
- (198) Kuehlewind, H.; Neusser, H. J.; Schlag, E. W. Production and Unimolecular Decay Rate of Internal Energy Selected Molecular Ions in a Laser Reflectron Time-of-Flight Mass Spectrometer. *J. Chem. Phys.* **1984**, *88*, 6104–6106.
- (199) Bergmann, T.; Martin, T. P.; Schaber, H. High-Resolution Time-of-Flight Mass Spectrometer. *Rev. Sci. Instrum.* **1989**, *60*, 792.
- (200) Boesl, U.; Weinkauff, R.; Schlag, E. W. Reflectron Time-of-Flight Mass Spectrometry and Laser Excitation for the Analysis of Neutrals, Ionized Molecules and Secondary Fragments. *Int. J. Mass Spectrom. Ion Processes* **1992**, *112*, 121–166.
- (201) Mamyrin, B. A.; Karataev, V. I.; Shmikk, D. V.; Zagulin, V. A. The Mass-Reflectron, a New Non-Magnetic Time-of-Flight Mass Spectrometer with High Resolution. *Soviet Physics -JEPT* **1973**, *64*, 45–48.
- (202) Brause, R.; Fricke, H.; Gerhards, M.; Weinkauff, R.; Kleinermanns, K. Double Resonance Spectroscopy of Different Conformers of the Neurotransmitter Amphetamine and Its Clusters with Water. *Chem. Phys.* **2006**, *327*, 43–53.
- (203) Dian, B. C.; Longarte, A.; Zwier, T. S. Conformational Dynamics in a Dipeptide after Single-Mode Vibrational Excitation. *Science* **2002**, *296*, 2369-2373.
- (204) Ebata, T. Study on the Structure and Vibrational Dynamics of Functional Molecules and Molecular Clusters by Double Resonance Vibrational Spectroscopy. *Bull. Chem. Soc. Jpn.* **2009**, *82*, 127–151.
- (205) Snoek, L. C.; Robertson, E. G.; Kroemer, R. T.; Simons, J. P. Conformational Landscapes in Amino Acids: Infrared and Ultraviolet Ion-Dip Spectroscopy of Phenylalanine in the Gas Phase. *Chem. Phys. Lett.* **2000**, *321*, 49-56.
- (206) Wilson, K. R.; Jimenez-Cruz, M.; Nicolas, C.; Belau, L.; Leone, S. R.; Ahmed, M. Thermal Vaporization of Biological Nanoparticles: Fragment-Free Vacuum Ultraviolet Photoionization Mass Spectra of Tryptophan, Phenylalanine-Glycine-Glycine, and, β -Carotene. *J. Phys. Chem. A* **2006**, *110*, 2106-2113.
- (207) Gaie-Levrel, F.; Garcia, G. A.; Schwell, M.; Nahon, L. Vuv State-Selected Photoionization of Thermally-Desorbed Biomolecules by Coupling an Aerosol Source to an Imaging Photoelectron/Photoion Coincidence Spectrometer: Case of the Amino Acids Tryptophan and Phenylalanine. *Phys. Chem. Chem. Phys.* **2011**, *13*, 7024-7036.
- (208) Grottemeyer, J.; Boesl, U.; Walter, K.; Schlag, E. W. A General Soft Ionization Method for Mass Spectrometry: Resonance-Enhanced Multi-Photon Ionization of Biomolecules. *Organic Mass Spectrometry* **1986**, *21*, 645–653.
- (209) Tembreull, R.; Lubman, D. M. Pulsed Laser Desorption of Biological Molecules in Supersonic Beam Mass Spectrometry with Resonant Two-Photon Ionization Detection. *Analytical Chemistry* **1987**, *59*, 1082–1088.
- (210) Tembreull, R.; Lubman, D. M. Pulsed Laser Desorption with Resonant Two-Photon Ionization Detection in Supersonic Beam Mass Spectrometry. *Analytical Chemistry* **1986**, *58*, 1299–1303.
- (211) Cable, J. R.; Tubergen, M. J.; Levy, D. H. Laser Desorption Molecular Beam Spectroscopy: The Electronic Spectra of Tryptophan Peptides in the Gas Phase. *J. Am. Chem. Soc.* **1987**, *109*, 6198-6199.

- (212) Cable, J. R.; Tubergen, M. J.; Levy, D. H. The Electronic-Spectra of Small Peptides in the Gas Phase. *Faraday Discuss.* **1988**, *86*, 143-152.
- (213) Handschuh, M.; Nettesheim, S.; Zenobi, R. Is Infrared Laser-Induced Desorption a Thermal Process? The Case of Aniline. *J. Phys. Chem. B* **1999**, *103*, 1719-1726.
- (214) Cohen, R.; Brauer, B.; Nir, E.; Grace, L.; de Vries, M. S. Resonance-Enhanced Multiphoton Ionization Spectroscopy of Dipeptides. *J. Phys. Chem. A* **2000**, *104*, 6351-6355.
- (215) Piuzzi, F.; Dimicoli, I.; Mons, M.; Tardivel, B.; Zhao, Q. A Simple Laser Vaporization Source for Thermally Fragile Molecules Coupled to a Supersonic Expansion: Application to the Spectroscopy of Tryptophan. *Chem. Phys. Lett.* **2000**, *320*, 282-288.
- (216) Hünig, I.; Seefeld, K. A.; Kleinermanns, K. Rempy and Uv-Uv Double Resonance Spectroscopy of Tryptophan Ethylester and the Dipeptides Tryptophan-Serine, Glycine- Tryptophan and Proline-Tryptophan. *Chem. Phys. Lett.* **2003**, *369*, 173-179.
- (217) Chin, W.; Dognon, J.-P.; Canuel, C.; Piuzzi, F.; Dimicoli, I.; Mons, M.; Compagnon, I.; von Helden, G.; Meijer, G. Secondary Structures of Short Peptide Chains in the Gas Phase: Double Resonance Spectroscopy of Protected Dipeptides. *J. Chem. Phys.* **2005**, *122*, 054317.
- (218) Cocinero, E. J.; Çarçabal, P.; Vaden, T. D.; Simons, J. P.; Davis, B. G. Sensing the Anomeric Effect in a Solvent-Free Environment. *Nature* **2011**, *469*, 76-80.
- (219) Biswal, H. S.; Loquais, Y.; Tardivel, B.; Gloaguen, E.; Mons, M. Isolated Monohydrates of a Model Peptide Chain: Effect of a First Water Molecule on the Secondary Structure of a Capped Phenylalanine. *J. Am. Chem. Soc.* **2011**, *133*, 3931-3942.
- (220) Alonso, J. L.; Pérez, C.; Eugenia Sanz, M.; López, J. C.; Blanco, S. Seven Conformers of L-Threonine in the Gas Phase: A LA-MB-FTMW Study. *Phys. Chem. Chem. Phys.* **2009**, *11*, 617-627.
- (221) Lee, K. T.; Sung, J.; Lee, K. J.; Kim, S. K.; Park, Y. D. Resonant Two-Photon Ionization Study of Jet-Cooled Amino Acid: L-Phenylalanine and Its Monohydrated Complex. *J. Chem. Phys.* **2002**, *116*, 8251-8254.
- (222) Çarçabal, P.; Kroemer, R. T.; Snoek, L. C.; Simons, J. P.; Bakker, J. M.; Compagnon, I.; Meijer, G.; Helden, G. v. Hydrated Complexes of Tryptophan: Ion Dip Infrared Spectroscopy in the 'Molecular Fingerprint' Region, 100-2000 cm^{-1} . *Phys. Chem. Chem. Phys.* **2004**, *6*, 4546-4552.
- (223) Wales, D. J. Energy Landscapes: Calculating Pathways and Rates. *Int. Rev. Phys. Chem.* **2006**, *25*, 237-282.
- (224) Imani, Z.; Mundlapati, V. R.; Goldsztejn, G.; Brenner, V.; Gloaguen, E.; Guillot, R.; Baltaze, J.-P.; Le Barbu-Debus, K.; Robin, S.; Zehnacker, A.; Mons, M.; Aitken, D. J. Conformation Control through Concurrent Hyperconjugation-Assisted N-H \cdots S and N-H \cdots O=C Hydrogen Bonding. *Chem. Sci*, *accepted*.
- (225) Snoek, L. C.; Van Mourik, T.; Simons, J. P. Neurotransmitters in the Gas Phase: A Computational and Spectroscopic Study of Noradrenaline. *Mol. Phys.* **2003**, *101*, 1239-1248.
- (226) Schermann, J. P. *Spectroscopy and Modelling of Biomolecular Building Blocks*; Elsevier: Amsterdam, 2008.
- (227) Ruoff, R. S.; Klots, T. D.; Emilsson, T.; Gutowsky, H. S. Relaxation of Conformers and Isomers in Seeded Supersonic Jets of Inert-Gases. *J. Chem. Phys.* **1990**, *93*, 3142-3150.
- (228) Řeha, D.; Valdés, H.; Vondrášek, J.; Hobza, P.; Abu-Riziq, A.; Crews, B.; de Vries, M. S. Structure and Ir Spectrum of Phenylalanyl-Glycyl-Glycine Tripeptide in the Gas-Phase: IR/UV Experiments, Ab Initio Quantum Chemical Calculations, and Molecular Dynamic Simulations. *Chem. Eur. J.* **2005**, *11*, 6803-6817.
- (229) Ebata, T.; Hashimoto, T.; Ito, T.; Inokuchi, Y.; Altunso, F.; Brutschy, B.; Tarakeshwar, P. Hydration Profiles of Aromatic Amino Acids: Conformations and Vibrations of L-Phenylalanine-(H₂O)_n Clusters. *Phys. Chem. Chem. Phys.* **2006**, *8*, 4783-4791.
- (230) Toennies, J. P.; Vilesov, A. F. Spectroscopy of Atoms and Molecules in Liquid Helium. *Annu. Rev. Phys. Chem.* **1998**, *49*, 1-41.
- (231) Lindinger, A.; Toennies, J. P.; Vilesov, A. F. High Resolution Vibronic Spectra of the Amino Acids Tryptophan and Tyrosine in 0.38 K Cold Helium Droplets. *J. Chem. Phys.* **1999**, *110*, 1429-1436.
- (232) Huisken, F.; Werhahn, O.; Ivanov, A. Y.; Krasnokutski, S. A. The O-H Stretching Vibrations of Glycine Trapped in Rare Gas Matrices and Helium Clusters. *J. Chem. Phys.* **1999**, *111*, 2978-2984.
- (233) Lindinger, A.; Lugovoj, E.; Toennies, J. P.; Vilesov, A. F. Splitting of the Zero Phonon Lines of Indole, 3-Methyl Indole, Tryptamine and N-Acetyl Tryptophan Amide in Helium Droplets. *Z. Phys. Chem.* **2001**, *215*, 401.

- (234) Chocholoušová, J.; Vacek, J.; Huisken, F.; Werhahn, O.; Hobza, P. Stacked Structure of the Glycine Dimer Is More Stable Than the Cyclic Planar Geometry with Two O–H···O Hydrogen Bonds: Concerted Action of Empirical, High-Level Nonempirical Ab Initio, and Experimental Studies. *J. Chem. Phys. A* **2002**, *106*, 11540–11549.
- (235) Lindinger, A.; Toennies, J. P.; Vilesov, A. F. The Effects of Isotope Substitution and Nuclear Spin Modifications on the Spectra of Complexes of Tetracene with Hydrogen Molecules in Ultracold 0.37 K He Droplets. *J. Chem. Phys.* **2004**, *121*, 12282–12292.
- (236) Toennies, J. P.; Vilesov, A. F. Superfluid Helium Droplets: A Uniquely Cold Nanomatrix for Molecules and Molecular Complexes. *Angew. Chem. Int. Ed.* **2004**, *43*, 2622–2648.
- (237) Choi, M. Y.; Miller, R. E. Four Tautomers of Isolated Guanine from Infrared Laser Spectroscopy in Helium Nanodroplets. *J. Am. Chem. Soc.* **2006**, *128*, 7320–7328.
- (238) Denifl, S.; Mähr, I.; Ferreira da Silva, F.; Zappa, F.; Märk, T. D.; Scheier, P. Electron Impact Ionization Studies with the Amino Acid Valine in the Gas Phase and (Hydrated) in Helium Droplets. *The European Physical Journal D* **2009**, *51*, 73–79.
- (239) Bierau, F.; Kupser, P.; Meijer, G.; Helden, G. v. Catching Proteins in Liquid Helium Droplets. *Phys. Rev. Lett.* **2010**, *105*, 133402.
- (240) Filsinger, F.; Ahn, D.-S.; Meijer, G.; Helden, G. v. Photoexcitation of Mass/Charge Selected Hemin⁺, Caught in Helium Nanodroplets. *Phys. Chem. Chem. Phys.* **2012**, *14*, 13370–13377.
- (241) Leavitt, C. M.; Moore, K. B.; Raston, P. L.; Agarwal, J.; Moody, G. H.; Shirley, C. C.; Schaefer, H. F.; Douberly, G. E. Liquid Hot NAGMA Cooled to 0.4 K: Benchmark Thermochemistry of a Gas-Phase Peptide. *J. Phys. Chem. A* **2014**, *118*, 9692–9700.
- (242) Verma, D.; Tanyag, R. M. P.; O'Connell, S. M. O.; Vilesov, A. F. Infrared Spectroscopy in Superfluid Helium Droplets. *Advances in Physics-X* **2018**, *4*, 32.
- (243) Lee, K. T.; Sung, J.; Lee, K. J.; Park, Y. D.; Kim, S. K. Conformation-Dependent Ionization Energies of L-Phenylalanine. *Angew. Chem. Int. Ed.* **2002**, *41*, 4114–4117.
- (244) Müller-Dethlefs, K.; Sander, M.; Schlag, E. W. A Novel Method Capable of Resolving Rotational Ionic States by the Detection of Threshold Photoelectrons with a Resolution of 1.2 cm⁻¹. *Z. Naturforsch. Sect. A-J. Phys. Sci.* **1984**, *39*, 1089–1091.
- (245) Reiser, G.; Dopfer, O.; Lindner, R.; Henri, G.; Mullerdethlefs, K.; Schlag, E. W.; Colson, S. D. A New Approach to Vibrational Spectroscopy of Ion Clusters - the Zero Kinetic-Energy (Zeke) Photoelectron Spectrum of the Phenol-Water Complex. *Chem. Phys. Lett.* **1991**, *181*, 1–4.
- (246) Muller-Dethlefs, K.; Schlag, E. W. Chemical Applications of Zero Kinetic Energy (Zeke) Photoelectron Spectroscopy. *Angew. Chem. Int. Ed.* **1998**, *37*, 1346–1374.
- (247) Zhu, L.; Johnson, P. Mass Analyzed Threshold Ionization Spectroscopy. *J. Chem. Phys.* **1991**, *94*, 5769.
- (248) Gerhards, M.; Schumm, S.; Unterberg, C.; Kleinermanns, K. Structure and Vibrations of Catechol in the S₁ State and Ionic Ground State. *Chem. Phys. Lett.* **1998**, *294*, 65–70.
- (249) Ishiuchi, S.-i.; Yamada, K.; Chakraborty, S.; Yagi, K.; Fujii, M. Gas-Phase Spectroscopy and Anharmonic Vibrational Analysis of the 3-Residue Peptide Z-Pro-Leu-Gly-NH₂ by the Laser Desorption Supersonic Jet Technique. *Chem. Phys.* **2013**, *419*, 145–152.
- (250) Fischer, J. L.; Elvir, B. R.; DeLucia, S. A.; Blodgett, K. N.; Zeller, M.; Kubasik, M. A.; Zwier, T. S. Single-Conformation Spectroscopy of Capped Aminoisobutyric Acid Dipeptides: The Effect of C-Terminal Cap Chromophores on Conformation. *J. Phys. Chem. A* **2019**, *123*, 4178–4187.
- (251) Jochims, H. W.; Schwell, M.; Chotin, J. L.; Clemino, M.; Dulieu, F.; Baumgärtel, H.; Leach, S. Photoion Mass Spectrometry of Five Amino Acids in the 6–22 eV Photon Energy Range. *Chem. Phys.* **2004**, *298*, 279–297.
- (252) Wilson, K. R.; Belau, L.; Nicolas, C.; Jimenez-Cruz, M.; Leone, S. R.; Ahmed, M. Direct Determination of the Ionization Energy of Histidine with Vuv Synchrotron Radiation. *International Journal of Mass Spectrometry* **2006**, *249*, 155–161.
- (253) Hu, Y.; Bernstein, E. R. Vibrational and Photoionization Spectroscopy of Biomolecules: Aliphatic Amino Acid Structures. *J. Chem. Phys.* **2008**, *128*, 164311.
- (254) Hu, Y.; Bernstein, E. R. Vibrational and Photoionization Spectroscopy of Neutral Valine Clusters. *J. Phys. Chem. A* **2009**, *113*, 8454–8461.

- (255) Woodward, J. R.; Watanabe, H.; Ishiuchi, S.-i.; Fujii, M. A Two-Color Tunable Infrared/Vacuum Ultraviolet Spectrometer for High-Resolution Spectroscopy of Molecules in Molecular Beams. *The Review of scientific instruments* **2012**, *83*, 014102.
- (256) Hu, Y.; Guan, J.; Bernstein, E. R. Mass-Selected IR-VUV (118 nm) Spectroscopic Studies of Radicals, Aliphatic Molecules, and Their Clusters. *Mass spectrometry reviews* **2013**, *32*, 484–501.
- (257) Yatsyna, V.; Mallat, R.; Gorn, T.; Schmit, M.; Feifel, R.; Rijs, A. M.; Zhaunerchyk, V. Conformational Preferences of Isolated Glycylglycine (Gly-Gly) Investigated with IRMPD-VUV Action Spectroscopy and Advanced Computational Approaches. *J. Phys. Chem. A* **2019**, *123*, 862-872.
- (258) Yatsyna, V.; Mallat, R.; Gorn, T.; Schmitt, M.; Feifel, R.; Rijs, A. M.; Zhaunerchyk, V. Competition between Folded and Extended Structures of Alanine (Ala) in a Molecular Beam. *Phys. Chem. Chem. Phys.* **2019**, *21*, 14126-14132.
- (259) Powis, I.; Rennie, E. E.; Hergenroth, U.; Kugeler, O.; Bussy-Socrate, R. Investigation of the Gas-Phase Amino Acid Alanine by Synchrotron Radiation Photoelectron Spectroscopy. *J. Phys. Chem. A* **2003**, *107*, 25-34.
- (260) Tia, M.; de Miranda, B. C.; Daly, S.; Gaie-Levrel, F.; Garcia, G. A.; Nahon, L.; Powis, I. VUV Photodynamics and Chiral Asymmetry in the Photoionization of Gas Phase Alanine Enantiomers. *J. Phys. Chem. A* **2014**, *118*, 2765-2779.
- (261) Plekan, O.; Feyer, V.; Richter, R.; Coreno, M.; de Simone, M.; Prince, K. C.; Carravetta, V. Investigation of the Amino Acids Glycine, Proline, and Methionine by Photoemission Spectroscopy. *J. Phys. Chem. A* **2007**, *111*, 10998-11005.
- (262) León, I.; Montero, R.; Longarte, A.; Fernández, J. A. Ir Mass-Resolved Spectroscopy of Complexes without Chromophore: Cyclohexanol-(H₂O)_n, n = 1-3 and Cyclohexanol Dimer. *J. Chem. Phys.* **2013**, *139*, 174312.
- (263) León, I.; Montero, R.; Longarte, A.; Fernández, J. A. Influence of Dispersive Forces on the Final Shape of a Reverse Micelle. *Phys. Chem. Chem. Phys.* **2015**, *17*, 2241–2245.
- (264) Mons, M.; Piuzzi, F.; Dimicoli, I.; Gorb, L.; Leszczynski, J. Near-UV Resonant Two-Photon Ionization Spectroscopy of Gas Phase Guanine: Evidence for the Observation of Three Rare Tautomers. *J. Phys. Chem. A* **2006**, *110*, 10921-10924.
- (265) Nosenko, Y.; Kunitski, M.; Stark, T.; Gobel, M.; Tarakeshwar, P.; Brutschy, B. Vibrational Signatures of Watson-Crick Base Pairing in Adenine-Thymine Mimics. *Phys. Chem. Chem. Phys.* **2013**, *15*, 11520-11530.
- (266) Valdes, H.; Spiwok, V.; Rezac, J.; Reha, D.; Abo-Riziq, A. G.; de Vries, M. S.; Hobza, P. Potential-Energy and Free-Energy Surfaces of Glycyl-Phenylalanyl-Alanine (Gfa) Tripeptide: Experiment and Theory. *Chem. Eur. J.* **2008**, *14*, 4886-4898.
- (267) Valdés, H.; Reha, D.; Hobza, P. Structure of Isolated Tryptophyl-Glycine Dipeptide and Tryptophyl-Glycyl-Glycine Tripeptide: Ab Initio SCC-DFTB-D Molecular Dynamics Simulations and High-Level Correlated Ab Initio Quantum Chemical Calculations. *J. Phys. Chem. B* **2006**, *110*, 6385-6396.
- (268) Lipert, R. J.; Colson, S. D. Persistent Spectral Hole Burning of Molecular Clusters in a Supersonic Jet. *J. Chem. Phys.* **1989**, *93*, 3894–3896.
- (269) Hünig, I.; Kleiner, K. Conformers of the Peptides Glycine-Tryptophan, Tryptophan-Glycine and Tryptophan-Glycine-Glycine as Revealed by Double Resonance Laser Spectroscopy. *Phys. Chem. Chem. Phys.* **2004**, *6*, 2650-2658.
- (270) Inokuchi, Y.; Kobayashi, Y.; Ito, T.; Ebata, T. Conformation of L-Tyrosine Studied by Fluorescence-Detected UV-UV and IR-UV Double-Resonance Spectroscopy. *J. Phys. Chem. A* **2007**, *111*, 3209-3215.
- (271) Ebata, T.; Fujii, A.; Mikami, N. Structures of Size-Selected Hydrogen-Bonded Phenol-(H₂O)_n Clusters in S₀, S₁ and Ion. *Int. J. Mass Spectrom. Ion Processes* **1996**, *159*, 111–124.
- (272) Carney, J. R.; Hagemester, F. C.; Zwier, T. S. Hydrogen-Bonding Topologies of Indole-(Water)_n Clusters from Resonant Ion-Dip Infrared Spectroscopy. *J. Chem. Phys.* **1998**, *108*, 3379-3382.
- (273) Palmer, P. M.; Chen, Y.; Topp, M. R. Simple Water Clusters of Coumarins 151 and 152A Studied by IR-UV Double Resonance Spectroscopy. *Chem. Phys. Lett.* **2000**, *318*, 440–447.
- (274) Stearns, J. A.; Das, A.; Zwier, T. S. Hydrogen Atom Dislocation in the Excited State of Anthranilic Acid: Probing the Carbonyl Stretch Fundamental and the Effects of Water Complexation. *Phys. Chem. Chem. Phys.* **2004**, *6*, 2605–2610.
- (275) Bartl, K.; Funk, A.; Gerhards, M. Ir/Uv Spectroscopy on Jet Cooled 3-Hydroxyflavone (H₂O)_n (n=1,2) Clusters Along Proton Transfer Coordinates in the Electronic Ground and Excited States. *J. Chem. Phys.* **2008**, *129*, 234306.

- (276) Bartl, K.; Funk, A.; Schwing, K.; Fricke, H.; Kock, G.; Martin, H.-D.; Gerhards, M. Ir Spectroscopy Applied Subsequent to a Proton Transfer Reaction in the Excited State of Isolated 3-Hydroxyflavone and 2-(2-Naphthyl)-3-Hydroxychromone. *Phys. Chem. Chem. Phys.* **2009**, *11*, 1173–1179.
- (277) Stamm, A.; Weiler, M.; Brächer, A.; Schwing, K.; Gerhards, M. A Combined IR/IR and IR/UV Spectroscopy Study on the Proton Transfer Coordinate of Isolated 3-Hydroxychromone in the Electronic Ground and Excited State. *Phys. Chem. Chem. Phys.* **2014**, *16*, 21795–21803.
- (278) Ebata, T.; Fujii, A.; Mikami, N. Vibrational Spectroscopy of Small-Sized Hydrogen-Bonded Clusters and Their Ions. *Int. Rev. Phys. Chem.* **1998**, *17*, 331–361.
- (279) Walther, T.; Bitto, H.; Minton, T. K.; Huber, J. R. Uv-Ir Double-Resonance Spectroscopy of Jet-Cooled Propynal Detected by the Fluorescence Dip Method. *Chem. Phys. Lett.* **1994**, *231*, 64–69.
- (280) Page, R. H.; Shen, Y. R.; Lee, Y. T. Local Modes of Benzene and Benzene Dimer, Studied by Infrared–Ultraviolet Double Resonance in a Supersonic Beam. *J. Chem. Phys.* **1988**, *88*, 4621.
- (281) Riehn, C.; Lahmann, C.; Wassermann, B.; Brutschy, B. IR Depletion Spectroscopy - a Method for Characterizing a Microsolvation Environment. *Chem. Phys. Lett.* **1992**, *197*, 443–450.
- (282) Tanabe, S.; Ebata, T.; Fujii, M.; Mikami, N. OH Stretching Vibrations of Phenol–(H₂O)_n (n=1–3) Complexes Observed by IR-UV Double-Resonance Spectroscopy. *Chem. Phys. Lett.* **1993**, *215*, 347–352.
- (283) Zwier, T. S. The Spectroscopy of Solvation in Hydrogen-Bonded Aromatic Clusters. *Annu. Rev. Phys. Chem.* **1996**, *47*, 205–241.
- (284) Gerhards, M.; Unterberg, C.; Gerlach, A. Structure of a β -Sheet Model System in the Gas Phase: Analysis of the C=O Stretching Vibrations. *Phys. Chem. Chem. Phys.* **2002**, *4*, 5563–5565.
- (285) Gerhards, M. High Energy and Narrow Bandwidth Mid IR Nanosecond Laser System. *Opt. Commun.* **2004**, *241*, 493–497.
- (286) Bakker, J. M.; Aleese, L. M.; Meijer, G.; Helden, G. v. Fingerprint IR Spectroscopy to Probe Amino Acid Conformations in the Gas Phase. *Phys. Rev. Lett.* **2003**, *91*, 203003.
- (287) Ishiuchi, S.-i.; Shitomi, H.; Takazawa, K.; Fujii, M. Nonresonant Ionization Detected IR Spectrum of Jet-Cooled Phenol. Ionization Mechanism and Its Application to Overtone Spectroscopy. *Chem. Phys. Lett.* **1998**, *283*, 243–250.
- (288) Omi, T.; Shitomi, H.; Sekiya, N.; Takazawa, K.; Fujii, M. Nonresonant Ionization Detected IR Spectroscopy for the Vibrational Study in a Supersonic Jet. *Chem. Phys. Lett.* **1996**, *252*, 287–293.
- (289) Fehrensens, B.; Hippler, M.; Quack, M. Isotopomer-Selective Overtone Spectroscopy by Ionization Detected IR+UV Double Resonance of Jet-Cooled Aniline. *Chem. Phys. Lett.* **1998**, *298*, 320–328.
- (290) James III, W. H.; Baquero, E. E.; Shubert, V. A.; Choi, S. H.; Gellman, S. H.; Zwier, T. S. Single-Conformation and Diastereomer Specific Ultraviolet and Infrared Spectroscopy of Model Synthetic Foldamers: α -/ β -Peptides. *J. Am. Chem. Soc.* **2009**, *131*, 6574–6590.
- (291) Cocinero, E. J.; Çarçabal, P.; Vaden, T. D.; Davis, B. G.; Simons, J. P. Exploring Carbohydrate-Peptide Interactions in the Gas Phase: Structure and Selectivity in Complexes of Pyranosides with *N*-Acetylphenylalanine Methylamide. *J. Am. Chem. Soc.* **2011**, *133*, 4548–4557.
- (292) Gloaguen, E.; Valdes, H.; Pagliarulo, F.; Pollet, R.; Tardivel, B.; Hobza, P.; Piuze, F.; Mons, M. Experimental and Theoretical Investigation of the Aromatic-Aromatic Interaction in Isolated Capped Dipeptides. *J. Phys. Chem. A* **2010**, *114*, 2973–2982.
- (293) Shubert, V. A.; Zwier, T. S. IR-IR-UV Hole-Burning: Conformation Specific IR Spectra in the Face of UV Spectral Overlap. *J. Phys. Chem. A* **2007**, *111*, 13283–13286.
- (294) Shubert, V. A.; Müller, C. W.; Zwier, T. S. Water's Role in Reshaping a Macrocyclic Binding Pocket: Infrared and Ultraviolet Spectroscopy of Benzo-15-Crown-5-(H₂O)_n and 4'-Aminobenzo-15-Crown-5-(H₂O)_n, n = 1, 2. *J. Chem. Phys. A* **2009**, *113*, 8067–8079.
- (295) Weiler, M.; Bartl, K.; Gerhards, M. Infrared/Ultraviolet Quadruple Resonance Spectroscopy to Investigate Structures of Electronically Excited States. *J. Chem. Phys.* **2012**, *136*, 114202.
- (296) Dian, B. C.; Longarte, A.; Winter, P. R.; Zwier, T. S. The Dynamics of Conformational Isomerization in Flexible Biomolecules. I. Hole-Filling Spectroscopy of *N*-Acetyl Tryptophan Methyl Amide and *N*-Acetyl Tryptophan Amide. *J. Chem. Phys.* **2004**, *120*, 133–147.

- (297) Dian, B. C.; Florio, G. M.; Clarkson, J. R.; Longarte, A.; Zwier, T. S. Infrared-Induced Conformational Isomerization and Vibrational Relaxation Dynamics in Melatonin and 5-Methoxy-*N*-Acetyl Tryptophan Methyl Amide. *J. Chem. Phys.* **2004**, *120*, 9033-9046.
- (298) Dian, B. C.; Clarkson, J. R.; Zwier, T. S. Direct Measurement of Energy Thresholds to Conformational Isomerization in Tryptamine. *Science* **2004**, *303*, 1169-1173.
- (299) Clarkson, J. R.; Dian, B. C.; Moriggi, L.; DeFusco, A.; McCarthy, V.; Jordan, K. D.; Zwier, T. S. Direct Measurement of the Energy Thresholds to Conformational Isomerization in Tryptamine: Experiment and Theory. *J. Chem. Phys.* **2005**, *122*, 214311.
- (300) Zwier, T. S. Laser Probes of Conformational Isomerization in Flexible Molecules and Complexes. *J. Phys. Chem. A* **2006**, *110*, 4133-4150.
- (301) Gerhards, M.; Stamm, A.; Bernhard, D. Structural Investigations on a Linear Isolated Depsipeptide: Importance of Dispersion Interactions. *Phys. Chem. Chem. Phys.* **2016**, *18*, 15327-15336.
- (302) Seaiby, C.; Zabuga, A. V.; Svendsen, A.; Rizzo, T. R. IR-Induced Conformational Isomerization of a Helical Peptide in a Cold Ion Trap. *J. Chem. Phys.* **2016**, *144*, 7.
- (303) Choi, M. Y.; Douberly, G. E.; Falconer, T. M.; Lewis, W. K.; Lindsay, C. M.; Merritt, J. M.; Stiles, P. L.; Miller, R. E. Infrared Spectroscopy of Helium Nanodroplets: Novel Methods for Physics and Chemistry. *Int. Rev. Phys. Chem.* **2006**, *25*, 15-75.
- (304) Bellina, B.; Merthe, D. J.; Kresin, V. V. Proton Transfer in Histidine-Tryptophan Heterodimers Embedded in Helium Droplets. *J. Chem. Phys.* **2015**, *142*.
- (305) González Flórez, A. I.; Ahn, D.-S.; Gewinner, S.; Schöllkopf, W.; Helden, G. v. IR Spectroscopy of Protonated Leu-Enkephalin and Its 18-Crown-6 Complex Embedded in Helium Droplets. *Phys. Chem. Chem. Phys.* **2015**, *17*, 21902-21911.
- (306) Vaden, T. D.; Gowers, S. A. N.; Snoek, L. C. Infrared Spectroscopy of 'Forbidden' Peptide Sequences. *Phys. Chem. Chem. Phys.* **2009**, *11*, 5843-5850.
- (307) Cable, J. R.; Tubergen, M. J.; Levy, D. H. Electronic Spectroscopy of Small Tryptophan Peptides in Supersonic Molecular Beams. *J. Am. Chem. Soc.* **1988**, *110*, 7349-7355.
- (308) Martinez, S. J.; Alfano, J. C.; Levy, D. H. The Electronic Spectroscopy of Tyrosine and Phenylalanine Analogs in a Supersonic Jet: Acidic Analogs. *J. Mol. Spectrosc.* **1991**, *145*, 100-111.
- (309) Edwards, G. S.; Austin, R. H.; Carroll, F. E.; Copeland, M. L.; Couprie, M. E.; Gabella, W. E.; Haglund, R. F.; Hooper, B. A.; Hutson, M. S.; Jansen, E. D.; Joos, K. M.; Kiehart, D. P.; Lindau, I.; Miao, J.; Pratisto, H. S.; Shen, J. H.; Tokutake, Y.; van der Meer, A. F. G.; Xie, A. Free-Electron-Laser-Based Biophysical and Biomedical Instrumentation. *Rev. Sci. Instrum.* **2003**, *74*, 3207.
- (310) Ullrich, J.; Rudenko, A.; Moshhammer, R. Free-Electron Lasers: New Avenues in Molecular Physics and Photochemistry. *Annu. Rev. Phys. Chem.* **2012**, *63*, 635-660.
- (311) Couprie, M. E. New Generation of Light Sources: Present and Future. *J. Electron. Spectrosc. Relat. Phenom.* **2014**, *196*, 3-13.
- (312) Ozerov, M.; Bernath, B.; Kamenskyi, D.; Redlich, B.; van der Meer, A. F. G.; Christianen, P. C. M.; Engelkamp, H.; Maan, J. C. A THz Spectrometer Combining the Free Electron Laser Flare with 33 T Magnetic Fields. *Applied Physics Letters* **2017**, *110*, 094106.
- (313) Chulkov, R.; Goryashko, V.; Arslanov, D. D.; Jongma, R. T.; van der Zande, W. J.; Zhaunerchyk, V. Multimode Dynamics in a Short-Pulse THz Free Electron Laser. *Physical Review Special Topics - Accelerators and Beams* **2014**, *17*, 050703.
- (314) Jaeqx, S.; Oomens, J.; Cimas, A.; Gaigeot, M.-P.; Rijs, A. M. Gas-Phase Peptide Structures Unraveled by Far-IR Spectroscopy: Combining IR-UV Ion-Dip Experiments with Born-Oppenheimer Molecular Dynamics Simulations. *Angew. Chem. Int. Ed.* **2014**, *53*, 3663-3666.
- (315) Polfer, N. C.; Paizs, B.; Snoek, L. C.; Compagnon, I.; Suhai, S.; Meijer, G.; Helden, G. v.; Oomens, J. Infrared Fingerprint Spectroscopy and Theoretical Studies of Potassium Ion Tagged Amino Acids and Peptides in the Gas Phase. *J. Am. Chem. Soc.* **2005**, *127*, 8571-8579.
- (316) Miyazaki, M.; Makara, K.; Ishiuchi, S.; Fujii, M. Gas-Phase Infrared Spectroscopy of Mono-peptides from 10 to 3 μm . *Chem. Lett.* **2011**, *40*, 1157-1158.

- (317) von Helden, G.; Compagnon, I.; Blom, M. N.; Frankowski, M.; Erlekam, U.; Oomens, J.; Brauer, B.; Gerber, R. B.; Meijer, G. Mid-IR Spectra of Different Conformers of Phenylalanine in the Gas Phase. *Phys. Chem. Chem. Phys.* **2008**, *10*, 1248-1256.
- (318) Cirtog, M.; Rijs, A. M.; Loquais, Y.; Brenner, V.; Tardivel, B.; Gloaguen, E.; Mons, M. Far/Mid-Infrared Signatures of Solvent Solute Interactions in a Microhydrated Model Peptide Chain. *J. Phys. Chem. Lett.* **2012**, *3*, 3307-3311.
- (319) Mahé, J.; Bakker, D. J.; Jaeqx, S.; Rijs, A. M.; Gaigeot, M.-P. Mapping Gas Phase Dipeptide Motions in the Far-Infrared and Terahertz Domain. *Phys. Chem. Chem. Phys.* **2017**, *19*, 13778-13787.
- (320) Mahé, J.; Jaeqx, S.; Rijs, A. M.; Gaigeot, M.-P. Can Far-IR Action Spectroscopy Combined with Bemd Simulations Be Conformation Selective? *Phys. Chem. Chem. Phys.* **2015**, *17*, 25905-25914.
- (321) Giordmaine, J. A.; Miller, R. C. Tunable Coherent Parametric Oscillation in LiNbO₃ at Optical Frequencies. *Phys. Rev. Lett.* **1965**, *14*, 973-976.
- (322) Eckardt, R. C.; Nabors, C. D.; Kozlovsky, W. J.; Byer, R. L. Optical Parametric Oscillator Frequency Tuning and Control. *Journal of the Optical Society of America B* **1991**, *8*, 646.
- (323) Huisken, F.; Kulcke, A.; Voelkel, D.; Laush, C.; Lisy, J. M. New Infrared Injection-Seeded Optical Parametric Oscillator with High Energy and Narrow Bandwidth Output. *Applied Physics Letters* **1993**, *62*, 805.
- (324) Bosenberg, W. R.; Guyer, D. R. Broadly Tunable, Single-Frequency Optical Parametric Frequency-Conversion System. *Journal of the Optical Society of America B* **1993**, *10*, 1716.
- (325) Miyazaki, M.; Saikawa, J.; Ishizuki, H.; Taira, T.; Fujii, M. Isomer Selective Infrared Spectroscopy of Supersonically Cooled Cis- and Trans-N-Phenylamides in the Region from the Amide Band to NH Stretching Vibration. *Phys. Chem. Chem. Phys.* **2009**, *11*, 6098-6106.
- (326) Häber, T.; Seefeld, K.; Engler, G.; Grimme, S.; Kleinermanns, K. Ir/Uv Spectra and Quantum Chemical Calculations of Trp-Ser: Stacking Interactions between Backbone and Indole Side-Chain. *Phys. Chem. Chem. Phys.* **2008**, *10*, 2844-2851.
- (327) Boyarkine, O. V. Cold Ion Spectroscopy for Structural Identifications of Biomolecules. *Int. Rev. Phys. Chem.* **2018**, *37*, 559-606.
- (328) Gloaguen, E.; Pagliarulo, F.; Brenner, V.; Chin, W.; Piuze, F.; Tardivel, B.; Mons, M. Intramolecular Recognition in a Jet-Cooled Short Peptide Chain: γ -Turn Helicity Probed by a Neighbouring Residue. *Phys. Chem. Chem. Phys.* **2007**, *9*, 4491-4497.
- (329) Schmitt, M.; Feng, K.; Boehm, M.; Kleinermanns, K. Low Frequency Backbone Vibrations of Individual Conformational Isomers: Tryptamine. *J. Chem. Phys.* **2006**, *125*.
- (330) Brenner, V.; Piuze, F.; Dimicoli, I.; Tardivel, B.; Mons, M. Spectroscopic Evidence for the Formation of Helical Structures in Gas-Phase Short Peptide Chains. *J. Phys. Chem. A* **2007**, *111*, 7347-7354.
- (331) Loquais, Y. Chaines Peptidiques Modèles En Détente Supersonique. *Ph.D. Thesis, University Paris-Sud* **2013**.
- (332) Gerlach, A.; Unterberg, C.; Fricke, H.; Gerhards, M. Structures of Ac-Trp-OMe and Its Dimer (Ac-Trp-OMe)₂ in the Gas Phase: Influence of a Polar Group in the Side-Chain. *Mol. Phys.* **2005**, *103*, 1521-1529.
- (333) Sohn, W. Y.; Brenner, V.; Gloaguen, E.; Mons, M. Local NH- π Interactions Involving Aromatic Residues of Proteins: Influence of Backbone Conformation and $\pi\pi^*$ Excitation on the π H-Bond Strength, as Revealed from Studies of Isolated Model Peptides. *Phys. Chem. Chem. Phys.* **2016**, *18*, 29969-29978.
- (334) Ishiuchi, S.; Yamada, K.; Oba, H.; Wako, H.; Fujii, M. Gas Phase Ultraviolet and Infrared Spectroscopy on a Partial Peptide of B(2)-Adrenoceptor SIVSF-NH₂ by a Laser Desorption Supersonic Jet Technique. *Phys. Chem. Chem. Phys.* **2016**, *18*, 23277-23284.
- (335) Stamm, A.; Maue, D.; Schaly, A.; Schlicher, S.; Bartl, J.; Kubik, S.; Gerhards, M. Structural Analyses of Isolated Cyclic Tetrapeptides with Varying Amino Acid Residues. *Phys. Chem. Chem. Phys.* **2017**, *19*, 10718-10726.
- (336) Otaki, H.; Yagi, K.; Ishiuchi, S.; Fujii, M.; Sugita, Y. Anharmonic Vibrational Analyses of Pentapeptide Conformations Explored with Enhanced Sampling Simulations. *J. Phys. Chem. B* **2016**, *120*, 10199-10213.
- (337) McDonald, D. Q.; Still, W. C. Amber* Torsional Parameters for the Peptide Backbone. *Tetrahedron Letters* **1992**, *33*, 7743-7746.
- (338) Case, D. A.; Cheatham, T. E.; Darden, T.; Gohlke, H.; Luo, R.; Merz, K. M.; Onufriev, A.; Simmerling, C.; Wang, B.; Woods, R. J. The Amber Biomolecular Simulation Programs. *J. Comput. Chem.* **2005**, *26*, 1668-1688.

- (339) Brooks, B. R.; Brooks, C. L.; Mackerell, A. D.; Nilsson, L.; Petrella, R. J.; Roux, B.; Won, Y.; Archontis, G.; Bartels, C.; Boresch, S.; Caflisch, A.; Caves, L.; Cui, Q.; Dinner, A. R.; Feig, M.; Fischer, S.; Gao, J.; Hodosek, M.; Im, W.; Kuczera, K. et al. Charmm: The Biomolecular Simulation Program. *J. Comput. Chem.* **2009**, *30*, 1545-1614.
- (340) Best, R. B.; Zhu, X.; Shim, J.; Lopes, P. E. M.; Mittal, J.; Feig, M.; MacKerell, A. D. Optimization of the Additive Charmm All-Atom Protein Force Field Targeting Improved Sampling of the Backbone ϕ , ψ and Side-Chain χ_1 and χ_2 Dihedral Angles. *J. Chem. Theo. Comp.* **2012**, *8*, 3257-3273.
- (341) Harder, E.; Damm, W.; Maple, J.; Wu, C. J.; Reboul, M.; Xiang, J. Y.; Wang, L. L.; Lupyan, D.; Dahlgren, M. K.; Knight, J. L.; Kaus, J. W.; Cerutti, D. S.; Krilov, G.; Jorgensen, W. L.; Abel, R.; Friesner, R. A. OPLS3: A Force Field Providing Broad Coverage of Drug-Like Small Molecules and Proteins. *J. Chem. Theo. Comp.* **2016**, *12*, 281-296.
- (342) Maple, J. R.; Hwang, M. J.; Jalkanen, K. J.; Stockfisch, T. P.; Hagler, A. T. Derivation of Class II Force Fields: V. Quantum Force Field for Amides, Peptides, and Related Compounds. *J. Comput. Chem.* **1998**, *19*, 430-458.
- (343) Halgren, T. A. MMFF VI. MMFF94s Option for Energy Minimization Studies. *J. Comput. Chem.* **1999**, *20*, 720-729.
- (344) Halgren, T. A. MMFF VII. Characterization of MMFF94, MMFF94s, and Other Widely Available Force Fields for Conformational Energies and for Intermolecular-Interaction Energies and Geometries. *J. Comput. Chem.* **1999**, *20*, 730-748.
- (345) Rezac, J.; Hobza, P. Advanced Corrections of Hydrogen Bonding and Dispersion for Semiempirical Quantum Mechanical Methods. *J. Chem. Theo. Comp.* **2012**, *8*, 141-151.
- (346) Holroyd, L. F.; van Mourik, T. Insufficient Description of Dispersion in B3LYP and Large Basis Set Superposition Errors in MP2 Calculations Can Hide Peptide Conformers. *Chem. Phys. Lett.* **2007**, *442*, 42-46.
- (347) van Mourik, T. Assessment of Density Functionals for Intramolecular Dispersion-Rich Interactions. *J. Chem. Theo. Comp.* **2008**, *4*, 1610-1619.
- (348) Becke, A. D. Density-Functional Thermochemistry. 3. The Role of Exact Exchange. *J. Chem. Phys.* **1993**, *98*, 5648-5652.
- (349) Becke, A. D. Density-Functional Thermochemistry .5. Systematic Optimization of Exchange-Correlation Functionals. *J. Chem. Phys.* **1997**, *107*, 8554-8560.
- (350) Grimme, S.; Antony, J.; Ehrlich, S.; Krieg, H. A Consistent and Accurate Ab Initio Parametrization of Density Functional Dispersion Correction (Dft-D) for the 94 Elements H-Pu. *J. Chem. Phys.* **2010**, *132*, 154104.
- (351) Grimme, S.; Ehrlich, S.; Goerigk, L. Effect of the Damping Function in Dispersion Corrected Density Functional Theory. *J. Comput. Chem.* **2011**, *32*, 1456-1465.
- (352) Chai, J. D.; Head-Gordon, M. Long-Range Corrected Hybrid Density Functionals with Damped Atom-Atom Dispersion Corrections. *Phys. Chem. Chem. Phys.* **2008**, *10*, 6615-6620.
- (353) Bouteiller, Y.; Pouilly, J. C.; Desfrancois, C.; Grégoire, G. Evaluation of MP2, DFT, AND DFT-D Methods for the Prediction of Infrared Spectra of Peptides. *J. Phys. Chem. A* **2009**, *113*, 6301-6307.
- (354) Bouteiller, Y.; Gillet, J.-C.; Grégoire, G.; Schermann, J. P. Transferable Specific Scaling Factors for Interpretation of Infrared Spectra of Biomolecules from Density Functional Theory. *J. Phys. Chem. A* **2008**, *112*, 11656-11660.
- (355) Habka, S.; Very, T.; Donon, J.; Vaquero-Vara, V.; Tardivel, B.; Charnay-Pouget, F.; Mons, M.; Aitken, D. J.; Brenner, V.; Gloaguen, E. Identification of Ion Pairs in Solution by IR Spectroscopy: Crucial Contributions of Gas Phase Data and Simulations. *Phys. Chem. Chem. Phys.* **2019**, *21*, 12798-12805.
- (356) Norris, L. S.; Ratner, M. A.; Roitberg, A. E.; Gerber, R. B. Moller-Plesset Perturbation Theory Applied to Vibrational Problems. *J. Chem. Phys.* **1996**, *105*, 11261-11267.
- (357) Yagi, K.; Otaki, H. Vibrational Quasi-Degenerate Perturbation Theory with Optimized Coordinates: Applications to Ethylene and trans-1,3-Butadiene. *J. Chem. Phys.* **2014**, *140*.
- (358) Barone, V.; Biczysko, M.; Bloino, J. Fully Anharmonic IR and Raman Spectra of Medium-Size Molecular Systems: Accuracy and Interpretation. *Phys. Chem. Chem. Phys.* **2014**, *16*, 1759-1787.
- (359) Panek, P. T.; Jacob, C. R. Efficient Calculation of Anharmonic Vibrational Spectra of Large Molecules with Localized Modes. *Chemphyschem* **2014**, *15*, 3365-3377.
- (360) Cheng, X. L.; Steele, R. P. Efficient Anharmonic Vibrational Spectroscopy for Large Molecules Using Local-Mode Coordinates. *J. Chem. Phys.* **2014**, *141*.
- (361) VandeVondele, J.; Krack, M.; Mohamed, F.; Parrinello, M.; Chassaing, T.; Hutter, J. Quickstep: Fast and Accurate Density Functional Calculations Using a Mixed Gaussian and Plane Waves Approach. *Computer Physics Communications* **2005**, *167*, 103-128.

- (362) Bakels, S.; Gageot, M.-P.; Rijs, A. M. Gas Phase Infrared Spectroscopy of Neutral Peptides: Insights from the Far-IR and THz Domain. *Chem. Rev.* **2020**, DOI: cr-2019-00547w.
- (363) Galimberti, D. R.; Bougueroua, S.; Mahé, J.; Tommasini, M.; Rijs, A. M.; Gageot, M. P. Conformational Assignment of Gas Phase Peptides and Their H-Bonded Complexes Using Far-IR/THz: IR-UV Ion Dip Experiment, DFT-MD Spectroscopy, and Graph Theory for Mode Assignment. *Faraday Discuss.* **2019**, *217*, 67-97.
- (364) Evans, D. A.; Wales, D. J.; Dian, B. C.; Zwier, T. S. The Dynamics of Conformational Isomerization in Flexible Biomolecules. II. Simulating Isomerizations in a Supersonic Free Jet with Master Equation Dynamics. *J. Chem. Phys.* **2004**, *120*, 148-157.
- (365) Pollet, R.; Brenner, V. Assessment of Time-Dependent Density Functional Theory for Predicting Excitation Energies of Bichromophoric Peptides: Case of Tryptophan-Phenylalanine. *Theoretical Chemistry Accounts* **2008**, *121*, 307-312.
- (366) Christiansen, O.; Koch, H.; Jorgensen, P. The 2nd-Order Approximate Coupled-Cluster Singles and Doubles Model CC2. *Chem. Phys. Lett.* **1995**, *243*, 409-418.
- (367) Ben Amor, N.; Hoyau, S.; Maynau, D.; Brenner, V. Low-Lying Excited States of Model Proteins: Performances of the CC2 Method Versus Multireference Methods. *J. Chem. Phys.* **2018**, *148*, 14.
- (368) Doslic, N. A.; Kovacevic, G.; Ljubic, I. Signature of the Conformational Preferences of Small Peptides: A Theoretical Investigation. *J. Phys. Chem. A* **2007**, *111*, 8650-8658.
- (369) Dupuy, M.-S.; Gloaguen, E.; Tardivel, B.; Mons, M.; Brenner, V. CC2 Benchmark for Models of Phenylalanine Protein Chains: O=O Transition Energies and IR Signatures of the $\pi\pi^*$ Excited State. *J. Chem. Theo. Comp.* **2020**, *16*, 601-611.
- (370) Féraud, G.; Broquier, M.; Dedonder, C.; Jouvet, C.; Grégoire, G.; Soorkia, S. Excited State Dynamics of Protonated Phenylalanine and Tyrosine: Photo-Induced Reactions Following Electronic Excitation. *J. Phys. Chem. A* **2015**, *119*, 5914-5924.
- (371) Reed, A. E.; Curtiss, L. A.; Weinhold, F. Intermolecular Interactions from a Natural Bond Orbital, Donor-Acceptor Viewpoint. *Chem. Rev.* **1988**, *88*, 899-926.
- (372) Brenner, V.; Gloaguen, E.; Mons, M. Ranking the Amide-Amide H-Bonding in Peptides: A Natural Bond Orbital Analysis of Electron Delocalization and the Corresponding NH Stretch Spectral Shift. *Phys. Chem. Chem. Phys.* **2019**, *21*, 24601-24619.
- (373) Johnson, E. R.; Keinan, S.; Mori-Sánchez, P.; Contreras-García, J.; Cohen, A. J.; Yang, W. Revealing Noncovalent Interactions. *J. Am. Chem. Soc.* **2010**, *132*, 6498-6506.
- (374) Bader, R. F. W. A Quantum-Theory of Molecular-Structure and Its Applications. *Chem. Rev.* **1991**, *91*, 893-928.
- (375) Chaudret, R.; de Courcy, B.; Contreras-García, J.; Gloaguen, E.; Zehnacker-Rentien, A.; Mons, M.; Piquemal, J.-P. Unraveling Non Covalent Interactions within Flexible Biomolecules: From Electron Density Topology to Gas Phase Spectroscopy. *Phys. Chem. Chem. Phys.* **2014**, *16*, 2285-2288.
- (376) Lomas, J. S. Steric Clashes, Doughnuts and Exploding Cigars: Some Comments on Non-Covalent Interactions. *Chemistry Select* **2019**, *4*, 4238-4243.
- (377) Gloaguen, E.; Loquais, Y.; Thomas, J. A.; Pratt, D. W.; Mons, M. Spontaneous Formation of Hydrophobic Domains in Isolated Peptides. *J. Phys. Chem. B* **2013**, *117*, 4945-4955.
- (378) Gonzalez, J.; Martinez, R.; Fernandez, J. A.; Millan, J. Conformational Landscape of Isolated Capped Amino Acids: On the Nature of Non-Covalent Interactions. *Eur. Phys. J. D* **2017**, *71*.
- (379) Joseph, J.; Jemmis, E. D. Red-, Blue-, or No-Shift in Hydrogen Bonds: A Unified Explanation. *J. Am. Chem. Soc.* **2007**, *129*, 4620-4632.
- (380) Abo-Riziq, A. G.; Grace, L.; Crews, B.; Callahan, M. P.; van Mourik, T.; de Vries, M. S. Conformational Structure of Tyrosine, Tyrosyl-Glycine, and Tyrosyl-Glycyl-Glycine by Double Resonance Spectroscopy. *J. Phys. Chem. A* **2011**, *115*, 6077-6087.
- (381) Shimozono, Y.; Yamada, K.; Ishiuchi, S.-I.; Tsukiyama, K.; Fujii, M. Revised Conformational Assignments and Conformational Evolution of Tyrosine by Laser Desorption Supersonic Jet Laser Spectroscopy. *Phys. Chem. Chem. Phys.* **2013**, *15*, 5163-5175.
- (382) Häber, T.; Seefeld, K.; Kleinermanns, K. Mid- and near-Infrared Spectra of Conformers of H-Pro-Trp-OH. *J. Phys. Chem. A* **2007**, *111*, 3038-3046.

- (383) Chin, W.; Mons, M.; Dognon, J.-P.; Mirasol, R.; Chass, G.; Dimicoli, I.; Piuze, F.; Butz, P.; Tardivel, B.; Compagnon, I.; von Helden, G.; Meijer, G. The Gas-Phase Dipeptide Analogue Acetyl-Phenylalanyl-Amide: A Model for the Study of Side Chain/Backbone Interactions in Proteins. *J. Phys. Chem. A* **2005**, *109*, 5281-5288.
- (384) Schwing, K.; Fricke, H.; Bartl, K.; Polkowska, J.; Schrader, T.; Gerhards, M. Isolated β -Turn Model Systems Investigated by Combined IR/UV Spectroscopy. *Chemphyschem* **2012**, *13*, 1576-1582.
- (385) Fricke, H.; Schäfer, G.; Schrader, T.; Gerhards, M. Secondary Structure Binding Motifs of the Jet Cooled Tetrapeptide Model Ac-Leu-Val-Tyr(Me)-NHMe. *Phys. Chem. Chem. Phys.* **2007**, *9*, 4592-4597.
- (386) Chin, W.; Piuze, F.; Dognon, J.-P.; Dimicoli, I.; Mons, M. Gas Phase Models of γ -Turns : Effects of Side-Chain/Backbone Interactions Investigated by IR/UV Spectroscopy and Quantum Chemistry. *J. Chem. Phys.* **2005**, *123*, 084301.
- (387) Chin, W.; Dognon, J. P.; Piuze, F.; Tardivel, B.; Dimicoli, I.; Mons, M. Intrinsic Folding of Small Peptide Chains: Spectroscopic Evidence for the Formation of β -Turns in the Gas Phase. *J. Am. Chem. Soc.* **2005**, *127*, 707-712.
- (388) Chin, W.; Dognon, J. P.; Piuze, F.; Dimicoli, I.; Mons, M. Secondary Structures of Val-Phe and Val-Tyr(Me) Peptide Chains in the Gas Phase: Effect of the Nature of the Protecting Groups. *Mol. Phys.* **2005**, *103*, 1579-1587.
- (389) Brenner, V.; Piuze, F.; Dimicoli, I.; Tardivel, B.; Mons, M. Chirality-Controlled Formation of β -Turn Secondary Structures in Short Peptide Chains: Gas-Phase Experiment Versus Quantum Chemistry. *Angew. Chem. Int. Ed.* **2007**, *46*, 2463-2466.
- (390) Goldsztejn, G.; Mundlapati, V.; Brenner, V.; Gloaguen, E.; Mons, M.; Cabezas, C.; León, I.; Alonso, J. L. Intrinsic Folding of the Cysteine Residue: Competition Between Compact and Extended Forms Mediated by the -SH Group, *Phys. Chem. Chem. Phys.*, submitted.
- (391) Schwing, K.; Reyheller, C.; Schaly, A.; Kubik, S.; Gerhards, M. Structural Analysis of an Isolated Cyclic Tetrapeptide and Its Monohydrate by Combined IR/UV Spectroscopy. *Chemphyschem* **2011**, *12*, 1981-1988.
- (392) Biswal, H. S.; Gloaguen, E.; Loquais, Y.; Tardivel, B.; Mons, M. Strength of NH...S Hydrogen Bonds in Methionine Residues Revealed by Gas-Phase IR/UV Spectroscopy. *J. Phys. Chem. Lett.* **2012**, *3*, 755-759.
- (393) Serrallach, A.; Meyer, R.; Gunthard, H. H. Methanol and Deuterated Species - Infrared Data, Valence Force-Field, Rotamers and Conformation. *J. Mol. Spec.* **1974**, *52*, 94-129.
- (394) Helden, G. v.; Compagnon, I.; Blom, M. N.; Frankowski, M.; Erlekam, U.; Oomens, J.; Brauer, B.; Gerber, R. B.; Meijer, G. Mid-IR Spectra of Different Conformers of Phenylalanine in the Gas Phase. *Phys. Chem. Chem. Phys.* **2008**, *10*, 1248-1256.
- (395) Chass, G. A.; Mirasol, R. S.; Setiadi, D. H.; Tang, T.-H.; Chin, W.; Mons, M.; Dimicoli, I.; Dognon, J.-P.; Viskolcz, B.; Lovas, S.; Penke, B.; Csizmadia, I. G. Characterization of the Conformational Probability of *N*-Acetyl-Phenylalanyl-NH₂ by RHF, DFT, and MP2 Computation and Aim Analyses, Confirmed by Jet-Cooled Infrared Data. *J. Phys. Chem. A* **2005**, *109*, 5289-5302.
- (396) Bakker, J. M.; Plützer, C.; Hünig, I.; Häber, T.; Compagnon, I.; Helden, G. v.; Meijer, G.; Kleinermanns, K. Folding Structures of Isolated Peptides as Revealed by Gas-Phase Mid-Infrared Spectroscopy. *Chemphyschem* **2005**, *6*, 120-128.
- (397) Fricke, H.; Gerlach, A.; Gerhards, M. Structure of a β -Sheet Model System in the Gas Phase: Analysis of the Fingerprint Region up to 10 μ m. *Phys. Chem. Chem. Phys.* **2006**, *8*, 1660-1662.
- (398) Unterberg, C.; Gerlach, A.; Schrader, T.; Gerhards, M. Structure of the Protected Dipeptide Ac-Val-Phe-OMe in the Gas Phase: Towards a β -Sheet Model System. *J. Chem. Phys.* **2003**, *118*, 8296-8300.
- (399) Buchanan, E. G.; James, W. H.; Choi, S. H.; Guo, L.; Gellman, S. H.; Müller, C. W.; Zwier, T. S. Single-Conformation Infrared Spectra of Model Peptides in the Amide I and Amide II Regions: Experiment-Based Determination of Local Mode Frequencies and Inter-Mode Coupling. *J. Chem. Phys.* **2012**, *137*, 094301.
- (400) Stanca-Kaposta, E. C.; Çarçabal, P.; Cocinero, E. J.; Hurtado, P.; Simons, J. P. Carbohydrate-Aromatic Interactions: Vibrational Spectroscopy and Structural Assignment of Isolated Monosaccharide Complexes with *p*-Hydroxy Toluene and *N*-Acetyl L-Tyrosine Methylamide. *J. Phys. Chem. B* **2013**, *117*, 8135-8142.
- (401) Gerhards, M. In *Principles of Mass Spectrometry Applied to Biomolecules*; Laskin, J.; Lifshitz, C., Eds.; Wiley-Interscience: Hoboken, N.J., 2006.
- (402) Vass, E.; Hollósi, M.; Besson, F.; Buchet, R. Vibrational Spectroscopic Detection of β - and γ -Turns in Synthetic and Natural Peptides and Proteins. *Chem. Rev.* **2003**, *103*, 1917 and ref. therein.
- (403) Biswal, H. S.; Wategaonkar, S. Nature of the N-H...S Hydrogen Bond. *J. Phys. Chem. A* **2009**, *113*, 12763-12773.

- (404) Trachsel, M. A.; Ottiger, P.; Frey, H.-M.; Pfaffen, C.; Bihlmeier, A.; Klopfer, W.; Leutwyler, S. Modeling the Histidine-Phenylalanine Interaction: The NH $\cdots\pi$ Hydrogen Bond of Imidazole-Benzene. *J. Chem. Phys. B* **2015**, *119*, 7778–7790.
- (405) Stearns, J. A.; Boyarkin, O. V.; Rizzo, T. R. Spectroscopic Signatures of Gas-Phase Helices: Ac-Phe-(Ala)₅-Lys-H⁺ and Ac-Phe-(Ala)₁₀-Lys-H⁺. *J. Am. Chem. Soc.* **2007**, *129*, 13820–13821.
- (406) Stearns, J. A.; Seaiby, C.; Boyarkin, O. V.; Rizzo, T. R. Spectroscopy and Conformational Preferences of Gas-Phase Helices. *Phys. Chem. Chem. Phys.* **2009**, *11*, 125–132.
- (407) Xie, Y. M.; Schaefer, H. F.; Silaghi-Dumitrescu, R.; Peng, B.; Li, Q. S.; Stearns, J. A.; Rizzo, T. R. Conformational Preferences of Gas-Phase Helices: Experiment and Theory Struggle to Agree: The Seven-Residue Peptide Ac-Phe-(Ala)₅-Lys-H⁺. *Chem. Eur. J.* **2012**, *18*, 12941–12944.
- (408) Zabuga, A. V.; Rizzo, T. R. Capping Motif for Peptide Helix Formation. *J. Phys. Chem. Lett.* **2015**, *6*, 1504–1508.
- (409) Moore, W. M.; A., S. C. Peptide Hydroxamic Acids Inhibit Skin Collagenase. *Biochemical and Biophysical Research Communications* **1986**, *136*, 390–395.
- (410) Moore, W. M.; A., S. C. Purification of Human Collagenases with a Hydroxamic Acid Affinity Column. *Biochemistry* **1986**, *25*, 5189–5195.
- (411) Abo-Riziq, A. G.; Bushnell, J. E.; Crews, B.; Callahan, M.; Grace, L.; de Vries, M. S. Gas Phase Spectroscopy of the Pentapeptide FDASV. *Chem. Phys. Lett.* **2006**, *431*, 227–230.
- (412) Toth, G.; Watts, C. R.; Murphy, R. F.; Lovas, S. Significance of Aromatic-Backbone Amide Interactions in Protein Structure. *Proteins-Structure Function and Bioinformatics* **2001**, *43*, 373–381.
- (413) Cabezas, C.; Varela, M.; Pena, I.; Mata, S.; Lopez, J. C.; Alonso, J. L. The Conformational Locking of Asparagine. *Chem. Commun.* **2012**, *48*, 5934–5936.
- (414) Blanco, S.; Lesarri, A.; López, J. C.; Alonso, J. L. The Gas-Phase Structure of Alanine. *J. Am. Chem. Soc.* **2004**, *126*, 11675–11683.
- (415) Pace, C. N.; Scholtz, J. M.; Grimsley, G. R. Forces Stabilizing Proteins. *FEBS Lett.* **2014**, *588*, 2177–2184.
- (416) Dill, K. A.; MacCallum, J. L. The Protein-Folding Problem, 50 Years On. *Science* **2012**, *338*, 1042–1046.
- (417) Donohue, J. Hydrogen Bonded Helical Configurations of the Polypeptide Chain *PNAS* **1953**, *39*, 470–478.
- (418) Eisenberg, D. The Discovery of the α -Helix and β -Sheet, the Principal Structural Features of Proteins. *PNAS* **2003**, *100*, 11207–11210.
- (419) Bolen, D. W.; Rose, G. D. Structure and Energetics of the Hydrogen-Bonded Backbone in Protein Folding. *Annual Review of Biochemistry* **2008**, *77*, 339–362.
- (420) Rose, G. D.; Fleming, P. J.; Banavar, J. R.; Maritan, A. A Backbone-Based Theory of Protein Folding. *PNAS* **2006**, *103*, 16623–16633.
- (421) Shubert, V. A.; Baquero, E. E.; Clarkson, J. R.; James, W. H.; Turk, J. A.; Hare, A. A.; Worrel, K.; Lipton, M. A.; Schofield, D. P.; Jordan, K. D.; Zwier, T. S. Entropy-Driven Population Distributions in a Prototypical Molecule with Two Flexible Side Chains: O-(2-Acetamidoethyl)-N-Acetyltyramine. *J. Chem. Phys.* **2007**, *127*, 234315.
- (422) LeGreve, T. A.; Clarkson, J. R.; Zwier, T. S. Experimental Determination of Conformational Isomerization Energy Thresholds in Serotonin. *J. Phys. Chem. A* **2008**, *112*, 3911–3920.
- (423) Vaden, T. D.; Gowers, S. A. N.; Snoek, L. C. Observation of β -Sheet Aggregation in a Gas-Phase Tau-Peptide Dimer. *J. Am. Chem. Soc.* **2009**, *131*, 2472–2474.
- (424) Kumar, S.; Mishra, K. K.; Singh, S. K.; Borish, K.; Dey, S.; Sarkar, B.; Das, A. Observation of a Weak Intra-Residue C5 Hydrogen-Bond in a Dipeptide Containing Gly-Pro Sequence. *J. Chem. Phys.* **2019**, *151*, 9.
- (425) Schafer, L.; Sellers, H. L.; Lovas, F. J.; Suenram, R. D. Theory Versus Experiment - the Case of Glycine. *J. Am. Chem. Soc.* **1980**, *102*, 6566–6568.
- (426) Godfrey, P. D.; Brown, R. D. Shape of Glycine. *J. Am. Chem. Soc.* **1995**, *117*, 2019–2023.
- (427) McGlone, S. J.; Elmes, P. S.; Brown, R. D.; Godfrey, P. D. Molecular Structure of a Conformer of Glycine by Microwave Spectroscopy. *J. Mol. Struct.* **1999**, *485*, 225–238.
- (428) Godfrey, P. D.; Firth, S.; Hatherley, L. D.; Brown, R. D.; Pierlot, A. P. Millimeter-Wave Spectroscopy of Biomolecules - Alanine. *J. Am. Chem. Soc.* **1993**, *115*, 9687–9691.

- (429) Pérez, C.; Mata, S.; Blanco, S.; López, J. C.; Alonso, J. L. Jet-Cooled Rotational Spectrum of Laser-Abated Phenylalanine. *J. Phys. Chem. A* **2011**, *115*, 9653-9657.
- (430) Toroz, D.; van Mourik, T. The Structure of the Gas-Phase Tyrosine-Glycine Dipeptide. *Mol. Phys.* **2006**, *104*, 559-570.
- (431) Gellman, S. H. Foldamers: A Manifesto. *Acc. Chem. Res.* **1998**, *31*, 173-180.
- (432) Horne, W. S.; Gellman, S. H. Foldamers with Heterogeneous Backbones. *Acc. Chem. Res.* **2008**, *41*, 1399-1408.
- (433) Lee, K. T.; Sung, J.; Lee, K. J.; Kim, S. K.; Park, Y. D. Conformation-Dependent Ionization of L-Phenylalanine: Structures and Energetics of Cationic Conformers. *Chem. Phys. Lett.* **2003**, *368*, 262-268.
- (434) Huang, Z.; Yu, W.; Lin, Z. Exploration of the Full Conformational Landscapes of Gaseous Aromatic Amino Acid Phenylalanine: An Ab Initio Study. *J. Mol. Struct.* **2006**, *758*, 195-202.
- (435) James, W. H.; Baquero, E. E.; Choi, S. H.; Gellman, S. H.; Zwier, T. S. Laser Spectroscopy of Conformationally Constrained α/β -Peptides: Ac-ACPC-Phe-NHMe and Ac-Phe-ACPC-NHMe. *J. Chem. Phys. A* **2010**, *114*, 1581-1591.
- (436) Alauddin, M.; Gloaguen, E.; Brenner, V.; Tardivel, B.; Mons, M.; Zehnacker-Rentien, A.; Declerck, V.; Aitken, D. J. Intrinsic Folding Proclivities in Cyclic β -Peptide Building Blocks: Configuration and Heteroatom Effects Analyzed by Conformer-Selective Spectroscopy and Quantum Chemistry. *Chem. Eur. J.* **2015**, *21*, 16479-16493.
- (437) Blodgett, K. N.; Zhu, X.; Walsh, P. S.; Sun, D.; Lee, J.; Choi, S. H.; Zwier, T. S. Conformer-Specific and Diastereomer-Specific Spectroscopy of $\alpha\beta\alpha$ Synthetic Foldamers: Ac-Ala- β ACHC-Ala-NHBn. *J. Chem. Phys. A* **2018**, *122*, 3697-3710.
- (438) James, W. H.; Buchanan, E. G.; Müller, C. W.; Dean, J. C.; Kosenkov, D.; Slipchenko, L. V.; Guo, L.; Reidenbach, A. G.; Gellman, S. H.; Zwier, T. S. Evolution of Amide Stacking in Larger γ -Peptides: Triamide H-Bonded Cycles. *J. Chem. Phys. A* **2011**, *115*, 13783-13798.
- (439) James, W. H.; Buchanan, E. G.; Guo, L.; Gellman, S. H.; Zwier, T. S. Competition between Amide Stacking and Intramolecular H Bonds in γ -Peptide Derivatives: Controlling Nearest-Neighbor Preferences. *J. Chem. Phys. A* **2011**, *115*, 11960-11970.
- (440) Buchanan, E. G.; James III, W. H.; Gutberlet, A.; Dean, J. C.; Guo, L.; Gellman, S. H.; Zwier, T. S. Single-Conformation Spectroscopy and Population Analysis of Model γ -Peptides: New Tests of Amide Stacking. *Faraday Discuss.* **2011**, *150*, 209-226.
- (441) Walsh, P. S.; Kusaka, R.; Buchanan, E. G.; James, W. H.; Fisher, B. F.; Gellman, S. H.; Zwier, T. S. Cyclic Constraints on Conformational Flexibility in γ -Peptides: Conformation Specific IR and UV Spectroscopy. *J. Phys. Chem. A* **2013**, *117*, 12350-12362.
- (442) Kusaka, R.; Zhang, D.; Walsh, P. S.; Gord, J. R.; Fisher, B. F.; Gellman, S. H.; Zwier, T. S. Role of Ring-Constrained Γ -Amino Acid Residues in α/γ -Peptide Folding: Single-Conformation UV and IR Spectroscopy. *J. Phys. Chem. A* **2013**, *117*, 10847-10862.
- (443) Gord, J. R.; Walsh, P. S.; Fisher, B. F.; Gellman, S. H.; Zwier, T. S. Mimicking the First Turn of an α -Helix with an Unnatural Backbone: Conformation-Specific IR and UV Spectroscopy of Cyclically Constrained β/γ -Peptides. *J. Phys. Chem. B* **2014**, *118*, 8246-8256.
- (444) Tan, N.-H.; Zhou, J. Plant Cyclopeptides. *Chem. Rev.* **2006**, *106*, 840-895.
- (445) Pomilio, A.; Battista, M.; Vitale, A. Naturally-Occurring Cyclopeptides: Structures and Bioactivity. *Curr. Org. Chem.* **2006**, *10*, 2075-2121.
- (446) Vetter, J. Toxins of Amanita Phalloides. *Toxicon* **1998**, *36*, 13-24.
- (447) Stoop, R. Neuromodulation by Oxytocin and Vasopressin. *Neuron* **2012**, *76*, 142-159.
- (448) Braun, V. Protein Structure: Pumping Iron through Cell Membranes. *Science* **1998**, *282*, 2202-2203.
- (449) Haubner, R.; Finsinger, D.; Kessler, H. Stereoisomeric Peptide Libraries and Peptidomimetics for Designing Selective Inhibitors of the $\alpha\beta3$ Integrin for a New Cancer Therapy. *Angew. Chem. Int. Ed.* **1997**, *36*, 1374-1389.
- (450) Kubik, S. Artificial Receptors for Chemical Sensors: Cyclopeptide Derived Synthetic Receptors. Mirsky, V. M.; Yatsimirsky, A., Eds.; Wiley-VCH: Weinheim, Germany, 2011.
- (451) Ranganathan, D. Designer Hybrid Cyclopeptides for Membrane Ion Transport and Tubular Structures. *Acc. Chem. Res.* **2001**, *34*, 919-930.
- (452) Gibson, S. E.; Lecci, C. Amino Acid Derived Macrocycles - an Area Driven by Synthesis or Application? *Angew. Chem. Int. Ed.* **2006**, *45*, 1364-1377.

- (453) Safiulina, D.; Veksler, V.; Zharkovsky, A.; Kaasik, A. Loss of Mitochondrial Membrane Potential Is Associated with Increase in Mitochondrial Volume: Physiological Role in Neurons. *J. Cell. Physiol.* **2006**, *206*, 347–353.
- (454) Rose, L.; Jenkins, A. T. A. The Effect of the Ionophore Valinomycin on Biomimetic Solid Supported Lipid DPPE/EPC Membranes. *Bioelectrochemistry* **2007**, *70*, 387–393.
- (455) Pettit, G. R.; Kamano, Y.; Dufresne, C.; Cerny, R. L.; Herald, C. L.; Schmidt, J. M. Isolation and Structure of the Cytostatic Linear Depsipeptide Dolastatin. *The Journal of Organic Chemistry* **1989**, *54*, 6005–6006.
- (456) Gallo, E. A.; Gellman, S. H. Hydrogen-Bond-Mediated Folding in Depsipeptide Models of β -Turns and α -Helical Turns. *J. Am. Chem. Soc.* **1993**, *115*, 9774–9788.
- (457) Kang, Y. K.; Byun, B. J. Conformational Preferences and Cis-Trans Isomerization of L-Lactic Acid Residue. *J. Chem. Phys. B* **2008**, *112*, 9126–9134.
- (458) Zhang, J.; King, M.; Suggs, L.; Ren, P. Molecular Modeling of Conformational Properties of Oligodepsipeptides. *Biomacromolecules* **2007**, *8*, 3015–3024.
- (459) Boussard, G.; Marraud, M.; Néel, J. Experimental and Theoretical Investigations on the Folding Modes of Depsipeptide Molecules. *Biopolymers* **1977**, *16*, 1033–1052.
- (460) Abo-Riziq, A. G.; Bushnell, J. E.; Crews, B.; Callahan, M. P.; Grace, L.; De Vries, M. S. Discrimination between Diastereoisomeric Dipeptides by IR-UV Double Resonance Spectroscopy and Ab Initio Calculations. *International Journal of Quantum Chemistry* **2005**, *105*, 437–445.
- (461) Petkova, A. T.; Leapman, R. D.; Guo, Z. H.; Yau, W. M.; Mattson, M. P.; Tycko, R. Self-Propagating, Molecular-Level Polymorphism in Alzheimer's β -Amyloid Fibrils. *Science* **2005**, *307*, 262–265.
- (462) Rijs, A. M.; Kabeláč, M.; Abo-Riziq, A.; Hobza, P.; de Vries, M. S. Isolated Gramicidin Peptides Probed by Ir Spectroscopy. *ChemPhysChem* **2011**, *12*, 1816–1821.
- (463) Prenner, E. J.; Lewis, R.; Neuman, K. C.; Gruner, S. M.; Kondejewski, L. H.; Hodges, R. S.; McElhaney, R. N. Nonlamellar Phases Induced by the Interaction of Gramicidin S with Lipid Bilayers. A Possible Relationship to Membrane-Disrupting Activity. *Biochemistry* **1997**, *36*, 7906–7916.
- (464) Sawyer, D. B.; Williams, L. P.; Whaley, W. L.; Koeppe, R. E.; Andersen, O. S. Gramicidin-A, Gramicidin-B, and Gramicidin-C Form Structurally Equivalent Ion Channels. *Biophysical Journal* **1990**, *58*, 1207–1212.
- (465) Kupser, P.; Pagel, K.; Oomens, J.; Polfer, N.; Kokschi, B.; Meijer, G.; Helden, G. v. Amide-I and -II Vibrations of the Cyclic β -Sheet Model Peptide Gramicidin S in the Gas Phase. *J. Am. Chem. Soc.* **2010**, *132*, 2085–2093.
- (466) Nagornova, N. S.; Rizzo, T. R.; Boyarkin, O. V. Highly Resolved Spectra of Gas-Phase Gramicidin S: A Benchmark for Peptide Structure Calculations. *J. Am. Chem. Soc.* **2010**, *132*, 4040–4041.
- (467) Nagornova, N. S.; Guglielmi, M.; Doemer, M.; Tavernelli, I.; Rothlisberger, U.; Rizzo, T. R.; Boyarkin, O. V. Cold-Ion Spectroscopy Reveals the Intrinsic Structure of a Decapeptide. *Angew. Chem. Int. Ed.* **2011**, *50*, 5383–5386.
- (468) Roy, T. K.; Kopysov, V.; Nagornova, N. S.; Rizzo, T. R.; Boyarkin, O. V.; Gerber, R. B. Conformational Structures of a Decapeptide Validated by First Principles Calculations and Cold Ion Spectroscopy. *ChemPhysChem* **2015**, *16*, 1374–1378.
- (469) Doemer, M.; Guglielmi, M.; Athri, P.; Nagornova, N. S.; Rizzo, T. R.; Boyarkin, O. V.; Tavernelli, I.; Rothlisberger, U. Assessing the Performance of Computational Methods for the Prediction of the Ground State Structure of a Cyclic Decapeptide. *International Journal of Quantum Chemistry* **2013**, *113*, 808–814.
- (470) Schoenenberger, G. A.; Maier, P. F.; Tobler, H. J.; Monnier, M. A Naturally Occurring Delta-EEG Enhancing Nonapeptide in Rabbits. *Pflügers Archiv European Journal of Physiology* **1977**, *369*, 99–109.
- (471) Kovalzon, V. M.; Strekalova, T. V. Delta Sleep-Inducing Peptide (DSIP): A Still Unresolved Riddle. *J. Neurochem.* **2006**, *97*, 303–309.
- (472) Oh, H.-B.; Lin, C.; Hwang, H. Y.; Zhai, H.; Breuker, K.; Zabrouskov, V.; Carpenter, B. K.; McLafferty, F. W. Infrared Photodissociation Spectroscopy of Electro sprayed Ions in a Fourier Transform Mass Spectrometer. *J. Am. Chem. Soc.* **2005**, *127*, 4076–4083.
- (473) Wu, R.; McMahon, T. B. Infrared Multiple Photon Dissociation Spectra of Proline and Glycine Proton-Bound Homodimers. Evidence for Zwitterionic Structure. *J. Am. Chem. Soc.* **2007**, *129*, 4864–4865.
- (474) Rajabi, K.; Fridgen, T. D. Structures of Aliphatic Amino Acid Proton-Bound Dimers by Infrared Multiple Photon Dissociation Spectroscopy in the 700–2,000 cm^{-1} Region. *J. Phys. Chem. A* **2008**, *112*, 23–30.

- (475) Steill, J. D.; Szczepanski, J.; Oomens, J.; Eyler, J. R.; Brajter-Toth, A. Structural Characterization by Infrared Multiple Photon Dissociation Spectroscopy of Protonated Gas-Phase Ions Obtained by Electrospray Ionization of Cysteine and Dopamine. *Anal. Bioanal. Chem.* **2011**, *399*, 2463–2473.
- (476) Wu, R.; Marta, R. A.; Martens, J. K.; Eldridge, K. R.; McMahon, T. B. Experimental and Theoretical Investigation of the Proton-Bound Dimer of Lysine. *J. Am. Soc. Mass. Spectrom.* **2011**, *22*, 1651–1659.
- (477) Hudgins, R. R.; Jarrold, M. F. Helix Formation in Unsolvated Alanine-Based Peptides: Helical Monomers and Helical Dimers. *J. Am. Chem. Soc.* **1999**, *121*, 3494–3501.
- (478) Kaleta, D. T.; Jarrold, M. F. Noncovalent Interactions between Unsolvated Peptides. *J. Chem. Phys. A* **2002**, *106*, 9655–9664.
- (479) Kaleta, D. T.; Jarrold, M. F. Noncovalent Interactions between Unsolvated Peptides: Dissociation of Helical and Globular Peptide Complexes. *J. Chem. Phys. B* **2003**, *107*, 14529–14536.
- (480) Kohtani, M.; Jones, T. C.; Schneider, J. E.; Jarrold, M. F. Extreme Stability of an Unsolvated α -Helix. *J. Am. Chem. Soc.* **2004**, *126*, 7420–7421.
- (481) Dugourd, P.; Antoine, R.; Breaux, G.; Broyer, M.; Jarrold, M. F. Entropic Stabilization of Isolated β -Sheets. *J. Am. Chem. Soc.* **2005**, *127*, 4675–4679.
- (482) Dougherty, D. A. Cation- π Interactions in Chemistry and Biology: A New View of Benzene, Phe, Tyr, and Trp. *Science* **1996**, *271*, 163–168.
- (483) Vogel, H. J. Calmodulin: A Versatile Calcium Mediator Protein. *Biochemistry and Cell Biology* **1994**, *72*, 357–376.
- (484) Svensson, B.; Etchebest, C.; Tuffery, P.; van Kan, P.; Smith, J.; Styring, S. A Model for the Photosystem II Reaction Center Core Including the Structure of the Primary Donor P680. *Biochemistry* **1996**, *35*, 14486–14502.
- (485) Rodgers, M. T.; Armentrout, P. B. A Thermodynamic "Vocabulary" for Metal Ion Interactions in Biological Systems. *Acc. Chem. Res.* **2004**, *37*, 989–998.
- (486) Armentrout, P. B.; Yang, B.; Rodgers, M. T. Metal Cation Dependence of Interactions with Amino Acids: Bond Energies of Rb^+ and Cs^+ to Met, Phe, Tyr, and Trp. *J. Chem. Phys. B* **2013**, *117*, 3771–3781.
- (487) Liu, H.; Håkansson, K. Divalent Metal Ion-Peptide Interactions Probed by Electron Capture Dissociation of Trications. *J. Am. Soc. Mass. Spectrom.* **2006**, *17*, 1731–1741.
- (488) Fung, Y. M. E.; Liu, H.; Chan, T.-W. D. Electron Capture Dissociation of Peptides Metalated with Alkaline-Earth Metal Ions. *J. Am. Soc. Mass. Spectrom.* **2006**, *17*, 757–771.
- (489) Turecek, F.; Jones, J. W.; Holm, A. I. S.; Panja, S.; Nielsen, S. B.; Hvelplund, P. Transition Metals as Electron Traps. I. Structures, Energetics, Electron Capture, and Electron-Transfer-Induced Dissociations of Ternary Copper-Peptide Complexes in the Gas Phase. *J. Mass. Spectrom.* **2009**, *44*, 707–724.
- (490) Bush, M. F.; Oomens, J.; Saykally, R. J.; Williams, E. R. Effects of Alkaline Earth Metal Ion Complexation on Amino Acid Zwitterion Stability: Results from Infrared Action Spectroscopy. *J. Am. Chem. Soc.* **2008**, *130*, 6463–6471.
- (491) Atkins, C. G.; Rajabi, K.; Gillis, E. A. L.; Fridgen, T. D. Infrared Multiple Photon Dissociation Spectra of Proton- and Sodium Ion-Bound Glycine Dimers in the N-H and O-H Stretching Region. *J. Phys. Chem. A* **2008**, *112*, 10220–10225.
- (492) Dunbar, R. C.; Steill, J. D.; Polfer, N. C.; Oomens, J. Peptide Length, Steric Effects, and Ion Solvation Govern Zwitterion Stabilization in Barium-Chelated Di- and Tripeptides. *J. Chem. Phys. B* **2009**, *113*, 10552–10554.
- (493) Polfer, N. C.; Oomens, J.; Moore, D. T.; Helden, G. v.; Meijer, G.; Dunbar, R. C. Infrared Spectroscopy of Phenylalanine Ag(I) and Zn(II) Complexes in the Gas Phase. *J. Am. Chem. Soc.* **2006**, *128*, 517–525.
- (494) Dunbar, R. C.; Steill, J. D.; Oomens, J. Encapsulation of Metal Cations by the PhePhe Ligand: A Cation- π Ion Cage. *J. Am. Chem. Soc.* **2011**, *133*, 9376–9386.
- (495) Bellina, B.; Compagnon, I.; MacAleese, L.; Chirot, F.; Lemoine, J.; Maître, P.; Broyer, M.; Antoine, R.; Kulesza, A.; Mitrić, R.; Bonačić-Koutecký, V.; Dugourd, P. Binding Motifs of Silver in Prion Octarepeat Model Peptides: A Joint Ion Mobility, IR and UV Spectroscopies, and Theoretical Approach. *Phys. Chem. Chem. Phys.* **2012**, *14*, 11433–11440.
- (496) Otsuka, R.; Hirata, K.; Sasaki, Y.; Lisy, J. M.; Ishiuchi, S.; Fujii, M. Alkali and Alkaline Earth Metal Ions Complexes with a Partial Peptide of the Selectivity Filter in K^+ Channels Studied by a Cold Ion Trap Infrared Spectroscopy. *Chemphyschem* **2020**, *21*, 712–724.
- (497) Massaouti, M.; Velegrakis, M. Gas-Phase Cu^+ - and Ag^+ -Glycine Complexes Produced with a New Source. *Int. J. Mass. Spectrom.* **2003**, *225*, 89–94.

- (498) Marksteiner, M.; Haslinger, P.; Ulbricht, H.; Sclafani, M.; Oberhofer, H.; Dellago, C.; Arndt, M. Gas-Phase Formation of Large Neutral Alkaline-Earth Metal Tryptophan Complexes. *J. Am. Soc. Mass. Spectrom.* **2008**, *19*, 1021–1026.
- (499) Marksteiner, M.; Haslinger, P.; Sclafani, M.; Ulbricht, H.; Arndt, M. UV and VUV Ionization of Organic Molecules, Clusters, and Complexes. *J. Phys. Chem. A* **2009**, *113*, 9952–9957.
- (500) Miller, D. J.; Lisy, J. M. Modeling Competitive Interactions in Proteins: Vibrational Spectroscopy of $M^+(N\text{-Methylacetamide})_1(\text{H}_2\text{O})_n$, $n=0\text{-}3$, $M=\text{Na}$ and K , in the $3\ \mu\text{m}$ Region. *J. Phys. Chem. A* **2007**, *111*, 12409–12416.
- (501) Bialach, P. M.; Martin, T. C.; Gerhards, M. IR and IR + UV Spectroscopy of Isolated $[\text{Al-AcPheOme}]_n^+$ Cluster Cations ($n = 1\text{-}3$). *Phys. Chem. Chem. Phys.* **2012**, *14*, 8185–8191.
- (502) Müller-Schiffmann, A.; März-Berberich, J.; Andreyeva, A.; Rönicke, R.; Bartnik, D.; Brener, O.; Kutzsche, J.; Horn, A. H. C.; Hellmert, M.; Polkowska, J.; Gottmann, K.; Reymann, K. G.; Funke, S. A.; Nagel-Steger, L.; Moriscot, C.; Schoehn, G.; Sticht, H.; Willbold, D.; Schrader, T.; Korth, C. Combining Independent Drug Classes into Superior, Synergistically Acting Hybrid Molecules. *Angew. Chem. Int. Ed.* **2010**, *49*, 8743–8746.
- (503) Hochdörffer, K.; März-Berberich, J.; Nagel-Steger, L.; Epple, M.; Meyer-Zaika, W.; Horn, A. H. C.; Sticht, H.; Sinha, S.; Bitan, G.; Schrader, T. Rational Design of β -Sheet Ligands against A β 42 -Induced Toxicity. *J. Am. Chem. Soc.* **2011**, *133*, 4348–4358.
- (504) Sinha, S.; Lopes, D. H. J.; Du, Z.; Pang, E. S.; Shanmugam, A.; Lomakin, A.; Talbiersky, P.; Tennstaedt, A.; McDaniel, K.; Bakshi, R.; Kuo, P.-Y.; Ehrmann, M.; Benedek, G. B.; Loo, J. A.; Klärner, F.-G.; Schrader, T.; Wang, C.; Bitan, G. Lysine-Specific Molecular Tweezers Are Broad-Spectrum Inhibitors of Assembly and Toxicity of Amyloid Proteins. *J. Am. Chem. Soc.* **2011**, *133*, 16958–16969.
- (505) Attar, A.; Ripoli, C.; Riccardi, E.; Maiti, P.; Li Puma, D. D.; Liu, T.; Hayes, J.; Jones, M. R.; Lichti-Kaiser, K.; Yang, F.; Gale, G. D.; Tseng, C.-h.; Tan, M.; Xie, C.-W.; Straudinger, J. L.; Klarner, F.-G.; Schrader, T.; Frautschy, S. A.; Grassi, C.; Bitan, G. Protection of Primary Neurons and Mouse Brain from Alzheimer's Pathology by Molecular Tweezers. *Brain* **2012**, *135*, 3735–3748.
- (506) Unterberg, C.; Gerlach, A.; Schrader, T.; Gerhards, M. Clusters of a Protected Amino Acid with Pyrazole Derivatives: β -Sheet Model Systems in the Gas Phase. *Eur. Phys. J. D* **2002**, *20*, 543-550.
- (507) Screen, J.; Stanca-Kaposta, E. C.; Gamblin, D. P.; Liu, B.; Macleod, N. A.; Snoek, L. C.; Davis, B. G.; Simons, J. P. IR-Spectral Signatures of Aromatic-Sugar Complexes: Probing Carbohydrate-Protein Interactions. *Angew. Chem. Int. Ed.* **2007**, *46*, 3644–3648.
- (508) Stanca-Kaposta, E. C.; Gamblin, D. P.; Screen, J.; Liu, B.; Snoek, L. C.; Davis, B. G.; Simons, J. P. Carbohydrate Molecular Recognition: A Spectroscopic Investigation of Carbohydrate-Aromatic Interactions. *Phys. Chem. Chem. Phys.* **2007**, *9*, 4444-4451.
- (509) Wang, C. W.; Ying, F. M.; Wu, W.; Mo, Y. R. Sensing or No Sensing: Can the Anomeric Effect Be Probed by a Sensing Molecule? *J. Am. Chem. Soc.* **2011**, *133*, 13731-13736.
- (510) Crews, B. O.; Abo-Riziq, A.; Pluhackova, K.; Thompson, P.; Hill, G.; Hobza, P.; de Vries, M. S. Guanine-Aspartic Acid Interactions Probed with IR-UV Resonance Spectroscopy. *Phys. Chem. Chem. Phys.* **2010**, *12*, 3597-3605.
- (511) Seefeld, K.; Brause, R.; Haber, T.; Kleinermanns, K. Imino Tautomers of Gas-Phase Guanine from Mid-Infrared Laser Spectroscopy. *J. Phys. Chem. A* **2007**, *111*, 6217-6221.
- (512) Marian, C. M. The Guanine Tautomer Puzzle: Quantum Chemical Investigation of Ground and Excited States. *J. Phys. Chem. A* **2007**, *111*, 1545–1553.
- (513) Nir, E.; Janzen, C.; Imhof, P.; Kleinermanns, K.; de Vries, M. S. Guanine Tautomerism Revealed by UV-Uv and IR-UV Hole Burning Spectroscopy. *J. Chem. Phys.* **2001**, *115*, 4604-4611.
- (514) Mons, M.; Dimicoli, I.; Piuze, F.; Tardivel, B.; Elhanine, M. Tautomerism of the DNA Base Guanine and Its Methylated Derivatives as Studied by Gas-Phase Infrared and Ultraviolet Spectroscopy. *J. Phys. Chem. A* **2002**, *106*, 5088-5094.
- (515) Alonso, J. L.; Pena, I.; Lopez, J. C.; Vaquero, V. Rotational Spectral Signatures of Four Tautomers of Guanine. *Angew. Chem. Int. Ed.* **2009**, *48*, 6141-6143.
- (516) Abo-Riziq, A. G.; Grace, L.; Nir, E.; Kabelac, M.; Hobza, P.; de Vries, M. S. Photochemical Selectivity in Guanine-Cytosine Base-Pair Structures. *Proc. Natl. Acad. Sci. USA* **2005**, *102*, 20–23.
- (517) Gloaguen, E.; Brenner, V.; Alauddin, M.; Tardivel, B.; Mons, M.; Zehnacker-Rentien, A.; Declerck, V.; Aitken, D. J. Direct Spectroscopic Evidence of Hyperconjugation Unveils the Conformational Landscape of Hydrazides. *Angew. Chem. Int. Ed.* **2014**, *53*, 13756-13759.

- (518) Weinhold, F. Natural Bond Orbital Analysis: A Critical Overview of Relationships to Alternative Bonding Perspectives. *J. Comput. Chem.* **2012**, *33*, 2363-2379.
- (519) Alabugin, I. V.; dos Pasos Gomes, G.; Abdo, M. A. Hyperconjugation. *Wiley Interdisciplinary Reviews-Computational Molecular Science* **2019**, *9*, e1389.
- (520) Donon, J.; Habka, S.; Vaquero-Vara, V.; Brenner, V.; Mons, M.; Gloaguen, E. Electronic Stark Effect in Isolated Ion Pairs. *J. Phys. Chem. Lett.* **2019**, *10*, 7458-7462.
- (521) Bakels, S.; Meijer, E.; Greuell, M.; Porskamp, S. B. A.; Rouwhorst, G.; Mahé, J.; Gaigeot, M. P.; Rijs, A. M. Interactions of Aggregating Peptides Probed by IR-UV Action Spectroscopy. *Faraday Discuss.* **2019**, *217*, 322-341.